

PROCEEDINGS OF THE AUSTRALIAN PHYSIOLOGICAL AND PHARMACOLOGICAL SOCIETY



PROCEEDINGS OF THE AUSTRALIAN PHYSIOLOGICAL AND PHARMACOLOGICAL SOCIETY

Volume 34

August 2004



Correspondence

Correspondence concerning literary and technical aspects of the journal should be addressed to the Editor. Correspondence concerning subscriptions to the journal should be addressed to the Treasurer and that involving all other Society business should be addressed to the National Secretary.

**AUSTRALIAN AUSTRALIAN PHYSIOLOGICAL AND PHARMACOLOGICAL
SOCIETY INC.**

- President: P.W. Gage (2000-)
Department of Physiology,
JCSMR, ANU
Canberra 2601
- National Secretary: D.A. Saint (2002-)
Molecular and Biomedical Sciences
University of Adelaide
Adelaide SA 5005
- Treasurer: C.B. Neylon (2002-)
Department of Anatomy & Cell Biology
University of Melbourne
VIC 3010
- Editor: D.F. Davey (2002-)
D'Entrecasteaux
378 Manuka Road
Kettering,
Tasmania 7155

Elected Members of Council (Year of retirement in parentheses)

- | | | |
|---------------|--------|--|
| D. Robertson | (2004) | University of Western Australia |
| D.J. Adams | (2005) | University of Queensland |
| L. Delbridge | (2005) | University of Melbourne |
| C. Chen | (2006) | Prince Henry's Institute of Medical Research |
| A. Mihailidou | (2006) | Royal North Shore Hospital |

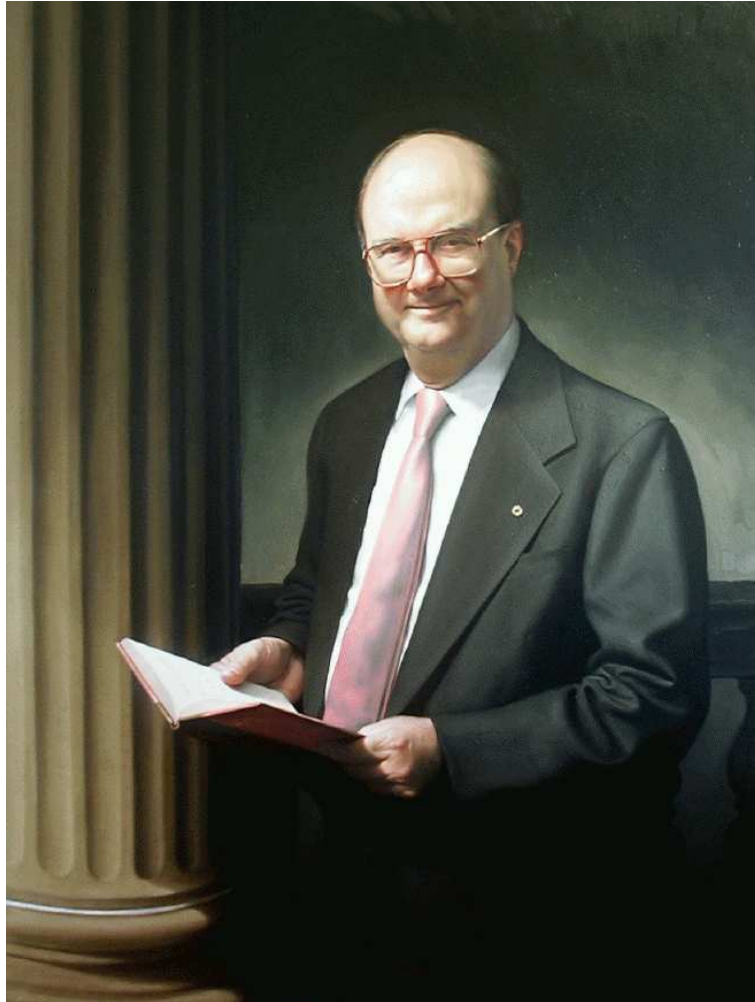
Appointed Members of Council (Year of retirement in parentheses)

- | | | |
|------------|--------|---|
| R. Haddock | (2003) | Australian National University (Student representative) |
|------------|--------|---|

Co-opted Members of Council

- | | | |
|---------------|--------|---|
| D. Tracey | (2004) | University of NSW (FASTS rep) |
| J. Brock | (2004) | Prince of Wales Medical Research Institute (AHMRC meeting representative) |
| S.C. Gandevia | (2004) | Prince of Wales Medical Research Institute (AHMRC meeting representative) |

© 2004 Australian Physiological and Pharmacological Society



Dedicated to the Memory of
John Atherton Young AO, FAA FRACP (1936-2004)

Councillor	1969-1973
Editor	1973-1975
National Secretary	1983-1988
President	1995-2000

Obituary - pages 151-155

This issue of the *Proceedings of the Australian Physiological and Pharmacological Society* contains papers resulting from presentations at the 70th scientific meeting of the *Society* held jointly with the *Physiological Society of New Zealand* at the University of Sydney, 29 September - 1 October 2003. At the Annual General Meeting held on 1 October, the *Society* took the first step towards changing its name to the *Australian Physiological Society*. This change of name was formalised by a postal vote of the *Society's* membership, declared carried on 9 February 2004. As a consequence this volume of the *Proceedings* will be the last to be published under the name *Proceedings of the Australian Physiological and Pharmacological Society*.

All scientific papers in this volume have been subject to peer review.

**PROCEEDINGS OF THE AUSTRALIAN
PHYSIOLOGICAL AND
PHARMACOLOGICAL SOCIETY**

Volume 34

August 2004

CONTENTS

APPS/PSNZ Sydney 2003 Meeting - Invited Lecture and Symposia

APPS Invited Lecture

Skeletal muscle function: the role of ionic changes in fatigue, damage and disease

D.G. Allen 1-11

Symposium: Stretch-induced muscle damage in sport and disease

Identification of a zebrafish model of muscular dystrophy

D. Bassett & P.D. Currie 13-17

Popping sarcomere hypothesis explains stretch induced muscle damage

D.L. Morgan & U. Proske 19-23

Identifying athletes at risk of hamstring strains and how to protect them

U. Proske, D.L. Morgan, C.L. Brockett & P. Percival 25-30

Stretch-activated channels in stretch-induced muscle damage

E.W. Yeung & D.G. Allen 31-37

The role of contraction-induced injury in the mechanisms of muscle damage in muscular dystrophy

G.S. Lynch 39-43

**Symposium: Potassium channels and endothelium-derived hyperpolarising factor:
Physiological and clinical roles**

Factors, fiction and endothelium-derived hyperpolarizing factor - EDH(F)

S.L. Sandow 45-54

Endothelial potassium channels, endothelium-dependent hyperpolarization, and the regulation of vascular tone in health and in disease

H.A. Coleman, M. Tare & H.C. Parkington 55-64

Changes in EDHF in hypertension and ageing: response to chronic treatment with renin-angiotensin system inhibitors

K. Goto, K. Fujii, Y. Kansui & M. Iida 65-70

Symposium: Hormonal, metabolic and neural control of the kidney

Activation of renal calcium and water excretion by novel physiological and pharmacological activators of the calcium-sensing receptor

A.D. Conigrave & H.C. Lok 71-74

Molecular changes in proximal tubule function in diabetes mellitus

D.H. Hryciw, E.M. Lee, C.A. Pollock & P. Poronnik 75-83

Differential neural control of glomerular ultrafiltration

K.M. Denton, S.E. Luff, A. Shweta & W.P. Anderson 85-91

Differential neural control of glomerular ultrafiltration

G.A. Eppel, S.C. Malpas, K.M. Denton & R.G. Evans 93-104

Symposium: Functional Imaging

Functional Imaging Introduction: Gaining new insight from biophotonic imaging

M.B. Cannell 105-106

Development of low affinity, membrane targeted Ca^{2+} sensors suitable for measuring presynaptic Ca^{2+}

M. Monif, M.L. Smart, C.A. Reid & D.A. Williams 107-112

Functional imaging: new views on lens structure and function

P.J. Donaldson, A.C. Grey, B.R. Merriman-Smith, A.M.G. Sisley, C. Soeller, M.B. Cannell & M.D. Jacobs 113-120

Quantitative phase microscopy – a new tool for investigating the structure and function of unstained live cells

C.L. Curl, C.J. Bellair, P.J. Harris, B.E. Allman, A. Roberts, K.A. Nugent & L.M.D. Delbridge 121-127

Microscopic imaging of extended tissue volumes

I.J. LeGrice, G. Sands, D.A. Hooks, D. Gerneke & B.H. Smaill 129-132

Symposium: Integrating cardiac function: From molecules to man

Inherited cardiac arrhythmia syndromes: What have they taught us about arrhythmias and anti-arrhythmic therapy?

R.N. Subbiah, T.J. Campbell & J.I. Vandenberg 133-140

Cardiac structure and electrical activation: Models and measurement

B.H. Smaill, I.J. LeGrice, D.A. Hooks, A.J. Pullan, B.J. Caldwell & P.J. Hunter 141-149

Dedication

John Atherton Young AO, FAA FRACP (1936-2004)

D.I. Cook 151-155

Index

Author index 156-157

Skeletal muscle function: the role of ionic changes in fatigue, damage and disease

D.G. Allen

*School of Biomedical Sciences and Institute for Biomedical Research,
University of Sydney F13,
NSW 2006, Australia*

Summary

1. Repeated activity of skeletal muscle causes a variety of changes in its properties; muscles become weaker with intense use (fatigue), may feel sore and weak after repeated contractions involving stretch, and can degenerate in some disease conditions. This review considers the role of early ionic changes in the development of each of these conditions.

2. Single fibre preparations of mouse muscle were used to measure ionic changes following activity-induced changes in function. Single fibres were dissected with intact tendons and stimulated to produce force. Fluorescent indicators were micro-injected into the fibres to allow simultaneous ionic measurements together with mechanical performance.

3. One theory to explain muscle fatigue is that it is caused by accumulation of lactic acid producing an intracellular acidosis which inhibits the myofibrillar proteins. In contrast we found that during repeated tetani there was little or no pH change but failure of calcium release was a major contributor to fatigue. Currently it is proposed that precipitation of calcium and phosphate in the sarcoplasmic reticulum contributes to the failure of calcium release.

4. Muscles can be used to shorten and produce force or they can be used to decelerate loads (stretched or eccentric contractions). A day after intense exercise involving stretched contractions muscles are weak, sore and tender and this damage can take a week to recover. In this condition sarcomeres are disorganised and there are increases in resting intracellular Ca^{2+} and Na^+ . Recently we demonstrated that the elevation of Na^+ occurs through a stretch-activated channel which can be blocked by either gadolinium or streptomycin. Preventing the rise of $[\text{Na}^+]_i$ with gadolinium also prevents part of the muscle weakness after stretched contractions.

5. Duchenne muscular dystrophy is a lethal degenerative disease of muscles in which the protein dystrophin is absent. Dystrophic muscles are more susceptible to stretch-induced muscle damage and the stretch-activated channel seems to be one pathway for the increases in intracellular Ca^{2+} and Na^+ which are a feature of this disease. We have recently shown that blockers of the stretch-activated channel can minimize some of the short-term damage in muscles from the *mdx* mouse, which also lacks dystrophin. Currently we are testing whether blockers of the stretch-activated channels given systemically to *mdx* mouse can protect against some features of this disease.

Introduction

Ionic changes are central to the activity of muscle. The action potential is caused by rapid movements of Na^+ into the cell and K^+ out of the cell. The action potential in the T-tubules triggers rapid release of Ca^{2+} from the sarcoplasmic reticulum into the myoplasm where it binds to troponin initiating cross bridge cycling. An early source of energy is the anaerobic breakdown of glycogen whose products are lactate and protons. Thus changes in the intracellular concentrations of Na^+ , Ca^{2+} and H^+ all occur as part of normal muscle activity. In the studies described in this review we are concerned with the changes in muscle function which accompany repeated activity. We show that each of the above cations can change during repeated muscle activity and analyse how this changes contribute to muscle function.

Our approach to these issues has been to develop the single mammalian muscle fibre preparation first described by Lännergren and Westerblad¹. Single fibres are dissected from the *flexor brevis* muscle of the mouse, clips are attached to the tendons at either end and the muscle fibre can then be attached to a tension transducer and a motor to impose length changes. Electrodes running parallel to the fibre allow stimulation. Normally fibres are continuously perfused by a physiological salt solution with pH buffered by $\text{HCO}_3^-/\text{CO}_2$. These fibres can be penetrated with microelectrodes and microinjected with fluorescent dyes or many other substances e.g. ions, drugs, peptides, proteins, DNA plasmids. At the end of the experiment fibres can be fixed for light or electron microscopy or subject to immunofluorescence. The attractions of this approach are that any sequence of stimulation (twitches, tetani, repeated in any pattern) or contraction type (isometric, shortening or lengthening) can be imposed on the fibre and the force and fluorescence can be monitored from a single cell during activity. In the experiments described in this review we have used fluorescent Ca^{2+} , Na^+ or pH indicators to allow continuous measurements of these ions. With use of an imaging microscope the distribution of these ions within a single cell can also be determined.

Muscle fatigue

It is a common experience that the performance of muscle gradually declines when muscles are used repeatedly at near their maximum force. This decline of performance, or muscle fatigue, is reflected in reduced force production, reduced shortening velocity and a slower time course of contraction and relaxation. Of course muscles

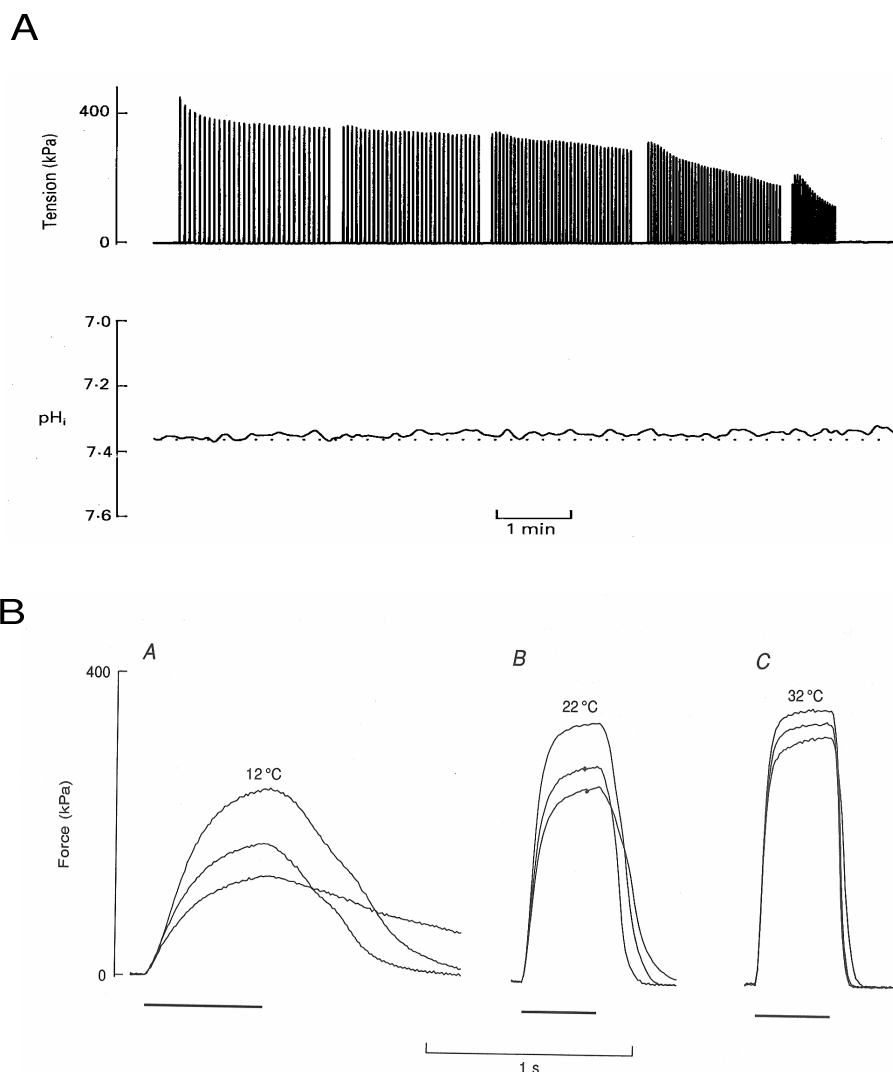


Figure 1. pH has minimal role in muscle fatigue.

Panel A shows measurement of myoplasmic pH throughout a period of fatigue caused by repeated brief tetani. Data from single mouse muscle fibre at 22°C. Note that myoplasmic pH changed little despite the development of fatigue. Data from Westerblad & Allen⁶. Panel B shows tetanic force from mouse single fibres at three different temperatures (12°C, 22°C and 32°C). At each temperature three tetani are shown with intracellular pH modified by changes in external [CO₂]. From above down, the intracellular pHs are respectively 0.5, 0 and -0.5 greater than the resting level. Note that the effect of a 1 pH unit change in intracellular pH is much greater at 12°C than at 32°C. Tension or force measurements are normalized as the force per cross-sectional area of the fibre and are quoted in units of kPa where a Pascal is one Newton metre⁻². Data from Westerblad et al.⁸ (reproduced with the permission of the copyright holder).

can be used near their maximal capacity in many different activities e.g. maximal continuous isometric contractions such as lifting a piano, repeated contractions such as running 100 m or a marathon, repeated stretched contractions such as walking down a mountain and it would be expected that these different activities would affect muscle function in different ways. Equally important many different diseases cause skeletal muscle weakness e.g. muscular dystrophies, cardiac failure, renal failure, starvation, chronic infections etc. and surveys show that complaints about muscle weakness and fatigue are among

the commonest presenting symptoms in medical consultations². Of particular importance is the fact that all elderly humans suffer a gradual loss of muscle mass and the consequent weakness and rapid fatigue during every day activities contribute to the loss of mobility and independence. Single fibres can be useful in the investigation of many of these situations by appropriate choice of conditions.

The present review will consider the muscle fatigue caused by repeated short isometric tetani e.g. Figs 1 & 2. These figures show that when short (0.3 s) maximal tetani

are repeated every few seconds, the force produced declines to 50% within a few minutes. The time scale of this experiment is similar that involved when running 1-2 km or swimming 200-500 m and it seems reasonable to suppose that the intracellular mechanisms within the muscles are similar.

Lactic acid as the cause of skeletal muscle fatigue

Since the pioneering research of A.V. Hill, the accumulation of intracellular lactic acid has been a dominant theory of muscle fatigue³. Lactic acid accumulates in many intense fatiguing regimes and can lead to an intracellular acidosis of about 0.5 pH units. There are two major lines of evidence that have been used to link this decline of intracellular pH to the contractile dysfunction in fatigue. First, studies on human muscle fatigue of rapid onset have often shown a good temporal correlation between the decline of intracellular muscle pH and the reduction of force or power production. Second, studies on skinned skeletal muscle fibres have shown that acidification reduces the isometric force by a direct effect on the isolated myofibrillar proteins⁴.

We therefore measured the intracellular pH in our mouse single fibre model of fatigue and found, to our initial surprise, that there was only a small acidosis of around 0.06 pH units (Fig. 1A). Later we showed in the same preparation that if the duty cycle (fraction of time the fibre is stimulated at 100 Hz) was increased the muscles fatigued more rapidly and the acidosis was greater⁵. We also found that blocking the lactate transporter with cinnamate, substantially increased the magnitude of the resulting acidosis⁶. Both these results suggest that lactic acid is produced during intense stimulation but can leave the cell at a substantial rate on the lactate transporter and consequently the intracellular acidosis is reduced. Because it is intracellular acidosis which affects the contractile proteins, it would be predicted that in longer or less intense stimulation protocols the acidosis would be smaller and that fatigue caused by this component would also be reduced. These experiments are compatible with the idea that when intracellular acidosis does occur it contributes to fatigue but, more important, they make it clear that there must be alternative mechanisms of fatigue which dominate when the timecourse is greater than a few minutes and are unrelated to acidosis.

Recent experiments have cast further doubt on the lactic acid theory. Early experiments showing that acidosis reduced the force produced by the myofibrillar proteins were generally performed at room or lower temperatures. When such experiments were repeated nearer body temperature, the magnitude of the inhibitory effect of acidosis was found to be much lower⁷. This is also true for intact fibres and Fig 1B illustrates the inhibitory effects of changes in intracellular acidosis produced by changes in extracellular CO₂⁸; in each panel the smallest tetanus is 1 pH unit more acid than the largest tetanus. Note that at 12°C an intracellular acidosis of 1 pH units reduces force by about 47% whereas at 32°C the same acidosis only

reduces force by about 11%.

To sum up, acidosis has little direct effect on the force production in mammalian muscles studied at physiological temperatures (for review see ⁹). However it remains true that production of lactic acid is of great importance in exercise physiology and the training of athletes. When glycogen is consumed anaerobically to produce lactic acid, the ATP production is 3 ATP per glycosyl unit whereas aerobic metabolism within the mitochondria supplies 39 ATP per glycosyl unit. Thus, the glycogen store is more rapidly depleted when large amounts of lactic acid are produced anaerobically and muscle performance is severely depressed at low glycogen levels. Also high levels of lactic acid in the blood contribute to the discomfort and breathlessness when performing at close to maximum levels of oxygen consumption¹⁰.

Role of intracellular calcium in skeletal muscle fatigue

Given that changes in intracellular pH are not the main cause of fatigue, we examined the role of intracellular calcium. The classic work of Eberstein and Sandow (1963) first suggested that changes in activation played an important role in fatigue¹¹. They fatigued intact muscles with repeated tetani until force was greatly reduced and then increased the level of activation by increasing extracellular K⁺ or application of caffeine; both agents cause increased Ca²⁺ release from the sarcoplasmic reticulum (SR). Both these manoeuvres increased force substantially in the fatigued muscle suggesting that a reversible failure of activation was an important contributor to fatigue. A recent example of this approach is shown in Fig. 2A which illustrates how a moderate concentration of caffeine can reverse much of the decline of force in a fatigued muscle. The rise in intracellular calcium concentration ([Ca²⁺]_i) which activates the contractile proteins (Fig. 2B(i)), initially increases tetanic [Ca²⁺]_i (Fig. 2B(ii)), but then tetanic [Ca²⁺]_i declines during fatigue (Fig. 2B(iii)). Agents such as caffeine, which increase the opening of the SR Ca²⁺ release channels (ryanodine receptors), can increase the amplitude of tetanic [Ca²⁺]_i (Fig. 2B(iv)) and thus overcome much of fatigue. Thus the partial failure of SR Ca²⁺ release is accepted to be one of the causes of muscle fatigue¹²⁻¹⁴.

What causes the reduced Ca²⁺ release which can be reversed by caffeine? In recent years it has become increasingly clear that increased inorganic phosphate (P_i) can affect fatigue development by acting on SR Ca²⁺ handling (for review see¹⁵). Studies in intact muscles show that the resting [P_i]_i is 1-5 mM¹⁶ while during intense contraction it can rise to 30-40 mM¹⁷. It is already established that increasing [P_i]_i reduces crossbridge force and Ca²⁺-sensitivity of the myofilaments¹⁸ and probably contributes to the early fall in force (within 1 min) shown in Fig. 2A. There are several mechanisms whereby P_i might influence SR Ca²⁺¹⁵; here we consider only the Ca²⁺ precipitation theory.

The solubility product of Ca²⁺ and P_i is 6 mM²¹⁹ and this product can be exceeded in the extracellular space

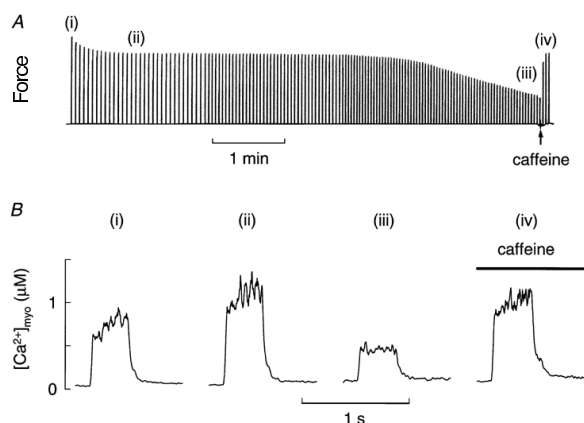


Figure 2. Muscle fatigue is partly caused by failure of SR Ca^{2+} release.

Panel A shows force production from a mouse single fibre stimulated to give repeated brief tetani at gradually reducing intervals until force had declined to ~40% of control. At that time caffeine (10 mM) was applied which reversed much of the decline of force. Panel B shows $[\text{Ca}^{2+}]_i$ records of selected tetani from experiments similar to Panel A. (i) is the first tetanus, (ii) is at the end of the early decline of force, (iii) is a fatigued tetanus just before the addition of caffeine, and (iv) is in the presence of caffeine. These data show that a caffeine-reversible decline in tetanic $[\text{Ca}^{2+}]_i$ is responsible for much of the late phase of decline of force. Figure reproduced from Allen & Westerblad¹⁵.

resulting in the production of bone. In the intracellular environment the very low $[\text{Ca}^{2+}]_i$ generally prevents precipitation but in the SR the $[\text{Ca}^{2+}]_{\text{SR}} = 1 \text{ mM}$, so if $[\text{P}_i]_{\text{SR}}$ exceeds 6 mM then CaP_i will start to precipitate. Thus if P_i enters the SR during fatigue, this could result in CaP_i precipitation and hence decrease the Ca^{2+} available for release.

This mechanism has recently gained support from studies using many different experimental approaches. In initial experiments on skinned fibres with intact T-tubular-SR system it was shown that increased P_i could depress SR Ca^{2+} release¹⁹. These authors also provided indirect evidence that P_i may reach a concentration in the SR high enough to exceed the threshold for CaP_i precipitation. A second indication that P_i has effects other than directly on the myofilaments came from a study in which P_i was directly injected into muscle cells²⁰. We were expecting to see reduced force and Ca^{2+} -sensitivity due to the direct effects of P_i on the myofilaments but, to our surprise, these effects were hardly apparent and instead there was a drastic reduction in SR Ca^{2+} release which caused a fall in force. Since the expected effects of P_i on myofilaments were largely absent, we reasoned that most of the injected P_i had entered the SR, precipitated as CaP_i , and consequently reduced SR Ca^{2+} release.

Another approach to this issue has been to measure SR Ca^{2+} stores in the expectation that the Ca^{2+} available for release might decline if free Ca^{2+} became sequestered as precipitated CaP_i within the SR. 4-Chloro-*m*-cresol (4-CmC) is a drug which, like caffeine, rapidly opens the SR Ca^{2+} channels allowing most of the rapidly-releasable SR Ca^{2+} to enter the myoplasm. Thus in Fig. 3 the initial vertical line represents the rise in $[\text{Ca}^{2+}]_i$ caused by tetanic stimulation while the application of 4-CmC produces a larger and slower rise in $[\text{Ca}^{2+}]_i$, whose magnitude represents the Ca^{2+} available for release in the SR. Note that during fatigue the peak tetanic $[\text{Ca}^{2+}]_i$ signal rises and then falls and that in the fatigued muscle, a second 4-CmC application shows the SR Ca^{2+} content to be reduced. Both the tetanic $[\text{Ca}^{2+}]_i$ and the SR Ca^{2+} content recover over the next 20 min. Measurements of the SR Ca^{2+} concentration ($[\text{Ca}^{2+}]_{\text{SR}}$) using a Ca^{2+} indicator located in the SR have also shown a decrease in fatigued cane toad fibres¹⁸.

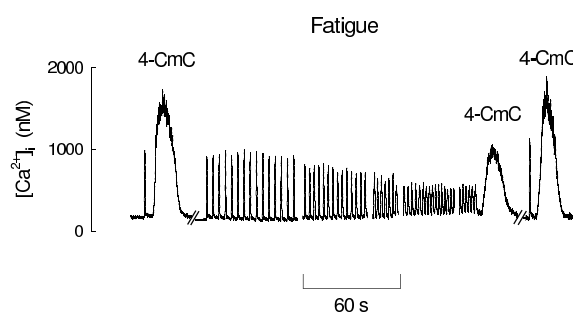


Figure 3. SR Ca^{2+} stores decline during fatigue.

$[\text{Ca}^{2+}]_i$ recorded from a single cane toad fibre from the lumbrical muscle at 22°C. The first record shows a single short tetanus followed by ~10 s application of 4-chloro-*m*-cresol (4-CmC). This drug opens SR Ca^{2+} release channels and the large rise in $[\text{Ca}^{2+}]_i$ represents the amount of rapidly releasable SR Ca^{2+} . Similar results can be obtained with caffeine. The fibre was then rested for 20 min and then fatigued with repeated brief tetani until the tetanic force (not shown) was reduced to 40%. 4-CmC was then reapplied and the amount of rapidly releasable SR Ca^{2+} was reduced compared to control. The fibre was then rested for 20 min and showed a recovery of tetanic $[\text{Ca}^{2+}]_i$ and the rapidly releasable Ca^{2+} . These data show that the rapidly-releasable Ca^{2+} in the SR store declines during fatigue and recovers after a period of rest. Adapted from Kabbara & Allen⁶⁸.

Dahlstedt and colleagues have made use of the creatine kinase knockout mouse as another way to investigate this possibility²¹. In this animal, because of the absence of creatine kinase, the usual rise of P_i observed during fatigue is absent. They found that in muscles which lack the rise of P_i , the late decline of tetanic $[\text{Ca}^{2+}]_i$ during fatigue was delayed. Thus results obtained with a variety of experimental approaches suggest that CaP_i precipitation in the SR is a possible cause of reduced tetanic $[\text{Ca}^{2+}]_i$ in

fatigue.

The CaP_i precipitation theory is obviously dependent on the ability of P_i to move from the myoplasm to the SR. The SR membrane contains small conductance chloride channels, which conduct P_i ²² and may be the pathway involved²³. Interestingly the open probability of these channels increases at low ATP. This dependence on ATP can explain one apparent weakness of the hypothesis that raised $[\text{P}_i]_i$ causes CaP_i precipitation in the SR: $[\text{P}_i]_i$ increases relatively early during fatiguing stimulation while the decline of tetanic $[\text{Ca}^{2+}]_i$ generally occurs quite late. Moreover, in mouse fibres the decline of tetanic $[\text{Ca}^{2+}]_i$ temporally correlates with an increase in Mg^{2+} , which presumably stems from a net breakdown of ATP²⁴, and it is not obvious why CaP_i precipitation in the SR should show a temporal correlation with ATP breakdown. The ATP-dependence of the presumed SR P_i channels can explain both why P_i enters the SR with a delay and why there is a temporal correlation between declining ATP and declining tetanic $[\text{Ca}^{2+}]_i$.

Stretch-induced muscle damage

Muscle damage is a common consequence of intense muscular activity²⁵ and is more severe when the activity involves stretch of contracting muscles (eccentric contraction). In this review the term 'stretched contractions' is used to mean contractions in which the muscle is stretched by an external force²⁶. Following repeated stretched contractions, particularly by untrained subjects, the muscles exhibit an immediate weakness and over the subsequent days they remain weak but also become tender, painful and stiff²⁷. These changes can take a week to fully recover.

The cellular mechanisms which underlie the immediate weakness and the subsequent muscle damage following stretched contractions have two separate components. Fridén (1981) performed electron microscopy on humans muscle biopsies following stretched contractions and showed that the sarcomere structure was disturbed with overstretched sarcomeres and wavy Z-lines distributed randomly throughout the affected fibres²⁸. Morgan (1990) pointed out that sarcomeres are unstable on the descending limb of the length-tension curve, particularly when undergoing stretch²⁹, and that this can lead individual weak sarcomeres to suddenly stretch (popping sarcomeres). Such overstretched sarcomeres normally reinterdigitate during relaxation but after repeated stretched contractions increasing numbers of sarcomeres will fail to reinterdigitate and areas of overstretched sarcomeres may gradually extend.

The earliest changes of sarcomere structure can be observed within a single stretched contraction^{30,31} and are probably the initiating factor in damage. Nevertheless there is good evidence that changes in excitation-contraction coupling also contribute to the muscle weakness caused by stretched contractions^{32,33}. For instance when intracellular calcium was measured during tetani before and after stretched contractions it was found that the resting $[\text{Ca}^{2+}]_i$

was increased while the tetanic $[\text{Ca}^{2+}]_i$ was reduced (Fig. 4). To test whether the reduction of tetanic $[\text{Ca}^{2+}]_i$ contributed to the reduced force production, caffeine was applied and shown to increase both the tetanic $[\text{Ca}^{2+}]_i$ and force after stretched contractions. This result establishes that part of the weakness following stretched contractions is caused by reduced Ca^{2+} release which can be overcome by caffeine. The results also suggests that the SR Ca^{2+} store is not greatly affected since caffeine was capable of increasing Ca^{2+} release and implies that the defect in release lies in the action potential or its coupling to the release channel or the release channel itself. However the mechanism of the disturbance to excitation-contraction coupling remains uncertain.

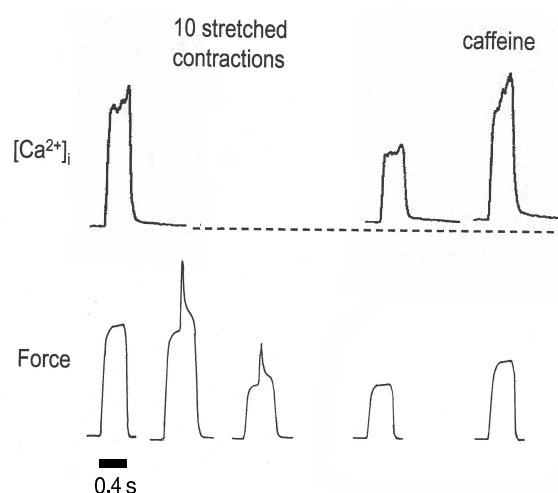


Figure 4. Stretched contractions cause a decline of tetanic $[\text{Ca}^{2+}]_i$ which can be reversed by caffeine.

Figure shows representative tetanic $[\text{Ca}^{2+}]_i$ and force records from a mouse single fibre. Initial $[\text{Ca}^{2+}]_i$ and force are an isometric control obtained at L_o (the length at which maximal tetanic tension is observed). The next two force records are the first and last (10th) stretched contractions in which the fibre was stretched by a motor from L_o to $L_o + 40\%$ over 100 ms. The next pair of records are an isometric tetanus at L_o after 20 min recovery. The last pair of records show that caffeine can overcome the reduced tetanic $[\text{Ca}^{2+}]_i$ and partially restore the force. These data show that stretch-induced muscle damage causes a reduction in tetanic $[\text{Ca}^{2+}]_i$ which is partly responsible for the decline of force. Time scale applies to each tetanus; the time between tetani was variable. Adapted from Balnave & Allen³³.

Another component of stretch-induced damage is an increase in membrane permeability. For example, both serum albumin and the fluorescent dye orange procion have been shown to enter some damaged fibres after a series of stretched contractions³⁴. Resting $[\text{Ca}^{2+}]_i$ increases within 10 minutes of eccentric contractions and, although the mechanism has not been established, this might also be a consequence of increased membrane permeability. The rise in resting $[\text{Ca}^{2+}]_i$ might initiate the impairment of

excitation-contraction coupling by activating proteases which damage the sarcoplasmic reticulum (SR) Ca^{2+} release channel³⁵⁻³⁷. It has also been proposed that Ca^{2+} -activated proteases might damage membranes and contribute to the increased membrane permeability.

We recently showed that following a series of stretched contractions, muscles developed vacuoles which filled with an extracellular marker (sulphorhodamine B) suggesting that they were attached to the T-system³⁸. Such vacuoles had previously been observed under a range of situations in which a muscle was eliminating an osmotic load^{39,40}. We proposed that stretch-induced damage produced T-tubular tears allowing the intracellular Na^+ ($[\text{Na}^+]_i$) to rise and that vacuoles were a consequence of the osmotic load caused by the Na^+ pump extruding the excess Na^+ along with osmotically-equivalent water.

To test these ideas we measured $[\text{Na}^+]_i$ in muscle subjected to stretched contractions⁴¹. Ten isometric tetani had no significant effect on resting $[\text{Na}^+]_i$ but 10 stretched contractions caused a significant increase in $[\text{Na}^+]_i$ (Fig. 5A) from about 7 to 15 mM. The rise was surprisingly slow taking several minutes to reach a maximum and only starting to decline after about 20 min. By removing the extracellular sodium, we showed that this rise in $[\text{Na}^+]_i$ was caused by increased Na^+ influx from the extracellular space. To test whether the Na^+ entry arose through T-tubular or membrane tears we imaged $[\text{Na}^+]_i$ expecting to observe localized elevations of $[\text{Na}^+]_i$ close to the putative tears. However we never observed any obvious areas of elevated $[\text{Na}^+]_i$ suggesting that the Na^+ influx was via multiple small sources below the spatial resolution of the confocal microscope. For this reason we decided to test blockers of various channels through which Na^+ might enter. Skeletal muscle is known to contain stretch-activated non-specific cation channels⁴² so we tested whether known blockers of this channel could prevent the rise of $[\text{Na}^+]_i$ following stretched contractions. Fig. 5B shows that 20 μM Gd^{3+} , applied after the stretched contractions, was capable of preventing the rise of $[\text{Na}^+]_i$. While Gd^{3+} is an established blocker of stretch-activated channels it is also capable of blocking many other channels (for review see⁴³), it is therefore important to note that Gd^{3+} had no effect on resting $[\text{Na}^+]_i$ (Fig. 5B) or on tetanic force⁴¹ in wild-type fibres. In addition, we showed that a chemically-unrelated blocker of stretch-activated channels, streptomycin, was also able to prevent the rise of $[\text{Na}^+]_i$ ⁴¹.

The above results suggest that entry of Na^+ may occur through a class of channels activated by the preceding stretch. Most stretch-activated channels open rapidly (<1 s) after distortion of the membrane and typically close briskly when the distortion is removed⁴⁴. A notable feature of the present experiments is that the rise of $[\text{Na}^+]_i$ occurred mainly after the stretches and that blockers applied after the stretches were capable of preventing the rise of $[\text{Na}^+]_i$. This suggests that the channels were opened by connection to a membrane component or cytoskeletal element which remains distorted long after the initial stretched contractions. For instance long lasting distortion of the T-tubular system following stretched contractions has been

demonstrated by electron-microscopy⁴⁵ and by diffusion of fluorescent markers³⁸. Alternatively changes in cytoskeletal elements such as desmin and titin have been observed after stretched contractions⁴⁶.

The above results also raised the possibility that the ionic changes associated with the stretch-contractions might be implicated in the reduction of force. For instance, if Ca^{2+} ions also entered through the same channel, this would provide an explanation for the raised resting $[\text{Ca}^{2+}]_i$ and we have previously speculated that this might cause the reduced Ca^{2+} release which is one of the causes of the reduced force. This possibility was tested by comparing the recovery of force after stretch-contractions with and without blockers of stretch-activated channels. Either Gd^{3+} or streptomycin increased the recovery of force from 36 to 49% strongly suggesting that ionic entry has some part in the processes which reduce the force.

Stretched contractions are a normal part of the repertoire of muscle activities and have an important role in the training of muscles⁴⁷. It has long been recognized that the damage caused by a series of stretched contractions is reduced on a second repeat⁴⁸. The mechanism of this training effect has been the subject of much investigation and one component is that stretched contractions seem to elicit a recovery in which synthesis of additional sarcomeres in series occurs^{49,50}. The net result of this is a shorter sarcomere length at a given muscle length thereby reducing the propensity to damage⁵¹. These findings suggest that stretched contractions stimulate a specialized sub-set of gene activation. Since $[\text{Ca}^{2+}]_i$ appears to be intimately involved in gene regulation⁵² this raises the possibility that Ca^{2+} entry by stretch-activated channels, perhaps because of some unidentified spatial or temporal feature, activates a group of genes which result in synthesis of additional sarcomeres in series.

Muscular dystrophy

Duchenne muscular dystrophy is an X-linked condition that affects approximately 1 in 3500 male births⁵³. It is a degenerative muscle disease causing death through respiratory and cardiac failure by the end of the second decade. The discovery that the disease was caused by absence of the protein dystrophin has revolutionized understanding of the disease and given new impetus to therapy⁵⁴. The effectiveness of gene replacement therapy has been demonstrated in mouse models of dystrophy but in humans gene therapy has so far proved of limited value because of the difficulties of obtaining adequate expression of the very large dystrophin gene in human muscle (for review see⁵⁵).

The mechanism by which the absence of dystrophin exacerbates stretch-induced damage is unclear. It is widely accepted that excessive Ca^{2+} entry is a feature of dystrophic muscle (for review see⁵⁶). One theory to explain the excessive Ca^{2+} entry is that stretch-induced contractions lead to membrane tears which then allow ionic entry³⁴. On this theory, the absence of dystrophin is assumed to increase the membrane fragility so that membrane tears are

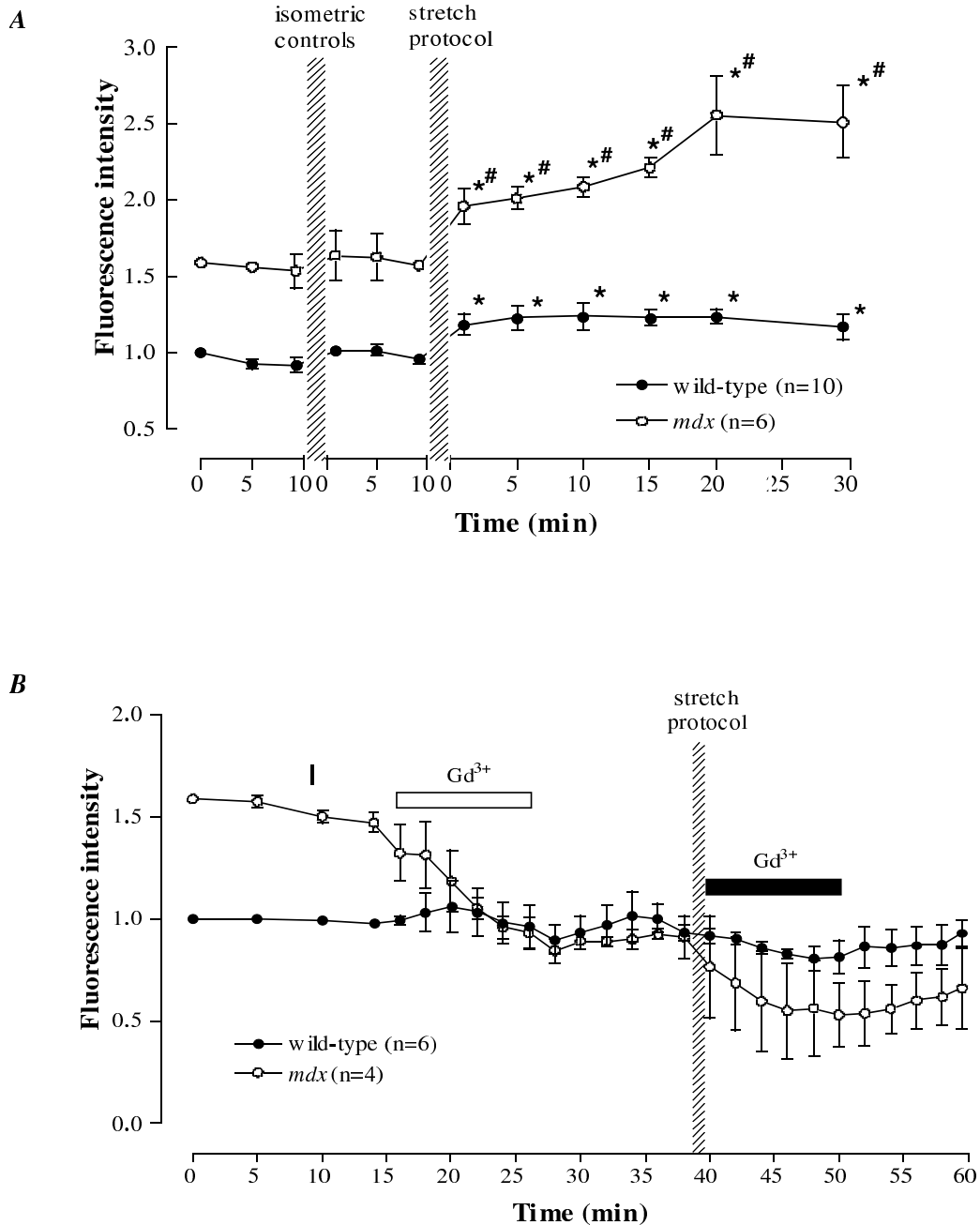


Figure 5. Intracellular sodium in wild-type and mdx mouse after stretched contractions.

$[Na^+]_i$ indicated by fluorescence intensity; the higher initial value in mdx fibres represents their higher $[Na^+]_i$. Panel A shows that a series of isometric contraction had no significant effect on $[Na^+]_i$ whereas a series of stretched contractions produced a rise of $[Na^+]_i$. Note that the rise in $[Na^+]_i$ caused by the stretched contractions was larger in mdx fibres compared to wild-type fibres. * significantly larger than initial level. # significantly larger increase compared to wild-type ($P < 0.05$). Panel B shows first the effect of Gd^{3+} on resting $[Na^+]_i$ in both mdx and wild-type fibres. Gd^{3+} had no effect on wild-type fibres but lowered $[Na^+]_i$ in the mdx fibres to about the level of the wild-type fibres. The fibres then underwent a series of stretched contractions and Gd^{3+} was applied immediately for 10 min (indicated by the bar). Gd^{3+} eliminated the rise of $[Na^+]_i$ caused by stretched contraction in both wild-type and mdx fibres. Values are mean \pm S.E.M. Data adapted from Yeung et al.^{41,65}.

more frequent and lead to greater ionic entry. Another possibility is that the stretch-activated channel in wild-type fibres⁴² has altered properties in the mdx fibres so that it

becomes more readily activated by stretch⁵⁷. The observation that mdx fibres have increased permeability to divalent cations using the Mn^{2+} quench approach would be

consistent with either of these hypotheses⁵⁸.

Studies of muscular dystrophy are very dependent on animals models of which the most widely used is the *mdx* mouse. This spontaneous mutant lacks dystrophin due to the presence of stop codon early in the sequence (for review see ⁵⁹). Although the genotype is similar to the human disease the phenotype is much milder. *Mdx* mice are fertile, live a near normal lifespan and show few overt signs of the disease. However, the creatine kinase levels are elevated and histology shows that the mild signs of muscle damage including centralized nuclei. Stretch-induced damage is generally more severe in *mdx* mice compared to wild-type mice⁶⁰⁻⁶² and the delivery of a dystrophin mini gene to *mdx* fibres reduces stretch-induced damage⁶³. The reasons that the *mdx* phenotype is so much milder than Duchenne muscular dystrophy are not entirely clear but one possibility is that utrophin can substitute to a limited extent for dystrophin and seems to be overexpressed in the *mdx* mouse⁵⁹. Another interesting observation is that muscle damage does not become apparent until about 3 weeks after birth which is close to the time when the animals are weaned and become more mobile, suggesting the possibility that mechanical factors contribute to the damage.

To investigate the mechanism of damage in *mdx* muscle we have measured $[Na^+]_i$ in single fibres dissected from *mdx* mice. An initial finding was that resting $[Na^+]_i$ was higher in *mdx* compared to wild-type fibres, confirming an earlier observation⁶⁴. An interesting feature was that the elevated resting $[Na^+]_i$ of the *mdx* muscle was reduced by Gd^{3+} or streptomycin (Fig. 5B) strongly suggesting that it is caused by increased opening of the same class of stretch-activated channels considered earlier. When the *mdx* fibres were exposed to our standard protocol of stretched contractions the rise in $[Na^+]_i$ started from a higher level and showed a significantly greater rise (Fig. 5A). Either Gd^{3+} or streptomycin were capable of preventing this rise and seemed to lower the $[Na^+]_i$ back towards the level observed in wild-type fibres (Fig 5B). Just as in wild-type fibres we found that either Gd^{3+} or streptomycin could prevent one component of the reduced muscle force after stretch-induced damage⁶⁵. We interpret these findings to mean that muscle contains a stretch-activated channel whose open probability is enhanced in the *mdx* mouse. Patch-clamp studies on *mdx* fibres have produced similar findings⁵⁷. Furthermore the channels seem to be more sensitive to the effects of stretch contractions in *mdx* fibres compared to wild-type fibres. Thus these channels may explain the elevated resting $[Na^+]_i$ in *mdx* mice and also the elevated $[Ca^{2+}]_i$ reported by others⁵⁷. These channels appear to be further opened by stretch and the ionic entry associated with this pathway appears to have a role in the reduction of force observed after muscle stretch.

Some of the pathways we hypothesize to be active in muscle as a consequence of stretch-activated channels are illustrated in Fig. 6. As discussed above, we suggest that stretched contractions lead to a persistent opening of stretch-activated channels. The mechanisms involved are unclear at present but could involve membrane stretch as a result of popped sarcomeres or T-tubular vacuoles or

perhaps changes in the cytoskeleton which modify channel activity. Since these channels are permeable to both Na^+ and Ca^{2+} ⁴² we would expect to observe increases in the resting $[Na^+]_i$ and $[Ca^{2+}]_i$ and, as discussed above, both have been observed. On this basis we would expect that blockers of the stretch-activated channels would be capable of preventing the rise of $[Na^+]_i$ and $[Ca^{2+}]_i$ and we have demonstrated that both Gd^{3+} and streptomycin can block the rise of $[Na^+]_i$ in *mdx* muscle⁶⁵. The functional changes in muscle as a consequence of raised $[Na^+]_i$ are not clear but we have previously suggested above that the vacuoles present after stretched contractions are because the Na^+ pump extrudes the excess Na^+ with osmotically equivalent water and this hydraulic load in the T-tubules causes dilation and vacuolation³⁸. The elevated $[Na^+]_i$ would be expected to reduce the amplitude of the action potential and might therefore reduce SR Ca^{2+} release. In addition a raised $[Na^+]_i$ will affect all Na^+ linked transporters with a range of possible consequences for the cell. Whether the changed properties of the T-tubules affect muscle function is unclear^{38,45}.

Current hypothesis

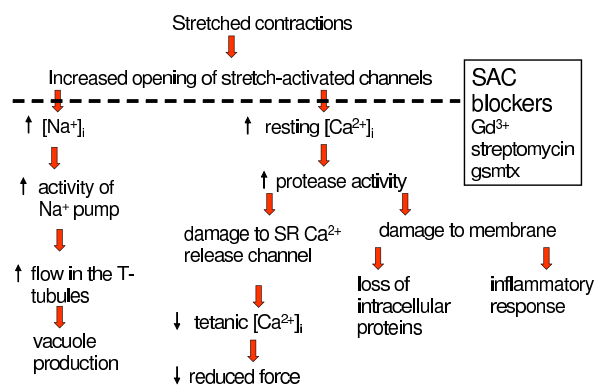


Figure 6. Role of stretch-activated channels in stretch-induced muscle damage.

Schematic to illustrate some of the pathways thought to be involved in the muscle damage caused by stretched contractions. For description see main text.

In Fig. 6 we propose that the elevated $[Ca^{2+}]_i$ activates proteases with consequent effects on intracellular proteins and membranes. This possibility has been extensively considered but a difficulty is that the proteases which have been described do not have sufficient Ca^{2+} sensitivity to be activated by the observed rises in $[Ca^{2+}]_i$ ⁶⁶⁻⁶⁷. One protein which might be damaged is the ryanodine receptor (SR Ca^{2+} release channel) and, as discussed earlier, there is good evidence that increases in $[Ca^{2+}]_i$ can lead to reduced SR Ca^{2+} release³⁵⁻³⁷. We also speculated in Fig. 6 that the loss of intracellular proteins and the inflammatory response are secondary consequences of membrane damage.

Therapeutic possibilities

Our experimental data so far show that in isolated single fibres stretch-induced damage involves changes in $[Na^+]_i$ and $[Ca^{2+}]_i$ which are probably attributable to stretch-activated channels. When these channels are blocked some of the reduced force associated with stretch-induced damage can be prevented. These results raise the possibility that if the damage in muscular dystrophy is partly or predominately through the same pathway then blockers of the stretch-activated channels may reduce part of the muscle damage. We are currently testing this idea by using the stretch-activated channel blocker to *mdx* mice and testing whether the muscle damage is reduced.

Conclusions

Single fibre preparations have proved a powerful experimental approach for studies of muscle function. The ability to make ionic measurements with good temporal and spatial resolution in single functioning fibres has greatly facilitated understanding of the functional changes during repeated muscle activity. Increasingly it will be possible to measure ionic concentrations in defined regions such as mitochondria, nuclei, SR and the near-membrane region. The possibilities of fluorescent tagging of signaling molecules, transcription factors, mRNA and proteins and following the distribution of these substances during different kinds of muscle activity offer exciting directions for the future.

Acknowledgements

Support from the Australian Research Council and the National Health & Medical Research Council is gratefully acknowledged.

Reference List

- Lännergren J, Westerblad H. The temperature dependence of isometric contractions of single, intact fibres dissected from a mouse foot muscle. *J. Physiol.* 1987;**390**:285-93.
- Hickie IB, Hooker AW, Hadzi-Pavlovic D, Bennett BK, Wilson AJ, Lloyd AR. Fatigue in selected primary care settings: sociodemographic and psychiatric correlates. *Med. J. Aust.* 1996;**164**:585-88.
- Hill AV, Kupalov P. Anaerobic and aerobic activity in isolated muscle. *Proc. Roy. Soc. (Lond. Series B)*. 1929;**105**:313-22.
- Fabiato A, Fabiato F. Effects of pH on the myofilaments and the sarcoplasmic reticulum of skinned cells from cardiac and skeletal muscles. *J. Physiol.* 1978;**276**:233-55.
- Chin ER, Allen DG. The contribution of pH-dependent mechanisms to fatigue at different intensities in mammalian single muscle fibres. *J. Physiol.* 1998;**512**:831-40.
- Westerblad H, Allen DG. Changes of intracellular pH due to repetitive stimulation of single fibres from mouse skeletal muscle. *J. Physiol.* 1992;**449**:49-71.
- Pate E, Bhimani M, Franks-Skiba K, Cooke R. Reduced effect of pH on skinned rabbit psoas muscle mechanics at high temperatures: implications for fatigue. *J. Physiol.* 1995;**486**:689-94.
- Westerblad H, Bruton JD, Lännergren J. The effect of intracellular pH on contractile function of intact, single fibres of mouse muscle declines with increasing temperature. *J. Physiol.* 1997;**500**:193-204.
- Westerblad H, Allen DG, Lännergren J. Muscle fatigue: lactic acid or inorganic phosphate the major cause? *News Physiol. Sci.* 2002;**17**:17-21.
- Killian KJ, Campbell EJ. Dyspnea and exercise. *Annu. Rev. Physiol.* 1983;**45**:465-79.
- Eberstein A, Sandow A. Fatigue mechanisms in muscle fibers. In: Gutman E, Hink P, eds. The effect of use and disuse on the neuromuscular functions. Amsterdam: Elsevier; 1963: 515-26.
- Allen DG, Lännergren J, Westerblad H. Muscle cell function during prolonged activity: cellular mechanisms of fatigue. *Exp. Physiol.* 1995;**80**:497-527.
- Williams JH, Klug GA. Calcium exchange hypothesis of skeletal muscle fatigue: a brief review. *Muscle and Nerve.* 1995;**18**:421-34.
- Favero TG. Sarcoplasmic reticulum Ca^{2+} release and muscle fatigue. *J. Appl. Physiol.* 1999;**87**:471-83.
- Allen DG, Westerblad H. Role of phosphate and calcium stores in muscle fatigue. *J. Physiol.* 2001;**536**:657-65.
- Kushmerick MJ, Moerlands TS, Wiseman RW. Mammalian skeletal muscle fibres distinguished by contents of phosphocreatine, ATP and Pi. *Proc. Nat. Acad. Sci. USA.* 1992;**89**:7521-25.
- Cady EB, Jones DA, Lynn J, Newham DJ. Changes in force and intracellular metabolites during fatigue of human skeletal muscle. *J. Physiol.* 1989;**418**:311-25.
- Cooke R, Pate E. The effects of ADP and phosphate on the contraction muscle fibers. *Biophys. J.* 1985;**48**:789-98.
- Fryer MW, Owen VJ, Lamb GD, Stephenson DG. Effects of creatine phosphate and P_i on Ca^{2+} movements and tension development in rat skinned skeletal muscle fibres. *J. Physiol.* 1995;**482**:123-40.
- Westerblad H, Allen DG. The effects of intracellular injections of phosphate on intracellular calcium and force in single fibres of mouse skeletal muscle. *Pflügers Arch.* 1996;**431**:964-70.
- Dahlstedt AJ, Katz A, Westerblad H. Role of myoplasmic phosphate in contractile function of skeletal muscle studies on creatine kinase deficient mice. *J. Physiol.* 2001;**533**:379-88.
- Ahern GP, Laver DR. ATP inhibition and rectification of a Ca^{2+} -activated anion channel in sarcoplasmic reticulum of skeletal muscle. *Biophys. J.* 1998;**74**:2335-51.
- Laver DR, Lenz GKE, Dulhunty AF. Phosphate ion channels in the sarcoplasmic reticulum of rabbit

- skeletal muscle. *J. Physiol.* 2001;**537**:763-78.
24. Westerblad H, Allen DG. Myoplasmic free Mg²⁺ concentration during repetitive stimulation of single fibres from mouse skeletal muscle. *J. Physiol.* 1992;**453**:413-34.
 25. Gissel H, Clausen T. Ca²⁺ uptake and cellular integrity in rat EDL muscle exposed to electrostimulation, electroporation, or A23187. *Am. J Physiol. Regul. Integr. Comp. Physiol.* 2003;**285**:R132-R142.
 26. Faulkner JA. Terminology for contractions of muscles during shortening, while isometric, and during lengthening. *J Appl. Physiol.* 2003;**95**:455-59.
 27. Newham DJ, Jones DA, Clarkson PM. Repeated high-force eccentric exercise: effects on muscle pain and damage. *J. Appl. Physiol.* 1987;**63**:1381-86.
 28. Fridén J, Sjöström M, Ekblom B. A morphological study of delayed muscle soreness. *Experientia.* 1981;**37**:506-7.
 29. Morgan DL. New insights into the behavior of muscle during active lengthening. *Biophys. J.* 1990;**57**:209-21.
 30. Brown LM, Hill L. Some observations on variations in filament overlap in tetanized muscle fibres and fibres stretched during a tetanus, detected in the electron microscope after rapid fixation. *J Mol. Cell. Cardiol.* 1991;**12**:171-82.
 31. Talbot JA, Morgan DL. Quantitative analysis of sarcomere non-uniformities in active muscle following a stretch. *J. Muscle Res. Cell Motility.* 1996;**17**:261-68.
 32. Warren GL, Lowe DA, Hayes DA, Karwoski CJ, Prior BM, Armstrong RB. Excitation failure in eccentric contraction-induced injury of mouse soleus muscle. *J. Physiol.* 1993;**468**:487-99.
 33. Balnave CD, Allen DG. Intracellular calcium and force in single mouse muscle fibres following repeated contractions with stretch. *J. Physiol.* 1995;**488**:25-36.
 34. McNeil PL, Khakee R. Disruptions of muscle fiber plasma membranes. Role in exercise-induced damage. *Am. J. Pathol.* 1992;**140**:1097-109.
 35. Lamb GD, Junankar PR, Stephenson DG. Raised intracellular [Ca²⁺] abolishes excitation-contraction coupling in skeletal muscle fibres of rat and toad. *J. Physiol.* 1995;**489**:349-62.
 36. Chin ER, Allen DG. The role of elevations in intracellular Ca²⁺ concentration in the development of low frequency fatigue in mouse single muscle fibres. *J. Physiol.* 1996;**491**:813-24.
 37. Bruton JD, Lannergren J, Westerblad H. Effects of repetitive tetanic stimulation at long intervals on excitation-contraction coupling in frog skeletal muscle. *J. Physiol.* 1996;**495**:15-22.
 38. Yeung EW, Balnave CD, Ballard HJ, Bourreau JP, Allen DG. Development of T-tubular vacuoles in eccentrically damaged mouse muscle fibres. *J. Physiol.* 2002;**540**:581-92.
 39. Lännergren J, Bruton JD, Westerblad H. Vacuole formation in fatigued skeletal muscle fibres from frog and mouse: effects of extracellular lactate. *J. Physiol.* 2000;**526**:597-611.
 40. Krolenko SA, Lucy JA. Reversible vacuolation of T-tubules in skeletal muscle: mechanisms and implications for cell biology. *Int. Rev. Cytol.* 2001;**202**:243-98.
 41. Yeung EW, Ballard HJ, Bourreau JP, Allen DG. Intracellular sodium in mammalian muscle fibers after eccentric contractions. *J Appl. Physiol.* 2003;**94**:2475-82.
 42. Franco A, Lansman JB. Stretch-sensitive channels in developing muscle cells from a mouse cell line. *J. Physiol.* 1990;**427**:361-80.
 43. Caldwell RA, Clemo HF, Baumgarten CM. Using gadolinium to identify stretch-activated channels: technical considerations. *Am. J. Physiol.* 1998;**275**:C619-C621.
 44. McBride DW, Jr., Hamill OP. Pressure-clamp: a method for rapid step perturbation of mechanosensitive channels. *Pflügers Arch.* 1992;**421**:606-12.
 45. Takekura H, Fujinami N, Nishizawa T, Ogasawara H, Kasuga N. Eccentric exercise-induced morphological changes in the membrane systems involved in excitation-contraction coupling in rat skeletal muscle. *J. Physiol.* 2001;**533**:571-83.
 46. Lieber RL, Thornell LE, Friden J. Muscle cytoskeletal disruption occurs within the first 15 min of cyclic eccentric contraction. *J Appl. Physiol.* 1996;**80**:278-84.
 47. Colliander EB, Tesch PA. Effects of eccentric and concentric muscle actions in resistance training. *Acta Physiol. Scand.* 1990;**140**:31-39.
 48. Balnave CD, Thompson MW. Effect of training on eccentric exercise-induced muscle damage. *J Appl. Physiol.* 1993;**75**:1545-51.
 49. Lynn R, Morgan DL. Decline running produces more sarcomeres in rat vastus intermedius muscle fibers than does incline running. *J Appl. Physiol.* 1994;**77**:1439-44.
 50. Lynn R, Talbot JA, Morgan DL. Differences in rat skeletal muscles after incline and decline running. *J Appl. Physiol.* 1998;**85**:98-104.
 51. Proske U, Morgan DL. Muscle damage from eccentric exercise: mechanism, mechanical signs, adaptation and clinical applications. *J. Physiol.* 2001;**537**:333-45.
 52. Olson EN, Williams RS. Remodeling muscles with calcineurin. *Bioessays.* 2000;**22**:510-519.
 53. Emery AE. Population frequencies of inherited neuromuscular diseases--a world survey. *Neuromuscul. Disord.* 1991;**1**:19-29.
 54. Hoffman EP, Brown RH, Jr., Kunkel LM. Dystrophin: the protein product of the Duchenne muscular dystrophy locus. *Cell.* 1987;**51**:919-28.
 55. Skuk D, Vilquin JT, Tremblay JP. Experimental and therapeutic approaches to muscular dystrophies. *Curr. Opin. Neurol.* 2002;**15**:563-69.
 56. Gillis JM. Understanding dystrophinopathies: an inventory of the structural and functional

- consequences of the absence of dystrophin in muscles of the mdx mouse. *J Muscle Res. Cell Motil.* 1999;**20**:605-25.
57. Franco-Obregon A, Lansman JB. Changes in mechanosensitive channel gating following mechanical stimulation in skeletal muscle myotubes from the mdx mouse. *J Physiol.* 2002;**539**:391-407.
58. Tutdibi O, Brinkmeier H, Rudel R, Fohr KJ. Increased calcium entry into dystrophin-deficient muscle fibres of MDX and ADR-MDX mice is reduced by ion channel blockers. *J Physiol.* 1999;**515**:859-68.
59. Blake DJ, Weir A, Newey SE, Davies KE. Function and genetics of dystrophin and dystrophin-related proteins in muscle. *Physiol. Rev.* 2002;**82**:291-329.
60. Head SI, Williams DA, Stephenson DG. Abnormalities in structure and function of limb skeletal muscle fibres of dystrophic mdx mice. *Proc. R. Soc. Lond. B Biol. Sci.* 1992;**248**:163-69.
61. Petrof BJ, Shrager JB, Stedman HH, Kelly AM, Sweeney HL. Dystrophin protects the sarcolemma from stresses developed during muscle contraction. *Proc. Natl. Acad. Sci. USA.* 1993;**90**:3710-3714.
62. Moens P, Baatsen PH, Marechal G. Increased susceptibility of EDL muscles from mdx mice to damage induced by contractions with stretch. *J Muscle Res. Cell Motil.* 1993;**14**:446-51.
63. Deconinck N, Ragot T, Marechal G, Perricaudet M, Gillis JM. Functional protection of dystrophic mouse (mdx) muscles after adenovirus-mediated transfer of a dystrophin minigene. *Proc. Natl. Acad. Sci. USA.* 1996;**93**:3570-3574.
64. Dunn JF, Bannister N, Kemp GJ, Publicover SJ. Sodium is elevated in mdx muscles: ionic interactions in dystrophic cells. *J Neurol. Sci.* 1993;**114**:76-80.
65. Yeung EW, Head SI, Allen DG. Gadolinium reduces short-term stretch-induced muscle damage in isolated mdx mouse muscle fibres. *J. Physiol.* 2003;**552**:449-58.
66. Belcastro AN, Shewchuk LD, Raj DA. Exercise-induced muscle injury: a calpain hypothesis. *Mol. Cell. Biochem.* 1998;**179**:135-45.
67. Goll DE, Thompson VF, Li H, Wei W, Cong J. The calpain system. *Physiol. Rev.* 2003;**83**:731-801.
68. Kabbara AA, Allen DG. The role of calcium stores in fatigue of isolated single muscle fibres from the cane toad. *J. Physiol.* 1999;**519**:169-76.

Author for correspondence:

Professor D.G. Allen

Department of Physiology

University of Sydney F13,

NSW 2006, Australia

Tel: +61 2 9351 4602

Fax: +61 2 9351 2058

Email: davida@physiol.usyd.edu.au

Received 17 December 2003; in revised form 12 March 2004. Accepted 24 March 2004.

©D.G. Allen 2004

Identification of a zebrafish model of muscular dystrophy

David Bassett* and Peter D. Currie†

*Institute of Human Genetics, Centre for Life,
University of Newcastle upon Tyne,
Central Parkway, Newcastle upon Tyne, NE1 3BZ, United Kingdom
and

†Victor Chang Cardiac Research Institute,
384 Victoria St., Darlinghurst 2010,
Sydney, Australia

Summary

1. Large-scale mutagenic screens of the zebrafish genome have identified a number of different classes of mutations that disrupt skeletal muscle formation. Of particular interest and relevance to human health are a class of recessive lethal mutations in which muscle differentiation occurs normally but is followed by tissue-specific degeneration reminiscent of human muscular dystrophies.

2. We have shown that one member of this class of mutations, the *sapje* (*sap*), results from mutations within the zebrafish orthologue of the human *Duchenne muscular dystrophy* (*DMD*) gene. Mutations in this locus cause Duchenne or Becker muscular dystrophies in human patients and are thought to result in a dystrophic pathology by disrupting the link between the actin cytoskeleton and the extracellular matrix in skeletal muscle cells.

3. We have found that the progressive muscle degeneration phenotype of *sapje* mutant zebrafish embryos is caused by the failure of somitic muscle attachments at the embryonic myotendinous junction (MTJ).

4. Although a role for dystrophin at MTJ's has been postulated previously and MTJ structural abnormalities have been identified in the Dystrophin-deficient, *mdx* mouse model, *in vivo* evidence of pathology based on muscle attachment failure is thus far lacking. Therefore the *sapje* mutation may provide a model for a novel pathological mechanism of Duchenne muscular dystrophy and other muscle diseases. In this review we discuss this finding in light of previously postulated models of Dystrophin function.

advantage of these qualities to examine early stages of muscle development in the zebrafish with a particular focus on the mechanisms utilised to determine the different fibre types present within the embryonic myotome¹. However, until recently the later stages of muscle development have been relatively little studied.

Axial muscle in fish initially forms from segmented paraxial mesoderm, the somites, which in turn give rise to the myotomes. In zebrafish, the different classes of muscle fibres, slow and fast twitch, are topographically separable in the embryonic myotome. The most medial cells of the forming myotome are specified by midline derived signals to form exclusively slow-twitch fibres. These cells subsequently migrate from their medial origin to traverse the entire extent of the myotome to form a subcutaneous layer of slow twitch muscle. The remainder of the myotome differentiates as fast twitch fibres behind this migration². Regardless of fate or position within the myotome, muscle fibres initially differentiate to span an entire somite in the anterior-posterior axis (Fig. 1A). The somite adopts its distinctive chevron shape early on, by 24 hours post fertilisation (hpf), with the dorsal and ventral halves being separated by a sheet of extracellular matrix called the horizontal myoseptum and each pair of adjacent somites being separated by the vertical myoseptum which is similarly constructed (see Fig. 1A). The myosepta serve as the attachment sites for somitic muscle fibres. These muscle attachment sites have now come under the spotlight with the finding that their mechanical failure is the pathological mechanism in a zebrafish mutation that provides the first zebrafish model of an inherited disease of skeletal muscle.

Introduction

Muscle development in the zebrafish

A number of attributes of the zebrafish embryo and larvae lend themselves to the study of skeletal muscle development. Zebrafish embryos develop externally, are optically transparent and are therefore accessible to *in vivo* embryological manipulations. As zebrafish employ precocious motor locomotor strategies, generating muscle load even before the completion of the first 24 h of development, mutations that disrupt muscle development are easily identifiable in large-scale mutagenic screens. Both embryological and genetic studies have taken

A novel mechanism of pathology in a model of muscular dystrophy

The zebrafish dystrophic class mutants and human muscular dystrophy

Large-scale genetic screens in zebrafish have identified a large number of mutants that affect muscle formation, with one class showing a very specific degeneration of skeletal muscle³. Preliminary investigations revealed that mutations at several independent loci share the broad phenotype of developing visible lesions in the trunk muscle during the second day of development which gradually accumulate until the animals

die before reaching adulthood, a phenotype superficially similar to muscular dystrophy in humans. Consequently, this class of mutations have been identified by the authors as the "Dystrophic class mutants"⁴.

In humans, muscular dystrophy is most often caused by mutations within genes encoding components of the Dystrophin associated protein complex (DAPC) which is a multi-protein assembly that provides a transmembrane link between the cytoskeleton and the extracellular matrix^{5,6}. The complex consists of several sub-complexes, with the main structural link being provided by a series of three proteins that attach intracellular F-actin via the sarcolemma to laminin outside the cell. The laminin receptor within the DAPC is dystroglycan, which is formed by the cleavage of a precursor protein into extracellular α and transmembrane β subunits. Dystrophin is a large rod-like protein related to the spectrin family, which binds to β -dystroglycan at its C-terminus and to actin filaments via its N-terminus. A second sub-complex of the DAPC is comprised of a group of related transmembrane proteins called sarcoglycans, a third is based on syntrophin proteins and nitric oxide synthase, and several further proteins are known to associate with the complex. The DAPC is found at the membrane of skeletal muscle fibres and several other cell types in the body, while a similar complex in which dystrophin is replaced by the related protein utrophin is distributed widely throughout the body.

Dystrophin is the product of the DMD or Duchenne Muscular Dystrophy gene, which is responsible for a spectrum of X-linked conditions including Duchenne and the milder Becker muscular dystrophies, cardiomyopathies and mental retardation^{7,8}. Although the exact pathological consequence of dystrophin loss has yet to be elucidated, the structural model of dystrophin function suggests that Duchenne muscular dystrophy results from sarcolemmal tearing during muscle contraction. This consequently leads to a cycle of death and replacement of muscle fibres which results in an accumulation of scar tissue in the muscle and a gradual loss of function and eventually to death^{9,10}. Furthermore, many other muscular dystrophies and congenital myopathies are caused by mutations affecting other components of the DAPC complex, such as a congenital dystrophy linked to laminin- α 2, and type-2 limb girdle muscular dystrophies (LGMD2) some of which are linked to sarcoglycans, calpain 3, caveolin 3 and dysferlin¹¹⁻¹⁵.

The sapje dystrophic class mutant results from mutations within the zebrafish (Zf) orthologue of dystrophin

An analysis of the expression of DAPC components within our zebrafish "dystrophic class" mutants has revealed loss of specific DAPC proteins within individual mutants. Within muscles of the zebrafish mutation *sap*, using antibodies raised against the mammalian dystrophin, which we have shown cross react with zf-dystrophin, we have found that zf-dystrophin is lost from the end of muscle fibres, confirming the class of muscle degeneration mutants may be valid genetic models of human muscular dystrophy

phenotypes⁴ (Fig. 1B and C). Histological examination and confocal imaging of skeletal muscle expressing green fluorescent protein (GFP) showed that the lesions occur where the ends of *sap* mutant muscle fibres become separated from their attachment sites (Fig. 1C and D). Many fibres are seen to detach at one end and contract to a fraction of their original length, showing compression or even collapse of the sarcomeric banding (Fig 1E and F). Furthermore, electron microscopy has revealed nuclear condensations within detached fibres indicating that these cells are undergoing cell death, a process not evident within intact neighbouring cells. A subset of these detached fibres take up the vital dye Evans Blue, which only enters cells with compromised plasma membranes, indicating that some membrane tearing does occur (Fig. 1 G and H)⁴. Thus, despite sharing the phenotype of muscle degeneration at the whole organism level at the cellular level, the pathology of *sap* mutant zebrafish is different to the pathological process that is currently thought to be involved in human muscular dystrophies, where membrane damage occurs along the length of the fibre. In zebrafish, the DAPC is localised embryonically to the ends of muscle fibres before it becomes detectable at the sarcolemma, suggesting that loss of the complex might compromise muscle attachments and possibly allowing detachment of the kind seen in *sap*. This is a surprising finding because this has not been reported in any human muscular dystrophy, and even in mouse mutants that show ultra-structural abnormalities of the cytoskeleton at the MTJ, there have been no reports of actual failure occurring *in vivo*¹⁶⁻²⁰.

By mapping analysis and mutation detection we have shown that *sap* is mutated at the zebrafish orthologue of the human Duchenne muscular dystrophy locus which encode zf-dystrophin. This finding therefore reveals a novel functional requirement for the DAPC in the stability of muscle attachments. We have identified a nonsense mutation within the N-terminal actin-binding domain of dystrophin that removes the large muscle-specific isoform and causes a progressive fatal muscle degeneration. Homozygous mutant *sap* embryos possess a far more severe phenotype than the mouse dystrophin mutant *mdx*, showing the same progression to early lethality as the human disease, perhaps because both human and zebrafish lack the regenerative capacity and compensatory levels of Utrophin that are thought to protect *mdx* mice²¹⁻²³. Utrophin is not found at embryonic muscle attachments in zebrafish, and is absent from the non-specialised sarcolemma along the length of muscle fibres during embryonic development, but is present in the skin and pronephros⁴. This lack of either Dystrophin or Utrophin in embryonic muscle perhaps makes *sap* mutant embryos most similar to mouse models thought to lack any functional DAPC link, notably the laminin- α 2 (*dy*), dystroglycan and *mdx*/utrophin double mutants²¹⁻²⁵. In these mice, the MTJ lacks folding almost completely and may be weaker than in *mdx* animals, but it is unclear whether it ever fails completely. Only very slight folding of the sarcolemma is present in wild-type zebrafish muscle²⁶, indicating that *sap* resembles these mouse models in its anatomical details, and that the complex involutions of

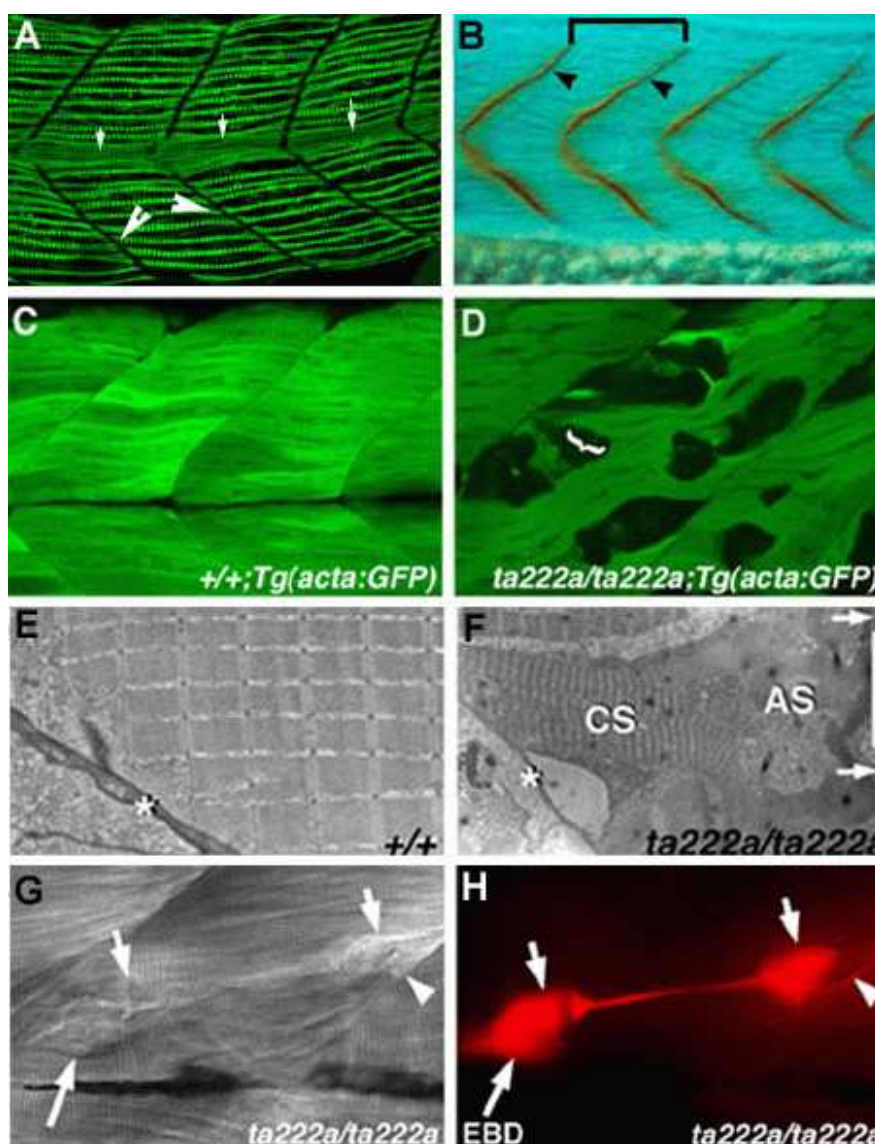


Figure 1. Phenotype of muscle detachment in sapje homozygote embryos.

A. Muscle fibres (Green) initially span the entirety of the myotome to attach to the vertical myosepta (Large arrows). The myotome is also bisected by the vertical myosepta, which separates the dorsal and ventral halves of the myotomes (Small arrows). Lateral view of a 24 hpf embryo stained with an antibody against slow MyHC. B. Dystrophin expression (yellow) is found exclusively at the end of muscle fibres at the vertical myosepta⁴. C, D. Confocal microscopy of GFP expressed in C, Wildtype and D, sap homozygote muscle. In D is an example of muscle fibres that detach from the vertical myosepta in sap homozygotes. Fibres within sap homozygotes (D) exhibit a club-like or faceted appearance at their newly detached membranes, not evident in wild type embryos (C). E, F. Electron microscopy shows that wild type embryonic myofibrils align to form a regular sarcomeric array that attaches obliquely to the myosepta (asterisks (E)). In sap homozygotes, fibres showing detached ends (arrows in F) and shortening of both the entire fibre and the sarcomeres, are visible. In these cells, the separation and regularity of sarcomeric banding is greatly reduced or collapsed compared to that in intact neighbouring cells, and absent in some places. G, H. In vivo observation of muscle attachment failure and molecular analysis of detached free ends. A single fibre (G, H short arrows) viewed in vivo in the process of detaching myosepta, under differential interference contrast (lateral view, 5 days post-fertilisation) and labelled with Evans blue dye. (H). A gap is visible between the separating posterior end of the fibre (right short arrow) and the myoseptum (arrowhead). A narrowed retraction zone has formed where the contractile apparatus has withdrawn from the centre of the fibre (between the short arrows). The anterior end of the fibre (left short arrow) is partly obscured by a second dye-positive detached cell (long arrow).

the mammalian MTJ may have evolved to withstand the rigours of life on land. A similarly severe loss of the mechanical function might occur in the merosin (laminin- α 2) deficient congenital muscular dystrophies²⁷, a group of very severe early muscle disorders, raising the possibility that such diseases might involve MTJ defects in human muscle.

Within some mammalian muscles, dystrophin is also enriched at specialised myomuscular junctions (MMJs) that also transmit force between the ends of muscle fibres²⁸. These occur as either intrafascicular fibre terminations, connecting single fibres into networks both end-to-end and end-to-side²⁹, or as fibrous sheets called tendinous intersections that separate segmented blocks of non-overlapping fibres. These, in particular, bear a striking structural resemblance to the dystrophin-dependent attachments between somites in zebrafish^{29,30}. If MMJ failure was a significant factor in mammalian muscle disease, their differential utilisation might contribute to the observed variations in pathology between individual muscles affected in muscular dystrophies, and between humans and the different dystrophic animal models.

As well as accurately representing the progressive nature of DMD, *sap* closely resembles known Duchenne-causing nonsense mutations in the N-terminal, making *sap* a new model of the disease and raising the possibility that muscle attachment failure contributes to the pathology of either Duchenne or other muscular dystrophies. The known localisation of the DAPC to this site is consistent with this, but it seems possible that such pathology might so far have been overlooked, as muscle biopsies are often deliberately taken from sites at a distance from the tendon in order to simplify histological examinations. It remains to be seen to what extent this novel requirement for the DAPC in the stability of muscle attachments might contribute to human muscle diseases, but it might be prudent to re-examine these structures, especially myomuscular junctions.

Future research directions for zebrafish models of muscular dystrophy

The discoveries outlined here provided us with the tantalising possibility of applying the sophisticated embryological and genetic methodologies afforded in zebrafish to the study of the human dystrophic conditions. In particular, applying second site enhancer and suppressor screens to identify genes that may act to modulate the dystrophic condition is a particularly promising research direction. Furthermore, the molecular defects present within the remainder of the class of "dystrophic" mutants has yet to be elucidated, and it remains likely that these may represent potentially novel genes that may also be mutated in human muscular dystrophies.

References

- Blagden, CS, Currie, PD, Ingham, PW, Hughes, SM. Notochord induction of zebrafish slow muscle mediated by Sonic hedgehog. *Genes Dev.* 1997; **11**: 2163–2175.
- Brennan, C, Amacher, SL and Currie, PD. Pattern formation in zebrafish. Aspects of organogenesis: Somitogenesis. *Res. Probl. Cell Differ.* 2002; **40**: 271–297.
- Granato M., van Eeden FJ., Schach U, Trowe T, Brand M, Furutani-Seiki M, Haffter P, Hammerschmidt M, Heisenberg CP, Jiang YJ, Kane DA, Kelsh RN, Mullins MC, Odenthal J, Nusslein-Volhard C. Genes controlling and mediating locomotion behavior of the zebrafish embryo and larva. *Development* 1996; **123**: 399–413.
- Bassett, D.I., Bryson-Richardson, R.J., Daggett, D.F., Gautier, P., Keenan, DG. and Currie, PD. Dystrophin is required for the formation of stable muscle attachments in the zebrafish embryo. *Development* 2003; **130**: 5851–5860.
- Blake, DJ., Weir, A., Newey, SE. and Davies, KE. Function and genetics of dystrophin and dystrophin-related proteins in muscle. *Physiol. Rev.* 2002; **82**: 291–329.
- Spence H.J., Chen Y.J, Winder, SJ. Muscular dystrophies, the cytoskeleton and cell adhesion. *BioEssays* 2002; **24**: 542–552.
- Ehmsen J, Poon E, Davies K. The dystrophin-associated protein complex. *J. Cell Sci.* 2002; **115**: 2801–3.
- Finsterer J, Stollberger C. The heart in human dystrophinopathies. *Cardiology* 2003; **99**: 1–19.
- Mokri B, and Engel AG. Duchenne dystrophy: electron microscopic findings pointing to a basic or early abnormality in the plasma membrane of the muscle fiber. *Neurology* 1975; **25**: 1111–1120.
- Straub V, Rafael JA, Chamberlain JS, and Campbell KP. Animal models for muscular dystrophy show different patterns of sarcolemmal disruption. *J. Cell Biol.* 1997; **139**: 375–385.
- Durbeej M, Cohn RD, Hrstka RF, Moore SA, Allamand V, Davidson BL, Williamson RA and Campbell KP. Disruption of the beta-sarcoglycan gene reveals pathogenetic complexity of limb-girdle muscular dystrophy type 2E. *Mol. Cell* 2000; **5**: 141–151
- Ettinger AJ, Feng G, Sanes JR. Epsilon-Sarcoglycan, a broadly expressed homologue of the gene mutated in limb-girdle muscular dystrophy 2D. *J. Biol. Chem.* 1997; **272**: 32534–32538.
- Nigro V, de Sa M, Piluso G, Vainzof M, Belsito A, Politano L, Puca AA, Passos-Bueno MR Zatz M. Autosomal recessive limb-girdle muscular dystrophy, LGMD2F, is caused by a mutation in the delta-sarcoglycan gene. *Nat. Genet.* 1996; **14**: 195–198.
- Cote PD, Moukhles H, Carbonetto S. Dystroglycan is not required for localization of dystrophin, syntrophin, and neuronal nitric-oxide synthase at the sarcolemma but regulates integrin alpha 7B expression and caveolin-3 distribution. *J. Biol. Chem.* 2002; **277**: 4672–4679.
- Cohn RD, Campbell KP. Molecular basis of muscular dystrophies. *Muscle Nerve* 2000; **23**:1456–71.

16. Law DJ, Tidball, JG. Dystrophin deficiency is associated with myotendinous junction defects in pre-necrotic and fully regenerated skeletal muscle. *Am. J. Pathol.* 1993; **142**: 1513–1523.
17. Law DJ, Caputo A, Tidball, JG. Site and mechanics of failure in normal and dystrophin-deficient skeletal muscle. *Muscle Nerve* 1995; **18**: 216–223.
18. Law DJ, Allen DL, Tidball JG. Talin, vinculin and DRP (utrophin) concentrations are increased at mdx myotendinous junctions following onset of necrosis. *J. Cell Sci.* 1994; **107**: 1477–1483.
19. Ridge JC, Tidball JG, Ahl K, Law DJ, Rickoll WL. Modifications in myotendinous junction surface morphology in dystrophin-deficient mouse muscle. *Exp. Mol. Pathol.* 1994; **61**: 58–68.
20. Tidball JG, Law DJ. Dystrophin is required for normal thin filament membrane associations at myotendinous junctions. *Am. J. Pathol.* 1991; **138**: 17–21.
21. Deconinck AE, Rafael JA, Skinner JA, Brown SC, Potter AC, Metzinger L, Watt DJ, Dickson JG, Tinsley JM and Davies KE. Utrophin–dystrophin-deficient mice as a model for Duchenne muscular dystrophy. *Cell* 1997; **90**: 717–727.
22. Deconinck N, Rafael JA, Beckers-Bleukx G, Kahn D, Deconinck AE, Davies KE, Gillis JM. Consequences of the combined deficiency in dystrophin and utrophin on the mechanical properties and myosin composition of some limb and respiratory muscles of the mouse. *Neuromusc. Disord.* 1998; **8**: 362–370.
23. Grady RM, Teng H, Nichol MC, Cunningham JC, Wilkinson RS, Sanes JR. Skeletal and cardiac myopathies in mice lacking utrophin and dystrophin: a model for Duchenne muscular dystrophy. *Cell* 1998; **90**: 729–738.
24. Cote PD, Moukhles H, Lindenbaum M., Carbonetto S. Chimaeric mice deficient in dystroglycans develop muscular dystrophy and have disrupted myoneural synapses. *Nat. Genet.* 1999; **23**: 338–342.
25. Desaki J. Scanning electron microscopical study of skeletal muscle fiber ends in normal and dystrophic mice. *Arch. Histol. Cytol.* 1992; **55**: 449–452.
26. Waterman RE. Development of the lateral musculature in the teleost, *Brachydanio rerio*: a fine structural study. *Am. J. Anat.* 1969; **125**: 457–493.
27. Tubridy N, Fontaine B, Eymard B. Congenital myopathies and congenital muscular dystrophies. *Curr. Opin. Neurol.* 2001; **14**: 575–582.
28. Paul AC, Sheard PW, Kaufman SJ, Duxson MJ. Localization of alpha7 integrins and dystrophin suggests potential for both lateral and longitudinal transmission of tension in large mammalian muscles. *Cell Tissue Res.* 2002; **308**: 255–265.
29. Snobl D, Binaghi LE, Zenker W. Microarchitecture and innervation of the human latissimus dorsi muscle. *J. Reconstr. Microsurg.* 1998; **14**: 171–177.
30. Hijikata T, Ishikawa H. Functional morphology of serially linked skeletal muscle fibers. *Acta Anat. (Basel)* 1997; **159**: 99–107.

Received 28 October 2003, in revised form 11 March 2004.

Accepted 24 March 2004

©P.D. Currie 2004.

Author for correspondence:

Assoc. Prof. P.D. Currie

Victor Chang Cardiac Research Institute,

384 Victoria St.,

Darlinghurst

NSW 2010, Australia

Phone: +61 2 9295 8536

Fax: +61 2 9295 8537

Email: p.currie@victorchang.unsw.edu.au

Popping sarcomere hypothesis explains stretch induced muscle damage

David L. Morgan & Uwe Proske

*Departments of Electrical Engineering and Physiology,
Monash University,
Clayton, Vic. 3800, Australia*

Summary

1. Exercise that involves stretching a muscle while active cause microscopic areas of damage, delayed onset muscle soreness, and adaptation to withstand subsequent similar exercise.

2. Longer muscle lengths are associated with greater damage, and recent animal experiments show that it is the length relative to optimum that determines the damage.

3. In humans walking down stairs, taking two at a time increases the length of the muscle during the lengthening and increases the delayed onset muscle soreness.

4. The observed pattern of damage is consistent with explanations based on sarcomere length instabilities

5. The pattern of adaptation is consistent with the number of sarcomeres in series in a muscle being modulated by exercise, especially the range of muscle lengths over which eccentric exercise regularly occurs.

Muscle stretch

When muscle is stretched during active tension generation, the event is commonly, though not intuitively, described as an eccentric contraction. Other terms include pliometric contraction, or active stretch. The muscle is being forcibly lengthened while trying to shorten. Energetically the muscle is absorbing work, not performing it. In common terms, the muscle is being used as a brake, not a motor.

Eccentric contraction is an important function of muscle, occurring during activities ranging from lowering a load to walking down hill. It is present in many forms of exercise, such as running, particularly when down hill is included, horse-riding and skiing, where the action could be better described as shock absorbing rather than braking. Eccentric contractions seldom occur in cycling, rowing or swimming.

Stretch induced muscle damage.

It is a long standing observation that "unaccustomed" eccentric exercise can lead to stiff and tender muscles next day, known as Delayed Onset Muscle Soreness, or DOMS¹. It has become apparent in recent years that "unaccustomed" can mean at unaccustomed length, as well as involving an unaccustomed number of repetitions or unaccustomed forces^{2,3}. This is a key observation that will be reinforced later. DOMS is accompanied by microscopic muscle damage, with multiple areas of damage scattered throughout the muscle, but each confined to a single fibre⁴. The maximum force is also reduced, the dependence of

force on stimulation rate is changed⁵, and the optimum length is immediately shifted to longer lengths⁶. In some experiments, usually in frog fibres, the tension at long length has been shown to increase, making the changes in activation unable to fully account for the shift in optimum length⁶.

Perhaps most importantly, eccentric exercise produces a rapid adaptation, so that a second similar bout of exercise produces substantially less soreness and injury⁷.

Popping sarcomere hypothesis

The popping sarcomere hypothesis⁸ states that stretch induced muscle damage results from very non-uniform lengthening of sarcomeres when active muscle is stretched beyond optimum length. If sarcomeres are beyond optimum length, then the longest sarcomeres will be the weakest, and so will be stretched more rapidly than the others, and so become weaker, until rising passive tension compensates for falling active tension. For at least some muscles, this corresponds to lengths beyond filament overlap. (The situation in other muscles is unclear, depending on the origins of the resting tension.) As the weakest sarcomeres are not at the same point along each myofibril, this non-uniform lengthening leads to shearing of myofibrils, exposing membranes, especially t-tubules, to large deformations. This is thought to lead to loss of calcium ion homeostasis, and hence damage, either through tearing of membranes or opening of stretch activated channels⁹. It is postulated⁸ that the adaptation to eccentric exercise consists of increasing the number of sarcomeres in series, so that a given muscle length corresponds to a shorter sarcomere length. In particular, the adapted muscle confines eccentric activity to muscle lengths less than optimum.

Optimum length

For a simple muscle where all fibres have the same number of sarcomeres in series, the optimum length for tension generation during maximal activation will be given by the length of tendons, plus the product of the number of sarcomeres in series and the optimum length of a sarcomere. For a muscle containing fibres with a range of the number of sarcomeres in series, the above relation will approximately hold if the number of sarcomeres in series is replaced with the average number of sarcomeres in series. As the optimum length of a sarcomere is fixed, and tendons are slow to remodel, shifts in the optimum length with exercise that occur within a few days can be confidently assigned to changes in the number of sarcomeres in series.

In the popping sarcomere hypothesis, the optimum

muscle length takes on three very important roles. In the first, optimum length becomes a prime determinant of the susceptibility; damage is predicted to occur only when sarcomeres are used beyond optimum length. In the second, the immediate shift in optimum length after eccentric exercise is a measure of damage, which is largely specific to eccentric exercise damage, and independent of fatigue or damage that involves fibres ceasing to contract, both of which contribute to force drop. Here it is proposed that the immediate shift indicates the number of overstretched sarcomeres, an early stage in the process leading to DOMS. Experimentally, the shift in optimum is closely correlated with the fall in tension, but typically shows less scatter². In its third role, the position of the optimum is a measure of adaptation. A muscle is expected to be protected from injury if the optimum length is near to or beyond the maximum length at which the muscle undergoes eccentric contraction.

The importance of long length in determining damage has been clearly demonstrated in frog sartorius muscles, rat vastus intermedius, and cat gastrocnemius. Furthermore it has been shown that damage to an individual motor unit within a muscle undergoing eccentric exercise depends on that motor unit's optimum length¹⁰.

Walking down stairs two at a time

A recent unpublished experiment from our laboratories also showed a dependence of damage on length for human knee extensor muscles. When we walk down stairs, the knee extensors of the supporting leg undergo an eccentric contraction as they support the body as it is lowered to place the extended leg on to the next step. This does not normally cause muscle soreness, as it is an everyday exercise. Descending the same distance two steps at a time causes the muscles to undergo eccentric contractions at an unaccustomed longer length, while still generating the same forces and absorbing the same amount of energy.

Twenty one students walked down ten flights of 24 stairs with instructions to land on their heels rather than their toes. For alternate flights, they stepped down one step with leg A leading, and then brought leg B alongside, so that leg B absorbed all the energy of descending one flight in 24 eccentric contractions at short length, while the knee extensors of leg A were essentially inactive. For the other flights, they stepped down two steps with leg B leading, and then brought leg A alongside, so that A was the supporting leg that underwent eccentric contraction at long length. The same amount of energy was absorbed as for the other flights, but spread over only 12 eccentric contractions extending to longer muscle length. The relations between left and right, dominant and non-dominant, and A and B were randomized.

Subjects rated soreness in their left and right quadriceps muscles twice daily for the next week on a scale of 0 to 10, representing no pain and extreme pain respectively. Most experienced only mild pain. Figure 1 shows that the mean pain rating for leg A, the support leg

during the double step, reached 2 between 24 and 48 hours, but leg B only reached 0.4. A General Linear Model of the 616 pain ratings was carried out for the following factors. The time of measurement was tested as a discrete variable, due to the rise and fall of pain with time, and reached $p < 0.0001$. The time course is shown in Figure 1. The comparison between the A and B legs, that is whether the leg had been supporting the body during single or double stepping had $p < 0.0001$, with the leg that was stretched to longer lengths showing more pain. The length of the subjects' legs, measured as the height of the iliac crest above the floor was significant as a linear factor with $p < 0.003$, with taller people experiencing less pain, presumably because the fixed step requires smaller angles of flexion for taller people. Subjects also graded their regular participation in eccentric and concentric exercise on a five point scale. From these, an exercise factor was calculated as the difference between the index of participation in eccentrically biased exercise and the index for concentrically biased exercise. This showed $p = 0.0001$, with high scores showing less damage. Gender had $p < 0.0001$ when leg length was removed as a factor, but this became $p < 0.02$ when leg length was included, suggestion that gender primarily acted through height. Weight was not a significant continuous factor. Measurements of optimum length were not made.

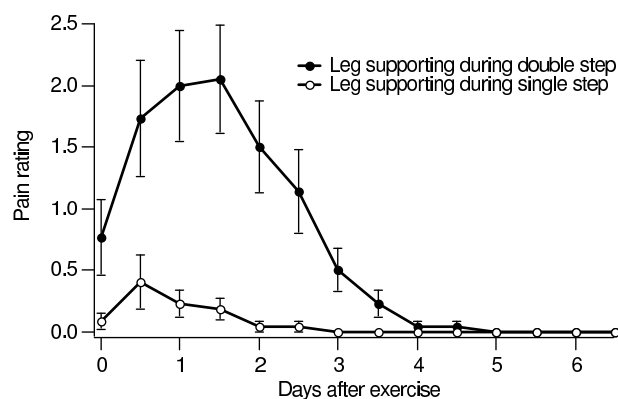


Figure 1. Mean with SEM of pain ratings of knee extensor muscles after walking down stairs supported by one leg for five flights taken one step at a time, and the other leg for five flights taken two steps at a time. The larger steps stretched the muscles to longer lengths and produced more soreness.

These results are all in accord with the hypothesis that damage only occurs when muscle is actively stretched beyond its optimum length, and that muscles adjust their optimum length by adjusting the number of sarcomeres so that active stretch normally occurs only at lengths less than optimum.

Sarcomere addition as a protective mechanism

The idea that adaptation to eccentric exercise consists of adding sarcomeres in series in fibres has a number of supporting observations. It ties in closely with the observations that damage depends critically on the range of lengths of the stretch compared to optimum. It also explains why biopsy studies have been unable to show differences with adaptation, as the sarcomeres are unchanged. It is consistent with previous observations that the number of sarcomeres in series is capable of relatively rapid change¹¹, though the mechanisms are yet to be fully elucidated. It also gives a reason for the reversal of training. Extra sarcomeres in series increase the energy consumption for isometric force development. This provides an incentive to shed un-needed sarcomeres in the interests of efficiency of tension generation. Extensive exercise involving only concentric contractions would be expected to increase this, supporting the anecdotal observation that "couch potatoes" are less prone to eccentric exercise damage to knee extensors than regular cyclists. In this view, the number of sarcomeres is continuously modulated up or down to maximise efficiency while avoiding damage during "normal" activity. Investigating the mechanisms of the adaptation is beyond our expertise.

Evidence for sarcomere number modulation

Direct evidence for sarcomere number modulation has come from rat vastus intermedius muscles, the postural knee extensors¹². Rats were trained by running on an climbing or descending treadmill for about 20 mins per day for five days, in a protocol that had been previously shown to cause damage to these muscle in the descending group but not the climbing group¹³. The muscles were fixed and then digested in acid. Intact fibres were identified in serial dilutions of the digested muscle, and the number of sarcomeres estimated from fibre length and sarcomere length, measured by laser diffraction. From these the number of sarcomeres in fibres was calculated. All groups had quite broad distributions of sarcomere numbers, but the means were significantly different between training groups. The descending trained animals had the largest sarcomere count, the climbing trained rats had the smallest counts, and sedentary rats had intermediate counts, though closer to the climbing group. This could be interpreted as the response to concentric exercise being either smaller or slower than the response to eccentric exercise.

In another series of experiments¹⁴, vastus intermedius muscles of treadmill trained rats were tested mechanically while still in situ, that is attached to the bones, but with all other muscles about the knee joint removed. This avoids introducing uncertainties into muscle length. In descending trained rats the knee angle for optimum torque generation corresponded to longer muscle lengths than in climbing trained rats, and the muscles of descending trained rats suffered less damage from an acute bout of eccentric contractions over the same range of knee angles.

In humans the hamstring muscles are of particular interest, because they are used relatively rarely for eccentric

contractions, and because they are subject to muscle tears, which are thought to occur during eccentric contractions in activities such as sprinting where they act as brakes on the forward swing of the leg, particularly the lower leg. They are also a convenient muscle to use experimentally, as passive tension about the knee is small over most of the anatomical range. The optimum knee angle for torque generation can be reliably measured by isokinetic dynamometry, where an angle torque curve is measured during maximum voluntary contraction with constant velocity shortening. Doing a number of cycles and averaging improves the reliability.

Using this measure before and after a series of eccentric exercises produced a significant shift of about 7° in optimum knee angle for torque generation¹⁵. The exercise was a series of "hamstring lowers", where the subject knelt on a pad with ankles restrained and hips straight, and leaned slowly forward from the knees as far as possible before collapsing. This led to muscle soreness in the hamstring group. Some subjects repeated the exercise ten days later, and suffered much less soreness. Again eccentric exercise, DOMS, increased optimum length and adaptation all occurred together.

A less well investigated consequence of the hypothesis is that the unloaded shortening velocity should increase with eccentric training, as the unloaded shortening velocity of a fibre is the sum of the velocities of the sarcomeres. Some indications of this have been reported¹⁶, though the long time course makes it difficult to rule out fibre type change as an alternative explanation.

It has been noted in tetanically stimulated animal muscles with multiple fibre types that the damaged fibres are largely fast twitch fibres¹⁷. In sub-maximal voluntary activity the opposite is true¹³, presumably because the fast twitch fibres are not likely to be activated. Hence the fast fibres can be seen as being susceptible in tetanic contractions because they are not recruited, and hence not trained, during normal submaximal activity. If training consists of increasing the number of sarcomeres, then slow motor units should have longer optima than fast units, or more precisely, the most susceptible units should have the shortest optima and be fast type. This was tested for cat gastrocnemius motor units¹⁰. It was found that all motor units with optimum length less than the whole muscle optimum had a time to peak twitch of less than 50msec, that is all slow motor units had long optima. Interestingly, a small number of fast twitch units had long optimum lengths, suggesting that they have adapted to, and hence were subject to, regular eccentric exercise. However as the experimental observation was that all damaged fibres were fast, not all fast fibres were damaged, the existence of units that are both fast and well adapted is not inconsistent.

Different optimum lengths may be due to different tendon lengths as well as different numbers of sarcomeres. Where a relatively rapid (hours to days) shift of optimum is shown, it is more likely that sarcomeres are involved than tendon. This is less clear with experiments such as the above comparison of motor units, where the adaptation has taken place over a lifetime, so that tendon adaptations

cannot be ruled out. However, the basic hypothesis that muscle adapts optimum length to avoid eccentric contractions beyond optimum is not affected by this complication.

Are other mechanisms involved?

It is possible that adaptation of optimum length does occur, but that other adaptation mechanisms are also important. This was tested by training more rats as described above, either climbing or descending. All animals were then anaesthetised, and the vastus intermedius subjected to a series of 20 eccentric contractions. All stretches had an amplitude of 27° of knee angle, but beginning at different knee angles. In some animals stretch began at the measured optimum angle, while in others it began from 90° of knee angle³. One way of analysing these data is shown in Figure 2. Damage has been quantified by the immediate shift in optimum angle, but the tension decrease shows similar results. When the damage is plotted against the absolute knee angle from which the eccentric contractions began, the climbing and descending trained muscles clearly fall on two distinct lines, confirming both the existence of a training effect and the dependence of damage on muscle length. When the same damage data are plotted against the angle relative to optimum from which the acute eccentric contractions began, the two groups fall on the same line. Damage still depends on sarcomere length, but not independently on training. Statistical analysis of the data confirmed these conclusions. If training group (discrete) and absolute knee angle (continuous) were used as factors in a General Linear Model, group was highly significant. If absolute knee angle was replaced by relative knee angle, group was no longer significant. This indicated that effect of training attributable to mechanisms other than the shift in optimum length was not statistically significant.

These ideas and observations have been useful in directing current research into eccentric exercise, such as examination of the role of transverse tubules⁹ and in muscle injury prevention¹⁸.

Summary

There is now an extensive body of evidence that damage from eccentric exercise is strongly dependent on the sarcomere lengths over which the stretching occurs. Adaptation in a number of preparations has been shown to be accompanied by a shift in optimum length, and the shift has been shown to account for the major portion of the adaptation. All of this provides evidence that damage occurs when sarcomeres are beyond optimum, the central prediction of the popping sarcomere hypothesis. This is true whether the stretch progresses to damage by tearing of structures or by opening of stretch activated channels.

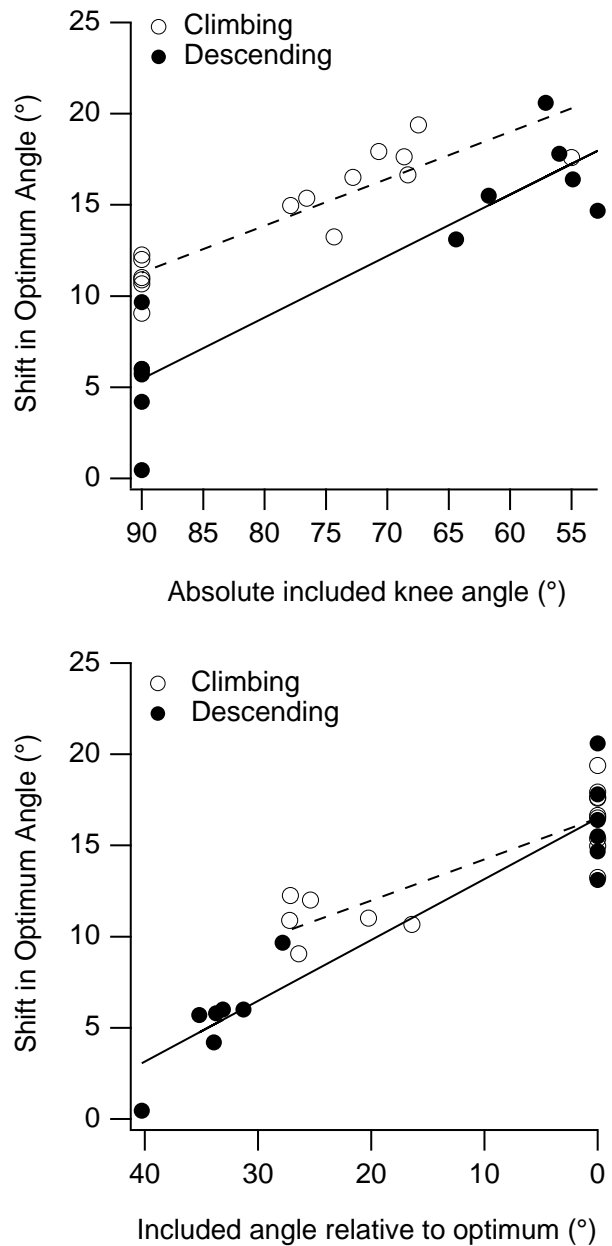


Figure 2. The shift in optimum angle after acute eccentric contractions from various initial lengths, in climbing and descending trained rats. In the upper panel, data are plotted against the absolute knee angle from which stretches began. The muscles stretched from 90° are on the left, and those stretched from optimum length were generally longer and more damaged. Most importantly, the climbing and descending animals are clearly separated. In the lower panel the same data are plotted against angle relative to optimum. In this case the muscles stretched from optimum all appear at zero, and those stretched from 90° are generally stretched from less than optimum and damaged less. In this case, the climbing and descending trained animals are not separated.

Acknowledgements

The authors wish to acknowledge the support of the NH&MRC, and the co-operation of the 2003 Biomechanics class in the stairs experiment.

References

1. Hough T. Ergographic studies in muscular soreness. *Am. J. Physiol.* 1902;**7**:76-92.
2. Talbot JA, Morgan DL. The effects of stretch parameters on eccentric exercise induced damage to toad skeletal muscle. *J. Musc. Res. Cell. Mot.* 1998;**19**:237-245.
3. Morgan DL, Talbot JA. The Addition of Sarcomeres in Series is the Main Protective Mechanism Following Eccentric Exercise. *J. Mech. Med. Biol.* 2002;**2**(3 & 4):421-431.
4. Ebbeling CB, Clarkson PM. Exercise-induced muscle damage and adaptation. *Sports Med* 1989;**7**:207-234.
5. Edwards RHT, Hill DK, Jones DA, Merton PA. Fatigue of long duration in human skeletal muscle after exercise. *J. Physiol. (Lond.)* 1977;**272**:769-778.
6. Morgan DL, Claffin DR, Julian FJ. The effects of repeated active stretches on tension generation and myoplasmic calcium in frog single fibres. *J. Physiol. (Lond.)* 1996;**497**(3):665-674.
7. Newham DJ, Jones DA, Clarkson PM. Repeated high-force eccentric exercise: effects on muscle pain and damage. *J. Appl. Physiol.* 1987;**63**(4):1381-1386.
8. Morgan DL. New insights into the behavior of muscle during active lengthening. *Biophys. J.* 1990;**57**(Feb):209-221.
9. Yeung EW, Balnave CD, Ballard HJ, Bourreau J-P, Allen DG. Development of T-tubular vacuoles in eccentrically damaged mouse muscle fibres. *J. Physiol. (Lond.)* 2002;**540**(2):581-592.
10. Brockett C, Morgan DL, Gregory JE, Proske U. Damage to different motor units from active lengthening of the medial gastrocnemius muscle of the cat. *J. Appl. Physiol.* 2002;**92**:1104-1110.
11. Goldspink G. Malleability of the motor system: a comparative approach. *J. Exp. Biol.* 1985;**115**:375-391.
12. Lynn R, Morgan DL. Decline running produces more sarcomeres in rat vastus intermedius muscle fibres than incline running. *J. Appl. Physiol.* 1994;**77**(5):1439-1444.
13. Armstrong RB, Ogilvie RW, Schwane JA. Eccentric exercise induced injury to rat skeletal muscle. *J. Appl. Physiol.* 1983;**54**(1):80-93.
14. Lynn R, Talbot JA, Morgan DL. Differences in rat skeletal muscles after incline and decline running. *J. Appl. Physiol.* 1998;**85**(1):98-104.
15. Brockett C, Morgan DL, Proske U. Human hamstring muscles adapt to damage from eccentric exercise by changing optimum lengths. *Med. Sci. Sports Exercise* 2001;**33**(5):783-790.
16. Fridén J, Seger J, Sjöström M, Ekblom B. Adaptive response in human skeletal muscle subjected to prolonged eccentric training. *Int. J. Sports Med.* 1983;**4**:177-183.
17. Lieber RL, Fridén J. Selective damage of fast glycolytic fibres with eccentric contraction of the rabbit tibialis anterior. *Acta Physiol. Scand.* 1988;**133**:587-588.
18. Brockett C, Morgan DL, Proske U. Predicting hamstring strain injury in elite athletes. *Med. Sci. Sports Exercise* 2004;**36**(3):379-387.

Received 16 January 2004, in revised form 4 May 2004.
Accepted 5 May 2004.
©D.L. Morgan 2004.

Author for correspondence:
Prof. David L. Morgan
Department of Electrical Engineering
Monash University,
Clayton, Vic. 3800, Australia

Tel: +61 3 9905 3483
Fax: +61 3 9905 1820
Email: david.morgan@ieee.org

Identifying athletes at risk of hamstring strains and how to protect them

U. Proske, D.L. Morgan*, C.L. Brockett & P. Percival*

*Department of Physiology
and*

**Department of Electrical and Computer Systems Engineering,
Monash University,
Clayton VIC 3800,
Australia*

Summary

1. One common soft-tissue injury in sports involving sprinting and kicking a ball is the hamstring strain. Strain injuries often occur while the contracting muscle is lengthened, an eccentric contraction. We have proposed that the microscopic damage to muscle fibres which routinely occurs after a period of unaccustomed eccentric exercise, can lead to a more severe strain injury.

2. An indicator of susceptibility for the damage from eccentric exercise is the optimum angle for torque. When this is at a short muscle length, the muscle is more prone to eccentric damage. It is known that subjects most at risk of a hamstring strain have a previous history of hamstring strains. By means of isokinetic dynamometry, we have measured the optimum angle for torque for 9 athletes with a history of unilateral hamstring strains. We also measured optimum angles for 18 athletes with no previous history of strain injuries. It was found that mean optimum angle in the previously injured muscles was at a significantly shorter length than for the uninjured muscles of the other leg and for muscles of both legs in the uninjured group. This result suggested that previously injured muscles were more prone to eccentric damage and therefore, according to our hypothesis, more prone to strain injuries than uninjured muscles.

3. After a period of unaccustomed eccentric exercise, if the exercise is repeated a week later, there is much less evidence of damage because the muscle has undergone an adaptation process which protects it against further damage. We propose that for athletes considered at risk of a hamstring strain, as indicated by the optimum angle for torque, a regular program of mild eccentric exercise should be carried out. This approach seems to work since evidence from one group of athletes, who have implemented such a program, shows a significant reduction in the incidence of hamstring strains.

Introduction

Hamstring strains are a common soft-tissue injury in sports such as Australian football and track and field events, including sprinting and hurdling. The Australian Football League (AFL) has the hamstring strain at the top of its injury list with 16% of all injuries attributed to it. Worse still, the re-injury rate for players who have at some time incurred a hamstring strain currently lies at 34%.¹ These

figures indicate that current preventative strategies for this kind of injury remain inadequate.

Epidemiological evidence suggests that hamstring strains are associated with eccentric contractions, where the contracting muscle is lengthened.^{2,3} Hamstrings undergo eccentric contractions during sprinting, kicking the ball and picking up the ball. Indeed, it is regularly observed that during these activities, players incur hamstring strains. This fact has led us to propose a new approach to hamstring strains, indeed, to all muscle strains, based on recent research.

We have been studying the mechanical changes in a muscle subjected to a series of eccentric contractions. Eccentric exercise is the only form of exercise which is routinely accompanied by muscle damage. For a review of the topic see Proske and Morgan.⁴ Here we have gone one step further and proposed that under certain conditions, the microscopic damage at the level of muscle fibres from eccentric contractions may, at times, progress to a more major strain injury.

Muscle damage from eccentric exercise

Eccentric exercise, in someone unaccustomed to it, produces stiffness and soreness next day. This is because the exercise has led to muscle damage which, in turn, leads to sensitisation of nociceptors.⁵ Why eccentric exercise produces muscle damage can be explained in terms of a theory based on sarcomere dynamics.⁶ This proposes that the descending limb of the length-tension curve for skeletal muscle is a region of instability. When a sarcomere, which is weaker than its neighbours, lengthens on the descending limb, it becomes progressively weaker. In addition, when the yield point of the force-velocity relation is reached, lengthening is rapid and uncontrolled, without the development of additional force. The rapid lengthening will only stop when tension in passive structures associated with the sarcomere has risen sufficiently to balance the tension being generated in adjacent still-functioning sarcomeres. Then the next weakest sarcomere begins to lengthen uncontrollably. This process continues for the duration of the applied lengthening during the eccentric contraction.

Once a sarcomere has been stretched to the point of no overlap, when the muscle relaxes, the sarcomere risks becoming disrupted, that is, the myosin and actin filaments no longer interdigitate properly.⁷ A non-functioning, disrupted sarcomere represents a point of weakness in the muscle. During repeated eccentric contractions the area of

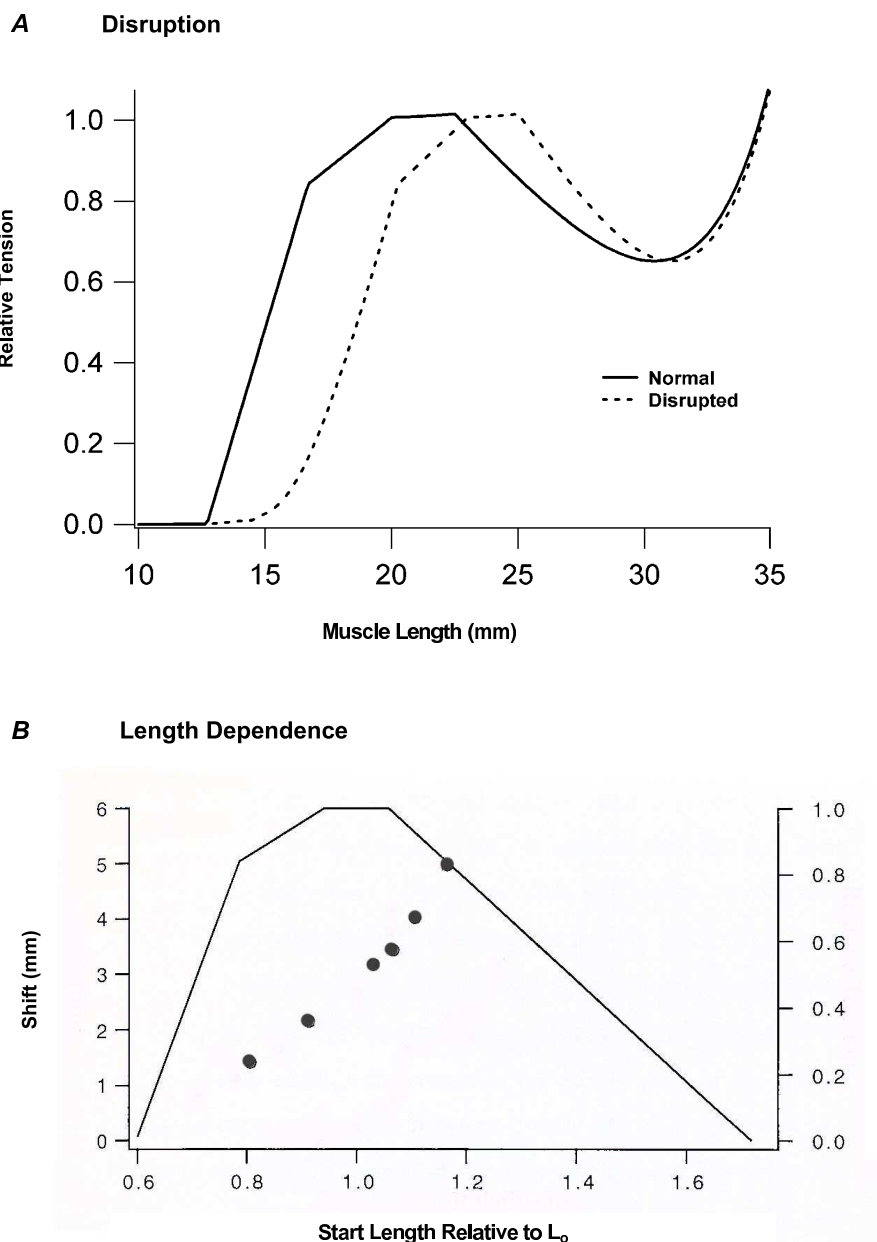


Figure 1. A: Changes in sarcomere length-tension relation following a series of eccentric contractions. A computer-simulated curve of total sarcomere tension has been represented, based on the active length-tension relation¹¹ to which the estimated, exponentially rising passive tension has been added. Tension has been normalized relative to the maximum active tension. Length is of a fibre postulated to comprise 10,000 sarcomeres with a sarcomere length of 2.5 μm at optimum length. The control curve (solid line) is on the left. After a series of eccentric contractions, 10% of sarcomeres have their tension output set to zero to simulate disruption. That shifts the length-tension relation in the direction of longer lengths by 3 mm, as shown by the dashed curve on the right. Redrawn from Proske and Morgan.⁴

B: Dependence of the shift in length-tension relation on the starting length. The filled circles represent the data from each of 6 toad sartorius muscles subjected to 20 eccentric contractions. These were active stretches of 3 mm (10% L_0) at 3 muscle lengths s^{-1} . They were applied at progressively longer lengths, the first at a starting length of 0.8 L_0 , the last at 1.2 L_0 . At longer starting lengths, the resultant shifts in optimum were larger. To provide an indication of where on the sarcomere length-tension relation these shifts lay, a superimposed active sarcomere length tension curve has been shown (from Gordon et al.¹¹) Figure redrawn from Talbot.¹²

disruption is likely to grow and a point is reached where membranes are torn and the muscle fibre begins to contract uncontrollably, leading to a rise in whole-muscle passive tension.⁸ Ultimately some of these fibres are likely to die.⁴

Signs of damage

Evidence for the presence of disrupted sarcomeres in series with still functioning sarcomeres is provided by a

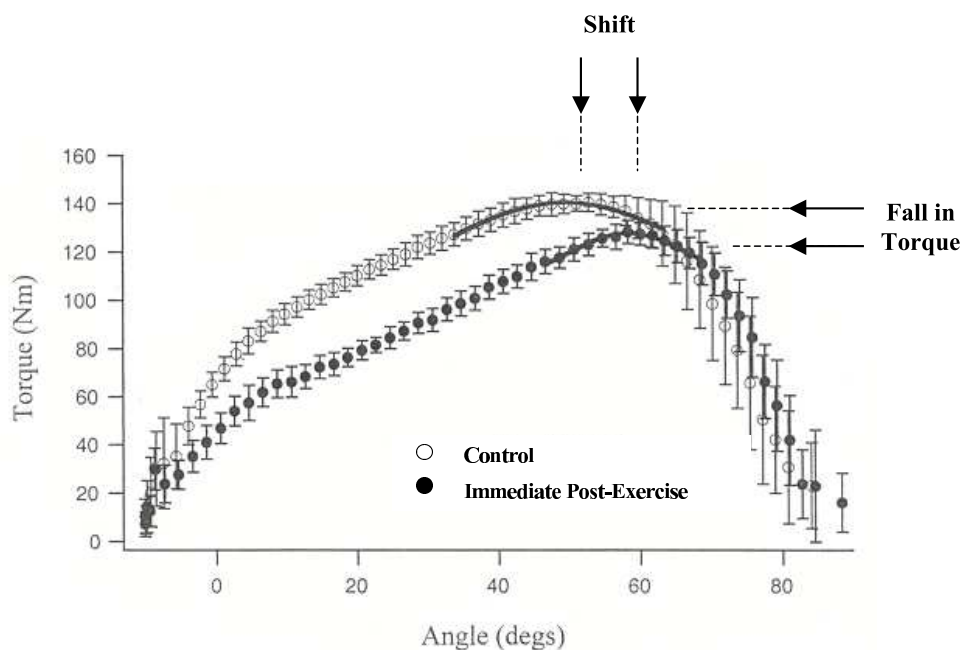


Figure. 2. Torque-angle curves for human hamstring muscles, before and after a series of eccentric contractions. Torque and angle values were obtained from a series of maximal knee extensions carried out on an isokinetic dynamometer. Gaussian curves were fitted by computer to the top 10% of the digitised and averaged values (continuous lines). These gave values for peak torque and optimum angle. Open circles (\pm S.E.M.), data acquired immediately before the exercise (Control), filled circles (\pm S.E.M.), immediately after the exercise (Immediate Post-Exercise). The exercise consisted of a series of controlled forward falls, using hamstrings to brake the fall. Figure redrawn from Brockett et al.¹³ Downwards directed arrows indicate the shift in optimum angle (7.2°). Horizontal arrows show the drop in torque (12.6 N).

shift in the muscle's length-tension relation in the direction of longer muscle lengths.^{9,10} This can be modelled by means of a sarcomere length-tension curve based on Gordon, Huxley and Julian.¹¹ A disruption of 10% of 10,000 sarcomeres, each with a length of 2.5 μ m at optimum, produces, in a muscle 25 mm long, a shift of 3 mm, in the direction of longer lengths (Fig. 1A).

Since the instability of sarcomeres is present only on the descending limb of the length tension curve, the single, most important determinant of the amount of damage and disruption from eccentric contractions is the length range over which the muscle is stretched. For amphibian muscle, the size of the shift in optimum length is directly dependent on the starting length for the stretch. The shift is small (1 – 2 mm) when the starting length is below the optimum. It increases steeply up to 5 mm when it exceeds the optimum (Fig. 1B).¹²

There has been much debate over the reliability of the various damage indicators after eccentric exercise. In our view the drop in force is not as reliable an indicator as a shift in optimum length. This is because during repeated eccentric contractions, as occurs in most sports, the force drop may be confounded by fatigue effects. The shift in optimum is present immediately after the exercise, not delayed like soreness, and the size of the shift is a direct indication of the amount of damage that has occurred.⁴

Our approach to the problem of hamstring strains is

based on the proposal that damage at the level of single muscle fibres can, at times, lead to a major tear, the muscle strain.¹³ If we are right, it means that evidence for a predisposition for eccentric damage is also an indication of vulnerability for strain injury.

We have tested this proposal by, first of all, measuring torque-angle curves for hamstring muscles in untrained subjects. Curves were constructed using an isokinetic dynamometer. Subjects were asked to carry out a series of isokinetic contractions and the torque and angle signals during each contraction were digitised, sorted according to length and averaged. A computer fitted a curve to values above 90% of torque to determine the optimum angle. Subjects were then asked to carry out a series of eccentric contractions with their hamstring muscles. For this they were asked to kneel on a padded board with their feet strapped to the board at the ankle. Subjects were instructed to lower their trunk down onto the board, using their hamstrings to brake the fall. Subjects carried out a series of such 'hamstring lowers' and then a second torque-angle curve was constructed immediately afterwards.

An example of a pair of torque angle curves constructed before and after a period of eccentric exercise is shown in Figure 2. For 10 subjects tested it was found that there was a fall in optimum torque, by an average of 25% (\pm 4%), and a shift of the optimum angle of 7° (\pm 3°).¹³ This result confirmed that it was indeed possible to obtain

evidence for muscle damage in hamstrings after a series of eccentric contractions.

Previously injured athletes are more prone to injury

As mentioned earlier, more than one third of all AFL players with a previous history of hamstring strains, subsequently re-injure. If we are right in our predictions, a greater-than-normal vulnerability for eccentric damage should mean an increased likelihood for a strain injury. This leads to the prediction that previous hamstring-injured subjects should show a greater-than-normal susceptibility for eccentric damage. It was decided to test this hypothesis.

Hamstring angle-torque curves, as described previously, were measured for 9 elite athletes, 5 AFL players and 4 track and field athletes all of whom had previously incurred one or more hamstring strains in one leg, 4 weeks or more previously. At the time of testing they had all returned to full training and no one experienced any soreness during testing. Measurements made on the previously injured hamstrings were compared with hamstrings of the other, uninjured leg. In addition measurements were made on both legs of 18 AFL players, none of whom had a previous history of hamstring strains.¹⁴

The values for optimum angles revealed dramatic differences. The mean optimum angle for the previously injured hamstrings was $12.1^\circ (\pm 2.7^\circ)$ shorter than for the uninjured muscle (Fig. 3). A shorter-than-normal optimum length means that more of the muscle's working range is on the descending limb of the length-tension relation, the region of instability and damage. Interestingly, the uninjured muscles of the other leg not only had longer optima but these were not significantly different from values for both legs of the uninjured subjects. So the uninjured muscles of subjects with a history of unilateral hamstring strains show no signs of a susceptibility for damage. If, as experience shows, differences between hamstrings on the two sides are usually small, this finding suggests that at-risk subjects within a population of uninjured players may not always be identified by their optimum angles. It also suggests that for the initial injury other factors are likely to play a role.

It has previously been proposed that a measure of susceptibility for hamstring strains is the quadriceps:hamstrings torque ratio.¹⁵ Other observations suggest that this ratio is not a reliable predictor of strain injuries.¹⁶ We have calculated quadriceps:hamstrings torque ratios for the muscle of the previously injured leg, the muscle of the other, uninjured leg and for the muscles of both legs in the athletes with no history of hamstring strains. Plotting ratios for muscles of one leg against the other leg showed no significant difference for the previously injured leg (Fig. 3B).

The "repeated bout effect" from eccentric training

We have all had the experience that a period of unaccustomed exercise, biased towards eccentric exercise, like walking downhill, leaves us stiff and sore next day. However the same exercise a week later is followed by

much less stiffness and soreness. This is the "repeated bout effect".¹⁷ Following damage from the first period of exercise, the muscle adapts to prevent further damage. It has been proposed that the adaptation process involves the incorporation of additional sarcomeres, in series, in muscle fibres.⁶ It is known that such an addition of sarcomeres can occur in less than a week.¹⁸ The presence of additional sarcomeres in myofibrils means that the average sarcomere length for a given fibre length becomes less, leading to a shift in the direction of longer muscle lengths of the optimum length for force. That, in turn, makes it less likely for the muscle, within its normal working range, to be stretched onto its descending limb, the region of potential damage.

We have measured the training effect in hamstrings. In non-athletic subjects optimum angle shifted by 7° immediately after a first period of eccentric exercise (see above). By 8 days after the exercise, there remained a persistent $6^\circ (\pm 4^\circ)$ shift. Following a second period of exercise at day 8, there was a further 1° shift accompanied by a smaller-than-previous drop in force and less soreness.¹³ Our interpretation is that the shift in optimum length after the first period of eccentric exercise reverses only partially since repair of damaged muscle fibres is accompanied by incorporation of additional sarcomeres. This, in turn, means that the second period of exercise is not stretching muscle fibres quite as far as previously, so avoiding the descending limb of the length-tension curve. As a consequence there is less damage and disruption. If we are right, and a susceptibility for eccentric damage signals a vulnerability for strain injuries, the training effect is likely to be a means of providing protection against further injury.

Training with eccentric exercise reduces the incidence of hamstring strains

In order to test some of our ideas, over the last 3 years we have been collaborating with one of the AFL clubs. In cooperation with the club's fitness coordinator a new training program has been implemented for all players. Our approach is based on the proposition that the precursor event to a hamstring strain is microscopic damage in muscle fibres from eccentric exercise. It follows that if it is possible to reduce the muscle's susceptibility for eccentric damage, this will lead to a reduced incidence of strain injuries.

Pre-season training before we began our study was mainly aimed at achieving greater aerobic fitness. The new program emphasised kicking and other exercises that stretched the active hamstrings. In addition, players carried out some specific, targeted eccentric exercises. These included "straight-legged deadlifts" and carrying out "knee-curls" on a GHG (gluteus-hamstrings-gastrocnemius) machine. For players who had incurred a hamstring strain, initially a rather mild program of exercise was given and this was gradually increased as the subject recovered from the injury.

In the 2001 season, which was before we began working with the club, they had reported a total of 16

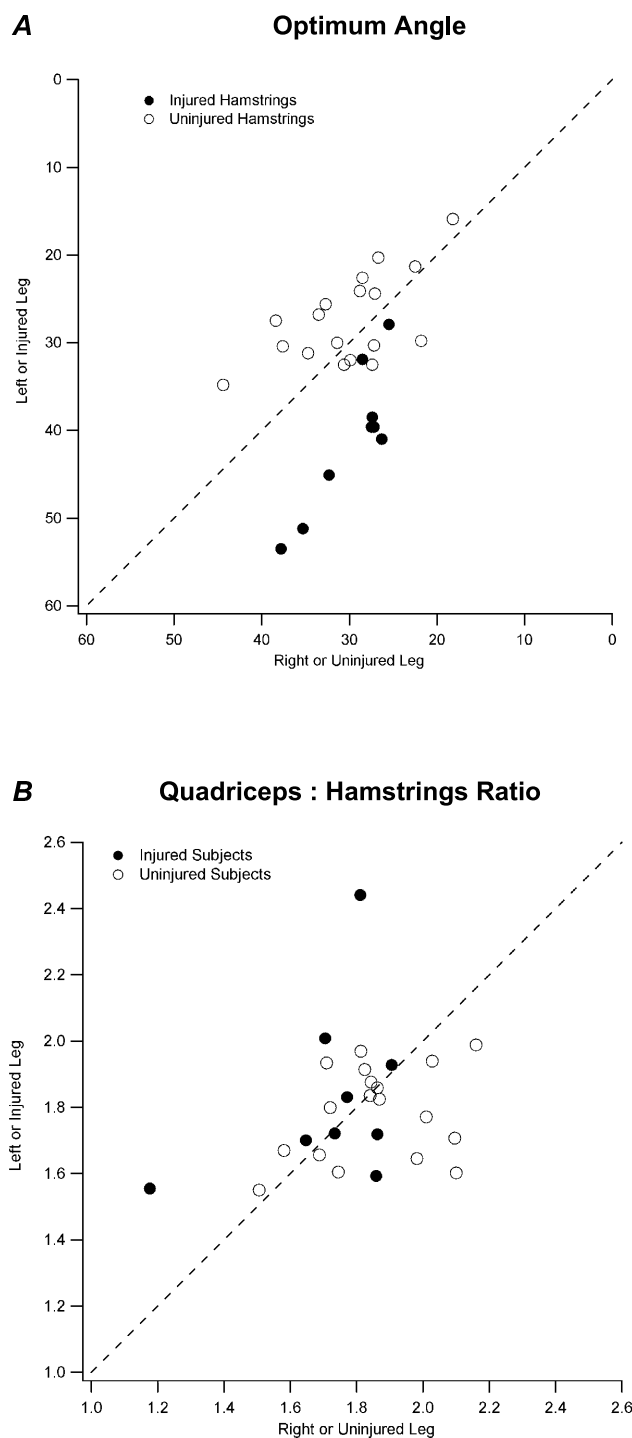


Figure 3. A: A plot of the optimum angle for torque in hamstrings for the left, or the injured leg against optimum angle for the right or the uninjured leg. Data from 9 athletes with a previous history of a unilateral hamstrings strain (filled circles) and from 18 athletes with no previous history of strain injuries (open circles). The dashed line indicates where values would lie if they were equal. Optimum angle has been expressed in degrees of knee flexion, where 0° is when the knee is fully extended and 110° when it is fully flexed. Optimum angles for the previously injured muscles were at significantly shorter muscle lengths, that is, a more flexed knee, than for muscles with no history of injury (Figure redrawn, in part, from Brockett et al.¹⁴).

B: Ratio of peak torque in quadriceps to peak torque in hamstrings. Values for athletes with a previous history of unilateral hamstring strains shown as filled circles. Values from athletes with no history of injury shown as open circles. Differences in ratios between injured and uninjured muscles were not significant.

hamstring strains amongst players. After introduction of the new training program, 5 hamstring strains were reported during the 2002 season. For the 2003 season, the club reported only 2 hamstring strains. This data remains preliminary, but is encouraging. Currently testing is continuing and other AFL clubs are beginning to participate. So we are hoping that in the future widespread implementation of a program of targetted eccentric exercise will lead to a dramatic fall in the incidence of hamstring strains.

Conclusions

The outcome of this first cooperative study has obviously delighted the AFL club. But it has also provided additional supporting evidence for our proposal of a link between the microscopic damage routinely incurred after eccentric exercise and development of a more major muscle tear. If protection against eccentric damage can be achieved with a regular program of eccentric exercise, this will be the means of preventing the occurrence of all such strain injuries. The evidence suggests that in athletes with a history of unilateral hamstring strains, the uninjured muscle is indistinguishable in its properties from muscles of athletes with no history of such injuries. It may, therefore, make it difficult, at times, to detect at risk athletes in an uninjured population. It means that all participants in sports known to be associated with the occurrence of hamstring strains should be subjected to regular eccentric exercise programs, carried out in combination with measurements of optimum angle for torque, to make sure that the exercise has led to the desired adaptive changes.

Now it remains for other AFL clubs, indeed, other sporting bodies confronted with the problem of hamstring strains, to participate in similar training programs, to help eliminate this kind of injury.

Acknowledgements

This work was supported by the National Health and Medical Research Council of Australia.

References

1. Seward H, Orchard J, Hazard H, et al. Football injuries in Australia at the elite level. *Med. J. Aust.* 1993; **159**: 298-301.
2. Garrett WE, Jr. Muscle strain injuries: clinical and basic aspects. *Med. Sci. Sports Exerc.* 1990; **22**: 436-43.
3. Kujala UM, Orava S, Jarvinen M. Hamstring injuries. Current trends in treatment and prevention. *Sports Med.* 1997; **23**: 397-404.
4. Proske U, Morgan DL. Muscle damage from eccentric exercise: mechanism, mechanical signs, adaptation and clinical applications. *J. Physiol.* 2001; **537**: 333-345.
5. Weerakkody NS, Percival P, Hickey MW, et al. Effects of local pressure and vibration on muscle pain from eccentric exercise and hypertonic saline. *Pain* 2003; **105**: 425-435.
6. Morgan DL. New insights into the behavior of muscle during active lengthening. *Biophys. J.* 1990; **57**: 209-221.
7. Talbot JA, Morgan DL. Quantitative analysis of sarcomere non-uniformities in active muscle following a stretch. *J. Muscle Res. Cell Motil.* 1996; **17**: 261-268.
8. Whitehead NP, Morgan DL, Gregory JE, et al. Rises in whole muscle passive tension of mammalian muscle after eccentric contractions at different muscle lengths. *J. Appl. Physiol.* 2003; **95**: 1224-1234.
9. Wood SA, Morgan DL, Proske U. Effects of repeated eccentric contractions on structure and mechanical properties of toad sartorius muscle. *Am. J. Physiol.* 1993; **265**: C792-800.
10. Jones C, Allen T, Talbot J, et al. Changes in the mechanical properties of human and amphibian muscle after eccentric exercise. *Eur. J. Appl. Physiol. Occup. Physiol.* 1997; **76**: 21-31.
11. Gordon AM, Huxley AF, Julian FJ. The variation in isometric tension with sarcomere length in vertebrate muscle fibres. *J. Physiol.* 1966; **184**: 170-92.
12. Talbot JA. Muscle damage and recovery Following eccentric contractions. PhD Thesis, Monash University, Melbourne, 1997.
13. Brockett CL, Morgan DL, Proske U. Human hamstring muscles adapt to eccentric exercise by changing optimum length. *Med. Sci. Sports Exerc.* 2001; **33**: 783-90.
14. Brockett CL, Morgan DL, Proske U. Predicting hamstring strain injury in elite athletes. *Med. Sci. Sports Exerc.* 2004; **36**: 379-387.
15. Orchard J, Marsden J, Lord S, et al. Preseason hamstring muscle weakness associated with hamstring muscle injury in Australian footballers. *Am. J. Sports Med.* 1997; **25**: 81-5.
16. Bennell K, Wajswelner H, Lew P, et al. Isokinetic strength testing does not predict hamstring injury in Australian Rules footballers. *Br. J. Sports Med.* 1998; **32**: 309-314.
17. McHugh MP. Recent advances in the understanding of the repeated bout effect: the protective effect against muscle damage from a single bout of eccentric exercise. *Scan. J. Med. Sci. Sports* 2003; **13**: 88-97.
18. Williams PE, Goldspink G. The effect of immobilization on the longitudinal growth of striated muscle fibres. *J. Anat.* 1973; **116**: 45-55.

Received 20 November 2003, in revised form 5 April 2004.
Accepted 6 April 2004 ©U. Proske 2004.

Author for correspondence:

Prof. U. Proske

Department of Physiology

Monash University,

Clayton VIC 3800, Australia

Tel: +61 3 9905 2526 Fax: +61 3 9905 2531

Email: uwe.proske@med.monash.edu.au

Stretch-activated channels in stretch-induced muscle damage - role in muscular dystrophy

Ella W. Yeung & David G. Allen*

*Department of Rehabilitation Sciences,
The Hong Kong Polytechnic University,
Hung Hom, Kowloon, Hong Kong
and*

**Institute for Biomedical Research and
Department of Physiology,
University of Sydney F13,
NSW 2006, Australia*

Summary

1. Stretch-induced muscle injury results in the damage which causes reduced force and increased membrane permeability. This muscle damage is partly caused by ionic entry through stretch-activated channels and blocking these channels with Gd^{3+} or streptomycin reduces the force deficit associated with damage.

2. Dystrophin-deficient muscles are more susceptible to stretch-induced muscle injury and the recovery from injury can be incomplete. We have found that Na^+ entry associated with stretch-induced injury is enhanced in dystrophin-deficient muscles and that blockers of stretch-activated channels are capable of preventing the ionic entry and reducing the muscle damage.

3. A model is presented which proposes links between stretch-induced injury, opening of stretch-activated channels, increased levels of intracellular ions and various forms of muscle damage. While changes in Na^+ accompany stretch-induced muscle injury, we believe that changes in Ca^{2+} probably have a more central role in the damage process.

Introduction

Muscles which are stretched during contraction are susceptible to damage particularly when the exercise is prolonged and unaccustomed. It is widely agreed that stretch-induced injury includes both structural disorganization and changes to ionic regulation of the muscle fibres. The structural and functional changes include focal sarcomeric disorganisation, increase membrane permeability, reduction in force, delayed muscle soreness and reduction in joint range.¹⁻³ Severely damaged fibres may degenerate and this is then normally followed by regeneration as evidenced by force recovery.⁴ In normal individuals, this cycle of damage and repair lasts 4-6 days and is associated with symptoms of transient muscle soreness, stiffness and weakness. However in patients with debilitating muscle diseases, the muscle damage more frequently leads to degeneration and the regeneration is insufficient to compensate for damage.

Duchenne muscular dystrophy (DMD) is an X-linked genetic disease caused by the absence of the protein dystrophin. This devastating disease affects approximately

1 in 3500 male births. The disease is characterized by progressive muscle wasting and weakness. Affected boys are usually confined to a wheelchair before the age of 12 and die in their late teens or early twenties through respiratory muscle failure. Several studies have shown that *mdx* muscle fibres (an animal model for human DMD) are more vulnerable to stretch-induced injury and the increases in membrane permeability were greater.⁵⁻⁷ Dystrophin, the protein absent in DMD and the *mdx* mouse, connects the cytoskeletal network to the sarcolemma, and is thought it to provide mechanical reinforcement to the sarcolemma and minimize damage induced by contractile activity in normal muscles.⁸ However the reasons why absence of dystrophin cause increased in susceptibility to stretch-induced injury and the sequence of events leading to muscle necrosis remain unclear.

In recent years, attempts have been made to replace or transform the defective dystrophin gene using genetic approaches such as viral and plasmid vector therapy and corrective gene conversion therapy. While such approaches have been effective in the *mdx* mice,⁹⁻¹⁰ in humans these therapeutic strategies have not so far been of therapeutic value because of inefficiencies in the delivery and expression of the very large dystrophin gene and because of immune responses to parts of the expressed dystrophin.¹¹

In this review we focus primarily on the mechanisms of damage associated with stretch-induced damage in both wild-type and *mdx* muscle fibres. Specifically, we discuss the evidence that the activity of the stretch-activated (or mechanosensitive) channels after stretch-induced contraction injury is enhanced. Given the higher opening probability of stretch-activated channels in *mdx* myotubes,¹² we postulate that this abnormally high activity provides a leak pathway for Ca^{2+} to enter the cell causing cellular damage. Blocking these channels may provide a therapeutic approach for reducing muscle damage in DMD patients.

Stretch-induced muscle injury in wild-type fibres

Changes following stretch-induced muscle injury

It has long been recognized that cellular and ultrastructural damage occur following stretch-induced muscle injury in humans and animals. This includes myofibrillar disruption especially at the Z-lines and loss of

the cytoskeletal proteins, such as titin and desmin.¹³⁻¹⁵ In addition to the morphological abnormalities, a decrease in the force production and the shift of optimum length (L_o) have been observed following stretch-induced muscle injury.¹⁶⁻¹⁸

The 'popping sarcomere hypothesis' proposed by Morgan¹⁹ suggested that when muscles are stretched during contraction on the descending limb of the tension-length relation the sarcomeres show non-uniform increases in length. In general the weakest sarcomere will stretch first making it weaker still and then it will stretch rapidly to some maximum set by structural proteins in the sarcomere i.e. it will 'pop'. If lengthening continues after the weakest sarcomere has 'popped', then the next weakest sarcomere will elongate. It is likely that repeated lengthening contractions lead to increased numbers of disrupted sarcomeres in which the myofilaments fail to re-interdigitate. Furthermore, the overstretched sarcomeres increase the series compliance so that there is a shift in the active length-tension relation to longer muscle lengths. This shift following stretch-induced damage was first described by Katz²⁰ and subsequently confirmed in whole muscles and humans.²¹⁻²⁴ Structural evidence of overstretched sarcomeres was obtained by electron microscopy of fibres fixed during contraction, and supported the non-uniform sarcomere hypothesis. The occurrence of over-stretched sarcomeres after a single bout of lengthening contraction has been quantified and has been shown to account for more than half of the stretch²⁵.

The primary injury in stretch-induced muscle damage appears to be mechanical in nature with localised regions of sarcomere inhomogeneities. There is also evidence that changes in excitation-contraction (E-C) coupling may play a role in triggering the biomechanical and biochemical changes following stretch-induced injury. Calcium has long been thought to play a central role in muscle damage.²⁶ Earlier study in our laboratory on single wild-type muscle fibres²⁷ showed that both tetanic $[Ca^{2+}]_i$ and force were reduced following lengthening contractions. Furthermore, a persistent elevation in resting $[Ca^{2+}]_i$ was also observed though the mechanism of this increase was unclear. Another indication of increases in resting $[Ca^{2+}]_i$ arises from measurements of passive tension which has been shown to rise after a series of eccentric contractions.²³

One possible cause for the increase in resting $[Ca^{2+}]_i$ would be if T-tubules were forcibly disconnected from the surface membrane during stretch-induced injury causing increased membrane permeability. To study this possibility we performed experiments on single muscle fibres and used an extracellular fluorescent dye (sulforhodamine B) which enters the T-tubules. Following a series of eccentric (or stretched) contractions the T-tubules were found to be distorted and extracellular vacuoles attached to T-tubules were observed. Previously it had been shown that such vacuoles were a consequence of increased activity of the Na^+ pump as it removes excess Na^+ from the intracellular space²⁸ and we confirmed that the vacuoles observed after stretch-induced damage were also prevented by inhibiting the Na^+ pump with ouabain.¹⁷

Does $[Na^+]_i$ increase following stretch-induced muscle damage?

If the mechanism proposed above for the development of vacuoles is correct, then a rise in $[Na^+]_i$ should followed stretch-induced muscle damage. To test this idea we measured $[Na^+]_i$ with a fluorescent indicator (SBFI). Following the stretch protocol, $[Na^+]_i$ rose from the resting level of 7.3 ± 0.2 mM reaching a new level of 16.3 ± 1.6 mM. It is interesting to note that the rise of $[Na^+]_i$ occurred slowly taking 5-10 minutes to reach to a steady state.

To determine if the rise was caused by increased Na^+ influx, the stretch protocol was performed in a low- Na^+ solution. This solution eliminated the rise in $[Na^+]_i$ suggesting that Na^+ influx from the extracellular space was responsible. To determine whether inhibition of the Na^+ pump, for instance by damage to the pump or isolation of the pump within sealed off T-tubules, contributed to the rise of $[Na^+]_i$ we performed experiments in ouabain. Blocking the Na^+ pump with ouabain caused a slow rise of $[Na^+]_i$ but the rise of $[Na^+]_i$ produced by stretched contractions was further increased suggesting that the this rise was not caused by inhibition of the Na^+ pump.¹⁸

Does Na^+ enter through tears in the membrane?

The SBFI experiments establish that $[Na^+]_i$ rises following stretch-induced muscle injury but they do not identify whether the increase in $[Na^+]_i$ was via membrane tears. Earlier experiments have established that resting $[Ca^{2+}]_i$ also rises following stretch-induced damage and this rise may be the stimulus that trigger calcium-activated proteases which initiate muscle fibre degeneration.²⁹ If Ca^{2+} entry were at sites of membrane damage one would expect to observe localised elevations of $[Ca^{2+}]_i$ in the region of overstretched sarcomeres. However published studies showed that the distribution of $[Ca^{2+}]_i$ was uniform.³⁰⁻³¹ One possible explanation for these findings is that the sarcoplasmic reticulum rapidly sequesters Ca^{2+} which enters the fibre. For this reason, imaging $[Na^+]_i$ might be a better strategy since there is no large and active sink for $[Na^+]_i$ in skeletal muscles and detection of localised elevations might therefore be easier.

We imaged $[Na^+]_i$ with a confocal microscope having loaded the fibres with sodium green. $[Na^+]_i$ increased after the stretch protocol consistent with the SBFI results but, similar to the earlier $[Ca^{2+}]_i$ experiments, no localised elevations of $[Na^+]_i$ were detected.¹⁸ These results probably exclude large membrane tears but obviously small, multiple, transient tears might have escaped detection. Another possibility is that the Na^+ entry occurs through a class of Na^+ permeable channels which are open for many minutes after stretch-induced muscle damage.

Stretch-activated ion channels in skeletal muscle fibres

One possible contributor to the increased membrane permeability following stretch-induced muscle damage is the involvement of stretch-activated channels. Involvement

of the stretch-activated channels leading to membrane depolarization in rat muscle fibres after lengthening contractions has been reported.³² These results suggested that membrane depolarization was due to an increase in Na^+ permeability and the accompanying increase in Na^+ influx. Stretch-activated channels of various ionic selectivities have been found in many cell types including striated muscles.³³ These channels were first described in cultured chick embryonic skeletal muscle cells.³⁴ They respond to mechanical stress by increasing the open probability^{12,35} and act as membrane-embedded mechano-electrical switches, opening a large water-filled pore in response to lipid bilayer deformations. This process is important in a wide array of cellular activities such as volume regulation, electrolyte homeostasis and sensory transduction, and is critical to the response of living organisms to mechanical stimulation.³⁵⁻³⁶ Non-selective stretch-activated cation channels pass Ca^{2+} as well as Na^+ and K^+ , whereas others classes of mechanosensitive channels are selectively permeable to K^+ or Cl^- .³⁷⁻³⁸

Gadolinium (Gd^{3+}) and streptomycin have been reported to block stretch-activated channels.^{36,39-42} They have been used to inhibit cation-permeable stretch-activated channels in cardiac and skeletal muscle cells. Although Gd^{3+} is the most widely used blocker of stretch-activated channels,⁴²⁻⁴³ it is relatively non-specific blocking L-type Ca^{2+} channels,⁴⁴ store-dependent Ca^{2+} channels⁴⁵ and Cl^- channels⁴⁶ though generally with lower potency. Identification of the physiological role of stretch-activated channels has been hampered by the absence of specific channel blockers or activators. The spider venom peptide GsmTx-4 described by Sachs and colleagues⁴⁷ is the most potent and specific inhibitor of stretch-activated ion channels described so far.

Given the failure to detect localised Na^+ entry in our imaging experiments, a blocker of stretch-activated channels (Gd^{3+} or streptomycin) was applied for 10 min following stretch-induced damage. Not only did the blockers prevent the increase of $[\text{Na}^+]_i$ after the stretch protocol but it also prevented part of the force deficit.¹⁸ We hypothesise that stretched contractions open stretch-activated channels and allow influx of Na^+ and Ca^{2+} ions. The consequent rise in $[\text{Na}^+]_i$ activates the Na^+ - K^+ pump and the efflux of Na^+ and H_2O through the T-tubules is thought to cause the vacuoles. The increased $[\text{Ca}^{2+}]_i$ may activate proteases and phospholipases which cause membrane damage and the increase in membrane permeability (see Fig. 2).⁴⁸⁻⁴⁹

Stretch-induced muscle damage in *mdx* muscle fibres

Function of dystrophin in the prevention of stretch-induced muscle damage

Duchenne muscular dystrophy (DMD) is caused by mutations in the dystrophin gene which prevent dystrophin expression. Lack of dystrophin causes disruption of the dystrophin-glycoprotein complex (DGC) and results in sarcolemmal instability. Studies performed on dystrophic muscles have shown that lengthening contractions induce

greater damage than in wild-type muscle fibres.^{5,7}

The cytoskeletal protein dystrophin is thought to provide mechanical reinforcement to the sarcolemmal membrane and minimize damage induced by contractile activity in normal muscles. Since dystrophin normally links the contractile proteins to the DGC membrane complex it may prevent the relative movement between the myofibrils and the surface membrane. In the absence of dystrophin there may be relative movement between the myofibrils and the T-tubules which attach to the surface membrane and then pass perpendicularly through the myofibrils. Relative movement would therefore be expected to damage both the T-tubules and the surface membrane. Another possibility is that the dystrophic cells are often abnormal in shape (branching, tapering)⁵ so that stretch might be more prone to cause cell damage because of the non-uniformity in shape.

Apart from mechanical reinforcement, it has been suggested that dystrophin is involved in the clustering of ion channels within the sarcolemma. Using the manganese quench technique, the membrane permeability for cations has been shown to be two times higher in resting *mdx* muscle fibres than the wild-type fibres.⁵⁰ These authors showed that this leak channel was blocked by 50 μM Gd^{3+} raising the possibility that a stretch-activated channel might be involved. This idea is also supported by patch-clamp recordings from *mdx* myotubes in which single channel activity was recorded and stretch-sensitivity tested by applying suction. The results showed a 3-fold higher opening probability of the stretch-activated channels¹² in *mdx* compared to wild type fibres. As these channels have been shown to be present in the sarcolemma, and are non-specific cation channels allowing influx of Ca^{2+} and Na^+ , this pathway could contribute to the elevated resting $[\text{Ca}^{2+}]_i$ and $[\text{Na}^+]_i$. Furthermore, stretched contractions can result in activation of these channels, and the resulting Ca^{2+} influx can trigger Ca^{2+} -dependent proteolysis and lead eventually to muscle necrosis.

Stretch-activated channel blockers in the prevention of stretch-induced muscle damage

The above results suggest that Ca^{2+} leak pathways which may be stretch-activated are more prevalent in *mdx* fibres. We therefore tested the changes in $[\text{Na}^+]_i$ in *mdx* fibres following stretch-induced muscle damage. Single *mdx* muscle fibres were isolated and loaded with sodium green for examination under confocal microscopy.⁵¹ We show that $[\text{Na}^+]_i$ in *mdx* muscles (15.4 ± 1.1 mM) was higher than control (9.7 ± 1.1 mM). Similar to other *mdx* muscle studies,⁵⁻⁷ there was a greater reduction in force following lengthening contractions than in wild-type fibres. We also observe a significantly greater rise in $[\text{Na}^+]_i$ following lengthening contractions than in wild-type fibres (see Fig. 1A). Just as in wild-type fibres, the increase in $[\text{Na}^+]_i$ was uniformly distributed across the cell and there was no detectable localized elevations. Given that Gd^{3+} and streptomycin reduced the elevated $[\text{Na}^+]_i$ in wild-type fibres, we applied these stretch-activated channel blockers

Stretch-induced muscle damage

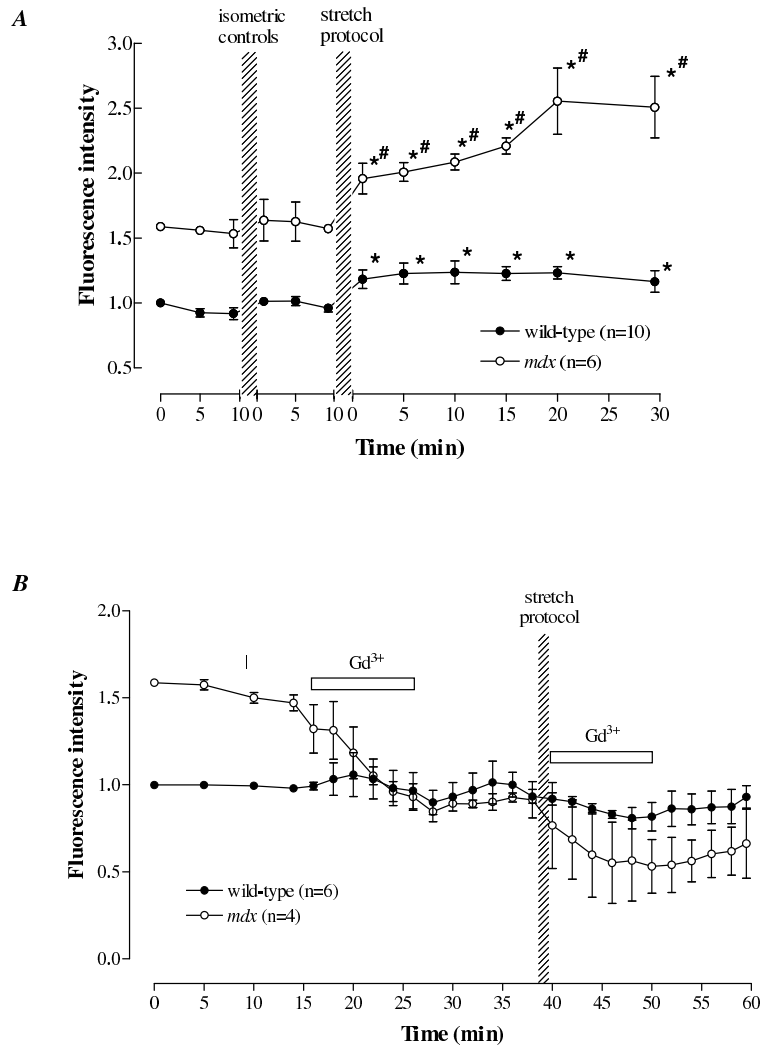


Figure 1. Na⁺ fluorescence following stretch-induced injury in wild-type and mdx muscle fibres. The fibres were loaded with sodium green and the fluorescence intensity was normalised to the initial value at the start of the experiment. Note that the initial fluorescence signal was adjusted for mdx muscle fibres based on the in vivo calibration procedures.

Panel A, there was a rise in Na⁺ fluorescence after the stretch-induced injury protocol in both wild-type and mdx fibres but the rise in mdx fibres was significantly higher. * significantly larger than initial wild-type control; # significantly larger than initial mdx control ($P < 0.05$).

Panel B, under control conditions, Gd³⁺ has no effect on wild-type fibres but lowered the Na⁺ fluorescence in the mdx fibres to the level of the wild-type fibres. The fibres underwent a stretch-induced protocol and Gd³⁺ was applied immediately for 10 min (as indicated by the bars). Gd³⁺ eliminated the rise of sodium green fluorescence following the stretch in both wild-type and mdx fibres. Values are mean \pm S.E.M.

to the mdx fibres immediately after the stretch protocol (Fig. 1B). Similar to the wild-type muscle data, not only did both agents eliminate the rise of [Na⁺]_i but, in addition, the force deficit was reduced. After the stretch protocol on mdx muscle fibres, the force was reduced to 23 ± 3 % of the control value at the original length but when Gd³⁺ was applied during or immediately after the lengthening contractions, the force was improved to 46 ± 4 %. When the muscle fibres were stretched to the new optimum length, the

force was improved to 96 ± 5 % of the control.

Based on these results, we postulate that the increase in Na⁺ permeability is caused by increased opening of the stretch-activated channels, and blocking these channels is capable of preventing the rise of [Na⁺]_i and, more interestingly, the force deficit. Furthermore, it is possible that the increased resting [Ca²⁺]_i observed²⁷ was caused by increased activity of these stretch-activated channels. This increased [Ca²⁺]_i may be responsible for the initiation of

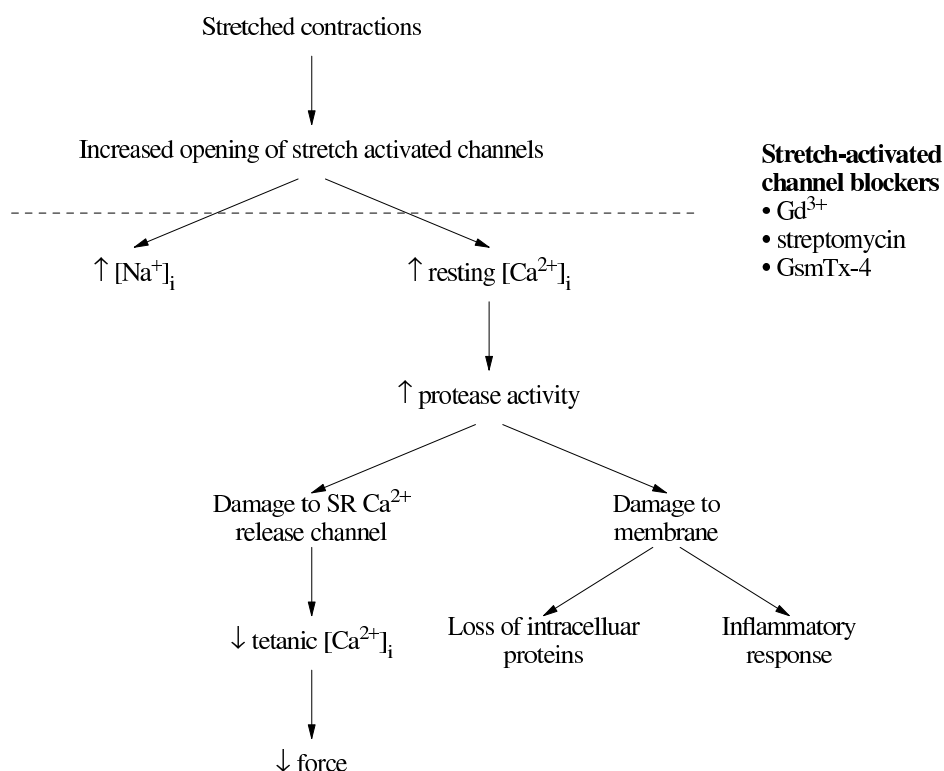


Figure 2. Working hypothesis linking stretch-activated channels, ionic changes and muscle damage. The causes of force reduction following stretch-induced muscle injury could be: (i) sarcomere inhomogeneity (not shown here) and (ii) damage arising through increased opening of the stretch-activated channels. It is likely that the opening of stretch-activated channels is a consequence of sarcomere inhomogeneity. In wild-type or mdx muscle fibres, elevated levels of $[Na^+]_i$ has been shown caused by the increased activity of the stretch-activated channels. One possibility is that elevations in resting $[Ca^{2+}]_i$ which occur following stretch-induced injury are a consequence of Ca^{2+} influx through the stretch-activated channels. It is possible that the associated inflammatory response, muscle weakness and pain observed following stretch-induced injury is caused by increased Ca^{2+} . If the stretch-activated channel blockers (Gd^{3+} , streptomycin, GsmTx-4) are capable of preventing the cascade of events following stretch-induced injury, they may prove valuable in reducing muscle damage.

protease activity causing damage to the SR Ca^{2+} release channel and to the membrane. Elevations in $[Ca^{2+}]_i$ have been shown to induce inactivation of E-C coupling associated with a decrease in tetanic $[Ca^{2+}]_i$ and reduction in force.⁵²⁻⁵³ The disruption to the membrane allows leakage of the intracellular contents out of the muscle cells and as evidenced by elevated serum levels of muscle enzymes and accumulation of inflammatory cells.^{1,54} An overview of this hypothesis is summarised in Fig. 2.

The force deficit provides an indication of the extent of muscle damage and the results seem to suggest that the stretch-activated channel blockers can protect against muscle damage at least over the 30 min post injury. Whether these blockers are capable of exerting protection for longer term damage is uncertain. Nevertheless these findings have potential implication in the treatment of DMD patients.

Clinical applications

DMD is a chronic, degenerative disease and there is no effective treatment at present despite attempts using

different genetic approaches. The exact role of dystrophin in the regulation of stretch-activated channels is not certain but we have evidence that these channels are abnormal in muscular dystrophy and cause part of the stretch-induced muscle damage. The various blockers of the stretch-activated channels and their capabilities of preventing Ca^{2+} and Na^+ meant that they hold as potential therapeutic agents to overcome irreversible muscle damage in DMD patients. However much work remains to be done before this therapy can be applied to patients.

Conclusion

Dystrophin deficiency is the precipitating feature in the muscle pathology of patients with Duchenne muscular dystrophy. The role of dystrophin in normal muscles remains unclear; possible roles include contributing to structural stability by connecting the cytoskeleton to the dystrophin-associated proteins in the membrane and contributing to channel function by anchoring and/or regulating ion channels. One channel whose function is altered in the absence of dystrophin is the stretch-activated

channel which allows increased influx of Na⁺ and Ca²⁺ following stretch-induced injury. The alteration of Ca²⁺ homeostasis in muscular dystrophy may be responsible for muscle degeneration. Consequently blockers of stretch-activated channels may have therapeutic potential by reducing stretch-induced muscle damage in DMD patients.

References

- Chleboun GS, Howell JN, Conatser RR, Giesey JJ. Relationship between muscle swelling and stiffness after eccentric exercise. *Med. Sci. Sports. Exerc.* 1998; **30**: 529-35
- Friden J, Lieber RL. Segmental muscle fiber lesions after repetitive eccentric contractions. *Cell Tissue Res.* 1998; **293**: 165-71.
- Howell JN, Chleboun G, Conatser R. Muscle stiffness, strength loss, swelling and soreness following exercise-induced injury in humans. *J. Physiol.* 1993; **464**: 183-96.
- Sayers SP, Clarkson PM. Force recovery after eccentric exercise in males and females. *Eur. J. Appl. Physiol.* 2001; **84**: 122-6.
- Head SI, Williams DA, Stephenson DG. Abnormalities in structure and function of limb skeletal muscle fibres of dystrophic *mdx* mice. *Proc. R. Soc. Lond., B, Biol. Sci.* 1992; **248**: 163-9.
- Moens P, Baatsen PH, Marechal G. Increased susceptibility of EDL muscles from *mdx* mice to damage induced by contractions with stretch. *J. Muscle. Res. Cell. Motil.* 1993; **14**: 446-51.
- Petrof BJ, Shrager JB, Stedman HH, Kelly AM, Sweeney HL. Dystrophin protects the sarcolemma from stresses developed during muscle contraction. *Proc. Natl. Acad. Sci.* 1993; **90**: 3710-14.
- Consolino CM, Brooks SV. Susceptibility to sarcomere injury induced by single stretches of maximally activated muscles of *mdx* mice. *J. Appl. Physiol.* 2004; **96**: 633-8.
- Acsadi G, Lochmuller H, Jani A, Huard J, Massie B, Prescott S, Simoneau M, Petrof BJ, Karpati G. Dystrophin expression in muscles of *mdx* mice after adenovirus-mediated in vivo gene transfer. *Hum. Gene Ther.* 1996; **7**: 129-40.
- Danko I, Fritz JD, Latendresse JS, Herweijer H, Schultz E, Wolff JA. Dystrophin expression improves myofiber survival in *mdx* muscle following intramuscular plasmid DNA injection. *Hum. Mol. Genet.* 1993; **2**: 2055-61.
- Kapsa, R, Kornberg AJ, Byrne E. Novel therapies for Duchenne muscular dystrophy. *Lancet Neurol.* 2003; **2**: 299-310.
- Franco-Obregon A, Lansman JB. Changes in mechanosensitive channel gating following mechanical stimulation in skeletal muscle myotubes from the *mdx* mouse. *J. Physiol.* 2002; **539**: 391-407.
- Clarkson PM, Nosaka K, Braun B. Muscle function after exercise-induced muscle damage and rapid adaptation. *Med. Sci. Sports Exerc.* 1992; **24**: 512-20.
- Lieber RL, Schmitz MC, Mishra DK, Fridén J. Contractile and cellular remodeling in rabbit skeletal muscle after cyclic eccentric contractions. *J. Appl. Physiol.* 1994; **77**: 1926-34.
- Lieber RL, Thornell LE, Fridén J. Muscle cytoskeletal disruption occurs within the first 15 min of cyclic eccentric contraction. *J. Appl. Physiol.* 1996; **80**: 278-84.
- Yeung EW, Bourreau JP, Allen DG, Ballard HJ. Effect of eccentric contraction-induced injury on force and intracellular pH in rat skeletal muscles. *J. Appl. Physiol.* 2002; **92**: 93-9.
- Yeung EW, Balnave CD, Ballard HJ, Bourreau JP, Allen DG. Development of T-tubular vacuoles in eccentrically damaged mouse muscle fibres. *J. Physiol.* 2002; **540**: 581-92.
- Yeung EW, Ballard HJ, Bourreau JP, Allen DG. Intracellular sodium in mammalian muscle fibers after eccentric contractions. *J. Appl. Physiol.* 2003; **94**: 2475-82.
- Morgan DL. New insights into the behavior of muscle during active lengthening. *Biophys. J.* 1990; **57**: 209-21.
- Katz B. The relation between force and speed in muscular contraction. *J. Physiol.* 1939; **96**: 45-64.
- Brockett CL, Morgan DL, Proske U. Human hamstring muscles adapt to eccentric exercise by changing optimum length. *Med. Sci. Sports Exerc.* 2001; **33**: 783-90.
- Jones C, Allen T, Talbot J, Morgan DL, Proske U. Changes in the mechanical properties of human and amphibian muscle after eccentric exercise. *Eur. J. Appl. Physiol. Occup. Physiol.* 1997; **76**: 21-31.
- Whitehead NP, Morgan DL, Gregory JE, Proske U. Rises in whole muscle passive tension of mammalian muscle after eccentric contractions at different lengths. *J. Appl. Physiol.* 2003; **95**: 1224-1234.
- Wood SA, Morgan DL, Proske U. Effects of repeated eccentric contractions on structure and mechanical properties of toad sartorius muscle. *Am. J. Physiol.* 1993; **265**: C792-800.
- Talbot JA, Morgan DL. Quantitative analysis of sarcomere non-uniformities in active muscle following stretch. *J. Muscle. Res. Cell. Motil.* 1996; **17**: 261-268.
- Duncan CJ. Role of intracellular calcium in promoting muscle damage: a strategy for controlling the dystrophic condition. *Experientia* 1978; **34**: 1531-35.
- Balnave CD, Allen DG. Intracellular calcium and force in single mouse muscle fibres following repeated contractions with stretch. *J. Physiol.* 1995; **488**: 25-36.
- Casademont J, Carpenter S, Karpati G. Vacuolation of muscle fibers near sarcolemmal breaks represents T-tubule dilatation secondary to enhanced sodium

- pump activity. *J. Neuropathol. Exp. Neurol.* 1988; **47**: 618-28.
29. Belcastro AN, Shewchuk LD, Raj DA. Exercise-induced muscle injury: a calpain hypothesis. *Mol. Cell. Biochem.* 1998; **179**: 135-45.
 30. Balnave CD, Davey DF, Allen DG. Distribution of sarcomere length and intracellular calcium in mouse skeletal muscle following stretch-induced injury. *J. Physiol.* 1997; **502**: 649-59.
 31. Ingalls CP, Warren GL, Williams JH, Ward CW, Armstrong RB. E-C coupling failure in mouse EDL muscle after in vivo eccentric contractions. *J. Appl. Physiol.* 1998; **85**: 58-67.
 32. McBride TA, Stockert BW, Gorin FA, Carlsen RC. Stretch-activated ion channels contribute to membrane depolarization after eccentric contractions. *J. Appl. Physiol.* 2000; **88**: 91-101.
 33. Sachs F, Morris CE. Mechanosensitive ion channels in nonspecialized cells. *Rev. Physiol. Biochem. Pharmacol.* 1998; **132**: 1-77.
 34. Guharay F, Sachs F. Stretch-activated single ion channel currents in tissue-cultured embryonic chick skeletal muscle. *J. Physiol.* 1984; **352**: 685-701.
 35. Perozo E, Cortes DM, Sompornpisut P, Kloda A, Martinac B. Open channel structure of MscL and the gating mechanism of mechanosensitive channels. *Nature* 2002; **418**: 942-8.
 36. Sackin H. Mechanosensitive channels. *Annu. Rev. Physiol.* 1995; **57**: 333-53.
 37. Hagiwara N, Masuda H, Shoda M, Irisawa H. Stretch-activated anion currents of rabbit cardiac myocytes. *J. Physiol.* 1992; **456**: 285-302.
 38. Ruknudin A, Sachs F, Bustamante JO. Stretch-activated ion channels in tissue-cultured chick heart. *Am. J. Physiol.* 1993; **264**: H960-72.
 39. Hansen DE, Borganelli M, Stacy GP Jr, Taylor LK. Dose-dependent inhibition of stretch-induced arrhythmias by gadolinium in isolated canine ventricles. Evidence for a unique mode of antiarrhythmic action. *Cardiovasc. Res.* 1991; **69**: 820-31.
 40. Komuro I, Kudo S, Yamazaki T, Zou Y, Shiojima I, Yazaki Y. Mechanical stretch activates the stress-activated protein kinases in cardiac myocytes. *FASEB J.* 1996; **10**: 631-36.
 41. Sokabe M, Hasegawa N, Yamamori K. Blockers and activators for stretch-activated ion channels of chick skeletal muscle. *Ann. N. Y. Acad. Sci.* 1993; **707**: 417-20.
 42. Yang XC, Sachs F. Block of stretch-activated ion channels in *Xenopus* oocytes by gadolinium and calcium ions. *Science* 1989; **243**: 1068-71.
 43. Franco A Jr, Lansman JB. Stretch-sensitive channels in developing muscle cells from a mouse cell line. *J. Physiol.* 1990; **427**: 361-80.
 44. Lacampagne A, Gannier F, Argibay J, Garnier D, Le Guennec JY. The stretch-activated ion channel blocker gadolinium also blocks L-type calcium channels in isolated ventricular myocytes of the guinea-pig. *Biochim. Biophys. Acta* 1994; **1191**: 205-08.
 45. Flemming R, Cheong A, Dedman AM, Beech DJ. Discrete store-operated calcium influx into an intracellular compartment in rabbit arteriolar smooth muscle. *J. Physiol.* 2002; **543**: 455-64.
 46. Thinnes FP, Walter G, Hellmann KP, Hellmann T, Merker R, Kiafard Z, Eben-Brunnen J, Schwarzer C, Gotz H, Hilschmann N. Gadolinium as an opener of the outwardly rectifying Cl(-) channel (ORCC). Is there relevance for cystic fibrosis therapy? *Pflugers Arch.* 2001; **443**: S111-16.
 47. Suchyna TM, Johnson JH, Hamer K, Leykam JF, Gage DA, Clemo HF, Baumgarten CM, Sachs F. Identification of a peptide toxin from *Grammostola spatulata* spider venom that blocks cation-selective stretch-activated channels. *J. Gen. Physiol.* 2000; **115**: 583-98.
 48. McNeil PL, Khakee R. Disruptions of muscle fiber plasma membranes: role in exercise-induced damage. *Am. J. Pathol.* 1992; **140**: 1097-109.
 49. Deconinck N, Ragot T, Marechal G, Perricaudet M, Gillis JM. Functional protection of dystrophic mouse (*mdx*) muscles after adenovirus-mediated transfer of a dystrophin minigene. *Proc. Natl. Acad. Sci. U.S.A.* 1996; **93**: 3570-74.
 50. Tutdibi O, Brinkmeier H, Rudel R, Fohr KJ. Increased calcium entry into dystrophin-deficient muscle fibres of MDX and ADR-MDX mice is reduced by ion channel blockers. *J. Physiol.* 1999; **515**: 859-68.
 51. Yeung EW, Head SI, Allen DG. Gadolinium reduces short-term stretch-induced muscle damage in isolated mdx mouse muscle fibres. *J. Physiol.* 2003; **552**: 449-58.
 52. Chin ER, Allen DG. The role of elevations in intracellular [Ca²⁺] in the development of low frequency fatigue in mouse single muscle fibres. *J. Physiol.* 1996; **491**: 813-24.
 53. Lamb GD, Junankar PR, Stephenson DG. Raised intracellular [Ca²⁺] abolishes excitation-contraction coupling in skeletal muscle fibres of rat and toad. *J. Physiol.* 1995; **489**: 349-62.
 54. Schwane JA, Johnson SR, Vandenaeker CB, Armstrong RB. Delayed-onset muscular soreness and plasma CPK and LDH activities after downhill running. *Med. Sci. Sports Exerc.* 1983; **15**: 51-6.
-
- Received 16 November 2003, in revised form 8 April 2004.
 Accepted 10 April 2004.
 ©D.G. Allen 2004.
- Author for correspondence:*
 Professor D. G. Allen
 Department of Physiology
 University of Sydney F13,
 NSW 2006, Australia
 Tel: +61 2 9351 4602 Fax: +61 2 9351 2058
 Email: david.a@physiol.usyd.edu.au

The role of contraction-induced injury in the mechanisms of muscle damage in muscular dystrophy

Gordon S. Lynch

Department of Physiology,
The University of Melbourne,
Victoria 3010,
Australia

Summary

1. Duchenne muscular dystrophy (DMD) is a severe disease of skeletal muscle, characterised by an X-linked recessive inheritance and a lack of dystrophin in muscle fibres. It is associated with progressive and severe wasting and weakness of nearly all muscles, and premature death by cardiorespiratory failure.

2. Studies investigating the susceptibility of dystrophic skeletal muscles to contraction-mediated damage, especially after lengthening actions where activated muscles are stretched forcibly, have concluded that dystrophin may confer protection to muscle fibres by providing a mechanical link between the contractile apparatus and the plasma membrane. In the absence of dystrophin, there is disruption to normal force transmission and greater stress placed upon myofibrillar and membrane proteins, leading to muscle damage.

3. Contraction protocols (involving activation and stretch of isolated muscles or muscle fibres) have been developed to assess the relative susceptibility of dystrophic (and otherwise healthy) muscles to contraction-induced injury. These protocols have been used successfully to determine the relative efficacy of different (gene, cell, or pharmacological) interventions designed to ameliorate or cure the dystrophic pathology. More research is needed to develop specific 'contraction assays' that will assist in the evaluation of the clinical significance of different therapeutic strategies for muscular dystrophy.

Duchenne muscular dystrophy and the *mdx* mouse

Duchenne muscular dystrophy (DMD) is a severe X chromosome-linked myopathy caused by a variety of mutations and deletions in the dystrophin gene.^{1,2} In the absence of dystrophin expression, the skeletal muscles of boys with DMD undergo continuous cycles of degeneration and insufficient regeneration that leads to progressive muscle wasting and weakness. Patients are confined to wheelchairs by their early teens and die of respiratory or heart failure by their early twenties.³ The *mdx* mouse, a commonly used animal model for DMD, carries a mutation in the dystrophin gene and lacks the native protein similar to the human condition, but exhibits a more benign pathological phenotype. The diaphragm muscles of *mdx* mice show progressive structural and functional deterioration consistent with DMD, whereas limb muscles exhibit a relatively mild pathology for much of the life span.⁴⁻⁷ Despite an early period of severe degeneration in

the limb muscles of *mdx* mice at 3-4 weeks of age, the muscles regenerate extremely well. In fact, despite ongoing cycles of (less severe) degeneration and regeneration throughout adulthood, the muscles of *mdx* mice are actually hypertrophied compared to wild type mice. However, despite their larger size they are comparatively weaker, since their maximum force output per muscle cross-sectional area is usually lower.⁸

Dystrophin and the costamere

Dystrophin links actin in the cytoskeleton through the transmembrane dystrophin-associated glycoprotein complex (or dystrophin-glycoprotein complex, DGC) to laminin in the extracellular matrix (ECM).⁹ The DGC and other cytoskeletal proteins form rib-like lattices on the cytoplasmic face of the sarcolemma, called costameres. Costameres help stabilise the cytoskeleton to the ECM; they act as mechanical couplers to distribute contractile forces from the sarcomere through to the sarcolemma and basal lamina; and they help facilitate uniform sarcomere length between fibres, at rest and during contraction.^{10,11} Dystrophin has also been found at the myotendinous junction and has therefore been postulated to play a role in the transmission of force to tendons.^{12,13}

The precise functional role of dystrophin and the DGC has not been described definitively, but it has been postulated that its primary role is to anchor the sarcolemma to costameres and thus stabilize the sarcolemma against physical forces transduced through costameres during muscle contraction, most especially when muscles are activated and stretched forcibly. Such muscle lengthening actions usually occur when muscles act as brakes during slowing movements (e.g. when running downhill), and they are commonly referred to as 'eccentric' or 'plyometric' contractions.^{14,15}

In addition to its membrane stabilising role, the DGC is postulated to play a role in the regulation of intracellular calcium, molecular signalling, and in signal transduction, such as neuronal nitric oxide synthase (nNOS)-mediated regulation of blood flow to contracting muscles.¹⁶ For the purpose of this review I will limit my discussion to dystrophin's role in protecting muscle fibres against contraction-induced injury.

Evidence for a functional role of dystrophin

Contraction-induced injury is associated with a mechanical disruption of sarcomeres that are stretched

excessively. Whether dystrophin helps maintain sarcomere stability is not known, but there are several lines of evidence supporting a functional role of dystrophin in skeletal muscle fibres, including: increased susceptibility to osmotic stress^{17,18}; increased permeability of the sarcolemma in *mdx* mice indicated by increased serum concentrations of muscle enzymes (e.g. creatine kinase); and elevated intracellular Ca²⁺ concentration.¹⁹ An uptake of Evans blue dye (EBD) by fibres in quiescent muscles of *mdx*, but not control mice, provides further support for an increased permeability of the sarcolemma of fibres lacking dystrophin.²⁰ Furthermore, when *mdx* and wild type mice are subjected to downhill running exercise, there is extensive EBD uptake in muscle fibres of *mdx* but not wild type mice, indicating increased sarcolemmal fragility and permeability in the absence of dystrophin.²¹

Intact Muscles

A number of different contraction protocols^{6,22-26} have demonstrated that skeletal muscles of *mdx* mice have a greater susceptibility to injury, particularly when maximally activated muscles are stretched. Whether whole muscles are studied *in vitro*, *in situ*, or *in vivo*, the overwhelming evidence indicates that intact skeletal muscles of adult *mdx* mice show a greater susceptibility to contraction-induced injury than muscles of control mice. Interestingly, the muscles of very young (9-12 day old) *mdx* mouse pups are relatively resistant to injury from acute mechanical injury, suggesting that the early onset of the dystrophic process might be independent of a mechanical perturbation to the sarcolemma.¹³ The few reports that muscles of adult *mdx* and control mice do not differ in their susceptibility to contraction-induced injury involved protocols with hundreds of these lengthening actions.^{27,28} These arduous protocols may have produced such severe damage to muscles in both *mdx* and control mice that they did not discriminate the differences between the two.

It should be noted that the majority of these studies have not reported the sarcomere length range or the region of the length tension curve over which the damaging contractions occurred. This is important since recent studies have indicated that this is a major determinant of the extent of damage in normal muscles.¹⁵ Whether the optimum length of a muscle corresponds to the same joint angle in normal and dystrophic muscles has not been described. In examining the relative susceptibility of normal and dystrophic muscles to contraction-mediated damage, experiments conducted over the same joint angle, the same part of the length-tension curve (relative to optimum), or the same range of sarcomere lengths, are worthy of consideration and would provide interesting information about the differences and similarities between normal and dystrophic muscles.

Studies have recently focused on developing contraction-induced injury 'assays', with some employing as few as two lengthening contractions, to differentiate between the injury susceptibility of muscles from dystrophic and wild type mice, especially after gene

therapies such as injection of viruses carrying full-length dystrophin or microdystrophins.^{29,30} DelloRusso and colleagues³¹ developed an assay based on the high susceptibility to injury of limb muscles in *mdx* mice for use in evaluating such therapeutic interventions. The assay involved two stretches of maximally activated tibialis anterior (TA) muscles *in situ*. The stretches of 40% strain relative to muscle fibre length were initiated once peak isometric force was attained. Damage (injury) was assessed one minute later by the deficit in isometric force. They found that the force deficits were four- to seven-fold higher for muscles of *mdx* compared with control mice. Such an *in situ* lengthening contraction protocol was used to assess whether intramuscular injection of gutted adenoviral vectors expressing full-length dystrophin into TA muscles of *mdx* mice could confer protection from contraction-mediated injury. The force deficit after each of the two stretches was used to determine the muscle resistance to injury. Despite a relative inefficiency of the intramuscular injection delivery leading to only 25% of the muscle cross-sectional area being transduced, this level of dystrophin expression conferred an ~40% correction of the functional difference between muscles of *mdx* and wild type mice.³²

More recently, Consolino and Brooks³³ examined the susceptibility to sarcomere injury induced by single stretches of maximally activated muscles of *mdx* mice. Single stretch protocols are less likely to result in fatigue or depletion of energy stores, factors that can complicate the mechanistic interpretation of muscle injury after protocols involving many repeated contractions. In this elegant study, the authors hypothesised that on the basis that muscles of *mdx* mice would be more susceptible to injury, stretches of lesser strains would be expected to cause more damage (i.e. cause a greater force deficit) to muscles of *mdx* compared with wild type mice.³³ In fast extensor digitorum longus (EDL) muscles of wild type mice, single stretches of 30% strain were necessary to cause a significant deficit in isometric force, whereas in *mdx* mice, single stretches of only 20% strain caused significant loss of force producing capacity. After stretches of 30, 40, and 50% strain, force deficits were two- to three-fold greater for EDL muscles of *mdx* than for wild type mice.³³ Interestingly, analysis of dye uptake into muscles following the single stretch protocols revealed no membrane damage. The authors concluded that on the basis of greater force deficits, in the absence of fatigue, depletion of energy stores, or significant membrane damage, the differences in the force deficits from single stretches were due to differences in the extent of disruption to the ultrastructure of force-generating or force-transmitting structures within or between sarcomeres, and that in addition to a compromised membrane, the lack of dystrophin in EDL muscles of *mdx* mice results in a mechanically compromised cytoskeleton.³³ These findings support a role for the DGC in the maintenance of the structural stability of sarcomeres and hence "activities involving either single or repeated contractions that are innocuous for muscles in control animals may be injurious to dystrophic muscles".³³ However, it should be noted that the precise mechanism for the protective role of the DGC

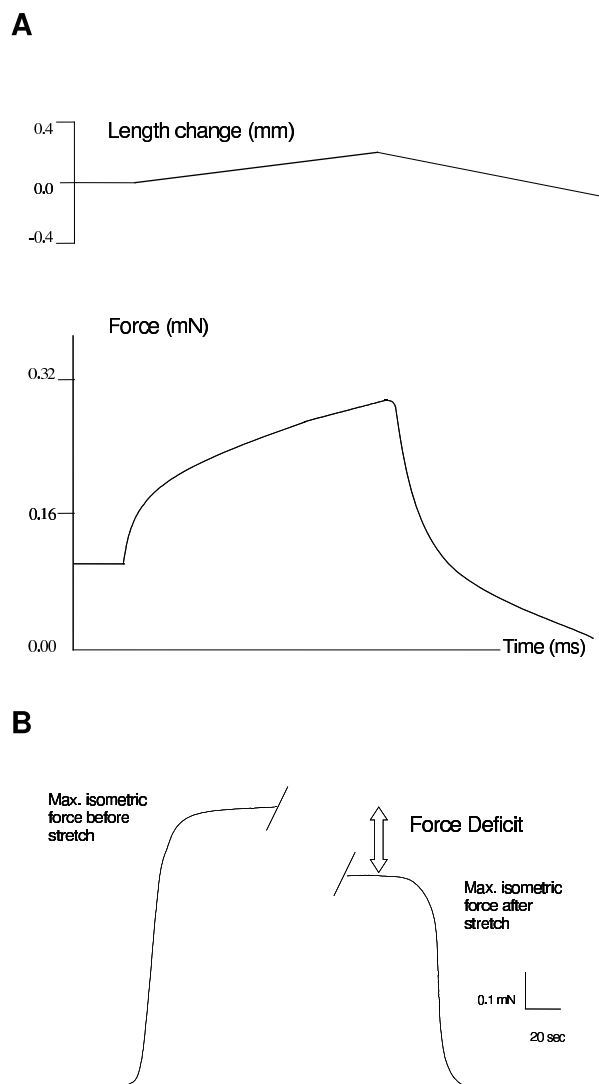
remains elusive. Other contributing mechanisms to the loss of force transmission after damage, including alterations in excitation-contraction coupling, cannot be ruled out.³⁴

Single Fibres

Similar studies have investigated the susceptibility of dystrophic muscle to contraction-induced injury at the cellular (single fibre level) using membrane permeabilized and intact single muscle fibre preparations. Yeung and colleagues³⁵ reported that single (flexor brevis) muscle fibres from *mdx* mice were more susceptible to stretch-induced damage and showed an associated rise in intracellular sodium concentration that was greater than in wild type mice. Each muscle fibre was subjected to 10 isometric tetani followed by 10 eccentric tetani of 40% strain relative to muscle length. Following the stretch-induced injury protocol, isometric force decreased to ~34% of the control in fibres from wild type mice and to ~23% in fibres from *mdx* mice.³⁵

Chemical permeabilization of muscle fibres disrupts the integrity of the sarcolemma severely.³⁶ In a study comparing the susceptibility of muscle fibres from *mdx* and wild type mice to contraction-induced injury, Lynch and colleagues³⁷ proposed that since the integrity of membranes of muscle fibres from *mdx* and control mice would be compromised equally, any protection conferred by dystrophin and the DGC to intact fibres from muscles of wild type mice would be eliminated, and thus the susceptibility to contraction-induced injury (as determined from the force deficit) would not be different (Fig. 1). Fibres from EDL muscles of wild type and *mdx* mice were maximally activated by Ca^{2+} and then subjected to a single stretch of either 10, 20, or 30% strain relative to muscle fibre length. The observation of no difference in the force deficits of fibres from muscles of *mdx* and wild type mice provided indirect evidence that the protection conferred on skeletal muscle fibres by dystrophin and the DGC is a stabilisation in the alignment of sarcomeres through the lateral transmission of force from the myofilaments to the laminin 2 and, eventually, collagen IV in the ECM. Taken together, the findings on permeabilized fibres and membrane-intact fibres indicate that dystrophic symptoms do not arise from factors within the myofibrillar structure of fibres but, rather, through a disruption of sarcolemmal integrity that normally confers significant protection from contraction-induced injury. The greater force deficits for single permeabilized fibres compared with intact muscles (following single stretches of identical magnitude) indicates the significance of the overall protection from injury afforded the myofibrils by the linkages among the myofibres, the sarcolemma, and the ECM.^{9-11,21,38} The findings also supported the premise that the dystrophin and DGC are major factors in the stabilisation of the membrane,²¹ the lateral transmission of force,¹⁰ and the alignment of sarcomeres, particularly during stretches of activated muscles.^{33,37} One other possibility, not immediately apparent when using permeabilized fiber preparations, is that the susceptibility of dystrophic muscles

to contraction-mediated damage could also disrupt normal excitation-contraction coupling, and thus subsequently affect (post-stretch) force generation.



A. Typical force trace of a maximally activated single permeabilized fibre before and after a single stretch of 20% strain. Upper trace shows the magnitude (20% strain relative to muscle fibre length) and duration (400 ms) of the ramp stretch, performed at 0.5 fibre lengths/s. Lower trace shows the corresponding force response during stretch. Note that the fibre has attained maximum isometric force before the stretch has been imposed. **B.** Force deficit is calculated as the difference in maximum isometric force (P_o) after stretch compared with before stretch, expressed as a percentage of the pre-stretch maximum isometric force.

New directions for clinical strategies: Protecting dystrophic muscles from contraction-induced injury

For clinical application, any therapy for muscular dystrophy, whether it be gene-based, cell-based, or

pharmacological in nature, must not increase the likelihood of contraction-mediated damage. This is especially relevant for therapies that do not replace the functional protein and serve to ameliorate the dystrophic pathology and either increase or decrease muscle fibre size. A long-held contention was that larger, fast muscle fibres were most susceptible to contraction-induced injury and that this explained why smaller calibre fibres were relatively spared from the dystrophic pathology.^{39,40} This notion has been challenged more recently by studies in mice that have blocked the myostatin gene product (a negative regulator of muscle size) either through transgenic approaches or through the use of antibodies, and produced *mdx* mice with larger and stronger muscles and with an attenuated dystrophic pathology.^{41,42} Although assessments of muscle function were not performed on the more severely affected diaphragm, the lesser dystrophic pathology highlighted the possibility that larger muscle fibres might be less susceptible to contraction-mediated damage.⁴³ This is an important question that needs to be addressed carefully through future experiments employing the contraction-induced injury assays described earlier. One approach could be to increase muscle fibre size through administration of anabolic agents, such as a β_2 -agonist. In a preliminary study, Lynch and colleagues⁴⁴ examined whether long-term (18 weeks') clenbuterol treatment in mice affected muscle fibre susceptibility to contraction-induced injury. After a single stretch of 20% strain relative to fibre length, no difference was evident in the force deficit of permeabilized fibres from EDL muscles of treated and untreated mice. These preliminary findings suggest that although β_2 -agonists increase skeletal muscle mass and fibre size, they do not increase muscle fibre susceptibility to contraction-induced injury.⁴⁴

Given the continual development of new therapeutic strategies for treating neuromuscular disorders, assessments of muscle (fibre) susceptibility to contraction-induced injury will become increasingly important as a tool for evaluating treatment efficacy and their overall clinical significance.

Acknowledgements

Supported by grants from the Muscular Dystrophy Association (USA).

References

1. Koenig M, Monaco AP, Kunkel LM. The complete sequence of dystrophin predicts a rod-shaped cytoskeletal protein. *Cell* 1988; **53**: 219-226.
2. Durbeej M, Campbell KP. Muscular dystrophies involving the dystrophin-glycoprotein complex: an overview of current mouse models. *Curr. Opin. Gen. Dev.* 2002; **12**: 349-361.
3. Hoffman EP, Brown RH, Kunkel LM. Dystrophin: the protein product of the Duchenne muscular dystrophy locus. *Cell* 1987; **51**: 919-928.
4. Stedman HH, Sweeney HL, Shrager JB, Maguire HC, Panettieri RA, Petrof BJ, Narusawa M, Leferovich JM, Sladky JT, Kelly AM. The *mdx* mouse diaphragm reproduces the degenerative changes of Duchenne muscular dystrophy. *Nature* 1991; **352**: 536-538.
5. Dupont-Versteegden EE, McCarter RJ. Differential expression of muscular dystrophy in diaphragm versus hind limb muscles of *mdx* mice. *Muscle Nerve* 1992; **15**: 1105-1110.
6. Petrof BJ, Shrager JB, Stedman HH, Kelly AM, Sweeney HL. Dystrophin protects the sarcolemma from stresses developed during muscle contraction. *Proc. Natl. Acad. Sci. USA* 1993; **90**: 3710-3714.
7. Lynch GS, Rafael JA, Hinkle RT, Cole NM, Chamberlain JS, Faulkner JA. Contractile properties of diaphragm muscle segments from old *mdx* and old transgenic *mdx* mice. *Am. J. Physiol.* 1997; **272**: C2063-C2068.
8. Lynch GS, Hinkle RT, Chamberlain JS, Brooks SV, Faulkner JA. Force and power output of fast and slow skeletal muscles from *mdx* mice 6-28 months old. *J. Physiol.* 2001; **535**: 591-600.
9. Williams MW, Bloch RJ. Extensive but coordinated reorganization of the membrane skeleton in myofibers of dystrophic (*mdx*) mice. *J. Cell Biol.* 1999; **144**: 1259-1270.
10. Bloch RJ, Gonzalez-Serratos H. Lateral force transmission across costameres in skeletal muscle. *Exerc. Sport Sci. Rev.* 2003 **3**: 73-78.
11. Ervasti JM. Costameres: the Achilles' heel of Herculean muscle. *J. Biol. Chem.* 2003; **278**: 13591-13594.
12. Tidball JG, Law DJ. Dystrophin is required for normal thin filament-membrane associations at myotendinous junctions. *Am. J. Pathol.* 1991; **138**: 17-21.
13. Grange RW, Gainer TG, Marschner KM, Talmadge RJ, Stull JT. Fast-twitch skeletal muscles of dystrophic mouse pups are resistant to injury from acute mechanical stress. *Am. J. Physiol.* 2002; **283**: C1090-C1101.
14. Faulkner JA. Terminology for contractions of muscles during shortening, while isometric, and during lengthening. *J. Appl. Physiol.* 2003; **95**: 455-459.
15. Morgan DL, Proske U. Popping sarcomere hypothesis explains stretch induced muscle damage. *Proc. Aust. Physiol. Pharmacol. Soc.* 2004; **34**: ???-???
16. Crosbie, R.H. NO vascular control in Duchenne muscular dystrophy. *Nature Med.* 2001; **7**: 27-29.
17. Hutter OF, Burton FL, Bovell DL. Mechanical properties of normal and *mdx* mouse sarcolemma: bearing on function of dystrophin. *J. Muscle Res. Cell Motil.* 1991; **12**: 585-589.
18. Menke A, Jockusch H. Decreased osmotic stability of dystrophin-less muscle cells from the *mdx* mouse. *Nature* 1991; **349**: 69-71.
19. Reeve JL, McArdle A, Jackson MJ. Age-related changes in muscle calcium content in dystrophin-deficient *mdx* mice. *Muscle Nerve* 1997; **20**: 357-360.

20. Straub V, Rafael JA, Chamberlain JS, Campbell KP. Animal models for muscular dystrophy show different patterns of sarcolemmal disruption. *J. Cell Biol.* 1997; **139**: 375-385.
21. Bansal D, Miyake K, Vogel SS, Groh S, Chen CC, Williamson R, McNeil PL, Campbell KP. Defective membrane repair in dysferlin-deficient muscular dystrophy. *Nature* 2003; **423**: 168-172.
22. Weller B, Karpati G, Carpenter S. Dystrophin-deficient *mdx* muscle fibers are preferentially vulnerable to necrosis induced by experimental lengthening contractions. *J. Neurol. Sci.* 1990; **100**: 9-13.
23. Clarke MSF, Khakee R, McNeil PL. Loss of cytoplasmic basic fibroblast growth factor from physiologically wounded myofibers of normal and dystrophic muscle. *J. Cell Sci.* 1993; **106**: 121-133.
24. Moens P, Baatsen PHWW, Maréchal G. Increased susceptibility of EDL muscles from *mdx* mice to damage induced by contractions with stretch. *J. Muscle Res. Cell Motil.* 1993; **14**: 446-451.
25. Deconinck N, Ragot T, Maréchal G, Perricaudet M, Gillis JM. Functional protection of dystrophic mouse (*mdx*) muscles after adenovirus-mediated transfer of a dystrophin minigene. *Proc. Natl. Acad. Sci. USA.* 1996; **93**: 3570-3574.
26. Brooks SV. Rapid recovery following contraction-induced injury to *in situ* skeletal muscles in *mdx* mice. *J. Muscle Res. Cell Motil.* 1998; **19**: 179-187.
27. Sacco P, Jones DA, Dick JRT, Vrbová G. Contractile properties and susceptibility to exercise-induced damage of normal and *mdx* mouse tibialis anterior muscle. *Clin. Sci.* 1992; **82**: 227-236.
28. Decrouy A, Renaud J-M, Davis HL, Lunde JA, Dickson G, Jasmin BJ. Mini-dystrophin gene transfer in *mdx^{Acv}* diaphragm muscle fibers increases sarcolemmal stability. *Gene Ther.* 1997; **4**: 401-408.
29. McArdle A, Edwards RHT, Jackson MJ. Effects of contractile activity on muscle damage in the dystrophin-deficient *mdx* mouse. *Clin. Sci.* 1991; **80**: 367-371.
30. Harper SQ, Hauser MA, DelloRusso C, Duan D, Crawford RW, Phelps SF, Harper HA, Robinson AS, Engelhardt JF, Brooks SV, Chamberlain JS. Modular flexibility of dystrophin: implications for gene therapy of Duchenne muscular dystrophy. *Nature Med.* 2002; **8**: 253-261.
31. DelloRusso C, Crawford RW, Chamberlain JS, Brooks SV. Tibialis anterior muscles in *mdx* mice are highly susceptible to contraction-induced injury. *J. Muscle Res. Cell Motil.* 2001; **22**: 467-475.
32. DelloRusso C, Scott JM, Hartigan-O'Connor D, Salvatori G, Barjot C, Robinson AS, Crawford RW, Brooks SV, Chamberlain JS. Functional correction of adult *mdx* mouse muscle using gutted adenoviral vectors expressing full-length dystrophin. *Proc. Natl. Acad. Sci. USA.* 2002; **99**: 12979-12984.
33. Consolino CM, Brooks SV. Susceptibility to sarcomere injury induced by single stretches of maximally activated muscles of *mdx* mice. *J. Appl Physiol.* 2004; **96**: 633-638.
34. Plant DR, Lynch GS. Depolarization-induced contraction and SR function in mechanically skinned fast muscle fibers from dystrophic *mdx* mice. *Am. J. Physiol.* 2003; **285**: C522-C528.
35. Yeung EW, Head SI, Allen DG. Gadolinium reduces short-term stretch-induced muscle damage in isolated *mdx* mouse muscle fibres. *J. Physiol.* 2003; **552**: 449-458.
36. Eastwood AM, Wood DS, Bock KL, Sorenson MM. Chemically skinned mammalian skeletal muscle. I. The structure of skinned rabbit psoas. *Tissue Cell* 1979; **11**: 553-566.
37. Lynch GS, Rafael JA, Chamberlain JS, Faulkner JA. Contraction-induced injury to single permeabilized muscle fibers from *mdx*, transgenic *mdx*, and control mice. *Am. J. Physiol.* 2000; **279**: C1290-C1294.
38. Street, S.F. Lateral transmission of tension in frog myofibers: a myofibrillar network and transverse cytoskeletal connections are possible transmitters. *J. Cell. Physiol.* 1983; **114**: 346-364.
39. Karpati G, Carpenter S, Prescott S. Small-caliber skeletal muscle fibers do not suffer necrosis in *mdx* mouse dystrophy. *Muscle Nerve* 1988; **11**: 795-803.
40. Bogdanovich S, Krag TOB, Barton ER, Morris LD, Whittenmore L-A, Ahima RS, Khurana TS. Functional improvement of dystrophic muscle by myostatin blockade. *Nature* 2002; **420**: 418-421.
41. Webster C, Silberstein L, Hays AP, Blau HM. Fast muscle fibers are preferentially affected in Duchenne muscular dystrophy. *Cell* 1988; **52**: 503-513.
42. Wagner KR, McPherron AC, Winik N, Lee, S-J. Loss of myostatin attenuates severity of muscular dystrophy in *mdx* mice. *Ann. Neurol.* 2002; **52**: 832-836.
43. Zammit PS, Partridge TA. Sizing up muscular dystrophy. *Nature* 2002; **8**: 1355-1356.
44. Lynch GS, Cole NM, Hinkle RT, Faulkner JA. Muscle force and power and single fiber susceptibility to contraction-induced injury following chronic clenbuterol treatment in mice. *Med. Sci. Sports Exerc.* 1996; **28** (Suppl): 167.

Received 24 March 2004, in revised form 14 April 2004.

Accepted 15 April 2004.

©G.S. Lynch 2004.

Author for correspondence:

Assoc. Prof. Gordon S. Lynch
Department of Physiology
The University of Melbourne
Victoria 3010, Australia

Tel: +61 3 8344 0065

Fax: +61 3 8344 5818

Email: gsl@unimelb.edu.au

Factors, fiction and endothelium-derived hyperpolarizing factor - EDH(F)

Shaun L. Sandow

Division of Neuroscience,
John Curtin School of Medical Research,
Australian National University,
Canberra, ACT 0200 Australia
and
Department of Pharmacy and Pharmacology,
University of Bath,
Claverton Down, Bath, BA2 7AY, UK

Summary

1. The principal mediators of vascular tone are neural, endothelial and physical stimuli that result in the initiation of dilator and constrictor responses to facilitate the control of blood pressure. Two primary vasodilatory stimuli produced by the endothelium are nitric oxide (NO) and prostaglandins. An additional endothelium dependent vasodilatory mechanism is characterized as the hyperpolarization mediated relaxation that remains after the inhibition of the synthesis of NO and prostaglandins. This mechanism is due to the action of a so-called endothelium-derived hyperpolarizing factor (EDHF) and is dependent on either the release of diffusible factor(s) and/or to a direct contact-mediated mechanism.

2. Most evidence supports the concept that 'EDHF' activity is dependent on contact-mediated mechanisms. This involves the transfer of an endothelium-derived electrical current, as an endothelium-derived hyperpolarization (EDH), through direct heterocellular coupling of endothelial cells (ECs) and smooth muscle cells (SMCs) via myoendothelial gap junctions (MEGJs). However, there is a lack of consensus with regard to the nature and mechanism of action of EDHF/EDH (EDH(F)), which has been shown to vary within and between vascular beds, as well as among species, strains, sex and during development, ageing and disease.

3. In addition to actual heterogeneity in EDH(F), further heterogeneity has resulted from the less than optimal design, analysis and interpretation of data in some key papers in the EDHF literature; with such views being perpetuated in the subsequent literature.

4. The focus of this brief review is to examine what factors are proposed as EDH(F), and highlight the correlative structural and functional studies from our laboratory that demonstrate an integral role for MEGJs in the conduction of EDH which account for the heterogeneity in EDH(F); whilst incorporating the reported diffusible mechanisms in the regulation of this activity. Furthermore, in addition to the reported heterogeneity in the nature and mechanism of action of EDH(F), the contribution of experimental design and technique to this heterogeneity will be examined.

What is EDH(F)?

The aim of this brief review is to provide a critical overview of the EDH(F) field, with a focus on the role of gap junctions in the EDH(F) phenomenon. More extensive reviews on EDHF are provided by McGuire *et al.*,¹ Campbell and Gauthier,² Ding and Triggle,³ and Griffith.⁴

Briefly, the arterial endothelium produces three vasodilatory factors; NO, prostaglandins and EDH(F). Classically, EDH(F) is the hyperpolarization and associated relaxation remaining after the inhibition of the synthesis of NO synthase (and thus NO) and prostaglandins. The two primary mechanisms that can account for EDH(F) activity rely on either diffusible- and/or contact-mediated mechanisms. Those that are dependent on the release of a diffusible substance, for which there is yet to be unequivocal evidence, are due to EDHF. Those that are dependent on the direct contact of ECs and SMCs via MEGJs are due to the transfer of an electrical current, as an EDH.⁴⁻⁹ In both cases, the net result is the hyperpolarization of the adjacent smooth muscle with subsequent vessel dilation. For clarity the term EDH(F) will be used here to refer to both a diffusible or contact-mediated mechanism.

Regardless of whether a diffusible- or contact-mediated mechanism is involved in EDH(F) activity, it is accepted that its action is dependent on the release of intracellular calcium and the activation of a specific pattern of potassium channels. The activation of receptors and/or application of physical stimuli such as shear stress results in a rise in intracellular EC calcium.^{1,4,10} Subsequently, this results in the activation of small (S) and intermediate (I) conductance calcium activated potassium channels (K_{Ca}) located on ECs, and in some cases the activation of EC or SMC large (B) K_{Ca} .¹ This channel activation results in the generation of an EDH or the release of an EDHF, which is subsequently transmitted to the adjacent SMC layer either via MEGJs or by diffusion.^{1,2} Indeed, it is agreed that EDH(F) activity is blocked by the application of K_{Ca} antagonists, such as apamin (SK_{Ca} antagonist) and charybdotoxin (non-selective IK_{Ca} and BK_{Ca} antagonist, with additional effects at voltage-dependent potassium channels³) in combination,^{1,2} or apamin and TRAM-34 (IK_{Ca} antagonist) in combination,^{4,11,12} in the case of SK_{Ca} and IK_{Ca} dependent responses, or by iberiotoxin in the case of BK_{Ca} dependent responses.²

The nature and mechanism of EDH(F) apparently

varies within and between vascular beds and amongst species, strains, sex and during development, ageing and disease,¹⁻³ as well as with variable experimental conditions and between laboratories.⁴ A proposal for unifying the role of EDH(F) and heterocellular coupling has recently been put forward by Griffith⁴ This scheme incorporates many of the proposed EDH(F)s, and questions others, for which there is debatable evidence.

Diffusible factors

Contact-mediated mechanisms represent the simplest explanation of EDH(F) activity, as a purely electrical event. However, the release of diffusible factors/s from the endothelium, at a concentration sufficient to change that of the internal elastic lamina and the local environment surrounding the innermost layer of SMCs, has also been proposed to account for EDH(F) activity. This substance then putatively effects the activation of SMC receptors and ion channels, to initiate smooth muscle hyperpolarization and relaxation.¹⁻⁴

Diffusible factors proposed as an EDHF include K⁺ ions, epoxyeicosatrienoic acids (EETs), H₂O₂,^{1,2} and C-type natriuretic peptide (CNP)¹³. N^ω-nitro-L-arginine methyl ester (L-NAME) insensitive nitric oxide has also been suggested to account for EDHF activity.^{14,15} In addition, S-nitrosothiols have been suggested to contribute to EDHF activity,¹⁶ although the evidence for the endothelial dependence of this response requires further investigation.

Potassium ions

Several studies have supported the proposal that K⁺ ions are an EDHF in some vessels (for references see 1,3,4,17). Indeed, since the original proposition that K⁺ ions were an EDHF, this hypothesis has received much attention. Basically, this scheme involves the activation of EC K_{Ca} and the subsequent EC efflux of K⁺ from these channels. The resultant potassium 'cloud'¹⁷ then reportedly diffuses across the internal elastic lamina to act as an EDHF by evoking smooth muscle hyperpolarization and relaxation, via the activation of smooth muscle Na⁺/K⁺ATPase and inwardly rectifying potassium channels;¹⁷ key channels for the modulation of ionic mechanisms that are reportedly sensitive to the application of ouabain and barium, respectively. Antagonism of the EDHF response by these blockers is used as defining evidence for K⁺ as an EDHF. In its current form this mechanism is referred to as the 'potassium cloud hypothesis'.¹⁷

A complication to this hypothesis is the efflux of K⁺ from SMCs that arises as a result of depolarization, which would thus contribute to the basal level of K⁺ surrounding vascular cells, and will thus suppress the K⁺/EDHF effect. At a simplistic level the term 'potassium cloud' is misleading, in that it implies the presence of a global cloud of potassium surrounding the vascular cells, when in fact any physiologically relevant change in the K⁺ concentration will be transient and localized. Indeed, a more plausible scenario is that the K⁺ flux acts at restricted localized sites (microdomains), as has been described in SMCs and other

cell types.¹⁸

Interestingly, the most recent version of the 'potassium cloud hypothesis' includes a role for MEGJs in the action of K⁺ as EDHF.¹⁷ However, once a role for MEGJs is included in this mechanism, a role for K⁺ as a diffusible EDHF may be redundant, since the EDHF phenomenon can be simply explained through the action of EDH. As alluded to above, a potential scenario where the diffusion of K⁺ may play a role in the EDHF activity could arise if there is a close spatial relationship between MEGJs and K_{Ca} distribution (as well as perhaps with sites of calcium extrusion), in the form of microdomains, where highly localized changes in K⁺ concentrations could play a role in the coordination and modulation of heterocellular-EDH(F) signaling (Garland and Sandow, personal communication). Whilst evidence for similar functional microdomains in SMCs and other cell types is well documented,¹⁸ it is interesting to speculate that this scenario may be the case in ECs of resistance vessels such as the mesenteric bed of the rat where functional studies have suggested this to occur.¹⁹ Further anatomical support for the existence of microdomains in ECs is not currently available in resistance vessels, and thus a role for a K⁺ in this scenario is speculative.

Epoxyeicosatrienoic acids (EETs)

There is evidence of a role for EETs in EDH(F) activity in some vascular beds.^{1,2} EETs are cytochrome P450 epoxygenase metabolites of phospholipase dependent arachidonic acid production, which putatively activate smooth muscle BK_{Ca}²⁰ to result in hyperpolarization and arterial relaxation in cerebral, coronary and renal arteries of several species.^{1,2} Indeed, although there is evidence that EETs play an integral role in EDH(F) activity in some vascular beds, EETs are not a universal EDH(F), in that in many vascular beds, EDH(F) activity is not sensitive to the application of iberiotoxin, a BK_{Ca} antagonist.⁴ Furthermore, it is not clear if EETs activity is related to their participation in the facilitation of autocrine pathways that generate hyperpolarization via mechanisms that are indistinct from alternative agonist-induced pathways that result in an analogous activation of an EDH(F) type response.⁴

Hydrogen peroxide

In human and mouse mesenteric and porcine coronary arteries, H₂O₂ has been proposed to act as an EDHF.²¹⁻²⁴ However, a primary problem with these studies is that the appropriate time and concentration controls for catalase, as a H₂O₂ antagonist, were not undertaken and indeed the proposal that H₂O₂ is an EDHF in these vascular beds is not consistent with several other studies undertaken in the same vascular beds (see below). Beny and von der Weid,²⁵ for example, have shown that EDHF and H₂O₂ are distinct factors in porcine coronary arteries, whilst Pomposiello *et al.*²⁶ demonstrate that catalase, an enzyme inhibitor H₂O₂ of activity, has no effect in porcine coronary vessels; although at 300U/ml it did abolish the endothelium

independent relaxation to exogenously generated H_2O_2 after 45min incubation. Catalase has been shown to have no effect on EDHF in the bovine ciliary, rat saphenous and mesenteric and human radial and subcutaneous arteries.^{9,27-30} In this light, several studies have shown that H_2O_2 can cause a vasoconstriction (see ^{31,32}, for example) which can be attenuated by a 20min incubation in 100U/ml catalase.³³ Furthermore, in a membrane potential independent manner, reactive oxygen species such as H_2O_2 have been reported to variably activate SMC K_{Ca} , ATP-sensitive potassium channels, Na^+/K^+ ATPase and modulate the sensitivity of the contractile apparatus to calcium,^{4,10} thus playing additional roles unrelated to EDHF, but complicating any speculative role for H_2O_2 in EDHF activity. Indeed, in contrast to the original proposition that H_2O_2 was an EDHF in mouse mesenteric vessels Ellis *et al.*³⁴ provide evidence that H_2O_2 is not an EDHF in these vessels. Indeed, Ellis *et al.*³⁴ found that an inhibitory effect of catalase does not provide definitive evidence that H_2O_2 is critical to a given vascular response.¹⁰

In any event, the physiological relevance of H_2O_2 as an EDHF is simply questioned based on the observation that the concentration of H_2O_2 produced in response to endothelial stimulation (10-60nM³⁵; see ⁴) is substantially less than the 3 μ M to 100 μ M of H_2O_2 required to elicit a 30 to 90% relaxation in human mesenteric vessels²² or the 0.1mM and 1mM of H_2O_2 required to elicit a 60 and 100% relaxation in porcine coronary arteries.²⁵ In addition, concentration dependent effects of H_2O_2 are critical to the question of whether physiological or pathophysiological effects are observed, since H_2O_2 can mediate vascular cell proliferation, apoptosis, hyperplasia, cell adhesion and migration, as well as having effects on arterial tone.¹⁰ Indeed, predominant evidence supports the proposition that H_2O_2 is not involved in the hyperpolarization dependent EDHF response and that it is not an EDHF.^{10,36}

C-type natriuretic peptide (CNP)

C-type natriuretic peptide has been proposed to act as an EDHF¹³ and indeed the data presented in Chauhan *et al.*¹³ are consistent with the activation of the CNP receptor C subtype playing a role in the EDH(F) phenomenon. However, in the same mesenteric vessels as examined in Sprague-Dawley rats by Chauhan *et al.*,¹³ but in the mature Wistar rat, Sandow *et al.*³⁷ demonstrate that heterocellular coupling of ECs and SMCs accounts for EDH activity in this bed. Whilst the difference between the two studies could be related to strain variation, such a fundamental difference is unlikely and the specific reason for the discrepancy is unknown. Interestingly, in this light, the use of the non-selective gap junction antagonist glycyrrhetic acid (GA) and its derivatives have implicated a primary role for gap junctional coupling in EDH(F) activity in this vascular bed.³⁸⁻⁴¹ Indeed, Chauhan *et al.*,¹³ implicate a role for MEGJs in the proposal that CNP is EDH(F) via the use of α -GA, although at present this role is currently unknown, but is being investigated (Ahluwalia, personal communication). In any case, a role for MEGJs in the

activity of CNP as EDH(F) is based on the assumption that GA is a specific antagonist for MEGJs and since no control studies for the effects of GA were undertaken in the Chauhan *et al.*¹³ study, this claim is open to question. Indeed, GA and its derivatives have been shown to block homocellular and MEGJs in this vessel,^{39,41} as well as having direct effects on the EC hyperpolarization to acetylcholine (ACh), via effects on phospholipase activity, and EC SK_{Ca} , IK_{Ca} and Na^+/K^+ ATPase, irrespective of its putative effect at gap junctions.^{6,42} A limitation of future studies examining a potential role for CNP as an EDH(F), is the lack of availability of selective antagonists for the CNP receptor-C subtype that is reported to mediate this response. Furthermore, specific limitations of the Chauhan *et al.* study¹³ include; the lack of a demonstration that the CNP-mediated relaxation can occur independently of the endothelium (which would thus demonstrate CNP action at the smooth muscle) and a lack of explanation of the observations that CNP evokes ~60 to 70% relaxation, whilst EDHF evokes ~100% relaxation. Additionally, there is also a lack of explanation as to why the (non-specific) blockade of gap junctions with GA suppresses CNP activity, or what effects barium alone has on the CNP- and EDHF-mediated relaxations, or the inclusion of appropriate control data to determine if there was a basal release of CNP in these mesenteric vessels. Thus, a definitive role for CNP in EDH(F) activity remains to be elucidated.

L-NAME insensitive nitric oxide

Endogenous or basal NO activity, which is insensitive to the application of NO synthase antagonists used in the routine study of EDH(F), has been suggested to account for EDH(F) activity.^{14,15} Current evidence suggests that in some vascular beds, under specific experimental conditions, this L-NAME insensitive NO may account for a *minor* degree of EDH(F) activity and one not consistently observed in studies of the same vascular bed. For example, in the Chauhan *et al.* study,¹⁵ purporting to show that L-NAME insensitive NO accounts for a *significant* portion of EDH(F) activity, 63% of hyperpolarization and 70% of relaxation to ACh remain after the addition of the NO scavenger oxyhaemoglobin (in the presence of L-NAME and indomethacin). Furthermore, in the caudal and saphenous arteries of the rat and mesenteric artery of the mouse the NO scavengers hydroxocobalamin and carboxy-PTIO have no effect on EDH(F);^{9,24,43} thus demonstrating a lack of an L-NAME insensitive NO component in these vascular beds. The contribution of endogenous NO to EDH(F) activity therefore appears variable and in many cases non-existent. Further studies are required to determine the physiological relevance of this phenomenon.

Contact-mediated mechanisms

Evidence supporting the critical role of MEGJs in EDH(F) activity comes primarily from structural and functional studies from our laboratory in Canberra and Tudor Griffith's^{4,36,44,45} laboratory in Cardiff. These studies, which illustrate the simplest explanation of EDH(F)

activity, utilize the electron microscopic identification of MEGJs, electrophysiological recordings from dye identified ECs and SMCs and myography with pharmacological interventions, as well as immunohistochemical methods for identifying the connexins and ion channels involved in the EDH(F) phenomenon. These studies are consistent with the hypothesis that EDH(F) is an electrical phenomenon involving the gap junctional transfer of an EDH, from ECs to the innermost layer of intimal SMCs in the arterial wall, for the subsequent generation of an arterial relaxation.

Studies from our laboratory, which are the focus of this section of the review, have examined the role of MEGJs in EDH activity. We have found that the distribution and activity of MEGJs is correlated with the presence of EDH within and between vascular beds, during development and in disease. In the proximal and distal mesenteric arteries of the rat, for example, gap junctions play a critical role in EDH activity,^{39,41} where MEGJs are prevalent.⁴⁶ In this vascular bed, in collaborative studies with Marianne Tare in Helena Parkington's laboratory in Melbourne, we showed that the presence of EDH is correlated with the presence of MEGJs, whilst in the femoral artery a lack of MEGJs is correlated with the absence of EDH.³⁷ A similar situation is present in the lateral saphenous artery of the juvenile rat, where MEGJs are prevalent and EDH-mediated relaxation present.⁹ This is in contrast to the saphenous artery of the adult, where MEGJs were rare and EDH absent.⁹ The relationship between EDH and MEGJs is somewhat more complicated in disease states, such as in hypertension. In a comparative study of the caudal artery of the hypertensive SHR and normotensive WKY rat, EDH activity was maintained, in spite of an increase in the number of SMC layers in the vessels from the hypertensive rat. This maintenance was found to be correlated with a concomitant increase in the incidence of MEGJs in the caudal artery of the hypertensive rat.⁴³

The above studies demonstrate there is a direct relationship between the degree of EDH and the incidence of MEGJs. Indeed, EDH increases with an increase in the number of MEGJs per EC, whilst, conversely, it generally decreases with an increase in the number of SMC layers and vessel diameter (Figure 1). Interestingly, whilst EDH is the predominant vasodilator in smaller vessels, it is present in some larger vessels (Figure 1), such as the rabbit iliac, rat caudal and superior mesenteric arteries.^{41,43,45} In the rabbit iliac artery cAMP has been proposed to enhance the spread of EDH via modulating gap junctional coupling within the multiple SMC layers, as well as at MEGJs.⁴⁷ Whilst conclusive biophysical evidence for this mechanism being relevant in larger vessels is lacking,⁴⁸ this mechanism may be of some importance for EDH activity in larger vessels.

These studies demonstrate that there is a consistent positive correlation between MEGJs and EDH activity within and between vascular beds and during development and disease. Whilst this correlation is not definitive evidence that contact-mediated mechanisms account for EDH(F) activity, to date, these data provide the most conclusive and plausible explanation for this activity.

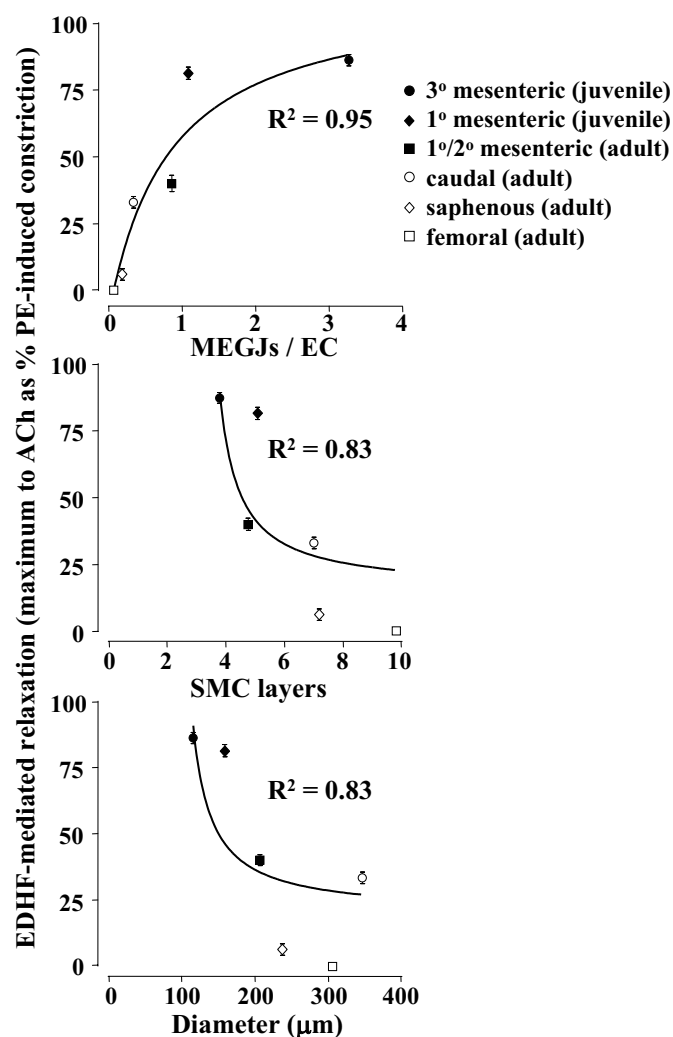


Figure 1. Summary data demonstrating the relationship between acetylcholine (ACh)-induced EDH(F) activity and arterial morphology as the number of myoendothelial gap junctions (MEGJs) per endothelial cell (EC), per number of medial smooth muscle cell (SMC) layer and per vessel diameter. Individual data points are presented as the mean \pm SEM with data being derived from earlier studies.^{9,37,43,46} Data were fitted with a one phase exponential curve using Graphpad Prism. PE, phenylephrine.

Role of diffusible factors in contact-mediated mechanisms

Direct electrical coupling is the most plausible mechanism to fully account for EDH activity. Indeed, there is increasing evidence that the diffusible factors, that act as credible EDHFs, may in fact be associated with the modulation of gap junction activity and specifically of MEGJs,⁴ for the transfer of EDH, as the most plausible mechanism of their activity. These mechanisms are outlined below.

Potassium ions

The original hypothesis regarding the mechanism of action of K^+ as EDHF has been modified to include a role for MEGJs.¹⁷ However, although K^+ are involved in mediating EDH(F) activity, once a role for such MEGJs is included, no direct role for K^+ as a diffusible EDHF is necessary for the transfer of an EDH. Indeed, in a series of experiments that repeated those in the original proposal that K^+ was EDHF, the data in the original study could not be repeated.⁴⁹ In addition, several studies have questioned the nature of K^+ as EDHF, since barium and ouabain, which are used to define the role of K^+ as an EDHF, do not universally block EDHF-mediated responses (for references see 1,3,4,17,50). Indeed, the efficacy of ouabain as a selective Na^+/K^+ ATPase antagonist has been questioned,^{4,51,52} whereby it has inhibitory effects on cell coupling via modulating gap junction function.⁵³ Indeed, ouabain may directly attenuate the transfer of EDH by its action at gap junctions.^{4,51,52} This action includes direct effects on gap junctional coupling, such as reducing connexin (Cx) expression through reduced Cx trafficking to the cell membrane, as well as modulating gap junction conductance.⁵² The implication of these observations is that the attenuation of an EDH(F) response by ouabain, as with high concentrations of potassium, does not necessarily provide evidence of the EDH(F) nature of the response.^{4,6,52} The demonstration that ouabain has direct effects on gap junctions, and thus on EDH(F), are essentially control studies for the earlier work that relied on the use of ouabain to show that K^+ was EDHF. Thus, based on these 'control' data^{4,51,52} K^+ ions are not an EDH(F), but rather may simply be involved in the modulation of the signal transduction pathways associated with gap junction function^{54,55} and thus with EDH activity.⁴ Further investigation is required to elucidate any potentially specific effects of ouabain on vasomotor responses and those at gap junctions. Indeed, this point is critical for the accurate interpretation of future EDH(F) data.

Epoxyeicosatrienoic acids (EETs)

In studies of cultured ECs, EETs have been shown to modulate homocellular gap junctions,⁵⁶ thus providing a potential mechanism for a modulatory role for EETs in EDH action.⁴ Griffith⁴ suggests that EETs activity may be related to a complex interaction of calcium and potassium homeostasis, cAMP and arachidonic acid activity and electrotonic signaling (see Figure 3 in ⁴ and also ⁵⁰). Indeed, EETs have also been suggested to be modulate EC K_{Ca} activity,⁵⁷ thus providing a further mechanism for their potential role in modulating EDH, independent of acting directly as an EDHF. Further studies of the role of EETs in EDH activity in intact vessels are required to clarify these proposals.

Hydrogen peroxide

There is some evidence that H_2O_2 can effect gap junction activity and calcium homeostasis; two factors that

are integral for EDH activity. Depending on the experimental conditions, studies have shown that H_2O_2 can both increase⁵⁸ and decrease⁵⁹ gap junctional coupling, and effect changes in intracellular calcium homeostasis, both in cultured cells and in intact arteries.⁵⁹⁻⁶¹ Although no specific evidence is currently available to support this proposal, these observations provide potential support for a mechanism to link the putative role of H_2O_2 as an EDH(F), with the MEGJ dependence of the EDH phenomenon.

C-type natriuretic peptide (CNP)

The putative action of CNP as an EDH(F)¹³, may be via acting as yet another factor that facilitates electrical coupling through gap junctions; although any putative mechanism for this is unknown. Indeed, any putative action for CNP as EDH(F) cannot be directly associated with the gap junctional transfer of CNP from ECs to SMCs, since gap junctions are limited to passing substances of ≤ 1 kD and CNP has a molecular weight of ~ 2.2 kD (Ahluwalia, personal communication). Interestingly, in the Chauhan *et al.* study¹³, proposing that CNP is an EDH(F), the response is sensitive to the combination of barium and ouabain, an observation that this is not a universal characteristic of EDH(F) in this, the rat mesenteric vascular bed.⁴⁹ Indeed, since ouabain is recognized as a non-specific gap junction antagonist, this result may in fact reflect a MEGJ dependence of EDH(F) in the mesenteric bed of the rat, as demonstrated by Sandow *et al.*³⁷

Myoendothelial gap junctions, EDH and gap junction inhibitors

The demonstration of the dependence of EDH activity on gap junctions relies, in part, on the specific pharmacological inhibition of gap junctions. Unfortunately, there are a number of limitations regarding this methodology. The primary one of these relates to the dependence on the use of gap junction inhibitors that have not been adequately characterized in terms of their specificity and mechanism of action. Currently, there is no unequivocal evidence that the available gap junction inhibitors are specific;⁶² let alone selective for gap junctions, be they heterocellular or homocellular. Indeed, unfortunately to date, few studies have examined this problem in detail and few have carried out the defining experiment of examining the effect of these agents on cell input resistance, whereby an increase in input resistance would provide key data on the gap junction antagonist effects of these agents. Of the studies that have carried out such technically demanding experiments, the data are not consistent and are incomplete; although this may in part reflect the heterogeneity in the Cx composition of vascular gap junctions.⁶³

Much of the current evidence for the gap junction and specifically MEGJ dependence of EDH relies on the utilization of the licorice derivatives (the GAs and carbenoxolone; see above for an outline of non-specific actions), the Cx-mimetic peptides (Gap26,⁴³ Gap27,⁴⁰ Gap27;^{37,43} which, based on putative selectivity, are the

current gap junction inhibitors of choice^{4,9,44}) and decreasingly, with the long chain alcohols, such as heptanol. However, there is little equivocal evidence that these agents are gap junction specific and that they do not induce other non-gap junctional effects. Whilst there is well documented (and often ignored) evidence for the non-specific effects of the licorice derivatives (see above) and heptanol (for example, ⁶⁴) the Cx-mimetic peptides, have not yet been equivocally tested for specificity, nor is their mechanism of action known. In this regard, a primary issue with the use of the Cx-mimetic peptides relates to the apparent requirement to use very high concentrations and long incubation times to attenuate gap junction activity.⁴ Interestingly, others report significant effects with lesser concentrations of the peptide/s and reduced incubation times.^{62,65,66} Clearly, there is a pressing need for these issues to be addressed.

Why is there such a disparity of views as to the nature and mechanism of action of EDH(F)?

The conventional reason given for the disparity of views as to the nature and mechanism of action of EDH(F) is that there is heterogeneity within and between arteries, species, sex, strain and disease states.^{1-4,10,17} However, a further cause of the heterogeneity relates to the less than optimal design, analysis and interpretation of data present in some key papers in the EDH(F) literature. Whilst some earlier studies can be seen as flawed with hindsight, this is not necessarily the case, since they may in fact represent significant contributions to the EDHF literature through their role in advancing the evolution of the field. Unfortunately, this is not always the case, and the perpetuation of now potentially misleading data is problematic. In any case, it is recognized that there is variation in the nature and mechanism of EDH(F) between laboratories,⁴ thus questioning the relevance of the data and conclusions of some studies.

The problems of experimental technique, with regard to the design, analysis and interpretation of data that contribute to the reported heterogeneity in the nature and mechanism of action of EDH(F) in the literature include:

1. The use of *selected* agonists, antagonists and/or modulators of the investigators choice and interest, but not those which may indicate an alternative nature or mechanism of EDH(F)(for references see ^{1,3,4,17}). That is, for example, an investigator may be interested in EETs or gap junctions to account for EDH(F) activity, but may thus limit the investigation to the use of antagonists of the mechanism of their interest, rather than of alternative pathways. This results in a potential for a bias in favor of a particular putative EDH(F)(for references see ^{1,3,4,17}).
2. The lack of control data for the effects of agonists, antagonists and other modulators. For instance, in the Matoba *et al.* studies²¹⁻²³ examining the role of H₂O₂ as an EDH(F), justification should be provided

as to the incubation time with catalase (2 hours or longer) as well as the high (and variable) concentration of catalase that was used.

3. The clear need for greater transparency with regard to variability in cell, vessel and species specific responses, as a result of a specific receptor and channel population, and associated signal transduction pathways (for references see ⁶³).
4. Making inappropriate comparative analyses between studies, including a lack of consideration of strain,^{67,68} age,^{9,69-71} sex,⁷²⁻⁷⁵ the use of intact versus isolated tissue and tension versus pressurized myography (for references see page 15 in ⁶³), as well as variation in the classification of arterial branching patterns.^{39,41,46} Indeed, such characteristics are often not stated in the methods section of papers and thus result in an inability to make comparative analyses between studies.
5. Lack of clarity and relevance as to the experimental protocol. For instance, under conditions of little or no vascular tone, use of buffers [such as HEPES],⁷⁷ that have non-physiological effects, the use of preconstrictor agents that adversely effect channel activity⁴ such as the effect of U46619 on SK_{Ca}⁷⁸ and the effect of the GA and related compounds on a variety of cell processes, as outlined above.
6. Extrapolation of data to other vascular beds. For example, Chauhan *et al.*^{13,15} examined EDH(F) in mesenteric vessels of the mature male Sprague Dawley rat, but extrapolate the data to be applicable to the vasculature as a whole. Whilst several studies have made such claims (for references see ^{1,3,4}), this contention merely confuses the field, as there is no evidence to justify this point of view.

Conclusions

The nature and mechanism of action of EDH(F) can apparently differ along and between vascular beds, between species, strains, sex and during development, ageing and disease. This heterogeneity can be explained through the action of heterocellular coupling. Indeed, contact-mediated mechanisms represent the simplest explanation of EDH(F) activity and involve the transfer of an endothelium-derived electrical signal to the smooth muscle via MEGJs, as EDH. Of the putative diffusion-mediated mechanisms, K⁺ ions have received much attention in the literature and whilst they might not be an EDHF, they are involved in the signal transduction pathways associated with the generation of the EDH and they may be involved in the modulation of gap junction activity. In a similar manner, there is good evidence of a role for EETs in EDH(F) activity in some vascular beds, although this role may be confined to a modulatory role of homo- and heterocellular coupling, as well as modulating the K_{Ca} component of the EDH mechanism. The role of CNP as an EDH(F) is yet to be clarified, but may also be related to the modulation of EDH

activity. Predominant evidence supports the proposition that H_2O_2 is not an EDH(F), although again, its activity may also be related to the modulation of gap junction function, and thus of EDH. L-NAME insensitive NO may account for a degree of EDH(F) activity in some vascular beds, but the extent of this is limited to only a minor part of such activity. Whilst the nature and mechanism of action of EDH(F) is in part be due to actual heterogeneity, it is also unfortunately due to a lack of consistent and sound scientific methodology.

Acknowledgements

This work was supported by the National Heart Foundation and National Health and Medical Research Council of Australia (NHMRC) and the Wellcome Trust. SLS was supported by a NHMRC Peter Doherty Fellowship. I thank Dr Alister McNeish for critical comments on the manuscript.

References

- McGuire JJ, Ding H, Triggle CR. Endothelium-derived relaxing factors: a focus on endothelium-derived hyperpolarizing factor(s). *Can. J. Physiol. Pharmacol.* 2001; **79**: 443-470.
- Campbell WB, Gauthier KM. What is new in endothelium-derived hyperpolarizing factors? *Curr. Opin. Nephrol. Hyperten Res.* 2002; **11**: 177-183.
- Ding H, Triggle CR. Contribution of EDHF and the role of potassium channels in the regulation of vascular tone. *Drug Dev. Res.* 2003; **58**: 81-89.
- Griffith TM. Endothelium-dependent smooth muscle hyperpolarization: do gap junctions provide a unifying hypothesis? *Brit. J. Pharmacol.* 2004; **141**: 881-903.
- Yamamoto Y, Imaeda K, Suzuki H. Endothelium-dependent hyperpolarization and intercellular electrical coupling in guinea-pig mesenteric arterioles. *J. Physiol.* 1999; **514**: 505-513.
- Coleman HA, Tare M, Parkington HC. K^+ currents underlying the action of endothelium-derived hyperpolarizing factor in guinea-pig and human blood vessels. *J. Physiol.* 2001; **531**: 359-373.
- Coleman HA, Tare M, Parkington HC. EDHF is not K^+ but may be due to spread of current from the endothelium in guinea pig arterioles. *Am. J. Physiol.* 2001; **280**: H2478-H2483.
- Coleman HA, Tare M, Parkington HC. Myoendothelial electrical coupling in arteries and arterioles and its implications for endothelium-derived hyperpolarizing factor. *Clin. Exp. Pharmacol. Physiol.* 2002; **29**: 630-637.
- Sandow SL, Goto K, Rummery N, Hill CE. Developmental dependence of EDHF on myoendothelial gap junctions in the saphenous artery of the rat. *J. Physiol.* 2004; **556**: 875-886.
- Ellis A, Triggle CR. Endothelium-dependent reactive oxygen species: their relationship to endothelium-dependent hyperpolarization and the regulation of vascular tone. *Can. J. Physiol. Pharmacol.* 2003; **81**: 1013-1028.
- Crane GJ, Walker SD, Dora KA, Garland CJ. Evidence for a differential cellular distribution of inward rectifier K channels in the rat isolated mesenteric artery. *J. Vasc. Res.* 2003; **40**: 159-168.
- Eichler I, Wibawa J, Grgic I, Knorr A, Brakemeier S, Pries AR, Hoyer J, Kohler R. Selective blockade of endothelial $Ca(2+)$ -activated small- and intermediate-conductance $K(+)$ -channels suppresses EDHF-mediated vasodilation. *Br. J. Pharmacol.* 2003; **138**: 594-601.
- Chauhan SD, Nilsson H, Ahluwalia A, Hobbs AJ. Release of C-type natriuretic peptide accounts for the biological activity of endothelium-derived hyperpolarizing factor. *Proc. Natl. Acad. Sci.* 2003; **100**: 1426-1431.
- Cohen RA, Plane F, Najibi S, Huk I, Malinski T, Garland CJ. Nitric oxide is the mediator of both endothelium-dependent relaxation and hyperpolarization of the rabbit carotid artery. *Proc. Natl. Acad. Sci.* 1997; **94**: 4193-4198.
- Chauhan S, Rahman A, Nilsson H, Clapp L, MacAllister R, Ahluwalia A. NO contributes to EDHF-like responses in rat small arteries: a role for NO stores. *Cardiovasc. Res.* 2003; **57**: 207-216.
- Batenburg WW, Popp R, Fleming I, de Vries R, Garredts IM, Saxena PR, Danser AH. Bradykinin-induced relaxation of coronary microarteries: S-nitrosothiols as EDHF? *Brit. J. Pharmacol.* 2004; **In Press**.
- Busse R, Edwards G, Feletou M, Fleming I, Vanhoutte PM, Weston A. EDHF: bringing the concepts together. *Trends Pharmacol. Sci.* 2002; **23**: 374-380.
- Poburko D, Kuo KH, Dai J, Lee CH, van Breemen C. Organellar junctions promote targeted Ca^{2+} signalling in smooth muscle: why two mechanisms are better than one. *Trends Pharmacol. Sci.* 2004; **25**: 8-15.
- Crane GJ, Gallagher NT, Dora KA, Garland CJ. Small and intermediate calcium-dependent K^+ channels provide different facets of endothelium-dependent hyperpolarization in rat mesenteric artery. *J. Physiol.* 2003; **553**: 183-189.
- Archer SL, Gragasin FS, Wu X, Wang S, McMurtry S, Kim DH, Platonov M, Koshal A, Hashimoto K, Campbell WB, Falck JR, Michelakis ED. Endothelium-derived hyperpolarizing factor in human internal mammary artery is 11,12-epoxyeicosatrienoic acid and causes relaxation by activating smooth muscle BK(Ca) channels. *Circulation.* 2003; **107**: 769-776.
- Matoba T, Shimokawa H, Nakashima M, Hirakawa Y, Mukai Y, Hirano K, Kanaide H, Takeshita A. Hydrogen peroxide is an endothelium-derived hyperpolarizing factor in mice. *J. Clin. Invest.* 2000; **106**: 1521-1530.
- Matoba T, Shimokawa H, Kubota H, Morikawa K, Fujiki T, Kunihiro I, Mukai Y, Hirakawa Y,

- Takeshita A. Hydrogen peroxide is an endothelium-derived hyperpolarizing factor in human mesenteric arteries. *Biochem. Biophys. Res. Commun.* 2002; **290**: 909-913.
23. Matoba T, Shimokawa H, Morikawa K, Kubota H, Kunihiro I, Urakami-Harasawa L, Mukai Y, Hirakawa Y, Akaike T, Takeshita A. Electron spin resonance detection of hydrogen peroxide as an endothelium-derived hyperpolarizing factor in porcine coronary microvessels. *Arterioscler. Thromb. Vasc. Biol.* 2003; **23**: 1224-1230.
 24. Morikawa K, Shimokawa H, Matoba T, Kubota H, Akaike T, Talukder MAH, Fujiki T, Maeda H, Takahashi S, Takeshita A. Pivotal role of Cu,Zn-superoxide dismutase in endothelium-dependent hyperpolarization. *J. Clin. Invest.* 2003; **112**: 1871-1879.
 25. Beny JL, der Weid PY. Hydrogen peroxide: an endogenous smooth muscle cell hyperpolarizing factor. *Biochem. Biophys. Res. Commun.* 1991; **176**: 378-384.
 26. Pomposiello S, Rhaleb NE, Alva M, Carretero OA. Reactive oxygen species: Role in the relaxation induced by bradykinin or arachidonic acid via EDHF in isolated porcine coronary arteries. *J. Cardiovasc. Pharmacol.* 1999; **34**: 567-574.
 27. Hamilton CA, McPhaden AR, Berg G, Pathi V, Dominiczak AF. Is hydrogen peroxide an EDHF in human radial arteries? *Am. J. Physiol.* 2001; **280**: H2451-H2455.
 28. McNeish AJ, Wilson WS, Martin W. Ascorbate blocks endothelium-derived hyperpolarizing factor (EDHF)-mediated vasodilatation in the bovine ciliary vascular bed and rat mesentery. *Br. J. Pharmacol.* 2002; **135**: 1801-1809.
 29. Kawabata A, Kubo S, Nakaya Y, Ishiki T, Kuroda R, Sekiguchi F, Kawao N, Nishikawa H. Distinct roles for protease-activated receptors 1 and 2 in vasomotor modulation in rat superior mesenteric artery. *Cardiovasc. Res.* 2004; **61**: 683-692.
 30. Luksha L, Nisell H, Kublickiene K. The mechanism of EDHF-mediated responses in subcutaneous small arteries from healthy pregnant women. *Am. J. Physiol.* 2004; **In Press**.
 31. Jin N, Packer CS, Rhoades RA. Reactive oxygen-mediated contraction in pulmonary arterial smooth muscle: cellular mechanisms. *Can. J. Physiol. Pharmacol.* 1998; **69**: 383-388.
 32. Gao YJ, Lee RM. Hydrogen peroxide induces a greater contraction in mesenteric arteries of spontaneously hypertensive rats through thromboxane A(2) production. *Br. J. Pharmacol.* 2001; **134**: 1639-1646.
 33. Ulker S, McMaster D, McKeown PP, Bayraktutan U. Impaired activities of antioxidant enzymes elicit endothelial dysfunction in spontaneous hypertensive rats despite enhanced vascular nitric oxide generation. *Cardiovasc. Res.* 2003; **59**: 488-500.
 34. Ellis A, Pannirselvam M, Anderson TJ, Triggle CR. Catalase has negligible inhibitory effects on endothelium-dependent relaxations in mouse isolated aorta and small mesenteric artery. *Br. J. Pharmacol.* 2003; **140**: 1193-1200.
 35. Cosentino F, Patton S, d'Uscio LV, Werner ER, Werner-Felmayer G, Moreau P, Malinski T, Luscher TF. Tetrahydrobiopterin alters superoxide and nitric oxide release in prehypertensive rats. *J. Clin. Invest.* 1998; **101**: 1530-1537.
 36. Chaytor AT, Edwards DH, Bakker LM, Griffith TM. Distinct hyperpolarizing and relaxant roles for gap junctions and endothelium-derived H₂O₂ in NO-independent relaxations of rabbit arteries. *Proc. Natl. Acad. Sci.* 2003; **100**: 15212-15217.
 37. Sandow SL, Tare M, Coleman HA, Hill CE, Parkington HC. Involvement of myoendothelial gap junctions in the actions of endothelium-derived hyperpolarizing factor. *Circ. Res.* 2002; **90**: 1108-1113.
 38. Edwards G, Feletou M, Gardener MJ, Thollon C, Vanhoutte PM, Weston AH. Role of gap junctions in the responses to EDHF in rat and guinea-pig small arteries. *Br. J. Pharmacol.* 1999; **128**: 1788-1794.
 39. Hill CE, Hickey H, Sandow SL. Role of gap junctions in acetylcholine-induced vasodilation of proximal and distal arteries of the rat mesentery. *J. Auton. Nerv. Syst.* 2000; **81**: 122-127.
 40. Doughty JM, Boyle JP, Langton PD. Blockade of chloride channels reveals relaxations of rat small mesenteric arteries to raised potassium. *Br. J. Pharmacol.* 2001; **132**: 293-301.
 41. Goto K, Fujii K, Kansui Y, Abe I, Iida M. Critical role of gap junctions in endothelium-dependent hyperpolarization in rat mesenteric arteries. *Clin. Exp. Pharmacol. Physiol.* 2002; **29**: 595-602.
 42. Tare M, Coleman HA, Parkington HC. Glycylrrhethinic derivatives inhibit hyperpolarization in endothelial cells of guinea pig and rat arteries. *Am. J. Physiol.* 2002; **282**: H335-H341.
 43. Sandow SL, Bramich NJ, Bandi HP, Rummery N, Hill CE. Structure, function and EDHF in the caudal artery of the SHR and WKY Rat. *Arterioscler. Thromb. Vasc. Biol.* 2003; **23**: 822-828.
 44. Chaytor AT, Martin PE, Edwards DH, Griffith TM. Gap junctional communication underpins EDHF-type relaxations evoked by ACh in the rat hepatic artery. *Am. J. Physiol.* 2001; **280**: H2441-H2450.
 45. Chaytor AT, Taylor HJ, Griffith TM. Gap junction-dependent and -independent EDHF-type relaxations may involve smooth muscle cAMP accumulation. *Am. J. Physiol.* 2002; **282**: H1548-H1555.
 46. Sandow SL, Hill CE. The incidence of myoendothelial gap junctions in the proximal and distal mesenteric arteries of the rat is suggestive of a role in EDHF-mediated responses. *Circ. Res.* 2000; **86**: 341-346.
 47. Griffith TM, Chaytor AT, Taylor HJ, Giddings BD, Edwards DH. cAMP facilitates EDHF-type relaxations in conduit arteries by enhancing electrotonic conduction via gap junctions. *Proc. Natl. Acad. Sci.* 2002; **99**: 6392-6397.

48. Diep HK, Vigmond EK, Welsh DG. Modelling of electrical communication in resistance arteries. *FASEB J.* 2004; **18**: A4236.
49. Vanheel B, Van de Voorde J: Effects of barium, ouabain and K⁺ on the resting membrane potential and endothelium-dependent responses in rat arteries; In: Vanhoutte PM (ed): EDHF 2000. London, Taylor and Francis, 2001, pp 146-155.
50. Dhein S. Pharmacology of gap junctions in the cardiovascular system. *Cardiovasc. Res.* 2004; **62**: 287-298.
51. Harris D, Martin PE, Evans WH, Kendall DA, Griffith TM, Randall MD. Role of gap junctions in endothelium-derived hyperpolarizing factor responses and mechanisms of K(+)-relaxation. *Eur. J. Pharmacol.* 2000; **402**: 119-128.
52. Martin PE, Hill NS, Kristensen B, Errington RJ, Griffith TM. Ouabain exerts biphasic effects on connexin functionality and expression in vascular smooth muscle cells. *Br. J. Pharmacol.* 2003; **140**: 1261-1271.
53. Ledbetter ML, Gatto CL. Concentrations of ouabain that prevent intercellular communication do not affect free calcium levels in cultured fibroblasts. *Cell Biochem. Funct.* 2003; **21**: 363-370.
54. Giaume C, Venance L: Characterization and regulation of gap junction channels in cultured astrocytes; In: Spray DC, Dermietzel R (eds): Gap junctions in the nervous system. Austin, TX, Landes, 1996, pp 136-157.
55. Pina-Benabou MH, Srinivas M, Spray DC, Scemes E. Calmodulin kinase pathway mediates the K⁺-induced increase in Gap junctional communication between mouse spinal cord astrocytes. *J. Neurosci.* 2001; **21**: 6635-6643.
56. Popp R, Brandes RP, Ott G, Busse R, Fleming I. Dynamic modulation of interendothelial gap junctional communication by 11,12-epoxyeicosatrienoic acid. *Circ. Res.* 2002; **90**: 800-806.
57. Baron A, Frieden M, Beny JL. Epoxyeicosatrienoic acids activate a high-conductance, Ca(2+)-dependent K⁺ channel on pig coronary artery endothelial cells. *J. Physiol.* 1997; **504**: 537-543.
58. Rouach N, Calvo CF, Duquenois H, Glowinski J, Giaume C. Hydrogen peroxide increases gap junctional communication and induces astrocyte toxicity: Regulation by brain macrophages. *Glia.* 2004; **45**: 28-38.
59. Todt I, Ngezahayo A, Ernst A, Kolb HA. Hydrogen peroxide inhibits gap junctional coupling and modulates intracellular free calcium in cochlear Hensen cells. *J. Membr. Biol.* 2001; **181**: 107-114.
60. Blanc EM, Bruce-Keller AJ, Mattson MP. Astrocytic gap junctional communication decreases neuronal vulnerability to oxidative stress-induced disruption of Ca²⁺ homeostasis and cell death. *J. Neurochem.* 1998; **70**: 958-970.
61. Touyz RM. Activated oxygen metabolites: do they really play a role in angiotensin II-regulated tone? *J. Hypertens.* 2003; **21**: 2235-2238.
62. Spray DC, Rozental R, Srinivas M. Prospects for rational development of pharmacological gap junction channel blockers. *Curr. Drug Targets.* 2002; **3**: 455-464.
63. Hill CE, Phillips JK, Sandow SL. Heterogeneous control of blood flow amongst different vascular beds. *Med. Res. Rev.* 2001; **21**: 1-60.
64. Hashitani H, Suzuki H. K⁺ channels which contribute to the acetylcholine-induced hyperpolarization in smooth muscle of the guinea-pig submucosal arteriole. *J. Physiol.* 1997; **501**: 505-513.
65. Dahl G, Nonner W, Werner R. Attempts to define functional domains of gap junction proteins with synthetic peptides. *Biophys. J.* 1994; **67**: 1816-1822.
66. Hill CE, Haddock RE, Brackenbury T. Role of the endothelium and gap junctions in cerebral vasomotion. *FASEB J.* 2004; **18**: A3631.
67. Kurtz TW, Morris RC, Jr. Biological variability in Wistar-Kyoto rats. Implications for research with the spontaneously hypertensive rat. *Hypertension.* 1987; **10**: 127-131.
68. Louis WJ, Howes LG. Genealogy of the spontaneously hypertensive rat and Wistar-Kyoto rat strains: implications for studies of inherited hypertension. *J. Cardiovasc. Pharmacol.* 1990; **16**: S1-S5.
69. Fujii K, Ohmori S, Tominaga M, Abe I, Takata Y, Ohya Y, Kobayashi K, Fujishima M. Age-related changes in endothelium-dependent hyperpolarization in the rat mesenteric artery. *Am. J. Physiol.* 1993; **265**: H509-H516.
70. Goto K, Fujii K, Onaka U, Abe I, Fujishima M. Angiotensin-converting enzyme inhibitor prevents age-related endothelial dysfunction. *Hypertension.* 2000; **36**: 581-587.
71. Goto K, Fujii K, Kansui Y, Iida M. Changes in EDHF in hypertension and ageing: response to chronic treatment with renin-angiotensin system inhibitors. *Clin. Exp. Pharmacol. Physiol.* 2004.
72. Huang A, Sun D, Koller A, Kaley G. Gender difference in flow-induced dilation and regulation of shear stress: role of estrogen and nitric oxide. *Am. J. Physiol.* 1998; **275**: R1571-R1577.
73. Golding EM, Kepler TE. Role of estrogen in modulating EDHF-mediated dilations in the female rat middle cerebral artery. *Am. J. Physiol.* 2001; **280**: H2417-H2423.
74. Xu HL, Santizo RA, Baughman VL, Pelligrino DA. ADP-induced pial arteriolar dilation in ovariectomized rats involves gap junctional communication. *Am. J. Physiol.* 2002; **283**: H1082-H1091.
75. Huang A, Sun D, Wu Z, Yan C, Carroll MA, Jiang H, Falck JR, Kaley G. Estrogen elicits cytochrome P450-mediated flow-induced dilation of arterioles in NO deficiency. Role of PI3K-Akt phosphorylation in genomic regulation. *Circ. Res.* 2004; **94**: 245-252.
76. Richards GR, Weston AH, Burnham MP, Feletou M,

- Vanhoutte PM, Edwards G. Suppression of K(+)-induced hyperpolarization by phenylephrine in rat mesenteric artery: relevance to studies of endothelium-derived hyperpolarizing factor. *Br. J. Pharmacol.* 2001; **134**: 1-5.
77. Edwards G, Feletou M, Gardener MJ, Glen CD, Richards GR, Vanhoutte PM, Weston AH. Further investigations into the endothelium-dependent hyperpolarizing effects of bradykinin and substance P in porcine coronary artery. *Br. J. Pharmacol.* 2001; **133**: 1145-1153.
78. Crane GJ, Garland CJ. Thromboxane receptor stimulation associated with loss of SKCa activity and reduced EDHF responses in the rat isolated mesenteric artery. *Brit. J. Pharmacol.* 2004; **142**: 43-50.

Received 9 January 2004, in revised form 30 April 2004.

Accepted 30 April 2004.

©S.L. Sandow 2004.

Author for correspondence:

Dr. Shaun L. Sandow

Division of Neuroscience,

John Curtin School of Medical Research,

Australian National University,

Canberra ACT 0200 Australia.

Tel: +61 2 6125 2149

Fax: +61 2 6125 8077

Email: Shaun.Sandow@anu.edu.au

Endothelial potassium channels, endothelium-dependent hyperpolarization, and the regulation of vascular tone in health and in disease

H.A. Coleman, Marianne Tare & Helena C. Parkington

Department of Physiology,
Monash University,
Victoria 3800, Australia

Summary

1. The elusive nature of endothelium-derived hyperpolarizing factor (EDHF) has hampered detailed study of the ionic mechanisms that underlie the EDHF hyperpolarization and relaxation. Most studies have relied on a pharmacological approach in which interpretations of results can be confounded by limited specificity of action of the drugs used. Nevertheless, small-, intermediate-, and large-conductance Ca^{2+} -activated K^+ channels (SK_{Ca} , IK_{Ca} , and BK_{Ca} , respectively), have been implicated, with inward rectifier K^+ channels (K_{IR}) and Na^+/K^+ ATPase also suggested by some studies.

2. Endothelium-dependent membrane currents recorded using single electrode voltage-clamp from electrically short lengths of arterioles in which the smooth muscle and endothelial cells remained in their normal functional relationship have provided useful insights into the mechanisms mediating EDHF. Charybdotoxin (ChTx) or apamin reduced, while apamin plus ChTx abolished the EDHF current. The ChTx and apamin sensitive currents both reversed near the expected K^+ equilibrium potential, were weakly outwardly rectifying, and displayed little, if any, time or voltage-dependent gating, thus having the biophysical and pharmacological characteristics of IK_{Ca} and SK_{Ca} channels, respectively.

3. IK_{Ca} and SK_{Ca} channels occur in abundance in endothelial cells and their activation results in EDHF-like hyperpolarization of these cells. There is little evidence for a significant number of these channels in healthy, contractile vascular smooth muscle cells.

4. In a number of blood vessels in which EDHF occurs, the endothelial and smooth muscle cells are electrically coupled via myoendothelial gap junctions. In contrast, in the adult rat femoral artery, in which the smooth muscle and endothelial layers are not coupled electrically, EDHF does not occur, even though acetylcholine evokes hyperpolarization in the endothelial cells.

5. *In vivo* studies indicate that EDHF contributes little to basal conductance of the vasculature, but it contributes appreciably to evoked increases in conductance.

6. EDHF responses are diminished in some diseases including hypertension, preeclampsia and some models of diabetes.

7. The most economical explanation for EDHF *in vitro* and *in vivo* in small vessels is that it arises from activation of IK_{Ca} and SK_{Ca} channels in endothelial cells. The resulting endothelial hyperpolarization spreads via myoendothelial junctions to result in the EDHF-attributed

hyperpolarization and relaxation of the smooth muscle.

Introduction

Endothelial K^+ channels have been widely implicated in endothelium-dependent vasodilation. Initially it was considered that endothelial cell hyperpolarization, via the opening of K^+ channels, would facilitate Ca^{2+} influx in these cells by increasing the driving force for this cation^{1,2} and in this way enhance production of the "classical" endothelium-dependent vasorelaxants NO and PGI_2 , which rely on an increase in cytoplasmic free Ca^{2+} . However, since the Ca^{2+} equilibrium potential is likely to be around +130 mV, a large driving force of +190 mV for Ca^{2+} influx exists at a resting potential of -60 mV. This means that endothelial hyperpolarization would be expected to contribute little extra to the driving force for Ca^{2+} influx. Under such conditions, block of endothelial hyperpolarization might be expected to have little effect on cytoplasmic Ca^{2+} levels. Such has been shown to be the case^{3,4}.

The discovery of the additional vasodilator phenomenon of endothelium-derived hyperpolarizing factor (EDHF) has prompted renewed interest in the role of endothelial K^+ channels in the regulation of vascular tone. EDHF is so-called because its vasodilator effects are strongly associated with smooth muscle hyperpolarization, and because the nature of EDHF was unknown⁵⁻⁷ and remains controversial^{8,9}. There are currently three main suggestions as to the nature of EDHF, which are not mutually exclusive but may represent differences between species, between vascular beds and between different endothelial stimulants. One suggestion is that EDHF represents endothelial hyperpolarization generated by the activation of Ca^{2+} -activated K^+ channels (K_{Ca}) that spreads passively via myoendothelial gap junctions to result in hyperpolarization of the smooth muscle cells¹⁰⁻¹⁷. According to this idea, endothelial K^+ channels would influence smooth muscle contractile activity by reducing Ca^{2+} influx via voltage-operated Ca^{2+} channels and by suppression of key enzymes involved in agonist-induced transduction pathways^{18,19}. Another suggestion is that EDHF is a product of the cytochrome P450 pathway, such as an epoxyeicosatrienoic acid (EET), and since EETs can activate large-conductance, Ca^{2+} -activated K^+ channels (BK_{Ca}), it has been inferred that EDHF evokes hyperpolarization via the activation of BK_{Ca} channels on the smooth muscle cells²⁰⁻²⁷. The third suggestion is that K^+ efflux from endothelial cells via intermediate- and small-conductance Ca^{2+} -activated K^+ channels (IK_{Ca} and

SK_{Ca}, respectively), activates inward rectifier K⁺ channels (K_{IR}) and the Na⁺/K⁺ATPase on the smooth muscle cells²⁸. Thus, different ionic mechanisms have been proposed to underlie the actions of EDHF. EDHF plays an increasingly prominent role in vasodilation as arterial diameter decreases, and is thus likely to be important in tissue perfusion. Since EDHF appears to decline with advancing age and to be targeted in diseases such as hypertension and diabetes, knowledge of the ionic mechanisms underlying EDHF would be expected to give an improved understanding of the nature of EDHF and to impact on our understanding of the regulation of vascular tone in health and in disease, and this will be the focus of the present article.

Pharmacology of EDHF relaxation and hyperpolarization

Earliest studies to identify the ionic mechanisms underlying EDHF utilized blockers of various ion pathways. Of concern was that the effects observed could have resulted from an action of the drugs used on the endothelial cells, thus affecting the production of EDHF, rather than the EDHF response in the smooth muscle. Early studies demonstrated an efflux of ⁸⁶Rb⁵, an increase in membrane conductance²⁹, and an insensitivity to the Na⁺/K⁺ATPase inhibitor ouabain³⁰ which suggested that EDHF activates a K⁺ conductance. The K⁺ channel blockers apamin (selective for SK_{Ca} channels)³¹ or charybdotoxin (ChTx, which blocks BK_{Ca}, IK_{Ca}, and some voltage-dependent K⁺ channels, K_V)³² abolished EDHF relaxations, but in other studies, either blocker by itself had little, if any, effect. However, total block was achieved by a combination of apamin plus ChTx^{4,33-39}. A general lack of effectiveness of blockers of K_{ATP} and K_V channels indicated that these channels were unlikely to be involved^{31,33-35,40}. Iberitoxin (IbTx), which selectively blocks BK_{Ca} channels, inhibited the EDHF relaxation in some studies *in vivo*⁴¹ and *in vitro*^{42,43} but was ineffective in other studies against the EDHF relaxation^{34,35,44-46} or hyperpolarization^{26,45,47}. This ineffectiveness of IbTx, together with at least partial block by ChTx, suggested that the ChTx-sensitive channel was the IK_{Ca} channel⁴⁴. Although tetraethylammonium (TEA, which blocks BK_{Ca} and some K_V channels) produced an effect in some studies^{32,35,44}, the anti-muscarinic actions of TEA⁴⁸ may cloud the interpretation of its effects. 4-Aminopyridine (4-AP, which blocks K_V channels) diminished the EDHF response in some studies, but an alternative explanation is that it did so through inhibition of the increase in endothelial cytoplasmic free Ca²⁺⁴.

In electrophysiological studies, K_V and K_{ATP} blockers did not affect the EDHF hyperpolarization in the guinea-pig coronary artery^{45,49-51}. However, the hyperpolarization was reduced by TEA (1-5mM), ChTx (5×10⁻⁸ M) and 4-AP⁴⁹⁻⁵¹, while apamin had no effect^{45,49} or caused a small reduction in the initial phase of the hyperpolarization⁵¹. Somewhat similarly, in guinea-pig carotid arteries and submucosal arterioles, the EDHF hyperpolarization was insensitive to blockers of K_{ATP} and K_V channels, but was

reduced by ChTx and further reduced by ChTx plus apamin⁵²⁻⁵⁴. In the rat, the EDHF hyperpolarization in the tail artery was abolished by a combination of ChTx plus apamin⁵⁵, while in the mesenteric artery, apamin was more effective than ChTx, but both were required to completely block the EDHF hyperpolarization and relaxation⁵⁶. In the mesenteric artery of the rabbit, apamin alone abolished the EDHF hyperpolarization, as did TEA (10mM), while it was unaffected by ouabain, 4-AP, or Ba²⁺⁵⁷.

Overall, the studies on EDHF-induced hyperpolarizations and relaxations produced no strong evidence for the involvement of K_V or K_{ATP} channels, evidence for the involvement of BK_{Ca} channels in several studies, and strongly implicated IK_{Ca} and SK_{Ca} channels in many other studies. More recently, selective and potent blockers of IK_{Ca} channels have been developed that are analogues of clotrimazole that lack the imidazole ring and therefore do not block cytochrome P450 enzymes⁵⁸. These compounds, TRAM-34 and TRAM-39, particularly in combination with apamin, block the EDHF hyperpolarization and relaxation, providing stronger pharmacological evidence for the involvement of IK_{Ca} channels, in addition to SK_{Ca} channels⁵⁹⁻⁶².

K⁺ as an EDHF

The elegant hypothesis that EDHF may be none other than K⁺ released from the endothelial cells raised additional candidates for the ionic mechanisms underlying EDHF²⁸. According to this scheme, stimulation of endothelial cells results in the activation of endothelial K_{Ca} channels. The resulting efflux of K⁺ is then proposed to accumulate in the myoendothelial space where it stimulates the Na⁺/K⁺ATPase and K_{IR} channels in the smooth muscle²⁸. This study gave a fresh boost to investigations into the ionic mechanisms underlying the EDHF hyperpolarization. Using low concentrations of Ba²⁺ to specifically block K_{IR} (typically around 30 μM), ouabain to block the Na⁺/K⁺ATPase, and attempted mimicry by the exogenous application of modest increases in KCl, a number of studies obtained evidence against the K⁺ hypothesis⁶³⁻⁶⁷, while other studies provided evidence in favour of the idea^{38,39,68-70}. Such studies have generally placed strong emphasis on block of EDHF responses by ouabain. However, the effects of ouabain need to be interpreted with considerable caution. Ca²⁺ overload⁷¹⁻⁷³ has been invoked to explain an inhibition of a K⁺ channel by a 10 minute exposure to ouabain in canine ventricular myocytes⁷⁴, while ouabain also inhibited the iloprost-induced hyperpolarization, which is inhibited by glibenclamide, in the rat hepatic artery¹⁶. In the bovine coronary artery, ouabain blocked relaxations induced by the NO donor glyceryl trinitrate³⁹. A recent study indicating that ouabain is capable of decreasing gap junction permeability⁷⁵ is particularly significant since such effects are consistent with EDHF being due to electrotonic spread of hyperpolarizing current from the endothelium to the smooth muscle (see below). In that study, the cells were exposed to ouabain for one hour, which is appreciably longer than in studies on the

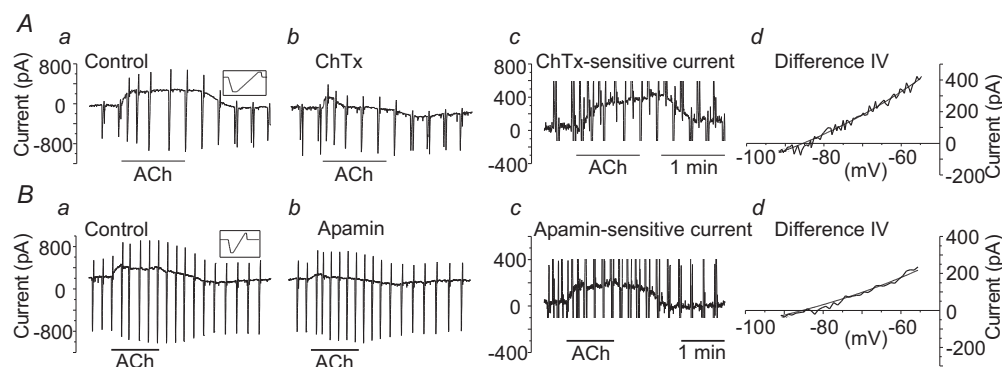


Figure 1. Components of EDHF current recorded from segments of guinea-pig submucosal arterioles.

Aa, Ba, ACh ($1 \mu\text{M}$) evoked an outward, EDHF current with the membrane clamped at -63 mV . Periodic transients are responses to voltage ramps (insets). Ab, ChTx (30 nM) and Bb, apamin ($0.5 \mu\text{M}$) reduced the EDHF current. Ac, Bc, subtraction of the current in Ab from Aa reveals the ChTx-sensitive component of current, and subtraction of the current in Bb from Ba reveals the apamin-sensitive component of current. Ad, Bd, the I-V relationships for the ChTx-sensitive and apamin-sensitive components, respectively, were well-described by the GHK equation for a K^+ current (smooth lines). Reproduced with permission of The Physiological Society from Coleman et al¹⁶.

effects of ouabain on EDHF. The effects of shorter duration exposures to ouabain on gap junction permeability were not determined.

Voltage-clamp studies

Ionic mechanisms are perhaps ideally studied by recording the membrane currents under voltage-clamp. Voltage-clamp studies of vascular tissues typically involve enzymatic isolation of either the smooth muscle or endothelial cells, and recording from the isolated cells using the patch-clamp technique. Such cellular isolation overcomes the problems of spatial clamp control in a syncytial tissue. However, to record the ionic currents underlying the elusive and controversial EDHF, a preparation was required in which the endothelial and smooth muscle cells remained in their normal functional relationship, especially in view of electrotonic spread as a potential mechanism. Such a preparation needed to be amenable to voltage-clamp, preferably without exposing the cells to digestive enzymes that could potentially disrupt mechanisms underlying EDHF. Hirst and Neild⁷⁶ demonstrated that the submucosal arterioles lying in the wall of the small intestine of the guinea-pig had an electrical length constant of about $1600 \mu\text{m}$, and that the arterioles could be cut into short segments that remained physiologically viable. Hirst and colleagues subsequently showed that if the arterioles were cut into sufficiently short lengths, they could be voltage-clamped with a single intracellular microelectrode using a switching amplifier⁷⁷, though the limited current-passing ability of the microelectrodes restricted the range of potentials over which the membrane could be clamped. The contractile activity of these arterioles could also be recorded using the video tracking hardware and software of diamtrak,

developed by Neild⁷⁸. These arterioles therefore seemed a good preparation in which to record the EDHF currents under voltage-clamp, and also to determine their functional significance in terms of contractile activity. However, it must be borne in mind that increasing the amount of stretch in the wall of the guinea-pig coronary artery increased the amplitude of hyperpolarization evoked by NO, iloprost, and EDHF, though the EDHF hyperpolarization was less sensitive to stretch than that of NO and iloprost⁷⁹. Thus, since the short segments of arterioles cannot be pressurized, there may be some differences in the activity of the underlying ion channels and their regulatory mechanisms compared with the more physiological, pressurized state, in which the ionic mechanisms cannot be readily studied.

In the submucosal arterioles, with the membrane potential clamped at around -65 mV , and in the presence of N^{ω} -nitro-L-arginine methylester (L-NAME) and indomethacin to inhibit NO production and cyclooxygenase activity, respectively, acetylcholine (ACh) and substance P evoked an outward current attributed to EDHF^{16,17} (Fig 1Aa, Ba) and also resulted in EDHF-induced relaxation^{16,17}. Current-voltage (I-V) relationships, obtained from the current responses to periodic voltage ramps, revealed that the EDHF current reversed at a potential around that for K^+ , indicating that the EDHF current involved the activation of K^+ channels. ChTx reduced the EDHF current (Fig 1Ab), and by subtraction of currents, the ChTx-sensitive component was revealed (Fig 1Ac). Its I-V relationship was well described by the Goldman-Hodgkin-Katz (GHK) equation for a K^+ current (Fig 1Ad), indicating that the ChTx-sensitive component of current involved the activation of K^+ channels whose gating was insensitive to membrane potential. This voltage-insensitivity, together with block by ChTx but not IbTx, provides both biophysical and pharmacological evidence that this component of

current was carried by IK_{Ca} channels¹⁶. Apamin similarly inhibited a component of current (Fig 1Bb,c) whose I-V relationship was well-described by the GHK equation for a K^+ current (Fig 1Bd). An insensitivity to gating by membrane potential, together with block by apamin, indicates that this component of current was carried by SK_{Ca} channels. In the combined presence of ChTx plus apamin, the EDHF current and relaxation were abolished, indicating that the only currents contributing to the EDHF response were those flowing through IK_{Ca} and SK_{Ca} channels in this preparation¹⁶.

Ba^{2+} inhibited a component of the holding current whose I-V relationship was inwardly rectifying, typical of K_{IR} channels, and very different to the I-V curves for the EDHF components of current^{16,17} (Fig 2). Ouabain also inhibited a component of the holding current, and its I-V relationship was typical of that for the Na^+/K^+ ATPase, and very different to that for the EDHF currents¹⁶ (Fig 2). The addition of 5 - 10 mM KCl activated a current which was largely blocked by Ba^{2+} ^{16,17}. These results indicate that K_{IR} channels and the Na^+/K^+ ATPase contribute to the resting current in the submucosal arterioles, and that the K_{IR} channels can be activated by the addition of K^+ . Significantly, however, these results provide strong evidence that K_{IR} channels and the Na^+/K^+ ATPase do not contribute to the EDHF current in these arterioles.

Myoendothelial electrical coupling and the location of IK_{Ca} and SK_{Ca} channels

The involvement of IK_{Ca} and SK_{Ca} channels in the EDHF response raises the critical question of where these channels are located. An associated question is whether the endothelial and smooth muscle cells are electrically coupled, since it has been suggested that EDHF may represent electrotonic spread of hyperpolarization from the endothelium to the smooth muscle¹⁴ (see above). Strong evidence indicates that such coupling occurs in a number of vessels (recently reviewed⁸⁰). To test this possibility in guinea-pig submucosal arterioles, recordings of membrane potential were made from dye (Lucifer Yellow)-identified endothelial and smooth muscle cells. Excitatory junction potentials (EJPs) in response to sympathetic nerve stimulation, and action potentials associated with vasoconstriction, all of which were initiated in the smooth muscle cells, were also recorded from endothelial cells. Significantly, the responses recorded from the endothelial cells were indistinguishable from those recorded from the smooth muscle cells, indicating that the electrical coupling is very strong and that the two layers function essentially as a single electrical syncytium^{16,17}. Such electrical coupling does not occur in all vessels. More recently, Sandow and colleagues found that in the more proximal parts of the adult rat femoral artery, there is a lack of both myoendothelial electrical coupling together with an absence of myoendothelial gap junctions⁸¹. Significantly, this lack of myoendothelial coupling was associated with a lack of EDHF-mediated hyperpolarization and relaxation in the smooth muscle, even though the endothelial cells

hyperpolarized when stimulated with agents such as ACh and the hyperpolarization was blocked by ChTx plus apamin⁸¹. Furthermore, in the rat mesenteric artery, in which myoendothelial coupling is strong^{81,82}, use of connexin mimetics inhibited the EDHF response recorded from the smooth muscle but not the endothelial cell hyperpolarization. Caution is required in interpreting the effects of the connexin mimetics such as the Gap compounds since they must be used at relatively high concentrations, and there have been very few electrophysiological studies of their effects on electrical coupling. Nevertheless, taken as a whole, the observations of Sandow and colleagues⁸¹ provide critical support for the idea that EDHF is generated in the endothelial cells and propagates via myoendothelial gap junctions to result in the smooth muscle EDHF hyperpolarization and relaxation.

An endothelial site for the initiation of the EDHF hyperpolarization suggests that the IK_{Ca} and SK_{Ca} channels are located in endothelial rather than in smooth muscle cells. Indeed, there is very little evidence that IK_{Ca} channels occur in normal, healthy, contractile smooth muscle cells, although electrophysiological and expression analysis reveal that IK_{Ca} channels can occur in cultured cells and during hyperplasia^{83,84}. There is also little evidence that SK_{Ca} channels occur in non-cultured vascular smooth muscle cells^{85,86}. In contrast, in endothelial cells, electrophysiology, immunohistochemistry, and expression analysis reveal an abundance of IK_{Ca} and SK_{Ca} channels⁸⁵⁻⁸⁹. Consistent with such observations, endothelial cells which are isolated and not in contact with vascular smooth muscles respond to ACh with hyperpolarization which can be reduced by ChTx^{90,91} and abolished by ChTx plus apamin^{81,91}. Furthermore, EDHF-induced relaxations of perfused mesenteric arteries were blocked when ChTx plus apamin were added to the perfusate in the lumen and thus applied selectively to the endothelial cells, but the relaxations were not blocked when these K^+ channel blockers were added to the superfusate⁹².

EDHF *in vivo*

Despite numerous studies indicating that EDHF is capable of evoking considerable relaxation in small vessels *in vitro*, an important consideration is whether EDHF is functionally important *in vivo*. Significant relaxation *in vivo* has been reported for an EDHF response attributed to a product of the cytochrome P450 pathway^{41,93-95} and blocked by IbTx, implicating BK_{Ca} channels⁴¹. This EDHF does not appear to contribute to basal tone *in vivo*⁴¹. The most widely reported EDHF response *in vitro* is that which is blocked by a combination of ChTx plus apamin and involves IK_{Ca} and SK_{Ca} channels located in the endothelium (discussed above). The *in vivo* significance of this form of EDHF was evaluated in the rat mesenteric and hindlimb beds⁹⁶. In the presence of L-NAME and indomethacin, local infusion of ChTx plus apamin selectively into these beds had no effect on basal blood flow or conductance. However, these agents abolished the appreciable increases in blood flow and conductance evoked by ACh and

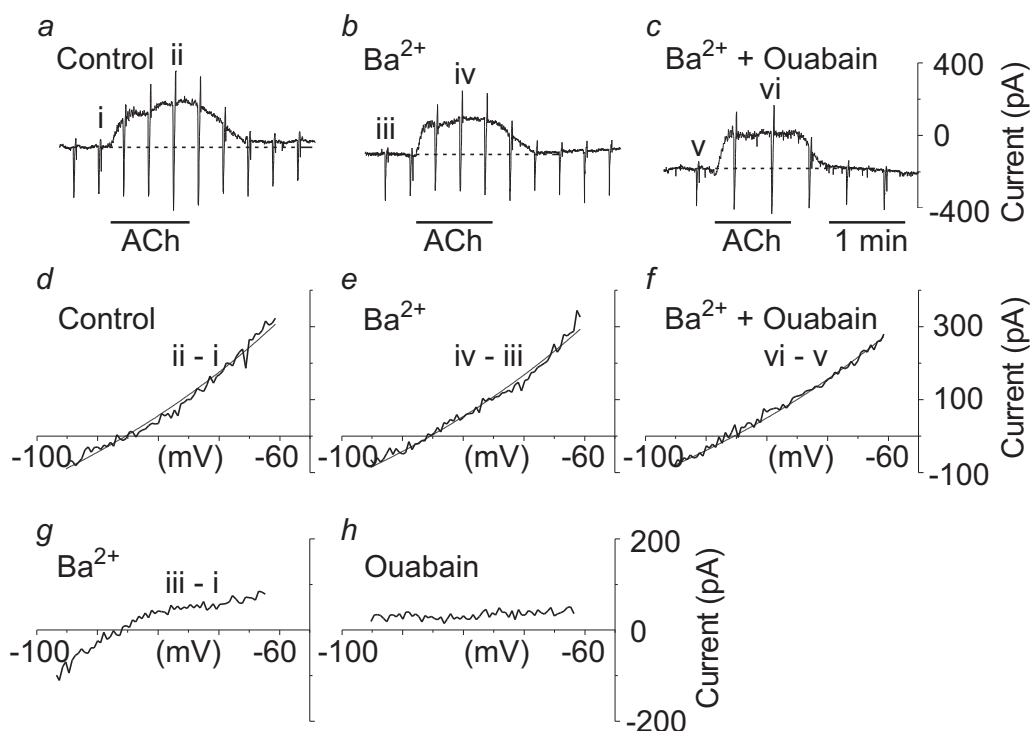


Figure 2. Contribution of K_{IR} and $Na^+/K^+ATPase$ to arteriole currents

a, ACh ($1 \mu M$) evoked an outward, EDHF current. b, the EDHF current was not reduced by Ba^{2+} ($30 \mu M$), or c, by the addition of ouabain ($200 \mu M$) in the continuing presence of Ba^{2+} . d, the I-V relationship for EDHF obtained from the current responses to periodic voltage ramps in panel a, was well-described by the GHK equation for a K^+ current (smooth line), but was not affected by Ba^{2+} (e) or ouabain plus Ba^{2+} (f). g, Ba^{2+} inhibited a component of the holding current (b – a) which had an inwardly-rectifying I-V relationship typical of K_{IR} channels. h, ouabain inhibited a component of holding current (c – b) with a relatively flat I-V relationship typical of the $Na^+/K^+ATPase$. Reproduced with permission of The Physiological Society from Coleman et al¹⁶.

bradykinin, whereas IbTx was ineffective. These results indicate that in these vascular beds, EDHF does not contribute to basal blood flow, but makes a significant contribution to evoked blood flow. These effects do not involve BK_{Ca} channels, but are due to activation of IK_{Ca} and SK_{Ca} K^+ channels located in the endothelial cells⁹⁶. These results support and extend an earlier *in vivo* study in which connexin-mimetic peptides, thought to inhibit gap junctions, abolished EDHF-mediated increases in blood flow in the rat renal microcirculation⁹⁷.

EDHF in disease

Endothelial dysfunction is a feature of a number of diseases and this has prompted investigations into the fate of EDHF in various diseases. The effects of hypertension on EDHF have been assessed in vessels from spontaneously hypertensive rats (SHR) compared with vessels from Wistar-Kyoto (WKY) rats. In the mesenteric artery, the EDHF hyperpolarization was halved and the relaxation significantly reduced⁹⁸, while in the tail artery the hyperpolarization was decreased by 28%⁵⁵. An increase in the number of layers of smooth muscle cells together with a

greater incidence of myoendothelial gap junctions (MEGJs) in SHRs⁵⁵ might explain the decreased EDHF response in terms of an increased electrical “sink” for the endothelium-derived hyperpolarizing current. In preeclampsia, a pregnancy-specific form of hypertension in women, the EDHF vasodilator response in myometrial arteries is also significantly reduced and this may represent a failure of its up regulation as occurs in these tissues in the normal adaptation to pregnancy in healthy women⁹⁹.

Changes in EDHF in diabetes have been studied in most detail in streptozotocin (STZ)- induced diabetes in rats. In the mesenteric bed, the EDHF hyperpolarization^{100,101} and relaxation¹⁰⁰⁻¹⁰² were significantly diminished compared with responses from control animals. EDHF-induced relaxations were also reduced *in vivo* in the renal circulation, with the most severe deficit occurring in the smallest arterioles¹⁰³. The EDHF relaxation was also impaired in the renal artery of obese Zucker rats, which is an animal model of insulin resistance and Type II diabetes¹⁰⁴. However, in a mouse model of Type II diabetes, the *db/db* $-/-$, the EDHF relaxation of first order mesenteric arteries was not diminished¹⁰⁵, indicating that EDHF is not impaired in all models of diabetes. The

mechanisms underlying disease-associated impairment of EDHF-attributed hyperpolarization and relaxation are far from clear and require further studies to determine whether the dysfunction arises in the smooth muscle cells, and/or the endothelial cells, and/or myoendothelial communication¹⁰⁶. This knowledge could provide the basis of novel therapeutic interventions in the amelioration or prevention of vascular complications of these diseases.

Conclusions

In many vessels, abolition of EDHF-attributed relaxation and/or hyperpolarization by apamin combined with ChTx, but not IbTx, or with a TRAM compound, implicate SK_{Ca} and IK_{Ca} as the ion channels carrying the current which underlies the EDHF hyperpolarization. Biophysical properties of the EDHF current, obtained from voltage-clamp results, strongly support the involvement of these channels and exclude the involvement of other ionic mechanisms such as K_{IR} channels and the Na⁺/K⁺ ATPase, at least in submucosal arterioles. In some vessels, EDHF is attributed to a product of the cytochrome P450 pathway and to involve the activation of BK_{Ca} channels. However, the poor selectivity of many blockers of cytochrome P450 pathways and differences in the actions of various agonists applied to stimulate the endothelial cells, means that further studies are required to better understand the role of the cytochrome P450 pathway in the EDHF response.

IK_{Ca} and SK_{Ca} channels occur in abundance on endothelial cells but not on smooth muscle cells and endothelial cells respond to agonists with EDHF-like hyperpolarization. Furthermore, there is strong myoendothelial electrical coupling in vessels with EDHF responses, but not in vessels without EDHF, although the range of vessels that have been tested is limited. Together, these observations suggest that EDHF likely involves the activation of K_{Ca} channels in the endothelial cells, and that the EDHF hyperpolarization of smooth muscle involves the spread of hyperpolarizing current from the endothelium via myoendothelial gap junctions. Some variations between vascular beds and species in the relative effectiveness of apamin, ChTx and IbTx is likely to reflect differences in the relative densities of the K_{Ca} channels. BK_{Ca} channels may be important in some vessels, while IK_{Ca} and SK_{Ca} channels are more important in many other vascular beds. These endothelial channels make an important contribution to vascular tone *in vivo*, and impairment of their effectiveness contributes to endothelial dysfunction in a range of diseases, thus raising the mechanisms underlying EDHF as potential therapeutic targets.

Acknowledgements

The authors' original work presented or cited in this review was supported by the National Health and Medical Research Council of Australia. This work was carried out during the tenure of a grant from the National Heart Foundation.

References

1. Adams DJ, Barakeh J, Laskey R, van Breemen C. Ion channels and regulation of intracellular calcium in vascular endothelial cells. *FASEB J.* 1989; **3**: 2389-400.
2. Cannell MB, Sage SO. Bradykinin-evoked changes in cytoplasmic calcium and membrane currents in cultured bovine pulmonary artery endothelial cells. *J. Physiol.* 1989; **419**: 555-68.
3. Yamanaka A, Ishikawa T, Goto K. Characterization of endothelium-dependent relaxation independent of NO and prostaglandins in guinea pig coronary artery. *J. Pharmacol. Exp. Ther.* 1998; **285**: 480-9.
4. Ghisda P, Morel N. Cellular target of voltage and calcium-dependent K⁺ channel blockers involved in EDHF-mediated responses in rat superior mesenteric artery. *Br. J. Pharmacol.* 2001; **134**: 1021-8.
5. Chen G, Suzuki H, Weston AH. Acetylcholine releases endothelium-derived hyperpolarizing factor and EDRF from rat blood vessels. *Br. J. Pharmacol.* 1988; **95**: 1165-74.
6. Félétou M, Vanhoutte PM. Endothelium-dependent hyperpolarization of canine coronary smooth muscle. *Br. J. Pharmacol.* 1988; **93**: 515-24.
7. Taylor SG, Weston AH. Endothelium-derived hyperpolarizing factor: a new endogenous inhibitor from the vascular endothelium. *Trends Pharmacol. Sci.* 1988; **9**: 272-4.
8. McGuire J, Ding H, Triggle C. Endothelium-derived relaxing factors: a focus on endothelium-derived hyperpolarizing factors. *Can. J. Pharmacol.* 2001; **79**: 443-70.
9. Busse R, Edwards G, Félétou M, Fleming I, Vanhoutte PM, Weston AH. EDHF: bringing the concepts together. *Trends Pharmacol. Sci.* 2002; **23**: 374-80.
10. Little TL, Xia J, Duling BR. Dye tracers define differential endothelial and smooth muscle coupling patterns within the arteriolar wall. *Circ. Res.* 1995; **76**: 498-504.
11. Bény J-L. Electrical coupling between smooth muscle cells and endothelial cells in pig coronary arteries. *Pflügers Arch.* 1997; **433**: 364-7.
12. Chaytor AT, Evans WH, Griffith TM. Central role of heterocellular gap junctional communication in endothelium-dependent relaxations of rabbit arteries. *J. Physiol.* 1998; **508**: 561-73.
13. Yamamoto Y, Fukuta H, Nakahira Y, Suzuki H. Blockade by 18β-glycyrrhetic acid of intercellular electrical coupling in guinea-pig arterioles. *J. Physiol.* 1998; **511**: 501-8.
14. Bény J-L. Information networks in the arterial wall. *News Physiol. Sci.* 1999; **14**: 68-73.
15. Edwards G, Félétou M, Gardener MJ, Thollon C, Vanhoutte PM, Weston AH. Role of gap junctions in the responses to EDHF in rat and guinea-pig small arteries. *Br. J. Pharmacol.* 1999; **128**: 1788-94.
16. Coleman HA, Tare M, Parkington HC. K⁺ currents underlying the action of endothelium-derived

- hyperpolarizing factor in guinea-pig, rat and human blood vessels. *J. Physiol.* 2001; **531**: 359-73.
17. Coleman HA, Tare M, Parkington HC. EDHF is not K⁺ but may be due to spread of current from the endothelium in guinea pig arterioles. *Am. J. Physiol.* 2001; **280**: H2478-83.
 18. Ganitkevich VY, Isenberg G. Membrane potential modulates inositol 1,4,5-trisphosphate-mediated Ca²⁺ transients in guinea-pig coronary myocytes. *J. Physiol.* 1993; **470**: 35-44.
 19. Itoh T, Seki N, Suzuki S, Ito S, Kajikuri J, Kuriyama H. Membrane hyperpolarization inhibits agonist-induced synthesis of inositol 1,4,5-trisphosphate in rabbit mesenteric artery. *J. Physiol.* 1992; **451**: 307-28.
 20. Hecker M, Bara AT, Bauersachs J, Busse R. Characterization of endothelium-derived hyperpolarizing factor as a cytochrome P450-derived arachidonic acid metabolite in mammals. *J. Physiol.* 1994; **481**: 407-14.
 21. Campbell WB, Gebremedhin D, Pratt PF, Harder DR. Identification of epoxyeicosatrienoic acids as endothelium-derived hyperpolarizing factors. *Circ. Res.* 1996; **78**: 415-23.
 22. Adeagbo ASO, Henzel MK. Calcium-dependent phospholipase A₂ mediates the production of endothelium-derived hyperpolarizing factor in perfused rat mesenteric prearteriolar bed. *J. Vasc. Res.* 1998; **35**: 27-35.
 23. Fisslthaler B, Popp R, Kiss L, Potente M, Harder DR, Fleming I, et al. Cytochrome P450 2C is an EDHF synthase in coronary arteries. *Nature* 1999; **401**: 493-7.
 24. Campbell WB, Harder DR. Endothelium-derived hyperpolarizing factors and vascular cytochrome P450 metabolites of arachidonic acid in the regulation of tone. *Circ. Res.* 1999; **84**: 484-8.
 25. Quilley J, McGiff JC. Is EDHF an epoxyeicosatrienoic acid? *Trends Pharmacol. Sci.* 2000; **21**: 121-4.
 26. Edwards G, Thollon C, Gardener MJ, Félétou M, Vilaine JP, Vanhoutte PM, et al. Role of gap junctions and EETs in endothelium-dependent hyperpolarization of porcine coronary artery. *Br. J. Pharmacol.* 2000; **129**: 1145-54.
 27. Fleming I. Cytochrome P-450 enzymes in vascular homeostasis. *Circ. Res.* 2001; **89**: 753-62.
 28. Edwards G, Dora KA, Gardener MJ, Garland CJ, Weston AH. K⁺ is an endothelium-derived hyperpolarizing factor in rat arteries. *Nature* 1998; **396**: 269-72.
 29. Chen G, Suzuki H. Some electrical properties of the endothelium-dependent hyperpolarization recorded from rat arterial smooth muscle cells. *J. Physiol.* 1989; **410**: 91-106.
 30. Chen G, Hashitani H, Suzuki H. Endothelium-dependent relaxation and hyperpolarization of canine coronary artery smooth muscles in relation to the electrogenic Na-K pump. *Br. J. Pharmacol.* 1989; **98**: 950-6.
 31. Adeagbo ASO, Triggle CR. Varying extracellular [K⁺]: A functional approach to separating EDHF- and EDNO-related mechanisms in perfused rat mesenteric arterial bed. *J. Cardiovasc. Pharmacol.* 1993; **21**: 423-9.
 32. Cowan CL, Palacino JJ, Najibi S, Cohen RA. Potassium channel-mediated relaxation to acetylcholine in rabbit arteries. *J. Pharmacol. Exp. Ther.* 1993; **266**: 1482-9.
 33. Waldron GJ, Garland CJ. Effect of potassium channel blockers on L-NAME insensitive relaxations in rat small mesenteric artery. *Can. J. Physiol. Pharmacol.* 1994; **72**: S1, 115.
 34. Zygmunt PM, Högestätt ED. Role of potassium channels in endothelium-dependent relaxation resistant to nitroarginine in the rat hepatic artery. *Br. J. Pharmacol.* 1996; **117**: 1600-6.
 35. Petersson J, Zygmunt PM, Hogestatt ED. Characterization of the potassium channels involved in EDHF-mediated relaxation in cerebral arteries. *Br. J. Pharmacol.* 1997; **120**: 1344-50.
 36. Plane F, Holland M, Waldron GJ, Garland CJ, Boyle JP. Evidence that anandamide and EDHF act via different mechanisms in rat isolated mesenteric arteries. *Br. J. Pharmacol.* 1997; **121**: 1509-11.
 37. Sunano S, Watanabe H, Tanaka S, Sekiguchi F, Shimamura K. Endothelium-derived relaxing, contracting and hyperpolarizing factors of mesenteric arteries of hypertensive and normotensive rats. *Br. J. Pharmacol.* 1999; **126**: 709-16.
 38. Büssemaker E, Wallner C, Fisslthaler B, Fleming I. The Na-K-ATPase is a target for an EDHF displaying characteristics similar to potassium ions in the porcine renal interlobar artery. *Br. J. Pharmacol.* 2002; **137**: 647-54.
 39. Nelli S, Wilson WS, Laidlaw H, Llano A, Middleton S, Price AG, et al. Evaluation of potassium ion as the endothelium-derived hyperpolarizing factor (EDHF) in the bovine coronary artery. *Br. J. Pharmacol.* 2003; **139**: 982-8.
 40. Zygmunt PM, Edwards G, Weston AH, Larsson B, Hogestatt ED. Involvement of voltage-dependent potassium channels in the EDHF-mediated relaxation of rat hepatic artery. *Br. J. Pharmacol.* 1997; **121**: 141-9.
 41. Nishikawa Y, Stepp DW, Chilian WM. In vivo location and mechanism of EDHF-mediated vasodilation in canine coronary microcirculation. *Am. J. Physiol.* 1999; **277**: H1252-9.
 42. Huang A, Sun D, Smith CJ, Connetta JA, Shesely EG, Koller A, et al. In eNOS knockout mice skeletal muscle arteriolar dilation to acetylcholine is mediated by EDHF. *Am. J. Physiol.* 2000; **278**: H762-8.
 43. Archer SL, Gragasin FS, Wu X, Wang S, McMurtry S, Kim DH, et al. Endothelium-derived hyperpolarizing factor in human internal mammary artery is 11,12-epoxyeicosatrienoic acid and causes

- relaxation by activating smooth muscle BK_{Ca} channels. *Circ.* 2003; **107**: 769-76.
44. Rapacon M, Mieyal P, McGiff JC, Fulton D, Quilley J. Contribution of calcium-activated potassium channels to the vasodilator effect of bradykinin in the isolated, perfused kidney of the rat. *Br. J. Pharmacol.* 1996; **118**: 1504-8.
 45. Eckman DM, Hopkins N, McBride C, Keef KD. Endothelium-dependent relaxation and hyperpolarization in guinea-pig coronary artery: role of epoxyeicosatrienoic acid. *Br. J. Pharmacol.* 1998; **124**: 181-9.
 46. Fulton D, McGiff JC, Quilley J. Pharmacological evaluation of an epoxide as the putative hyperpolarizing factor mediating the nitric oxide-independent vasodilator effect of bradykinin in the rat heart. *J. Pharmacol. Exp. Ther.* 1998; **287**: 497-503.
 47. Chataigneau T, Félétou M, Duhault J, Vanhoutte PM. Epoxyeicosatrienoic acids, potassium channel blockers and endothelium-dependent hyperpolarization in the guinea-pig carotid artery. *Br. J. Pharmacol.* 1998; **123**: 574-80.
 48. Balduini W, Costa LG, Murphy SD. Potassium ions potentiate the muscarinic receptor-stimulated phosphoinositide metabolism in cerebral cortex slices: A comparison of neonatal and adult rats. *Neurochem. Res.* 1990; **15**: 33-9.
 49. Parkington HC, Tonta MA, Coleman HA, Tare M. Role of membrane potential in endothelium-dependent relaxation of guinea-pig coronary arterial smooth muscle. *J. Physiol.* 1995; **484**: 469-80.
 50. Hammarström AK, Parkington HC, Coleman HA. The effects of some ion channel blockers on the hyperpolarisation evoked by EDHF in the guinea pig coronary artery. *Proc. Aust. Physiol. Pharmacol. Soc.* 1994; **25**: 63P.
 51. Nishiyama M, Hashitani H, Fukuta H, Yamamoto Y, Suzuki H. Potassium channels activated in endothelium-dependent hyperpolarization in guinea-pig coronary artery. *J. Physiol.* 1998; **510**: 455-65.
 52. Corriu C, Félétou M, Canet E, Vanhoutte PM. Endothelium-derived factors and hyperpolarization of the carotid artery of the guinea-pig. *Br. J. Pharmacol.* 1996; **119**: 959-64.
 53. Hashitani H, Suzuki H. K⁺ channels which contribute to the acetylcholine-induced hyperpolarization in smooth muscle of the guinea-pig submucosal arteriole. *J. Physiol.* 1997; **501**: 319-29.
 54. Coleman HA, Tare M, Parkington HC. Components of the potassium currents underlying the actions of endothelium-derived hyperpolarizing factor in arterioles. In: Vanhoutte PM, editor. EDHF 2000. London: Taylor & Francis, 2001:259-69.
 55. Sandow SL, Bramich NJ, Bandi HP, Rummery NM, Hill CE. Structure, function, and endothelium-derived hyperpolarizing factor in the caudal artery of the SHR and WKY rat. *Arterioscler. Thromb. Vasc. Biol.* 2003; **23**: 822-8.
 56. Chen G, Cheung DW. Effect of K⁺-channel blockers on ACh-induced hyperpolarization and relaxation in mesenteric arteries. *Am. J. Physiol.* 1997; **272**: H2306-12.
 57. Murphy ME, Brayden JE. Apamin-sensitive K⁺ channels mediate an endothelium-dependent hyperpolarization in rabbit mesenteric arteries. *J. Physiol.* 1995; **489**: 723-34.
 58. Wulff H, Miller MJ, Hänsel W, Grissmer S, Cahalan MD, Chandy KG. Design of a potent and selective inhibitor of the intermediate-conductance Ca²⁺-activated K⁺ channel, *IKCa1*: A potential immunosuppressant. *Proc. Natl. Acad. Sci. USA.* 2000; **97**: 8151-6.
 59. Eichler I, Wibawa J, Grgic I, Knorr A, Brakemeier S, Pries AR, et al. Selective blockade of endothelial Ca²⁺-activated small- and intermediate-conductance K⁺-channels suppresses EDHF-mediated vasodilation. *Br. J. Pharmacol.* 2003; **138**: 594-601.
 60. Hinton JM, Langton PD. Inhibition of EDHF by two new combinations of K⁺-channel inhibitors in rat isolated mesenteric arteries. *Br. J. Pharmacol.* 2003; **138**: 1031-5.
 61. Crane GJ, Gallagher N, Dora KA, Garland CJ. Small- and intermediate-conductance calcium-activated K⁺ channels provide different facets of endothelium-dependent hyperpolarization in rat mesenteric artery. *J. Physiol.* 2003; **553**: 183-9.
 62. Sandow SL, Goto K, Rummery NM, Hill CE. Developmental changes in myoendothelial gap junction mediated vasodilator activity in the rat saphenous artery. *J. Physiol.* 2004; **556**: 875-86.
 63. Quignard JF, Félétou M, Thollon C, Vilaine JP, Duhault J, Vanhoutte PM. Potassium ions and endothelium-derived hyperpolarizing factor in guinea-pig carotid and porcine coronary arteries. *Br. J. Pharmacol.* 1999; **127**: 27-34.
 64. Vanheel B, Van de Voorde J. Barium decreases endothelium-dependent smooth muscle responses to transient but not to more prolonged acetylcholine applications. *Pflügers Arch.* 1999; **439**: 123-9.
 65. Drummond GR, Selemidis S, Cocks TM. Apamin-sensitive, non-nitric oxide (NO) endothelium-dependent relaxations to bradykinin in the bovine isolated coronary artery: no role for cytochrome P₄₅₀ and K⁺. *Br. J. Pharmacol.* 2000; **129**: 811-9.
 66. Lacy PS, Pilkington G, Hanvesakul R, Fish HJ, Boyle JP, Thurston H. Evidence against potassium as an endothelium-derived hyperpolarizing factor in rat mesenteric small arteries. *Br. J. Pharmacol.* 2000; **129**: 605-11.
 67. Buus NH, Simonsen U, Pilegaard HK, Mulvany MJ. Nitric oxide, prostanoid and non-NO, non-prostanoid involvement in acetylcholine relaxation of isolated human small arteries. *Br. J. Pharmacol.* 2000; **129**: 184-92.
 68. Bény J-L, Schaad O. An evaluation of potassium ions as endothelium-derived hyperpolarizing factor in porcine coronary arteries. *Br. J. Pharmacol.* 2000;

- 131: 965-73.
69. Dora KA, Garland CJ. Properties of smooth muscle hyperpolarization and relaxation to K⁺ in the rat isolated mesenteric artery. *Am. J. Physiol.* 2001; **280**: H2424-9.
 70. Savage D, Perkins J, Lim CH, Bund SJ. Functional evidence that K⁺ is the non-nitric oxide, non-prostanoid endothelium-derived relaxing factor in rat femoral arteries. *Vasc. Pharmacol.* 2003; **40**: 23-8.
 71. Monteith GR, Blaustein MP. Different effects of low and high dose cardiotonic steroids on cytosolic calcium in spontaneously active hippocampal neurons and in co-cultured glia. *Brain Res.* 1998; **795**: 325-40.
 72. Zhu Z, Tepel M, Neusser M, Zidek W. Low concentrations of ouabain increase cytosolic free calcium concentration in rat vascular smooth muscle cells. *Clinical Science* 1996; **90**: 9-12.
 73. Korge P, Langer GA. Mitochondrial Ca²⁺ uptake, efflux, and sarcolemmal damage in Ca²⁺-overloaded cultured rat cardiomyocytes. *Am. J. Physiol.* 1998; **274**: H2085-93.
 74. Saxena NC, Fan JS, Tseng GN. Effects of elevating [Na]_i on membrane currents of canine ventricular myocytes: role of intracellular Ca ions. *Cardiovasc. Res.* 1997; **33**: 548-60.
 75. Martin PEM, Hill NS, Kristensen B, Errington RJ, Griffith TM. Ouabain exerts biphasic effects on connexin functionality and expression in vascular smooth muscle cells. *Br. J. Pharmacol.* 2004; **141**: 374-84.
 76. Hirst GDS, Neild TO. Some properties of spontaneous excitatory junction potentials recorded from arterioles of guinea-pigs. *J. Physiol.* 1980; **303**: 43-60.
 77. Finkel AS, Hirst GDS, Van Helden DF. Some properties of excitatory junction currents recorded from submucosal arterioles of guinea-pig ileum. *J. Physiol.* 1984; **351**: 87-98.
 78. Neild TO. Measurement of arteriole diameter changes by analysis of television images. *Blood Vessels* 1989; **26**: 48-52.
 79. Parkington HC, Tare M, Tonta MA, Coleman HA. Stretch revealed three components in the hyperpolarization of guinea-pig coronary artery in response to acetylcholine. *J. Physiol.* 1993; **465**: 459-76.
 80. Coleman HA, Tare M, Parkington HC. Myoendothelial electrical coupling in arteries and arterioles and its implications for Endothelium-Derived Hyperpolarizing Factor. *Clin. Exp. Pharmacol. Physiol.* 2002; **29**: 630-7.
 81. Sandow SL, Tare M, Coleman HA, Hill CE, Parkington HC. Involvement of myoendothelial gap junctions in the actions of endothelium-derived hyperpolarizing factor. *Circ. Res.* 2002; **90**: 1108-13.
 82. Sandow SL, Hill CE. Incidence of myoendothelial gap junctions in the proximal and distal mesenteric arteries of the rat is suggestive of a role in endothelium-derived hyperpolarizing factor-mediated responses. *Circ. Res.* 2000; **86**: 341-6.
 83. Neylon CB, Lang RJ, Fu Y, Bobik A, Reinhart PH. Molecular cloning and characterization of the intermediate-conductance Ca²⁺-activated K⁺ channel in vascular smooth muscle. *Circ. Res.* 1999; **85**: e33-43.
 84. Köhler R, Wulff H, Eichler I, Kneifel M, Neumann D, Knorr A, et al. Blockade of the intermediate-conductance calcium-activated potassium channel as a new therapeutic strategy for restenosis. *Circ.* 2003; **108**: 1119-25.
 85. Burnham MP, Bychov R, Féléto M, Richards GR, Vanhoutte PM, Weston AH, et al. Characterization of an apamin-sensitive small-conductance Ca²⁺-activated K⁺ channel in porcine coronary artery endothelium: relevance to EDHF. *Br. J. Pharmacol.* 2002; **135**: 1133-43.
 86. Taylor MS, Bonev AD, Gross TP, Eckman DM, Brayden JE, Bond CT, et al. Altered expression of small-conductance Ca²⁺-activated K⁺ (SK3) channels modulates arterial tone and blood pressure. *Circ. Res.* 2003; **93**: 124-31.
 87. Van Renterghem C, Vigne P, Frelin C. A charybdotoxin-sensitive, Ca²⁺-activated K⁺ channel with inward rectifying properties in brain microvascular endothelial cells: Properties and activation by endothelins. *J. Neurochem.* 1995; **65**: 1274-81.
 88. Marchenko SM, Sage SO. Calcium-activated potassium channels in the endothelium of intact rat aorta. *J. Physiol.* 1996; **492**: 53-60.
 89. Bychkov R, Burnham MP, Richards GR, Edwards G, Weston AH, Féléto M, et al. Characterization of a charybdotoxin-sensitive intermediate conductance Ca²⁺-activated K⁺ channel in porcine coronary endothelium: relevance to EDHF. *Br. J. Pharmacol.* 2002; **137**: 1346-54.
 90. Chen G, Cheung DW. Characterization of acetylcholine-induced membrane hyperpolarization in endothelial cells. *Circ. Res.* 1992; **70**: 257-63.
 91. Ohashi M, Satoh K, Itoh T. Acetylcholine-induced membrane potential changes in endothelial cells of rabbit aortic valve. *Br. J. Pharmacol.* 1999; **126**: 19-26.
 92. Doughty JM, Plane F, Langton PD. Charybdotoxin and apamin block EDHF in rat mesenteric artery if selectively applied to the endothelium. *Am. J. Physiol.* 1999; **276**: H1107-12.
 93. Widmann MD, Weintraub NL, Fudge JL, Brooks LA, Dellsperger KC. Cytochrome P-450 pathway in acetylcholine-induced canine coronary microvascular vasodilation in vivo. *Am. J. Physiol.* 1998; **274**: H283-9.
 94. De Wit C, Esser N, Lehr H, Bolz S, Pohl U. Pentobarbital-sensitive EDHF mediates ACh-induced arteriolar dilation in the hamster microcirculation. *Am. J. Physiol.* 1999; **276**: H1527-34.

95. Hungerford JE, Sessa WC, Segal SS. Vasomotor control in arterioles of the mouse cremaster muscle. *FASEB J.* 2000; **14**: 197-207.
96. Parkington HC, Chow J-AM, Evans RG, Coleman HA, Tare M. Role for endothelium-derived hyperpolarizing factor in vascular tone in rat mesenteric and hindlimb circulations *in vivo*. *J. Physiol.* 2002; **542**: 929-37.
97. De Vriese AS, Van de Voorde J, Lameire NH. Effects of connexin-mimetic peptides on nitric oxide synthase- and cyclooxygenase-independent renal vasodilation. *Kidney Int.* 2002; **61**: 177-85.
98. Fujii K, Tominaga M, Ohmori S, Kobayashi K, Koga T, Takata Y, et al. Decreased endothelium-dependent hyperpolarization to acetylcholine in smooth muscle of the mesenteric artery of spontaneously hypertensive rats. *Circ. Res.* 1992; **70**: 660-9.
99. Kenny LC, Baker PN, Kendall DA, Randall MD, Dunn WR. Differential mechanisms of endothelium-dependent vasodilator responses in human myometrial small arteries in normal pregnancy and pre-eclampsia. *Clinical Science* 2002; **103**: 67-73.
100. Fukao M, Hattori Y, Kanno M, Sakuma I, Kitabatake A. Alterations in endothelium-dependent hyperpolarization and relaxation in mesenteric arteries from streptozotocin-induced diabetic rats. *Br. J. Pharmacol.* 1997; **121**: 1383-91.
101. Wigg SJ, Tare M, Tonta MA, O'Brien RC, Meredith IT, Parkington HC. Comparison of effects of diabetes mellitus on an EDHF-dependent and an EDHF-independent artery. *Am. J. Physiol.* 2001; **281**: H232-40.
102. Makino A, Ohuchi K, Kamata K. Mechanisms underlying the attenuation of endothelium-dependent vasodilatation in the mesenteric arterial bed of the streptozotocin-induced diabetic rat. *Br. J. Pharmacol.* 2000; **130**: 549-56.
103. De Vriese AS, Van de Voorde J, Blom HJ, Vanhoutte PM, Verbeke M, Lameire NH. The impaired renal vasodilator response attributed to endothelium-derived hyperpolarizing factor in streptozotocin-induced diabetic rats is restored by 5-methyltetrahydrofolate. *Diabetologia* 2000; **43**: 1116-25.
104. Lau WAK, Reid JJ. Comparison of endothelial cell function in large and small arteries from the obese zucker rat. *Proc. Aust. Physiol. Pharmacol. Soc.* 2000; **31**: 66P.
105. Pannirselvam M, Verma S, Anderson TJ, Triggle CR. Cellular basis of endothelial dysfunction in small mesenteric arteries from spontaneously diabetic (*db/db* *-/-*) mice: role of decreased tetrahydrobiopterin bioavailability. *Br. J. Pharmacol.* 2002; **136**: 255-63.
106. Tare M, Coleman HA, Parkington HC. Regulation of vascular smooth muscle relaxation by the endothelium in health and in diabetes (with a focus on endothelium-derived hyperpolarizing factor). *Neurophys.* 2003; **35**: 284-9.

Received 10 December 2003, in revised form 25 May 2004.

Accepted 26 May 2004.

©H.A. Coleman 2004.

Author for correspondence:

Dr H.A. Coleman

Department of Physiology

Monash University, Victoria 3800

Australia

Tel: +61 3 9905 2520

Fax: +61 3 9905 2547

Email: harry.coleman@med.monash.edu.au

Changes in EDHF in hypertension and ageing: response to chronic treatment with renin-angiotensin system inhibitors

Kenichi Goto, Koji Fujii, Yasuo Kansui & Mitsuo Iida

Department of Medicine and Clinical Science,
Graduate School of Medical Sciences,
Kyushu University,
Fukuoka, Japan

Summary

1. Endothelial function is impaired in hypertension and ageing and this may be associated with an increase in cardiovascular disease. Several clinical studies have shown that blocking the renin-angiotensin system (RAS) improves endothelial function not only in hypertensive patients but also in normotensive patients with cardiovascular disease. The aim of the present study was to test whether endothelium-derived hyperpolarising factor (EDHF) - mediated smooth muscle hyperpolarisation and relaxation are altered in hypertension and ageing, and if so, whether chronic treatment with RAS inhibitors (the angiotensin-converting enzyme inhibitor enalapril and the angiotensin type 1 receptor antagonist candesartan) would correct such changes.

2. EDHF-mediated responses were examined in mesenteric arteries from 12-month-old spontaneously hypertensive rats (SHR) and 3-, 6-, 12-, and 24-month-old normotensive Wistar-Kyoto rats (WKY). Furthermore, both strains were treated for three months with either RAS blockers or a conventional therapy with hydralazine and hydrochlorothiazide from 9- to 12-month-old. In arteries of 12-month-old SHR, EDHF-mediated responses were impaired compared with age-matched WKY. In SHR, all the antihypertensive treatments improved the impairment of EDHF-mediated responses; however, RAS inhibitors tended to improve these responses to a greater extent compared with the conventional therapy with hydralazine and hydrochlorothiazide. In arteries of WKY, EDHF-mediated responses were impaired at the age of 12 and 24 months compared with those of 3- and 6-month-old rats, with the response tending to be impaired to a greater extent in 24-month-old rats. Three months of treatment of WKY until the age of 12 months with RAS inhibitors but not with a conventional therapy with hydralazine and hydrochlorothiazide improved the age-related impairment of EDHF-mediated responses, despite a similar reduction in blood pressure by both treatments.

3. These findings suggest that: (1) EDHF-mediated hyperpolarisation and relaxation decline with hypertension and ageing in rat mesenteric arteries; (2) antihypertensive treatment restores the impaired EDHF-mediated responses in hypertension; (3) RAS inhibitors may be more efficacious in improving endothelial dysfunction associated with hypertension; and (4) chronic treatment with RAS inhibitors improves the age-related impairment of EDHF-mediated responses presumably through the blockade of

RAS but not blood pressure lowering alone.

Introduction

Endothelial cells play an important role in the regulation of vascular tone through the release of several factors such as nitric oxide (NO), prostacyclin, and endothelium-derived hyperpolarising factor (EDHF).^{1,2} Although the nature of EDHF is still controversial, EDHF appears to be a dominant vasodilator in resistance arteries.³⁻⁵

Endothelial dysfunction is associated with various cardiovascular risk factors, such as hypertension, ageing, diabetes mellitus, and hypercholesterolemia.^{6,7} Endothelial dysfunction may facilitate the progress of atherosclerosis^{6,7}, thereby leading to cardiovascular diseases.⁸ It is, therefore, of clinical importance to find out the underlying mechanisms of, and effective treatments for endothelial dysfunction. In the present paper, the role of EDHF in hypertension and ageing and its modulation by drug treatment – especially the effects of renin-angiotensin system (RAS) inhibitors – will be discussed.

EDHF in hypertension

Endothelium-dependent relaxation is impaired both in animal models of experimental hypertension and in patients with hypertension.⁹ Several mechanisms have been proposed to explain the endothelial dysfunction in hypertension: reduced NO production, increased production of endothelium-derived contracting factors and increased generation of oxygen-derived free radicals.⁹

Fujii *et al.*¹⁰ have evaluated the relative contribution of EDHF in acetylcholine (ACh) -induced responses in the superior mesenteric arteries of spontaneously hypertensive rats (SHR). In this study, they showed that EDHF-mediated hyperpolarisation and relaxation were decreased in SHR compared with age-matched normotensive Wistar-Kyoto rats (WKY). In contrast, endothelium-dependent relaxation via NO was preserved in SHR.¹¹ Fujii *et al.* have also showed that neither NO synthase inhibitors nor a cyclooxygenase inhibitor affected ACh-induced hyperpolarisation in the rat superior mesenteric arteries,¹⁰ which suggests that ACh-induced hyperpolarisation is not mediated by endothelium derived NO or prostanoids in this vascular bed. Subsequent studies¹¹⁻¹⁴ confirmed the impairment of EDHF-mediated responses in mesenteric arteries from genetically hypertensive rats. Similar

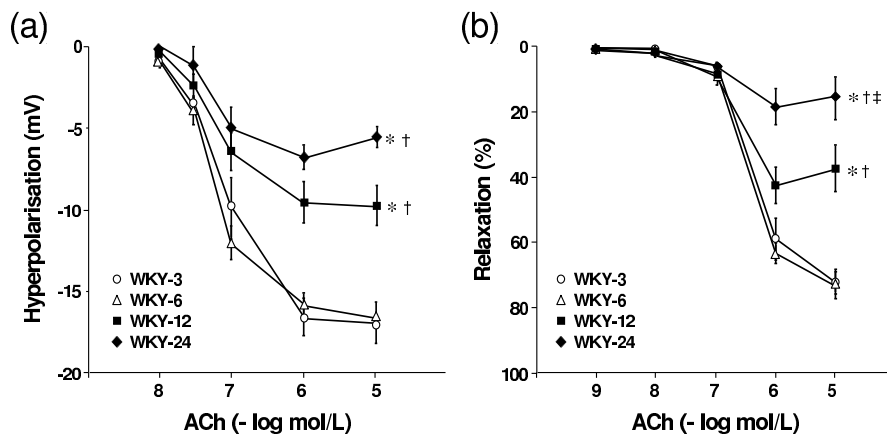


Figure 1. (a) Acetylcholine (ACh)-induced hyperpolarisation in mesenteric arteries of 3- (WKY-3), 6- (WKY-6), 12- (WKY-12), and 24-month-old Wistar Kyoto rats (WKY-24). ACh was applied under resting conditions without treatment. (b) ACh-induced relaxation in mesenteric arterial rings precontracted with norepinephrine (10^{-5} mol/L) in the presence of indomethacin (10^{-5} mol/L) and N^G -nitro-L-arginine (10^{-4} mol/L) of WKY-3, WKY-6, WKY-12, and WKY-24. Values are mean \pm SEM ($n=6-10$). * $P < 0.05$ vs. WKY-3; † $P < 0.05$ vs. WKY-6; ‡ $P < 0.05$ vs. WKY-12. (Reproduced from Fujii et al.,²¹ with permission).

observations were also reported in the aorta of two-kidney, one clip renal hypertensive rats¹⁵ and in the renal artery of aged SHR.¹⁶ These findings indicate that EDHF-mediated responses are impaired in hypertension, and the impairment of EDHF pathway may account, at least in part, for the endothelial dysfunction associated with hypertension. On the other hand, it has been recently reported that enhanced EDHF effect may compensate for the loss of NO and maintain the vasodilatory response to ACh in mesenteric arteries of Sprague-Dawley rats fed a high salt diet.¹⁷ Furthermore, Sandow *et al.* have reported that the incidence of myoendothelial gap junctions, which enables electrical and/or chemical coupling between endothelial cell and smooth muscle cell layers, was increased to maintain a functional role for EDHF in caudal artery of SHR.¹⁸

The reason for the difference in the results of these studies is not known, but may in part arise from differences in the type, severity and/or duration of hypertension.

EDHF in ageing

Ageing is associated with endothelial dysfunction both in humans and animal models.¹⁹ Reduced NO-mediated relaxation and/or increased cyclooxygenase-dependent constriction could partially underpin age-related endothelial dysfunction depending on the species and the vascular bed studied.¹⁹ In the present study, age related changes in EDHF-mediated hyperpolarisation and relaxation to ACh were studied in the superior mesenteric arteries from 3-, 6-, 12-, and 24-month-old WKY.^{20,21} EDHF-mediated hyperpolarisation was significantly smaller in arteries from 12- and 24-month-old rats compared with 3- and 6-month-old rats, with the response tending to be

smaller in 24-month-old rats than in 12-month-old rats. EDHF-mediated relaxation also decreased with increasing age (Fig. 1). In contrast, there was no difference in NO-mediated relaxation between 3- and 12-month-old rats. The age-related decline in EDHF-mediated responses observed here are consistent with previous studies by others.^{12,22} Thus, the impairment of the EDHF pathway may account, at least in part, for the age-related endothelial dysfunction in rat mesenteric arteries.

The EDHF pathway does exist in human arteries.^{23,24} Urakami-Harasawa *et al.*²⁴ have reported that EDHF-mediated relaxation was reduced with ageing in human gastroepiploic arteries. Thus, the reduced EDHF-mediated responses would also contribute to the age-related endothelial dysfunction in humans.

Effect of antihypertensive treatment on EDHF-mediated responses in hypertension

Hypertension is associated with endothelial dysfunction.⁹ Endothelial dysfunction may aggravate the progression of atherosclerosis, which could lead to cardiovascular disease.⁶⁻⁸ Hence, it is plausible to suggest that the improvement of endothelial function will reduce the occurrence of cardiovascular disease. Although several studies found that antihypertensive treatments improve endothelial function both in animal models of experimental hypertension⁹ and in patients with hypertension,²⁵ the effects of chronic antihypertensive treatment on EDHF-mediated hyperpolarisation *per se* are unknown.

The effects of chronic antihypertensive treatments on EDHF-mediated hyperpolarisation and relaxation were tested in the mesenteric arteries of SHR.^{11,14} SHR were

Table. Systolic blood pressure before and after 3 months of treatment. Values are mean \pm SEM. There were 7 to 12 rats in each group.

	Blood pressure (mmHg)			Blood pressure (mmHg)	
	Before	After		Before	After
SHR-12	241 \pm 6	253 \pm 6	WKY-12	150 \pm 4	156 \pm 5
SHR-12-H	242 \pm 6	163 \pm 6 *†	WKY-12-H	158 \pm 4	124 \pm 4 *§
SHR-12-ENA	245 \pm 5	135 \pm 6 *†	WKY-12-ENA	157 \pm 3	123 \pm 6 *§
SHR-12-CAN	239 \pm 7	120 \pm 6 *†‡	WKY-12-CAN	153 \pm 3	125 \pm 2 *§
SHR-12-C&E	246 \pm 7	111 \pm 3 *†‡			
WKY-12	151 \pm 5 †	155 \pm 4 †			

* $P < 0.05$ vs before treatment; † $P < 0.05$ vs SHR-12; ‡ $P < 0.05$ vs SHR-12-H; § $P < 0.05$ vs WKY-12

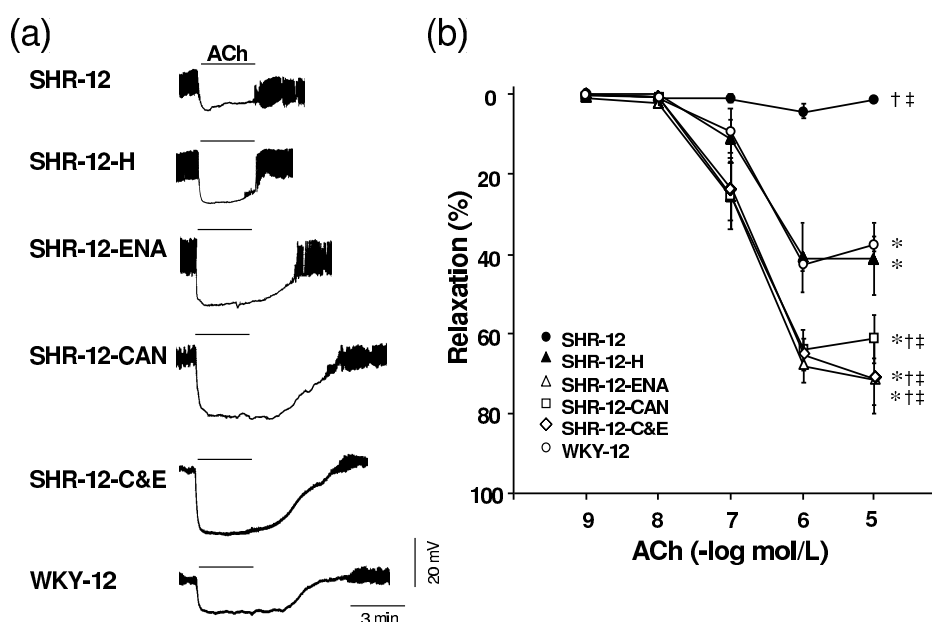


Figure 2. (a) Representative tracings showing hyperpolarisation to 10^{-5} mol/L acetylcholine (ACh) under conditions of depolarisation with norepinephrine (10^{-5} mol/L) in the presence of indomethacin (10^{-5} mol/L) in mesenteric arteries of untreated 12-month-old spontaneously hypertensive rats (SHR-12), SHR treated with a combination of hydralazine and hydrochlorothiazide (SHR-12-H), enalapril-treated SHR (SHR-12-ENA), candesartan-treated SHR (SHR-12-CAN), SHR treated with a combination of candesartan and enalapril (SHR-12-C&E), and untreated 12-month-old Wistar Kyoto rats (WKY-12). (b) ACh-induced relaxation in mesenteric arterial rings precontracted with norepinephrine (10^{-5} mol/L) in the presence of indomethacin (10^{-5} mol/L) and N^G -nitro-L-arginine (10^{-4} mol/L) of SHR-12, SHR-12-H, SHR-12-ENA, SHR-12-CAN, SHR-12-C&E, and WKY-12. Values are mean \pm SEM ($n=8-12$). * $P < 0.05$ vs. SHR-12; † $P < 0.05$ vs. WKY-12; ‡ $P < 0.05$ vs. SHR-12-H. (Modified from Goto et al.,¹⁴ with permission).

treated for 3 months with either the combination of hydralazine and hydrochlorothiazide, enalapril, an angiotensin converting enzyme (ACE) inhibitor, candesartan, an angiotensin type 1 (AT1) receptor antagonist, or the combination of enalapril and candesartan from 9- to 12-month-old. The combination of hydralazine and hydrochlorothiazide improved EDHF-mediated hyperpolarisation and relaxation to a similar level to that of WKY. Interestingly, however, the improvement achieved

by RAS inhibitors was significantly greater than that with a conventional therapy with hydralazine and hydrochlorothiazide, despite a similar, or only a slightly greater reduction in blood pressure (Table, Fig. 2). These results suggest that in addition to blood pressure lowering, inhibition of the RAS may play an important role in improving endothelial function.^{11,14}

Although both ACE inhibitors and AT1 receptor antagonists inhibit the RAS, each drug has its specific

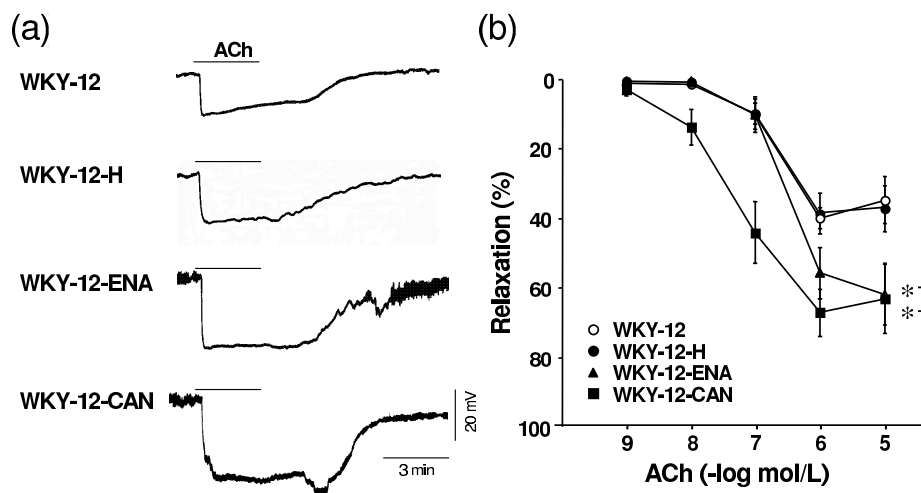


Figure 3. (a) Representative tracings showing hyperpolarisation to 10^{-5} mol/L acetylcholine (ACh) under conditions of depolarisation with norepinephrine (10^{-5} mol/L) in the presence of indomethacin (10^{-5} mol/L) in mesenteric arteries of untreated 12-month-old Wistar Kyoto rats (WKY-12), WKY treated with a combination of hydralazine and hydrochlorothiazide (WKY-12-H), enalapril-treated WKY (WKY-12-ENA), and candesartan-treated WKY (WKY-12-CAN). (b) ACh-induced relaxation in mesenteric arterial rings precontracted with norepinephrine (10^{-5} mol/L) in the presence of indomethacin (10^{-5} mol/L) and N^G -nitro-L-arginine (10^{-4} mol/L) of WKY-12, WKY-12-H, WKY-12-ENA, and WKY-12-CAN. Values are mean \pm SEM ($n=6-12$). * $P < 0.05$ vs. WKY-12; † $P < 0.05$ vs. WKY-12-H. (Modified from Goto et al.,³¹ with permission).

pharmacological profiles: ACE inhibitors prevent the degradation of bradykinin, a peptide that induces endothelium-dependent relaxation²³; AT1 receptor antagonists block the action of angiotensin II regardless of its generation pathway²⁶; under blockade of AT1 receptors, angiotensin II may stimulate unopposed angiotensin type 2 receptors.²⁷ However, in the present study, enalapril and candesartan were equally effective in improving EDHF-mediated responses, which indicates that the specific pharmacological profiles of each drug may not play a major role in improving EDHF-mediated responses in rat mesenteric arteries. Kähönen *et al.*²⁸ also showed that an ACE inhibitor and an AT1 receptor antagonist improved the EDHF-mediated relaxation to a similar extent in mesenteric arteries of SHR.

Several recent clinical studies^{29,30} have reported the beneficial effects of the combination therapy with an ACE inhibitor and an AT1 receptor antagonist. In the present study, however, the combination therapy did not appear to have definitive advantages over each therapy in improving EDHF-mediated responses (Fig. 2).

In summary, the above data indicate that: (1) chronic antihypertensive treatments restore the impaired EDHF-mediated responses in SHR; (2) RAS inhibitors may be more effective in improving endothelial dysfunction; and (3) the combination of an ACE inhibitor and an AT1 receptor antagonist does not seem to be more effective than treatment with either drug alone. The clinical relevance of the present finding remains to be determined.

Effect of renin-angiotensin system inhibitors on EDHF-mediated responses in ageing

Endothelial dysfunction associated with ageing may contribute in part to the frequent occurrence of cardiovascular disease with ageing in humans. Thus, it is clinically relevant to prevent or reverse endothelial dysfunction associated with ageing. In SHR, antihypertensive treatments with RAS inhibitors tended to be more effective in improving endothelial dysfunction compared with conventional antihypertensive drugs.^{11,14} These observations led to the hypothesis that RAS inhibitors may have a favourable effect on endothelial function independent of its blood pressure lowering effect.

The effects of RAS inhibitors on age-related impairment of EDHF-mediated responses were studied using mesenteric arteries of WKY.^{31,32} WKY were treated for 3 months with either enalapril, candesartan or a combination of hydralazine and hydrochlorothiazide from 9- to 12-month-old. All the treatments lowered blood pressure to a similar extent (Table). EDHF-mediated hyperpolarisation and relaxation were improved in the enalapril and candesartan treated groups. In contrast, a combination of hydralazine and hydrochlorothiazide failed to improve endothelial function, despite a similar reduction in blood pressure (Fig. 3). These findings suggest that RAS inhibitors restore the age-related impairment of EDHF-mediated responses presumably through the blockade of the RAS *per se*, although we cannot totally rule out the possibility that both RAS inhibition and blood pressure

lowering are required for the improvement of endothelial function. Thus, RAS inhibitors may serve as novel tools with which to prevent endothelial dysfunction associated with ageing.

Future directions

Because of the unidentified nature of EDHF,³⁻⁵ the mechanism of the alteration in EDHF associated with hypertension and ageing remains speculative. Likewise, how RAS inhibitors improve impaired EDHF-mediated responses remains an open question. However, considering the critical role of gap junctions in EDHF-mediated responses in rat mesenteric arteries^{33,34}, impairment of the EDHF pathway and its improvement by RAS inhibitors could be associated with structural and/or biochemical changes in gap junctions. This notion may be supported by the recent report by Rummery *et al.*³⁵ that showed expression of connexins, which comprise gap junctions, were decreased in the endothelium of the caudal artery in hypertension. Whether impairment of EDHF-mediated responses in disease states is attributable to abnormalities of gap junctions awaits further studies.

Conclusions

EDHF mediated hyperpolarisation and relaxation were impaired in hypertension and ageing. Chronic treatment with RAS inhibitors restored these impairments, and RAS inhibitors appear to have a favourable effect on endothelial function beyond its blood pressure lowering effect. Thus, RAS inhibitors may have a therapeutic potential in the prevention or treatment of cardiovascular diseases.

Acknowledgements

We thank Prof. Caryl Hill for critically reading the manuscript. The authors' original work presented or cited in this paper was supported by a Grant-in-Aid for Scientific Research from the Ministry of Education, Culture, Sports, Science and Technology of Japan, Tokyo, Japan. Fig. 1 was reproduced from: Fujii K, Goto K, Abe I. Inhibition of converting enzyme prevents the age-related decline in endothelium-dependent hyperpolarization. In: Vanhoutte PM (ed). *EDHF 2000* 2001; 410-6, permission granted by Taylor & Francis.

References

1. Hill CE, Phillips JK, Sandow SL. Heterogeneous control of blood flow amongst different vascular beds. *Med. Res. Rev.* 2001; **21**: 1-60.
2. Suzuki H, Chen G. Endothelium-derived hyperpolarizing factor (EDHF): An endogenous potassium-channel activator. *News Physiol. Sci.* 1990; **5**: 212-5.
3. McGuire JJ, Ding H, Triggler CR. Endothelium-derived relaxing factors: a focus on endothelium-derived hyperpolarizing factor(s). *Can. J. Physiol. Pharmacol.* 2001; **79**: 443-70.
4. Campbell WB, Gauthier KM. What is new in

- endothelium-derived hyperpolarizing factors? *Curr. Opin. Nephrol. Hypertens.* 2002; **11**: 177-83.
5. Busse R, Edwards G, Feletou M, Fleming I, Vanhoutte PM, Weston AH. EDHF: bringing the concepts together. *Trends Pharmacol. Sci.* 2002; **23**: 374-80.
6. Vanhoutte PM. Endothelial dysfunction and atherosclerosis. *Eur. Heart J.* 1997; **18**: E19-29.
7. Schiffrin EL. Beyond blood pressure: the endothelium and atherosclerosis progression. *Am. J. Hypertens.* 2002; **15**: 115S-22S.
8. Halcox JP, Schenke WH, Zalos G, Mincemoyer R, Prasad A, Waclawiw MA, Nour KR, Quyyumi AA. Prognostic value of coronary vascular endothelial dysfunction. *Circulation* 2002; **106**: 653-8.
9. Vanhoutte PM. Endothelial dysfunction in hypertension. *J. Hypertens.* 1996; **14**: S83-93.
10. Fujii K, Tominaga M, Ohmori S, Kobayashi K, Koga T, Takata Y, Fujishima M. Decreased endothelium-dependent hyperpolarization to acetylcholine in smooth muscle of the mesenteric artery of spontaneously hypertensive rats. *Circ. Res.* 1992; **70**: 660-9.
11. Onaka U, Fujii K, Abe I, Fujishima M. Antihypertensive treatment improves endothelium-dependent hyperpolarization in the mesenteric artery of spontaneously hypertensive rats. *Circulation* 1998; **98**: 175-82.
12. Mantelli L, Amerini S, Ledda F. Roles of nitric oxide and endothelium-derived hyperpolarizing factor in vasorelaxant effect of acetylcholine as influenced by aging and hypertension. *J. Cardiovasc. Pharmacol.* 1995; **25**: 595-602.
13. Sunano S, Watanabe H, Tanaka S, Sekiguchi F, Shimamura K. Endothelium-derived relaxing, contracting and hyperpolarizing factors of mesenteric arteries of hypertensive and normotensive rats. *Br. J. Pharmacol.* 1999; **126**: 709-16.
14. Goto K, Fujii K, Onaka U, Abe I, Fujishima M. Renin-angiotensin system blockade improves endothelial dysfunction in hypertension. *Hypertension* 2000; **36**: 575-80.
15. Van de Voorde J, Vanheel B, Leusen I. Endothelium-dependent relaxation and hyperpolarization in aorta from control and renal hypertensive rats. *Circ. Res.* 1992; **70**: 1-8.
16. Bussemaker E, Popp R, Fisslthaler B, Larson CM, Fleming I, Busse R, Brandes RP. Aged spontaneously hypertensive rats exhibit a selective loss of EDHF-mediated relaxation in the renal artery. *Hypertension* 2003; **42**: 562-8.
17. Sofola OA, Knill A, Hainsworth R, Drinkhill M. Change in endothelial function in mesenteric arteries of Sprague-Dawley rats fed a high salt diet. *J. Physiol.* 2002; **543**: 255-60.
18. Sandow SL, Bramich NJ, Bandi HP, Rummery NM, Hill CE. Structure, function, and endothelium-derived hyperpolarizing factor in the caudal artery of the SHR and WKY rat. *Arterioscler. Thromb. Vasc.*

- Biol.* 2003; **23**: 822-8.
19. Matz RL, Andriantsitohaina R. Age-related endothelial dysfunction: potential implications for pharmacotherapy. *Drugs Aging.* 2003; **20**: 527-50.
 20. Fujii K, Ohmori S, Tominaga M, Abe I, Takata Y, Ohya Y, Kobayashi K, Fujishima M. Age-related changes in endothelium-dependent hyperpolarization in the rat mesenteric artery. *Am. J. Physiol.* 1993; **265**: H509-16.
 21. Fujii K, Goto K, Abe I. Inhibition of converting enzyme prevents the age-related decline in endothelium-dependent hyperpolarization. In: Vanhoutte PM (ed). EDHF 2000. Taylor & Francis, London. 2001; Ch. 45.
 22. Nakashima M, Vanhoutte PM. Decreased endothelium-dependent hyperpolarization with aging and hypertension in the rat mesenteric artery. In: Vanhoutte PM (ed). Endothelium-Derived Hyperpolarizing Factor. Harwood Academic, Amsterdam. 1996; Ch. 28.
 23. Nakashima M, Mombouli JV, Taylor AA, Vanhoutte PM. Endothelium-dependent hyperpolarization caused by bradykinin in human coronary arteries. *J. Clin. Invest.* 1993; **92**: 2867-71.
 24. Urakami-Harasawa L, Shimokawa H, Nakashima M, Egashira K, Takeshita A. Importance of endothelium-derived hyperpolarizing factor in human arteries. *J. Clin. Invest.* 1997; **100**: 2793-9.
 25. Taddei S, Virdis A, Ghiadoni L, Sudano I, Salvetti A. Effects of antihypertensive drugs on endothelial dysfunction: clinical implications. *Drugs* 2002; **62**: 265-84.
 26. Urata H, Nishimura H, Ganten D. Chymase-dependent angiotensin II forming systems in humans. *Am. J. Hypertens.* 1996; **9**: 277-84.
 27. Matsubara H. Pathophysiological role of angiotensin II type 2 receptor in cardiovascular and renal diseases. *Circ. Res.* 1998; **83**: 1182-91.
 28. Kahonen M, Tolvanen JP, Kalliovalkama J, Wu X, Karjala K, Makynen H, Porsti I. Losartan and enalapril therapies enhance vasodilatation in the mesenteric artery of spontaneously hypertensive rats. *Eur. J. Pharmacol.* 1999; **368**: 213-22.
 29. McKelvie RS, Yusuf S, Pericak D, Avezum A, Burns RJ, Probstfield J, Tsuyuki RT, White M, Rouleau J, Latini R, Maggioni A, Young J, Pogue J. Comparison of candesartan, enalapril, and their combination in congestive heart failure: randomized evaluation of strategies for left ventricular dysfunction (RESOLVD) pilot study. The RESOLVD Pilot Study Investigators. *Circulation* 1999; **100**: 1056-64.
 30. McMurray JJ, Ostergren J, Swedberg K, Granger CB, Held P, Michelson EL, Olofsson B, Yusuf S, Pfeffer MA; CHARM Investigators and Committees. Effects of candesartan in patients with chronic heart failure and reduced left-ventricular systolic function taking angiotensin-converting-enzyme inhibitors: the CHARM-Added trial. *Lancet* 2003; **362**: 767-71.
 31. Goto K, Fujii K, Onaka U, Abe I, Fujishima M. Angiotensin-converting enzyme inhibitor prevents age-related endothelial dysfunction. *Hypertension* 2000; **36**: 581-7.
 32. Kansui Y, Fujii K, Goto K, Abe I, Iida M. Angiotensin II receptor antagonist improves age-related endothelial dysfunction. *J. Hypertens.* 2002; **20**: 439-46.
 33. Goto K, Fujii K, Kansui Y, Abe I, Iida M. Critical role of gap junctions in endothelium-dependent hyperpolarization in rat mesenteric arteries. *Clin. Exp. Pharmacol. Physiol.* 2002; **29**: 595-602.
 34. Sandow SL, Tare M, Coleman HA, Hill CE, Parkington HC. Involvement of myoendothelial gap junctions in the actions of endothelium-derived hyperpolarizing factor. *Circ. Res.* 2002; **90**: 1108-13.
 35. Rummery NM, McKenzie KU, Whitworth JA, Hill CE. Decreased endothelial size and connexin expression in rat caudal arteries during hypertension. *J. Hypertens.* 2002; **20**: 247-53..br

Received 1 December 2003; in revised form 8 February 2004. Accepted 9 February 2004.

©K. Goto 2004

Author for correspondence:
 Kenichi Goto
 Division of Neuroscience
 John Curtin School of Medical Research
 Australian National University,
 Canberra, A.C.T. 0200, Australia

Tel: +61 2 6125 2149
 Fax: +61 2 6125 8077
 Email: kenichi.goto@anu.edu.au

Activation of renal calcium and water excretion by novel physiological and pharmacological activators of the calcium-sensing receptor

Arthur D. Conigrave & Hiu Chuen Lok

School of Molecular and Microbial Biosciences, University of Sydney, NSW 2006, Australia.

Summary

1. Activated Ca²⁺-sensing receptors (CaRs) play key roles in the regulation of whole body calcium metabolism by inhibiting the secretion of the key calcitropic hormone, PTH and promoting urinary calcium excretion.

2. We have now examined the effects of intravenous administration of novel calcium receptor activators on renal function in anaesthetized female Wistar rats.

3. The type-II calcimimetic, NPS R467 and the CaR-active amino acids, L-Phe and L-Ala, which act at distinct binding sites on the receptor all activated urinary flow rate, calcium and osmolar excretion and suppressed urinary osmolality.

4. The effects of L-Phe and NPS R-467 on urine flow rate and calcium excretion were stereoselective consistent with the idea that these effects were mediated by calcium-sensing receptors.

5. However, D-Phe also suppressed urinary osmolality and promoted osmolar excretion possibly by exceeding the transport maximum in the proximal tubule.

6. The data indicate that novel activators of calcium-sensing receptors, including L-amino acids at physiologically relevant serum concentrations, play a significant role in the regulation of urinary calcium and water excretion.

Introduction

The calcium-sensing receptor (CaR) is a member of group C of the G-protein coupled receptor super-family. These receptors play multiple roles in calcium homeostasis including key roles in mediating the feedback regulation of parathyroid hormone secretion and urinary calcium excretion. Inactivating mutations of the CaR underlie several human pathological states including the relatively benign condition familial hypocalciuric hypercalcemia and its more severe but much rarer homozygous form, neonatal severe hyperparathyroidism which requires parathyroidectomy within the first few weeks of life (review:¹). The widespread distribution of these receptors, together with their resistance to desensitization, points to much wider roles in mammalian physiology (review:²).

Recently, two new classes of calcium-sensing receptor (CaR) activators have been identified. The type-II calcimimetics (e.g., NPS R-467 and R-568) were developed from a lead phenylalkylamine compound identified in a large-scale drug screen³. Type-II calcimimetics sensitize the CaR to calcium ions by binding to a site in the receptor's transmembrane region⁴. More recently, several sub-classes of L-amino acids (including aromatic, polar, and aliphatic amino acids) have been shown to act as

allosteric activators of the CaR. Furthermore, physiologically relevant fluctuations in the concentration of physiological amino acid mixtures can modulate receptor activity⁵. The amino acid binding site is likely to lie in the conserved N-terminal, Venus FlyTrap domain⁶.

In the kidney, the CaR is expressed in multiple sites. These include the apical membrane of the proximal tubule, the basolateral membrane of the cortical thick ascending limb (CTAL) and the apical membrane of the medullary collecting ducts (review:⁷). Thus, fluctuations in the serum levels of Ca²⁺ and amino acids might be expected to modulate CaR activity in the CTAL and fluctuations in the tubular fluid levels of Ca²⁺ and amino acids might be expected to modulate CaR activity in the proximal tubule and collecting ducts. Consistent with a role for the CaR in the regulation of urinary phosphate excretion, dietary phosphate loading has been shown to suppress the expression of the CaR in the apical brush border membrane of the proximal tubule⁸. Furthermore, the CaR agonist gadolinium (Gd³⁺) and the type-II calcimimetic NPS R-467 reversed PTH suppression of phosphate reabsorption in cultured proximal tubule cells⁹. On the other hand, expression of the CaR in the CTAL has been linked to the control of urinary calcium excretion and expression of the CaR in the collecting tubule has been linked to the control of urinary water excretion and osmolality. In particular, CaR activation suppresses vasopressin-induced water reabsorption, facilitating the excretion of solutes such as calcium, phosphate and oxalate that might otherwise contribute to the formation of renal calculi¹⁰.

The patterns of expression described above imply roles for CaR activators in the regulation of multiple renal functions including proximal tubular transport, calcium excretion and urinary concentration. For example, CaR-active amino acids (e.g., L-Phe and L-Ala) and type-II calcimimetics are predicted to promote calcium excretion (Fig. 1) and raise urine flow and suppress urinary osmolality (Fig. 2). We have examined the impact of intravenously administered L-amino acids or the type-II calcimimetic, NPS R-467 on renal calcium and water excretion in rats and report herein our preliminary findings. The data provide support for the hypotheses that CaR activators including L-amino acids promote urinary calcium and water excretion.

Materials and Methods

NPS R-467 and its 100-fold less potent isomer S-467 were the generous gifts of Dr Edward Nemeth (NPS Pharmaceuticals, Toronto, Canada). Animal experiments on a total of approximately forty rats were performed with approval from the University of Sydney Animal Ethics

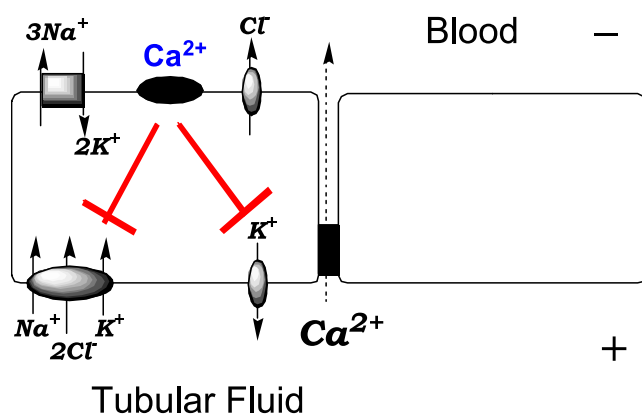


Figure 1. Schematic diagram of a thick ascending limb cell. The diagram shows the inhibitory effect of calcium-sensing receptor activation on apical $\text{Na}^+/\text{K}^+/\text{2Cl}^-$ co-transport and K^+ recycling. The impact of CaR activation is believed to be a reduction in the lumen-positive potential difference that drives Ca^{2+} reabsorption.

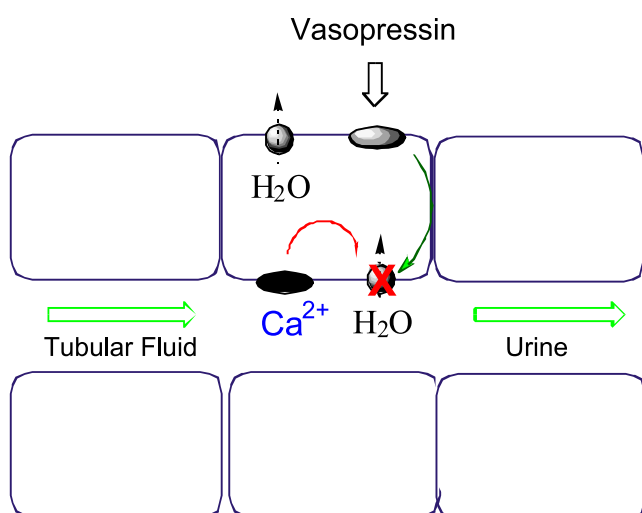


Figure 2. Schematic diagram of an epithelial cell from the collecting tubules. The diagram shows the inhibitory effect of CaR activation on vasopressin stimulated water reabsorption via aquaporin-2. In this way, CaR activators that have entered the renal filtrate and have not been reabsorbed in the proximal nephron may promote urinary water excretion.

Committee. Female Wistar rats (200-300 g) were anaesthetized with halothane (2% in oxygen; 0.8 mL/min) then catheterized. Both jugular veins were cannulated and the animals were infused at a constant rate (4 or 5 mL per h) with an isotonic physiological saline solution of the following composition: 140 mM NaCl, 4.0 mM KCl, 15 mM NaHCO_3 , 2.5 mM CaCl_2 , 1 mM MgCl_2 . After a 60 min equilibration period, continuous infusions of D and/or L-

amino acids were commenced, continuing for 60 min prior to return to the control solution. Blood samples (0.25 mL) were collected at regular intervals for analysis of serum creatinine, osmolality, total calcium and various amino acids. Urine samples were collected at 15 min intervals to assess flow rate, osmolality and the concentrations of creatinine, calcium and amino acids. Osmolality was determined by vapour pressure osmometry. Creatinine was determined by an adaptation of the alkaline picrate method¹¹ using a Wallac Victor2 multi-well plate reader and serum and urine total calcium concentrations were determined using an autoanalyzer (Roche/Hitachi 912). Amino acid levels in serum and urine were determined by HPLC separation and fluorimetric detection of O-phthalaldehyde-conjugates¹². In some experiments, bolus injections were administered to test for acute effects of R-467, S-467 and amino acids including L-Phe and L-Ala. The data are routinely expressed as means \pm SEM (number of experiments).

Results and Discussion

The type-II calcimimetic R-467 administered as a bolus intravenous injection of 2 μmol stereoselectively enhanced urinary calcium excretion (by 3-4 fold; Fig. 3A) and also promoted urinary flow rate (Fig. 3B). In addition, R-467 stereoselectively suppressed urinary osmolality from a baseline level of 946 ± 70 mosm/kg to 723 ± 80 mosm/kg ($n = 4$; $p = 0.01$) after 15 min consistent with an inhibitory action of the CaR on vasopressin-induced water reabsorption in the collecting ducts. Although the osmolality dropped, the osmolar excretion rate increased following exposure to R-467. The baseline osmolar excretion rate was 12.5 ± 2.4 $\mu\text{mol}/\text{min}$ and this increased to 34.6 ± 0.8 $\mu\text{mol}/\text{min}$ following R-467 ($n = 3$; $p = 0.01$). R-467 also lowered serum total calcium levels (not shown) as previously reported for the related calcimimetic R-568¹³. The 100-fold less potent isomer, S-467 was much less effective than R-467 on all of the parameters tested.

Infusions of the CaR-active L-amino acid, L-Phe sufficient to raise the serum level from 0.05 mM to about 2 mM (determined by HPLC), also elevated urinary calcium excretion (by about 2-fold; Fig. 4A) and urinary flow rate (Fig. 4B). Both effects were L/D selective (Fig. 4). In addition, both D-Phe and L-Phe reversibly suppressed urinary osmolality. In the case of L-Phe, urinary osmolality was maximally suppressed from 767 ± 20 mosm/kg to 599 ± 17 mosm/kg ($n = 3$) after 60 min. The reason for the apparent lack of L/D selectivity of this effect is not clear. However, it may have arisen from higher local D-amino acid concentrations in the tubular fluid as a result of the selectivity of proximal tubular amino acid transporters for L-amino acids. In addition, the osmolar excretion rate was significantly increased following exposure to L-Phe and D-Phe. The baseline osmolar excretion rate was 13.2 ± 3.6 $\mu\text{mol}/\text{min}$ and this increased to 33.4 ± 4.2 $\mu\text{mol}/\text{min}$ following D-Phe ($n = 3$; $p < 0.01$) and 36.7 ± 5.3 $\mu\text{mol}/\text{min}$ following L-Phe ($n = 3$; $p < 0.01$). Bolus injections of L-Phe and L-Ala also acutely elevated urinary

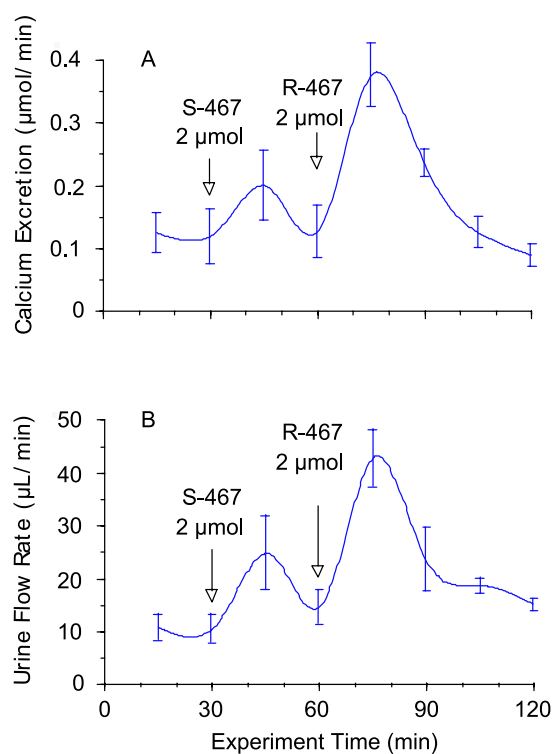


Figure 3. Effects of NPS R-467 on urinary calcium excretion and flow rate. Female Wistar rats were anaesthetised and infused intravenously with physiological saline at a rate of 4 mL/h via a jugular vein cannula. The CaR activator, R-467 and its stereoisomer S-467 were delivered intravenously as bolus injections (0.5 mL) in physiological saline. The data are means \pm SEM ($n=4$).

calcium excretion and flow rate and lowered urinary osmolality (not shown).

Taken together the data are consistent with the idea that novel activators of the CaR including L-amino acids and type-II calcimimetics such as R-467 mimic the effects of elevated plasma Ca^{2+} concentration on urinary calcium excretion, flow rate and osmolality. Increased serum and urinary amino acid concentrations associated, for example, with elevated dietary protein intake appear to act as physiological signals for enhanced solute and water excretion. CaR activators from distinct structural groups and targeting distinct binding sites on the receptor have similar effects on renal calcium and water excretion consistent with the proposed sites of CaR action in the thick ascending limb and collecting tubules.

Acknowledgements

The author's work is supported by the NHMRC of Australia.

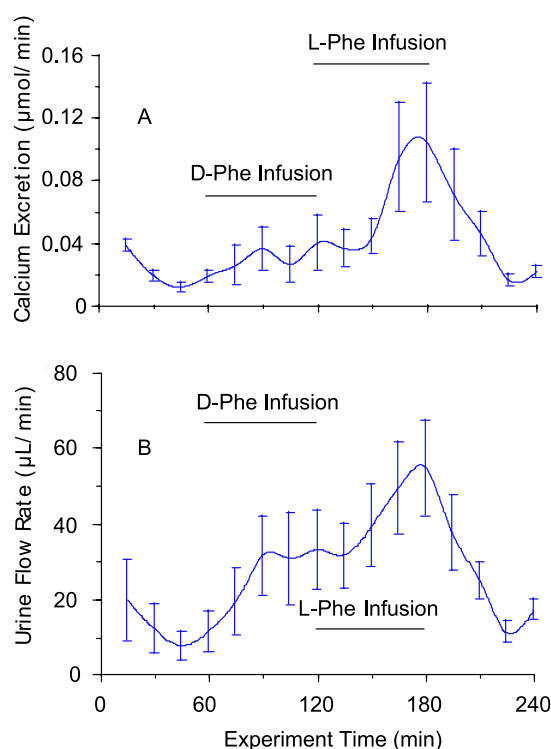


Figure 4. Effects of L-Phe and D-Phe infusions on urinary calcium excretion and flow rate. Female Wistar rats were anaesthetised and infused intravenously with physiological saline at a rate of 4 mL/h via a jugular vein cannula. After 60 min, the infusion was switched to saline that contained D-Phe (200 mM) and, after 120 min, to saline that contained L-Phe (200 mM). The maximum plasma amino acid concentration observed under the conditions of these experiments was approximately 2 mM (baseline level around 0.05 mM) and the urine amino acid concentration rose to around 20 mM in the case of D-Phe and around 10 mM in the case of L-Phe. The data are means \pm SEM ($n=4$).

References

1. Brown EM, Pollak M, Seidman CE, Seidman JG, Riccardi D, Hebert, SC. Calcium-ion-sensing cell-surface receptors. *N. Engl. J. Med.* 1995; **333**: 234-40.
2. Brown EM, MacLeod RJ. Extracellular calcium sensing and extracellular calcium signaling, *Physiol. Rev.* 2001; **81**: 239-97.
3. Nemeth EF, Steffey ME, Hammerland LG, Hung BCP, Vanwagenen BC, Delmar EG, Balandrin, MF. Calcimimetics with potent and selective activity on the parathyroid calcium receptor, *Proc. Natl. Acad. Sci. USA* 1998; **95**: 4040-5.
4. Hauache OM, Hu J, Ray K, Xie R, Jacobson KA, Spiegel AM. Effects of a calcimimetic compound and naturally activating mutations on the human Ca^{2+} receptor and on Ca^{2+} receptor/metabotropic glutamate chimeric receptors, *Endocrinology* 2000;

141: 4156-63.

5. Conigrave AD, Quinn SJ, Brown EM. L-amino acid sensing by the extracellular Ca²⁺-sensing receptor, *Proc. Natl. Acad. Sci. USA* 2000; **97**: 4814-9.
6. Zhang Z, Qiu W, Quinn SJ, Conigrave AD, Brown EM, Bai M. Three adjacent serines in the extracellular domains of the CaR are required for L-amino acid-mediated potentiation of receptor function, *J. Biol. Chem.* 2002; **277**: 33727-35.
7. Ward DT, Riccardi D. Renal physiology of the extracellular calcium-sensing receptor, *Pflügers Arch.* 2002; **445**: 169-76.
8. Riccardi D, Traebert M, Ward DT, Kaissling B, Biber J, Hebert SC, Murer H. Dietary phosphate and parathyroid hormone alter the expression of the calcium-sensing receptor (CaR) and the Na⁺-dependent Pi transporter (NaPi-2) in the rat proximal tubule, *Pflügers Arch.* 2000; **441**: 379-87.
9. Ba J, Brown D, Friedman PA. Calcium-sensing receptor regulation of PTH-inhibitable proximal tubule phosphate transport, *Am. J. Physiol.* 2003; **285**: F1233-F1243
10. Sands JM, Naruse M, Baum M, Jo I, Hebert SC, Brown EM, Harris HW. Apical extracellular calcium/polyvalent cation-sensing receptor regulates vasopressin-elicited water permeability in rat kidney inner medullary collecting duct, *J. Clin. Invest.* 1997; **99**: 1399-405.
11. Peters JH. The determination of creatinine and creatine in blood and urine with the photoelectric colorimeter, *J. Biol. Chem.* 1942; **146**: 179-86.
12. Jones BN, Paabo S, Stein S. Amino acid analysis and enzymatic sequence determination of peptides by an improved o-phthaldialdehyde precolumn labeling procedure, *J. Liquid Chromatography* 1981; **4**: 565-86.
13. Fox J, Lowe SH, Petty BA, Nemeth EF. NPS R-568: a type II calcimimetic compound that acts on parathyroid cell calcium receptor of rats to reduce plasma levels of parathyroid hormone and calcium, *J. Pharmacol. & Exp. Therapeut.* 1999; **290**: 473-9.

Received 30 October 2003; revised 27 January 2004.

Accepted 29 January 2004.

©A.D. Conigrave 2004

Author for Correspondence:

A/Prof. Arthur D. Conigrave
School of Molecular and Microbial Biosciences
The University of Sydney
NSW 2006 Australia

Tel: +61 2 9351 3883

Fax: +61 2 9351 4726

Email: a.conigrave@mmb.usyd.edu.au

Molecular changes in proximal tubule function in diabetes mellitus

Deanne H. Hryciw¹, Erwin M. Lee², Carol A. Pollock² & Philip Poronnik¹

¹School of Biomedical Sciences, University of Queensland, St Lucia, 4072, Queensland, Australia, and

²Department of Medicine, Kolling Institute of Medical Research, University of Sydney, Royal North Shore Hospital, St Leonards 2065, New South Wales, Australia

Summary

1. Diabetic kidney disease is initially associated with hypertension and increased urinary albumin excretion. The hypertension is mediated by enhanced volume expansion due to enhanced salt and water retention by the kidney. The increased urinary albumin is not only due to increased glomerular leak but to a decrease in albumin reabsorption by the proximal tubule. The precise molecular mechanisms underlying these two phenomena and whether there is any link between the increase Na^+ retention and proteinuria remain unresolved.

2. There is significant evidence to suggest that increased Na^+ retention by the proximal tubule $\text{Na}^+\text{-H}^+$ exchange isoform 3 (NHE3) can play a role in some forms of hypertension. Increased NHE3 activity in models of diabetes mellitus, may explain in part the enhanced salt retention observed in patients with diabetic kidney disease.

3. NHE3 also plays a role in receptor mediated albumin uptake in the proximal tubule. The uptake of albumin requires the assembly of a macromolecular complex that is thought to include the megalin/cubulin receptor, NHE3, the vacuolar type $\text{H}^+\text{-ATPase}$ ($\text{v-H}^+\text{-ATPase}$), the Cl^- channel, CIC-5 and interactions with the actin cytoskeleton. NHE3 seems to exist in two functionally distinct membrane domains, one involved with Na^+ reabsorption and the other involved in albumin uptake.

4. This review focuses on the evidence derived from *in vivo* studies as well as complementary studies in cell culture models for a dual role of NHE3 in both Na^+ retention and albumin uptake. We suggest a possible mechanism by which disruption of the proximal tubule albumin uptake mechanism in diabetes mellitus may lead to both increased Na^+ retention and proteinuria.

Diabetes mellitus, hypertension and albuminuria

Diabetic nephropathy is the most prevalent cause of chronic renal failure and end-stage renal disease in the Western world and can account for up to 40% of the patients requiring renal replacement therapy¹. The onset of renal failure in patients with diabetes mellitus is associated with hypertension and increased urinary albumin excretion². Although mesangial expansion, glomerular hypertrophy and thickening of the glomerular basement membrane leading to hyperfiltration and microalbuminuria are hallmarks of diabetic nephropathy, it is the degree of interstitial fibrosis that more closely correlates with the decline in glomerular filtration rate³. The tubulointerstitium represents a dynamic environment that maintains the structural and functional homeostasis within the kidney and

it is the dysregulation of this highly integrated system that may lead to many of the complications associated with diabetic kidney disease⁴.

The hypertension usually observed in patients with diabetic nephropathy is well recognised to be mediated by volume expansion due to enhanced salt and water retention by the kidney⁵. This suggests a dysregulation of the normal mechanisms to maintain volume homeostasis occurs in the 'diabetic milieu' long before a functional decline in renal function develops. Microalbuminuria is well recognised as being associated with primary glomerular pathology⁶. However, there is now clear evidence that the renal tubule has a critical role in the reabsorption of filtered albumin and in the development of albuminuria⁷. As microalbuminuria and volume-mediated hypertension occur in patients with diabetes mellitus, this may suggest a more direct relationship between albumin handling and Na^+ reabsorption. This review will focus on the possible compartmentalised roles of NHE3 in Na^+ reabsorption and albumin uptake in the proximal tubule and how the trafficking of NHE3 between the two functional compartments may provide a link to explain the co-existence of hypertension and albuminuria in diabetic nephropathy.

Under normal conditions, the kidneys filter approximately 180 litres of blood and reabsorb approximately 1.7 kg of NaCl per day⁸. The proximal tubule facilitates 'bulk' reabsorption of Na^+ , responsible for 50-75% of tubular Na^+ reabsorption. At the brush border membrane of proximal tubules approximately 0.7 moles of sodium are reabsorbed per hour⁹. Thus relatively small changes in the capacity of the proximal tubule to reabsorb Na^+ and water in response to elevations in plasma glucose or cytokine levels may result in dramatic changes in Na^+ retention and volume expansion.

$\text{Na}^+\text{-H}^+$ Exchanger Isoform 3 and Na^+ Retention

The luminal reabsorption of Na^+ in the proximal tubule is achieved primarily by the secondary active transport of the $\text{Na}^+\text{-H}^+$ exchanger isoform 3 (NHE3) mediated by the Na^+ gradient generated by the basolateral $\text{Na}^+\text{-K}^+\text{-ATPase}$ ⁸. There are now several lines of evidence to suggest that changes in the activity of NHE3 may be linked to hypertension. Importantly, a recent study in hypertensive patients found that proximal tubule Na^+ reabsorption was an independent determinant of the blood pressure in volume-dependent hypertension¹⁰. Similarly, a reduction in NHE3 activity has been reported in acute hypertension^{11,12} implicating a role for NHE3 in pressure natriuresis.

Several studies in spontaneously hypertensive rats (SHR), a commonly used model for human essential hypertension, are consistent with a role for NHE3 in the genesis of volume expansion. In the tubules of normal rats, $\text{Na}^+\text{-H}^+$ exchange activity was inhibited by parathyroid hormone (PTH) and dopamine but stimulated by angiotensin II (AngII) and norepinephrine. Tubules obtained from SHR tubules, however, were not responsive to PTH or dopamine and the levels of stimulation by AngII and norepinephrine were significantly reduced¹³. These imbalances could contribute to the development and maintenance of hypertension in this model¹³. NHE3 activity was also found to be elevated in a further study in SHR rats, with $\text{v-H}^+\text{-ATPase}$ also implicated in the regulation of Na^+ transport in the proximal tubule¹⁴. Consistent with the above studies, proximal tubule cells freshly isolated from SHR demonstrate a 3-fold increase in NHE3 activity with a 50% increase in NHE3 protein¹⁵. Furthermore, in SHR there appears to be defective coupling of the dopamine receptor to adenylyl cyclase, resulting in an alleviation of the cAMP mediated inhibition of NHE3, with subsequent elevation in Na^+ retention¹⁶. In a more recent study, it was found that proximal tubules of 5 week old SHR had greater levels of NHE3 and $\text{v-H}^+\text{-ATPase}$ activity compared to age matched normotensive Donryu rats. These findings led the authors to conclude that enhanced proximal tubule fluid reabsorption is likely to contribute to the development of high blood pressure in young SHR¹⁷. Immunofluorescence studies revealed that there was a significant level of redistribution of NHE3 in the proximal tubules in both SHR and Goldblatt hypertensive rats providing evidence for the dynamic role of NHE3 in states known to alter proximal tubular Na^+ reabsorption¹².

Further conclusive evidence for the role of NHE3 in control of blood pressure was demonstrated using NHE3 knockout transgenic mice. Microperfusion studies revealed that fluid and HCO_3^- reabsorption were reduced by ~60-70%, demonstrating that NHE3 is the major apical transporter mediating Na^+ and HCO_3^- reabsorption in the proximal tubule. These changes were associated with small but significant decreases in blood pH and HCO_3^- ¹⁸. Importantly, the systolic and mean arterial blood pressures in these mice were significantly reduced. These data therefore support the view that the major renal Na^+ transporters, including NHE3, play a central role in long-term control of arterial blood pressure^{19,20}.

NHE3 in diabetes mellitus

As discussed above, diabetes mellitus is associated with renal NaCl retention and expanded extracellular fluid volume, characterised by systemic suppression of the renin-angiotensin system. Volume expansion is largely responsible for hypertension in diabetes mellitus and may contribute to the altered haemodynamics responsible for diabetic nephropathy. Diabetes mellitus is associated with chronic or intermittently high plasma glucose levels, which are implicated in a number of adverse effects on the kidney. There is evidence to suggest that increased Na^+ flux with

glucose via SGLT-1 transporters may contribute to increased Na^+ reabsorption by the kidney²¹. However, when the significant role that NHE3 plays in Na^+ and fluid reabsorption in the proximal tubule is taken into account, hyperglycaemia-induced increases in the activity of NHE3 potentially also contribute to increased Na^+ retention and related volume expansion.

The first evidence that NHE3 was increased in the proximal tubule in diabetes was provided by Harris and co-workers in 1986²² who demonstrated increased $\text{Na}^+\text{-H}^+$ exchange in brush border vesicles from rats induced to diabetes with streptozocin (STZ). Micropuncture studies in our own laboratories have also clearly demonstrated in STZ rats that there is a pronounced increase in tubular Na^+ reabsorption^{23,24} and that this increase was primarily due to enhanced NHE3 activity²⁵. *In vivo* models of diabetes mellitus using STZ rats have also demonstrated altered renal handling of H^+ and increased HCO_3^- absorption, a result attributable to increased NHE3 activity²⁶. *In vitro* analysis of intact tubules and freshly isolated proximal tubule cells from STZ rats has shown increased NHE3 protein expression and activity²⁷. In addition, studies from our lab and others in cultured opossum kidney (OK) cells have shown that exposure to high glucose for 48 hours results in a significant increase in both NHE3 mRNA and protein^{28,29}.

Furthermore, there have been at least two reports in humans that show increased proximal tubular Na^+ reabsorption in patients with diabetes mellitus. A study in children with Type 1 diabetes found a significant increase (~20%) in proximal tubular reabsorption as determined by fractional lithium clearance³⁰. Similar studies in adults with Type 2 diabetes also found a ~20% change in reabsorption rates³¹. Thus, considerable evidence exists that the NHE3 mediated component of renal salt reabsorption may be at least in part responsible for the hypertension observed in patients with diabetes mellitus.

Albumin uptake in the proximal tubule - a macromolecular complex reliant on NHE3 activity?

It has long been recognised that the proximal tubule has a crucial role in reabsorbing any filtered albumin³². The concentration of albumin in the glomerular filtrate in rats and dogs ranges from <1 to 50 mg/l³². Recently, the concentration of albumin in humans has been estimated to be 3.5 mg/l³³ which translates to approximately 630 mg of albumin being filtered per day by the human kidneys. However, only around 30 mg is normally excreted in the urine per day, indicating that the tubules reabsorb at least 95% of all albumin filtered at the glomerulus. The uptake of albumin by the proximal tubule from the glomerular filtrate has been shown to occur by a highly active receptor-mediated endocytotic pathway involving the megalin/cubulin complex³⁴ (Figure 1). The albumin is then trafficked to the lysosomes where it is broken down to its constituent amino acids³⁴. Importantly, the C-terminus of megalin contains numerous potential protein binding domains³⁵. Recently it has been demonstrated that efficient

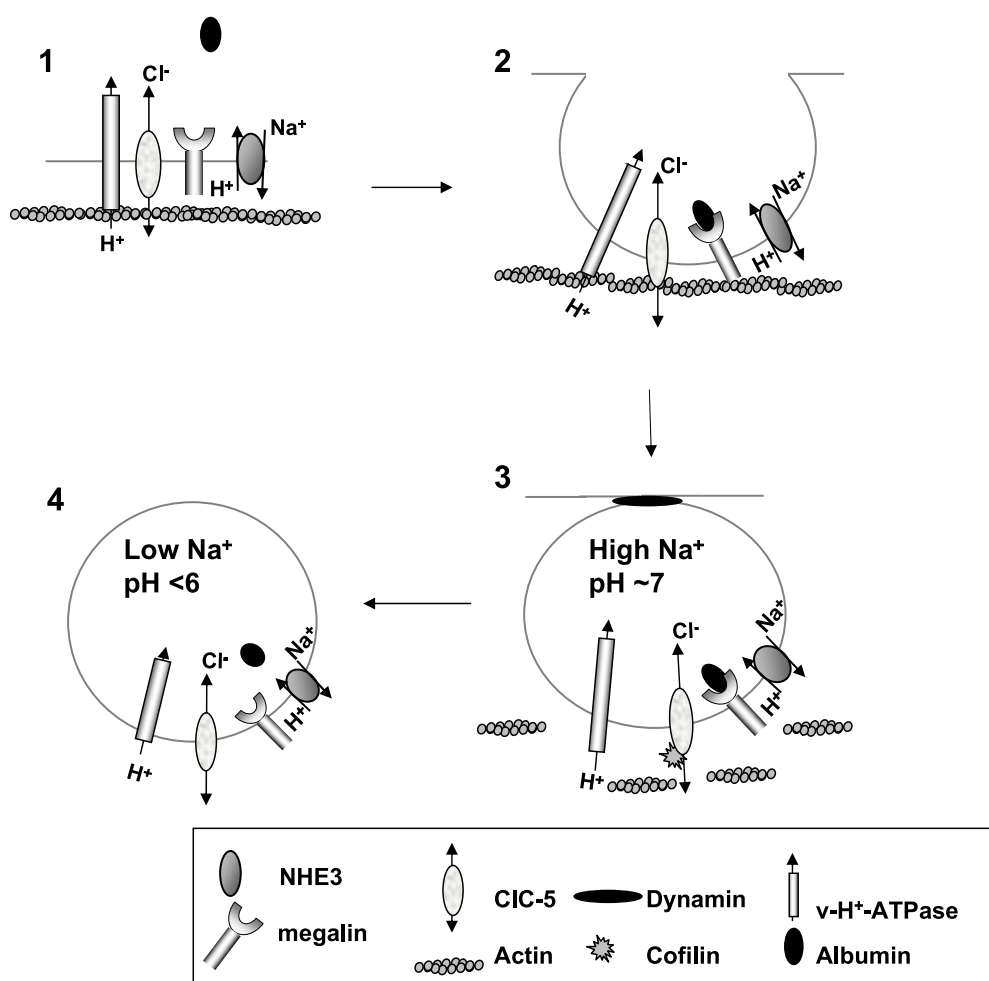


Figure 1. Macromolecular complex involved in proximal tubule albumin endocytosis. (1) In the plasma membrane at the intravillar cleft *ClC-5*, *v-H⁺-ATPase*, *NHE3* and megalin associate by C-terminal tail interactions with scaffold proteins that anchor the complex to the actin cytoskeleton. (2) When albumin binds the megalin/cubulin complex, endocytosis is initiated. (3) As the nascent endosome forms it is pinched off from the membrane by dynamin. Entry into the cytoplasm requires the dissolution of the local actin filaments. This involves the C-terminal tail of *ClC-5* recruiting the actin depolymerising protein cofilin to the complex. At this stage the endosome contains extracellular fluid high in Na^+ with a neutral pH. It is thought that *NHE3* may initiate endosomal acidification by electroneutral exchange of endosomal Na^+ for cytosolic H^+ . (4) When the Na^+ gradient is dissipated, the *v-H⁺-ATPase* continues the acidification and *ClC-5* provides the necessary anion shunt and albumin dissociates from the megalin/cubulin complex.

trafficking of megalin through the endosomal pathway is dependent on interactions of its C-terminus with the adaptor protein ARH³⁶. The dependence on the megalin/cubulin complex for the constitutive reabsorption of albumin is evident in megalin knock-out mice³⁷ and cubulin deficient dogs³⁸, both of which have pronounced low molecular weight proteinuria and albuminuria.

In addition to the megalin/cubulin receptor complex, there is now increasing evidence derived from knockout models and disease states that the albumin endocytic complex consists of a number of accessory plasma membrane transport proteins³⁹. There is a clear requirement for the *v-H⁺-ATPase*, the pump that is responsible for the acidification of the endosome and lysosomes³⁹ (Figure 1). It

has also been demonstrated *in vitro* using OK cells, that *NHE3* plays a role in albumin uptake. This is based on several papers from the laboratory of Gekle and our own^{29,40} showing that pharmacological inhibition of *NHE3* with amiloride analogues or HOE694, or inhibition of *NHE3* with cyclic adenosine monophosphate, results in pronounced decreases in albumin uptake⁴⁰. Most convincingly, in *NHE3* deficient OK cells, albumin uptake is effectively abolished while reintroduction of *NHE3* normalises albumin uptake⁴⁰. The most likely explanation for this effect of *NHE3* is that it plays a role in the initial acidification of the nascent endosome, by acting to dissipate the high intraendosomal Na^+ concentration in exchange for cytosolic H^+ . Interestingly, it has been reported that *NHE3*

binds megalin via a C-terminal tail interaction, suggesting that NHE3 may play an additional role as a molecular scaffold⁴¹. Although there are no reports of proteinuria in NHE3 knockout mice, this model is characterised by severe volume depletion, a significant reduction in glomerular filtration and an associated reduction in filtered protein¹⁸. Hence the specific role of NHE3 in Na⁺ reabsorption in this model is difficult to ascertain.

The critical role of epithelial ion transport in tubular albumin transport is exemplified in Dent's disease, where inactivating mutations of the Cl⁻ channel, CIC-5, significantly inhibit tubular albumin reabsorption⁴². In patients with Dent's disease there are genetic abnormalities in CIC-5 leading to defects in channel trafficking or channel function^{42,43} that in turn result in low molecular weight proteinuria as well as albuminuria due to defective proximal tubular protein reabsorption. A similar effect on tubular protein uptake is observed in CIC-5 knockout mice^{44,45}. It has been considered that the main role of CIC-5 was to provide an anion shunt for the positive charge translocated by the v-H⁺-ATPase into the endosome during acidification⁴⁶ (Figure 1). In support of this, in the kidneys of CIC-5 knockout mice, the uptake of markers of receptor-mediated and fluid phase endocytosis is severely impaired^{44,45} and the acidification of the endosomes is decreased⁴⁴. This finding is also consistent with the fact that many channels of the CIC family are believed to be involved principally in regulating intracellular Cl⁻ movement.

More detailed analysis, however, of the CIC-5 knockout mouse suggests that CIC-5, as well as acting as an anion shunt, plays an additional role in albumin endocytosis⁴⁵. If CIC-5 were acting solely as an anion shunt, it would be predicted that the nascent endosome would be able to form and that the trafficking of the endosome would only be affected at a later (early endosome) stage when significant electrogenic H⁺ movement occurs. This is particularly relevant when considering the role of electroneutral NHE3 exchange in initiating endosomal acidification, because this would remove the need for electrogenic transport of H⁺ immediately following the budding of the endosome from the membrane. In support of this, there are reports indicating that the v-H⁺-ATPase is not required for acidification of the early endosome⁴⁷.

In the brush borders of CIC-5 knockout mice exposed to the endocytic marker horseradish peroxidase, the marker was found to be trapped in a sub-plasmalemmal pre-endocytotic compartment and failed to enter the endosomal pathway⁴⁵. This is somewhat surprising, since if the v-H⁺-ATPase and hence anion shunt are not required during nascent endosome formation, it would be expected that the label would enter the early endosomal compartment. This raises the important point that the endocytotic defect may also be occurring earlier, at the formation of the nascent endosome. Further investigations in patients with Dent's disease showing that the loss of part of the C-terminus of CIC 5 also results in mistrafficking of the v-H⁺-ATPase⁴⁸ and in CIC-5 knockout mice there are significantly reduced

levels of megalin/cubulin at the plasma membrane also attributed to defective trafficking⁴⁹. These findings strongly suggest that CIC-5 has an additional role in targeting key proteins involved in albumin uptake to the plasma membrane. Consistent with the role of CIC-5 at the plasma membrane, we have used surface biotinylation to demonstrate that CIC-5 is present at the cell surface (unpublished observations; cf⁵⁰).

We have recently investigated a potential mechanism by which the C-terminal tail of CIC-5 can regulate albumin uptake. We found using a yeast 2-hybrid screen and glutathione S-transferase (GST)-pulldowns that CIC-5 interacted with the ubiquitously expressed actin binding protein cofilin⁵⁰ that is involved in actin depolymerization⁵¹. We reasoned that the passage of the nascent endosome through the cortical actin web required remodelling of the actin microfilament network. By phosphorylating cofilin with LIM kinase and thereby inhibiting the remodelling of the actin web we were able to inhibit albumin uptake in OK and LLC-PK1 cells⁵⁰. This study demonstrates a critical role for CIC-5 via its C-terminal domain in mediating remodelling of actin microfilaments essential for albumin endocytosis. Our current hypothesis is that, although CIC-5 is expressed at the plasma membrane, the ion channel activity is redundant and that the protein plays a key role in mediating macromolecular complex assembly. This occurs via C-terminal tail scaffolding interactions with proteins directly involved in albumin endocytosis (v-H⁺-ATPase and megalin/cubulin) as well as accessory proteins such as cofilin to form a localised and specialised endocytic complex (Figure 1).

Taken together, these data suggest that albumin uptake by the proximal tubule requires the assembly of a macromolecular complex at the plasma membrane that involves megalin/cubulin, CIC-5, NHE3 and v-H⁺-ATPase. Determining the molecular composition and scaffolds associated with this complex and the precise regulatory mechanisms represents a key research focus in renal cell physiology.

Albumin uptake in diabetes mellitus

Patients with diabetes mellitus show a clear reduction in the capacity of the proximal tubule to reabsorb albumin⁵², and this may even precede glomerular damage, demonstrating the importance of preventing tubular dysfunction early in the course of diabetes mellitus. Further evidence comes from studies in rat models of diabetes mellitus. Absolute tubular reabsorption of albumin is decreased in STZ rats⁵² and ultrastructural studies have shown a decrease in albumin uptake and a reduction in the levels of megalin in the kidneys of STZ rats⁵³. It is important to note that the presence of increased tubular protein overload leads to the development of inflammation and fibrosis⁵⁴ via activation of the nuclear factor- κ B (NF- κ B) transcriptional pathway²². This in turn induces the production of a number of proinflammatory stimuli such as regulated upon activation, normal T cell expressed and

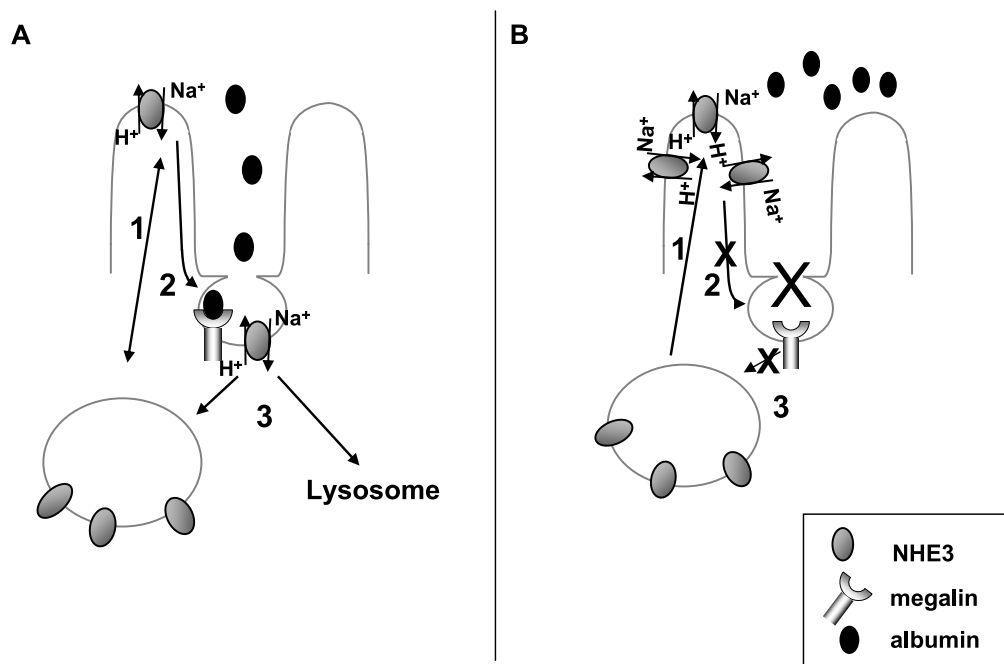


Figure 2. Possible alteration in NHE3 trafficking pathways in diabetes mellitus. Panel A: Under normal conditions in proximal tubule cells the majority of NHE3 exists in recycling endosomes from where it is inserted into the microvilli (1) to reabsorb Na⁺. Because of its role in albumin uptake, a proportion of the NHE3 may then translocate to the intravillar cleft where it associates with megalin/cubulin (2). This complex is then internalised and the NHE3 either returned to the recycling endosomes or degraded in the lysosomes (3). Panel B: The proteinuria associated with diabetes mellitus is in part due to an inhibition (x) of the normal albumin uptake pathway in the proximal tubule. As a result, the endocytosis of NHE3 via the megalin-associated pathway (2) is inhibited. However, insertion from the recycling endosomal pool is not affected (1), resulting in an accumulation of NHE3 in the microvillar pool and increased Na⁺ reabsorption with proteinuria.

secreted (RANTES), monocyte chemoattractant protein-1 (MCP-1) and transforming growth factor beta (TGF- β 1⁵⁵). TGF- β 1 is regarded as the key inflammatory cytokine in diabetic nephropathy. Furthermore, it has been shown that elevated levels of intrarenal Ang II may in fact mediate the autocrine production of TGF β 1. In fact, a recent study in STZ rats has shown that Ang II blockade restored tubular albumin uptake, further highlighting the renin-angiotensin system in the development of diabetic nephropathy⁵⁶. In the OK cell model of albumin uptake, it has been shown that TGF- β 1 can regulate albumin uptake, by decreasing the binding, internalization and trafficking of the megalin/albumin complex⁵⁷. Given that TGF β 1 levels are elevated in the diabetic kidney, this may provide a partial explanation for the molecular basis for the reduction in albumin uptake observed in vivo.

Interestingly, we have found that in OK cells, exposure to high glucose results in an increase in albumin uptake²⁹. This effect is specific for glucose and not due to an osmotic effect and may occur as a result of the increase in NHE3 activity that is known to accompany exposure to high glucose^{28,29}. It is likely that under these in vitro conditions, levels of autocrine TGF β 1 cannot reach the

levels required to inhibit albumin uptake. Thus there appears to be a direct link between NHE3 activity and albumin uptake in OK cells. Furthermore, it has been shown in OK cells exposed to pathophysiological levels of albumin similar to those expected in diabetic nephropathy, that albumin uptake is reduced. This is due to a decrease in the number of albumin binding sites by an as yet undetermined mechanism that may involve altered rates of trafficking of megalin to or from the cell membrane⁵⁸. It has been shown, however, in both primary cultures of human proximal cells⁵⁹ and OK cells^{29,60}, that exposure to high concentrations of albumin results in an increase in NHE3 expression and activity. A similar increase in NHE3 activity in response to increased tubular albumin has been reported in puromycin aminonucleoside nephrotic rats⁶¹.

These data collectively suggest that NHE3 may exist in different functional pools, one associated with albumin uptake and the other involved in Na⁺ reabsorption and not involved in albumin uptake (Figure 2). The evidence for the presence of NHE3 in two different pools in the proximal tubule brush border was presented in a recent review by McDonough and Biemesderfer⁹. One pool is located in the microvilli and the other in the intermicrovillar cleft where

NHE3 co-localises with megalin. A number of studies have shown that NHE3 can shuttle between the two pools in response to acute hypertension and other stimuli⁹. It is this association with megalin by an as yet uncharacterised molecular interaction that may explain the apparent role that NHE3 plays in albumin uptake. Furthermore, recent studies in OK cells have shown that a fraction of NHE3 is located in lipid rafts and that this may represent a different functional microdomain within the plasma membrane^{62,63}.

Based on the existence of different functional pools of NHE3, we postulate the following model that links increased Na⁺ retention and proteinuria in diabetic nephropathy (Figure 2). (i) NHE3 exists primarily in subplasmalemmal pools where it is available for insertion in to the plasma membrane in response to numerous stimuli. (ii) A significant proportion of NHE3 is recycled/ removed from the membrane in conjunction with albumin, such that NHE3 opportunistically exploits the highly active albumin endocytic pathway for its recycling and that this represents a constitutive regulatory pathway for regulation of surface levels of NHE3. (iii) The NHE3 associated with megalin is not primarily involved in Na⁺ reabsorption. (iv) When cells are exposed to high albumin, the endocytic pathway is reduced by an as yet uncharacterised mechanism, resulting in proteinuria (reduced albumin uptake) and a reduction in the internalisation rates of NHE3. (v) This in turn may result in a shift in the normal trafficking equilibrium of NHE3 with increased surface levels of NHE3 and potentiation of Na⁺ retention. We are currently investigating the exact molecular mechanisms that may underlie the differences in NHE3 trafficking and albumin uptake in conditions of high glucose and high albumin.

It is also reported that exposure to high glucose results in significant alterations in the cytoskeleton in many different cell types. In terms of the kidney, studies in mesangial cells exposed to high glucose have shown pronounced rearrangements of the actin cytoskeleton that may contribute to the hyperfiltration associated with diabetes mellitus⁶⁴. In addition, microarray analysis of mesangial cells have demonstrated altered levels of expression of actin regulatory proteins in response to high glucose⁶⁵. It is also clear that both the trafficking of NHE3 and albumin uptake depend on an intact cytoskeleton^{29,48,66}. In fact, we believe that it is critical to use the inhibition of albumin uptake by actin depolymerising agents to demonstrate that proximal tubule cells in culture are taking up albumin by a receptor-mediated pathway, as all cells have the ability to take up limited amounts of albumin by pinocytotic mechanisms. In proximal tubule cells, the actin at the microvillar core and in the terminal actin web must be in a constant state of remodelling to facilitate albumin endocytosis. Thus interactions between the membrane proteins and the cytoskeleton are essential for the regulation of ion transport activity and transporter/channel trafficking, control of vesicle movement and uptake as well as assembly of signalling and macromolecular complexes at the apical membrane^{67,68}.

It is important to note that, cultured proximal tubule cells do not have the extensive microvillar complex and

intermicrovillar clefts characteristic of their in vivo counterparts (for review see⁹) despite retaining the core functional features of the proximal tubule, namely NHE3 dependent Na⁺ uptake and megalin/cubulin mediated albumin uptake. Therefore, although much can be learned from studies in OK cells about endocytic complex assembly and regulation of albumin and NHE3, care must be exercised when extrapolating these data to the situation in the intact proximal tubule. Nevertheless, experiments in the cultured cell system can yield much valuable information regarding precise molecular interactions under defined conditions. For example, studies on the role of NHE3 uptake in OK cells have highlighted an apparently facilitative function of NHE3 in albumin uptake that may not have been as readily identified in studies in the intact proximal tubule or in NHE3 knockout mice.

Conclusion

There is now compelling evidence for increased proximal tubule NHE3 activity contributing to the Na⁺ retention that may underlie certain forms of hypertension including the hypertension often associated with diabetes mellitus. The existence of functionally different membrane domains and signalling/transporting complexes in the proximal tubule brush border may in part explain the relationship between increased Na⁺ retention and reduced albumin uptake observed in diabetic kidney disease. It is becoming apparent that the location of NHE3 in different membrane domains is a critical determinant of NHE3 function. In addition, albumin uptake by the proximal tubule involves a macromolecular complex at the plasma membrane that involves megalin/cubulin, CIC-5, NHE3 and v-H⁺-ATPase. Determining the molecular composition and scaffolds associated with this complex and the precise regulatory mechanisms represents a key research focus in renal cell physiology. A precise understanding of how these molecular interactions are altered in disease states such as diabetes mellitus will allow novel approaches to the diagnosis and management of diabetic kidney disease.

References

1. Collins AJ, Hanson G, Umen A, Kjellstrand C, Keshaviah P. Changing risk factor demographics in end-stage renal disease patients entering hemodialysis and the impact on long-term mortality. *Am. J. Kid. Dis.* 1990; **15**: 422-32.
2. Ibrahim HA, Vora JP. Diabetic Nephropathy. *Baillieres Best Pract. Res. Clin. Endocrinol. Metab.* 1999; **13**: 239-64.
3. Ziyadeh FN, Snipes ER, Watanabe M, Alvarez RJ, Goldfarb S, Haverty TP. High glucose induces cell hypertrophy and stimulates collagen gene transcription in proximal tubule. *Am. J. Physiol.* 1990; **259**: F704-14.
4. Kriz W, Napiwotzky P. Structural functional aspects of the renal interstitium. *Contrib. Nephrol.* 1979; **16**: 104-8.
5. Bickel CA, Knepper MA, Verbalis JG, Ecelbarger CA.

- Dysregulation of renal salt and water transport proteins in diabetic Zucker rats. *Kidney Int.* 2002; **61**: 2099-110.
6. Kriz W, Hosser H, Hahnel B, Gretz N, Provoost A. From segmental glomerulosclerosis to total nephron degeneration and interstitial fibrosis: a histopathological study in rat models and human glomerulopathies. *Nephrol. Dial. Transplant.* 1998; **12**: 2781-98.
 7. Russo LM, Bakris GL, Comper WD. Renal handling of albumin: a critical review of basic concepts and perspective. *Am. J. Kid. Dis.* 2002; **39**: 899-919.
 8. Greger R. Physiology of renal sodium transport. *Am. J. Med. Sci.* 2000; **319**: 51-62.
 9. McDonough AA, Biemesderfer D. Does membrane trafficking play a role in regulating the sodium/hydrogen exchanger isoform 3 in the proximal tubule? *Curr. Opin. Nephrol. Hypertens.* 2003; **12**: 533-41.
 10. Chiolero A, Maillard M, Nussberger J, Brunner HR, Burnier M. Proximal sodium reabsorption: an independent determinant of blood pressure response to salt. *Hypertens.* 2000; **36**: 631-7.
 11. Yip KP, Tse CM, McDonough AA, Marsh DJ. Redistribution of Na⁺/H⁺ exchanger isoform NHE3 in proximal tubules induced by acute and chronic hypertension. *Am. J. Physiol.* 1998; **275**: F565-75.
 12. Yip KP, Wagner AJ, Marsh DJ. Detection of apical Na⁺/H⁺ exchanger activity inhibition in proximal tubules induced by acute hypertension. *Am. J. Physiol. Regul. Integr. Comp. Physiol.* 2000; **279**: R1412-8.
 13. Gesek FA, Schoolwerth AC. Hormone responses of proximal Na⁺-H⁺ exchanger in spontaneously hypertensive rats. *Am. J. Physiol.* 1991; **261**: F526-36.
 14. Dagher G, Sauterey C. H⁺ pump and Na⁺-H⁺ exchange in isolated single proximal tubules of spontaneously hypertensive rats. *J. Hypertens.* 1992; **10**: 969-78.
 15. Kelly MP, Quinn PA, Davies JE, Ng LL. Activity and expression of Na⁺-H⁺ exchanger isoforms 1 and 3 in kidney proximal tubules of hypertensive rats. *Circ. Res.* 1997; **80**: 853-60.
 16. Felder RA, Kinoshita S, Ohbu K, Mouradian MM, Sibley DR, Monsma FJ, Jr., Minowa T, Minowa MT, Canessa LM, Jose PA. Organ specificity of the dopamine1 receptor/adenylyl cyclase coupling defect in spontaneously hypertensive rats. *Am. J. Physiol.* 1993; **264**: R726-32.
 17. Aldred KL, Harris PJ, Eitle E. Increased proximal tubule NHE-3 and H⁺-ATPase activities in spontaneously hypertensive rats. *J. Hypertens.* 2000; **18**: 623-8.
 18. Schultheis PJ, Clarke LL, Meneton P, Miller ML, Soleimani M, Gawenis LR, Riddle TM, Duffy JJ, Doetschman T, Wang T, Giebisch G, Aronson PS, Lorenz JN, Shull GE. Renal and intestinal absorptive defects in mice lacking the NHE3 Na⁺/H⁺ exchanger. *Nat. Genet.* 1998; **19**: 282-5.
 19. Lifton RP. Molecular genetics of human blood pressure variation. *Science* 1996; **272**: 676-0.
 20. Guyton AC. Blood pressure control-special role of the kidneys and body fluids. *Science* 1991; **252**: 1813-6.
 21. Vallon V, Blantz RC, Thomson S. Glomerular hyperfiltration and the salt paradox in early type 1 Diabetes Mellitus: A tubulo-centric view. *J. Am. Soc. Nephrol.* 2003; **14**: 530-7.
 22. Harris RC, Brenner BM, Seifter JL. Sodium-hydrogen exchange and glucose transport in renal microvillus membrane vesicles from rats with diabetes mellitus. *J. Clin. Invest.* 1986; **77**: 724-33.
 23. Pollock CA, Nobes MS, Gyory AZ, Heng PT, Field MJ. Transferable circulating factors and epithelial sodium transport after unilateral nephrectomy in the rat. *J. Physiol.* 1996; **490**: 257-64.
 24. Pollock C, Lawrence J, Field M. Tubular sodium handling and tubuloglomerular feedback in experimental diabetes mellitus. *Am. J. Physiol. Renal Fluid Electro. Physiol.* 1991; **260**: F946-52.
 25. Pollock CA, Bostrom TE, Dyne M, Gyory AZ, Field MJ. Tubular sodium handling and tubuloglomerular feedback in compensatory renal hypertrophy. *Pflugers Arch.* 1992; **420**: 159-66.
 26. Nascimento-Gomes G, Zaladek Gil F, Mello-Aires M. Alterations of the renal handling of H⁺ in diabetic rats. *Kidney Blood Press. Res.* 1997; **20**: 251-7.
 27. Hayashi M, Yoshida T, Monkawa T, Yamaji Y, Sato S, Saruta T. Na⁺/H⁺-exchanger 3 activity and its gene in the spontaneously hypertensive rat kidney. *J. Hypertens.* 1997; **15**: 43-8.
 28. Ambuhl P, Amemiya M, Preisig PA, Moe OW, Alpern RJ. Chronic hyperosmolality increases NHE3 activity in OKP cells. *J. Clin. Invest.* 1998; **101**: 170-7.
 29. Drumm K, Lee E, Stanners S, Gassner B, Gekle M, Poronnik P, Pollock C. Albumin and glucose effects on cell growth parameters, albumin uptake and Na⁺/H⁺-exchanger Isoform 3 in OK cells. *Cell. Physiol. Biochem.* 2003; **13**: 199-206.
 30. O'Hagan M, Howey J, Greene SA. Increased proximal tubular reabsorption of sodium in childhood diabetes mellitus. *Diabet. Med.* 1991; **8**: 44-8.
 31. Mbanya JC, Thomas TH, Taylor R, Alberti KG, Wilkinson R. Increased proximal tubular sodium reabsorption in hypertensive patients with type 2 diabetes. *Diabet. Med.* 1989; **6**: 614-20.
 32. Maack T. Renal filtration, transport, and metabolism of proteins. In: Seldwin DW, Giebisch, G. (eds) *The Kidney: Physiology and Pathophysiology 3rd Ed*, Lippincott Williams & Wilkins, New York, 2000, p 3005-38.
 33. Norden AGW, Lapsley M, Lee PJ, Pusey CD, Scheinman SJ, Tam FWK, Thakker RV, Unwin RJ, Wrong O. Glomerular protein sieving and implications for renal failure in Fanconi syndrom. *Kidney Int.* 2001; **60**: 1885-92.
 34. Christensen EI, Birn H. Megalin and cubulin: synergistic endocytic receptors in renal proximal

- tubule. *Am. J. Physiol. Renal Physiol.* 2001; **280**: F562-73.
35. Takeda T, Yamazaki H, Farquhar MG. Identification of an apical sorting determinant in the cytoplasmic tail of megalin. *Am. J. Physiol. Cell Physiol.* 2003; **284**: C1105-13.
 36. Nagai M, Meerloo T, Takeda T, Farquhar MG. The adaptor protein ARH escorts megalin to and through endosomes. *Mol. Biol. Cell* 2003; **14**: 4984-96.
 37. Willnow TE, Hilpert J, Armstrong SA, Rohlmann A, Hammer RE, Burns DK, Herz J. Defective forebrain development in mice lacking gp330/megalyn. *Proc. Natl Acad. Sci.* 1996; **93**: 8460-4.
 38. Birn H, Fyfe JC, Jacobsen C, Mounier F, Verroust PJ, Orskov H, Willnow TE, Moestrup SK, Christensen EI. Cubilin is an albumin binding protein important for renal tubular albumin reabsorption. *J. Clin. Invest.* 2000; **105**: 1353-61.
 39. Marshansky V, Ausiello DA, Brown D. Physiological importance of endosomal acidification: potential role in proximal tubulopathies. *Curr. Opin. Nephrol. Hypertens.* 2002; **11**: 527-37.
 40. Gekle M, Serrano OK, Drumm K, Mildenerger S, Freudinger R, Gassner B, Jansen HW, Christensen EI. NHE3 serves as a molecular tool for cAMP-mediated regulation of receptor-mediated endocytosis. *Am. J. Physiol. Renal Physiol.* 2002; **283**: F549-58.
 41. Biemesderfer D, Nagy T, DeGray B, Aronson PS. Specific association of megalin and the Na⁺/H⁺ exchanger isoform NHE3 in the proximal tubule. *J. Biol. Chem.* 1999; **274**: 17518-24.
 42. Lloyd SE, Pearce SH, Fisher SE, Steinmeyer K, Schwappach B, Scheinman SJ, Harding B, Bolino A, Devoto M, Goodyer P, Rigden SP, Wrong O, Jentsch TJ, Craig IW, Thakker RV. A common molecular basis for three inherited kidney stone diseases. *Nature* 1996; **379**: 445-9.
 43. Mo L, Xiong W, Qian T, Sun H, Wills NK. Coexpression of complementary cDNA fragments and restoration of chloride channel function in a Dent's disease mutation of CLC-5. *Am. J. Physiol. Cell Physiol.* 2003; **286**: C79-89.
 44. Piwon N, Gunther W, Schwake M, Bosl MR, Jentsch TJ. CLC-5 Cl⁻-channel disruption impairs endocytosis in a mouse model for Dent's disease. *Nature* 2000; **408**: 369-73.
 45. Wang SS, Devuyst O, Courtoy PJ, Wang XT, Wang H, Wang Y, Thakker RV, Guggino S, Guggino WB. Mice lacking renal chloride channel, CLC-5, are a model for Dent's disease, a nephrolithiasis disorder associated with defective receptor-mediated endocytosis. *Hum. Mol. Genet.* 2000; **9**: 2937-45.
 46. Devuyst O, Christie PT, Courtoy PJ, Beauwens R, Thakker RV. Intra renal and subcellular distribution of the human chloride channel, CLC-5, reveals a pathophysiological basis for Dent's disease. *Hum. Mol. Genet.* 1999; **8**: 247-57.
 47. Gekle M, Freudinger R, Mildenerger S. Inhibition of Na⁺-H⁺ exchanger-3 interferes with apical receptor-mediated endocytosis via vesicle fusion. *J. Physiol.* 2001; **531**: 619-29.
 48. Moulin P, Igarashi T, Van Der Smissen P, J-P. Cosyns, Verroust P, Thakker RV, Scheinman SJ, Courtoy PJ, Devuyst O. Altered polarity and expression of the H⁺-ATPase without ultrastructural changes in kidneys of Dent's disease patients. *Kidney Int.* 2003; **63**: 1285-95.
 49. Christensen E, Devuyst, O, Dom, G, Nielsen, R, Van Der Smissen, P, Verroust, P, Leruth, M, Guggino, WB, and Courtoy, PJ. Loss of chloride channel CLC-5 impairs endocytosis by defective trafficking of megalin and cubulin in kidney proximal tubules. *Proc. Natl Acad. Sci.* 2003; **100**: 8472-7.
 50. Hryciw DH, Wang Y, Devuyst O, Pollock CA, Poronnik P, Guggino WB. Cofilin interacts with CLC-5 and regulates albumin uptake in proximal tubule cell lines. *J. Biol. Chem.* 2003; **278**: 40169-76.
 51. Bamburg J. Proteins of the ADF/cofilin family: essential regulators of actin dynamics. *Annu. Rev. Cell. Dev. Biol.* 1999; **15**: 185-230.
 52. Tucker BJ, Rasch R, Blantz RC. Glomerular filtration and tubular reabsorption of albumin in preproteinuric and proteinuric diabetic rats. *J. Clin. Invest.* 1993; **92**: 686-94.
 53. Tojo A, Onozato ML, Ha H, Kurihara H, Sakai T, Goto A, Fujita T, Endou H. Reduced albumin reabsorption in the proximal tubule of early-stage diabetic rats. *Histochem. Cell Biol.* 2001; **116**: 269-76.
 54. Abbate M, Zoja C, Corna D, Capitanio M, Bertani T, Remuzzi G. In progressive nephropathies, overload of tubular cells with filtered proteins translates glomerular permeability dysfunction into cellular signals of interstitial inflammation. *J. Am. Soc. Nephrol.* 1998; **9**: 1213-24.
 55. Mezzano SA, Barria M, Droguett MA, Burgos ME, Ardiles LG, Flores C, Egado J. Tubular NF-κB and AP-1 activation in human proteinuric renal disease. *Kidney Int.* 2001; **60**: 1366-77.
 56. Tojo A, Onozato ML, Kurihara H, Sakai T, Goto A, Fujita T. Angiotensin II blockade restores albumin reabsorption in the proximal tubules of diabetic rats. *Hypertens. Res.* 2003; **26**: 413-9.
 57. Gekle M, Knaus P, Nielsen R, Mildenerger S, Freudinger R, Wohlfarth V, Sauvants C, Christensen EI. Transforming growth factor-β1 reduces megalin- and cubulin-mediated endocytosis of albumin in proximal-tubule-derived opossum kidney cells. *J. Physiol.* 2003; **552**: 471-81.
 58. Gekle M, Mildenerger S, Freudinger R, Silbernagl S. Long-term protein exposure reduces albumin binding and uptake in proximal tubule-derived opossum kidney cells. *J. Am. Soc. Nephrol.* 1998; **9**: 960-8.
 59. Lee EM, Pollock CA, Drumm K, Barden JA, Poronnik P. Effects of pathophysiological concentrations of albumin on NHE3 activity and cell proliferation in

- primary cultures of human proximal tubule cells. *Am. J. Physiol. Renal Physiol.* 2003; **285**: F748-57.
60. Klisic J, Zhang J, Nief V, Reyes L, Moe OW, Ambuhl PM. Albumin regulates the Na⁺/H⁺ exchanger 3 in OKP cells. *J. Am. Soc. Nephrol.* 2003;**14**:3008-16.
61. Besse-Eschmann V, Klisic J, Nief V, Le Hir M, Kaissling B, Ambuhl PM. Regulation of the proximal tubular sodium/proton exchanger NHE3 in rats with puromycin aminonucleoside (PAN)-induced nephrotic syndrome. *J. Am. Soc. Nephrol.* 2002; **13**: 2199-206
62. Li X, Galli T, Leu S, Wade JB, Weinman EJ, Leung G, Louvard D, Donowitz M. Na⁺-H⁺ exchanger 3 (NHE3) is present in lipid rafts in the rabbit ileal brush border: a role for rafts in trafficking and rapid stimulation of NHE3. *J. Physiol.* 2001; **537**: 537-52.
63. Akhter S, Kovbasnjuk O, Li X, Cavet M, Noel J, Arpin M, Hubbard AL, Donowitz, M. Na⁺/H⁺ exchanger 3 is in large complexes in the center of the apical surface of proximal tubule-derived OK cells. *Am. J. Physiol. Cell Physiol.* 2002; **283**: C927-40.
64. Zhou X, Hurst RD, Templeton D, Whiteside CI. High glucose alters actin assembly in glomerular mesangial and epithelial cells. *Lab Invest.* 1995; **73**: 372-83.
65. Clarkson MR, Murphy M, Gupta S, Lambe T, Mackenzie HS, Godson C, Martin F, Brady HR. High glucose-altered gene expression in mesangial cells. Actin-regulatory protein gene expression is triggered by oxidative stress and cytoskeletal disassembly. *J. Biol. Chem.* 2002; **277**: 9707-12.
66. Kurashima K, D'Souza S, Szaszi K, Ramjeesingh R, Orłowski J, Grinstein S. The apical Na⁺/H⁺ exchanger isoform NHE3 is regulated by the actin cytoskeleton. *J. Biol. Chem.* 1999; **274**: 29843-9.
67. Kim JH, Lee-Kwon W, Park JB, Ryu SH, Yun CH, Donowitz M. Ca²⁺-dependent inhibition of Na⁺/H⁺ exchanger 3 (NHE3) requires an NHE3-E3KARP- α -actinin-4 complex for oligomerization and endocytosis. *J. Biol. Chem.* 2002; **277**: 23714-24.
68. Naren AP, Cobb B, Li C, Roy K, Nelson D, Heda GD, Liao J, Kirk KL, Sorscher EJ, Hanrahan J, Clancy JP. A macromolecular complex of β 2 adrenergic receptor, CFTR, and ezrin/radixin/moesin-binding phosphoprotein 50 is regulated by PKA. *Proc. Natl Acad. Sci.* 2003; **100**: 342-6.

Author for correspondence:
Dr. Philip Poronnik
School of Biomedical Sciences,
University of Queensland,
St Lucia,
Queensland 4072, Australia

Tel: +61 7 3365 2299
Email: p.poronnik@uq.edu.au

Received 30 October 2003; in revised form January 21 2004. Accepted 29 January 2004.
©P. Poronnik 2004

Differential neural control of glomerular ultrafiltration

Kate M. Denton¹, Susan E. Luff², Amany Shweta¹ & Warwick P. Anderson¹.

¹Department of Physiology, Monash University, Victoria 3800, Australia, and

²Monash Micro Imaging, School of Biomedical Sciences, Monash University, Victoria 3800, Australia.

Summary

1. The renal nerves constrict the renal vasculature causing decreases in renal blood flow (RBF) and glomerular filtration rate (GFR). Whether renal haemodynamics are influenced by changes in renal nerve activity within the physiological range is a matter of debate.

2. We have identified two morphologically distinct populations of nerves within the kidney, which are differentially distributed to the renal afferent and efferent arterioles. TYPE I nerves almost exclusively innervate the afferent arteriole whereas TYPE II nerves are distributed equally on the afferent and efferent arterioles. We have also demonstrated that TYPE II nerves are immuno-reactive for neuropeptide Y while TYPE I nerves are not.

3. This led us to hypothesise that in the kidney, distinct populations of nerves innervate specific effector tissues and that these nerves may be selectively activated, setting the basis for the differential neural control of GFR. In physiological studies, we demonstrated that differential changes in glomerular capillary pressure occurred in response to graded reflex activation of the renal nerves, compatible with our hypothesis.

4. Thus, sympathetic outflow may be capable of selectively increasing or decreasing glomerular capillary pressure and hence GFR by differentially activating separate populations of renal nerves. This has important implications for our understanding of the neural control of body fluid balance in health and disease.

Introduction

Historical perspective

Opinion as to the importance of the renal nerves in controlling RBF and GFR has risen and fallen over the last 150 years. In the first study to demonstrate a role for the renal nerves in the control of renal function, Claude Bernard in 1859¹, transected the renal nerves and noted a marked diuresis, which he attributed to an increase in RBF. This and similar studies in the years following, demonstrating the phenomenon of denervation diuresis, dominated the understanding of the neural control of renal function (see ²). During this period the renal nerves were thought to exert a profound effect on the regulation of RBF and GFR.

Yet 80 years later, opinion had swung full circle, when Homer Smith dismissed the renal nerves in his landmark book *The Physiology of the Kidney* ² as having little importance in the control of renal function except in cases of severe stress. Smith damningly wrote of Bernard's study, stating that "His conclusion is admittedly correct, but his experiment was unfortunate in two respects."². In

the first instance, the development of clearance techniques to measure RBF and GFR demonstrated that changes in urine flow rate do not reflect changes in RBF. Secondly the anaesthesia and surgical stress to which the animals were subjected resulted in elevated basal levels of renal nerve activity. Bernard's finding of increased urine flow, probably was associated with an increase in RBF, but was due to the release of the kidney from the stress-induced increase in renal nerve activity. Smith's own studies, made painlessly in conscious and unstressed animals, failed to demonstrate any change in RBF or GFR following renal denervation. It was concluded that kidney function was not dependent on tonic renal sympathetic activity². Soon after the first kidney transplantations were performed, the apparent lack of long-term effects on body fluid balance was taken as confirmation of the independence from nervous system control of renal vascular and tubular function³.

However, in the 1970's there was a resurgence of interest in the neural control of renal function, sparked by quantitative analysis of the distribution and density of neuroeffector junctions in the kidney⁴ and appreciation that transplanted kidneys rapidly re-innervate⁵.

Significant role for nerves in renal function

Today it is widely accepted that changes in renal sympathetic nerve activity (RSNA) play a significant role in controlling body fluid homeostasis during normal daily activity and in the pathophysiology of many clinical conditions⁶⁻⁸. Whether this is primarily due to changes in renin release and tubular reabsorption, or also involves changes in RBF and GFR, is debated (see ^{9,10}).

In this review evidence is considered which supports the hypothesis that different populations of renal nerves selectively affect the afferent and efferent arterioles thereby allowing differential control of glomerular capillary pressure and hence single nephron glomerular filtration rate (SNGFR).

Control of glomerular ultrafiltration

A brief outline of the physiological basis of the control of glomerular ultrafiltration is necessary to understand how the renal nerves might contribute to its control. More detailed accounts can be found elsewhere (see ¹¹).

The primary force driving SNGFR is glomerular capillary pressure. Precise control of this pressure is important as significant falls in glomerular capillary pressure can lead to acute renal failure, whereas increased glomerular capillary pressure causes irreversible glomerular damage that leads to nephron loss and chronic renal disease¹².

The unique arrangement in the kidney of two resistance vessels in series, the afferent and efferent arterioles, allows fine regulation of pressure in the glomerular capillaries^{13,14}. RBF only becomes an important factor in determining SNGFR under conditions of filtration equilibrium, which is not the normal physiological state^{13,14}. Thus, glomerular capillary pressure and therefore SNGFR will increase if the pre (afferent) to post (efferent) glomerular resistance ratio decreases and decrease if this resistance ratio increases.

Importantly, for the majority of glomeruli the resting diameter of the efferent arteriole is smaller than the afferent arteriole¹⁵⁻¹⁸. Since resistance is inversely proportional to the fourth power of the radius this explains, in part, how this relatively small, sparsely muscled vessel can counterbalance the effects of constriction of the bigger, more muscular afferent arteriole (see ¹⁷ for a more detailed explanation). For juxtamedullary glomeruli - those 10% of glomeruli, whose efferent arterioles descend into the medulla to form the vasa recta - the situation is different since these efferent arterioles are as large if not larger than their afferent counterparts. Therefore the control of glomerular capillary pressure may well be different in juxtamedullary nephrons.

SNGFR can also be influenced by alterations in the glomerular capillary ultrafiltration coefficient (K_f), which represents the product of the glomerular capillary surface area available for filtration and hydraulic conductivity. K_f has been shown to decrease in response to a number of vasoactive stimuli, though the mechanisms are not well understood (see ¹¹).

Neural control of renal function

Renal innervation

The kidney receives an extensive sympathetic innervation. While it is generally agreed that all the major structural elements of the kidney are innervated, including vascular smooth muscle cells, renin secreting cells, mesangium and tubules (proximal, distal and loop of Henle)^{19,20}, the relative density of the innervation of each tissue type has been disputed²⁰. Whether functionally specific or non-specific renal sympathetic nerve fibres innervate the effector cells has also been questioned. Barajas concluded that the sympathetic innervation of the kidney was diffuse and non-specific, based on observations that each sympathetic axon made contact with multiple effector tissues (see ¹⁹). These studies powerfully influenced how the nerves were thought to control renal function (see ²¹). However, the definition of a neuroeffector contact in Barajas's studies is now considered very broad. Varicosities that were separated from the effector cell by up to 300 nm and in which two layers of basal lamina were present were included (see ¹⁹).

Our definition of a neuroeffector junction is much more specific^{20,22}. The varicosities along an axon can be divided into contacting and non-contacting. Contacting varicosities form specialized junctions with the effector cell; neuroeffector junctions. The vesicles are organized

within the varicosity in clusters associated with the region on the membrane that is in contact with the effector cells. At the point of contact, the varicosity and effector cell are separated by a gap that is less than 100 nm^{20,22}. Consequently, contacting varicosities release neurotransmitters directly onto junctional receptors rather than relying on diffusion of the transmitter to receptors across the surface of the smooth muscle cell membrane^{20,22}. Based on this definition of a neuroeffector junction, we re-examined the innervation of the kidney and drew vastly different conclusions to those drawn from the studies of Barajas (see ¹⁹).

Two structurally distinct types of sympathetic axons.

Using three dimensional reconstruction ultrastructural analysis of serial thin sections to examine the innervation of the juxtglomerular region, we identified two ultrastructurally distinct types of sympathetic axons²³. TYPE I axons were large in diameter with atypical varicosities and TYPE II axons resembled those innervating blood vessels in other organs, with typical fusiform varicosities²³. These axon types were identified in rats and rabbits²³. At the time the functional significance of two axon types was unknown, though conduction velocities would be expected to be different. Later, in support of our study, another study demonstrated that there was a bimodal distribution in the diameters of the renal nerves with different conduction velocities ²⁴.

Innervation density of TYPE I & II axons

Next we described the distribution and density of neuroeffector junctions made by these two types of axons²⁰. Several important findings were made: (i) The sympathetic axons were located in regions adjacent to the renal vasculature and therefore primarily the arterial vessels were innervated. However, the majority of tubular tissue in the cortex was not innervated. (ii) The afferent arteriole was the most densely innervated tissue. The afferent arterioles were 3 times more densely innervated than the efferent arterioles (Fig. 1 & 2). (iii) There was little evidence for individual axons innervating more than one effector cell type. (iv) Most significantly, it was shown that TYPE I axon varicosities made contact almost exclusively with afferent arterioles whereas TYPE II axons innervated both arterioles at similar densities (Fig. 1 & 2).

This finding was of great potential significance, and was also recognized as such by others, being rapidly incorporated into standard textbooks on the kidney^{25,26}. It raised the possibility that TYPE I and II axons originated from different populations of neurons.

Chemical coding of distinct nerve populations

The presence of distinct combinations of immunohistochemically detectable substances can be used to identify populations of nerves serving different functions^{27,28}. On this basis, we have recently shown that neuropeptide Y is located in TYPE II axons whereas TYPE

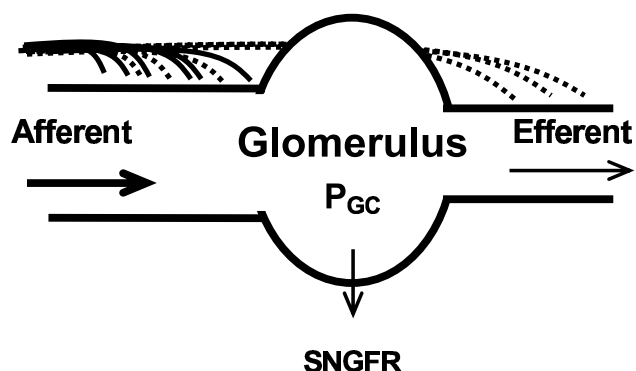


Figure 1. Diagram representing the relative TYPE I (solid line) and TYPE II (dashed line) axon innervation density on afferent and efferent arterioles. The afferent arteriole is 3 times more densely innervated than the efferent arteriole. TYPE I axons (solid lines) almost exclusively innervate the afferent arteriole. TYPE II axons (dotted lines) are equally distributed on the afferent and efferent arterioles. (P_{Gc} glomerular capillary pressure. SNGFR, single nephron glomerular filtration rate).

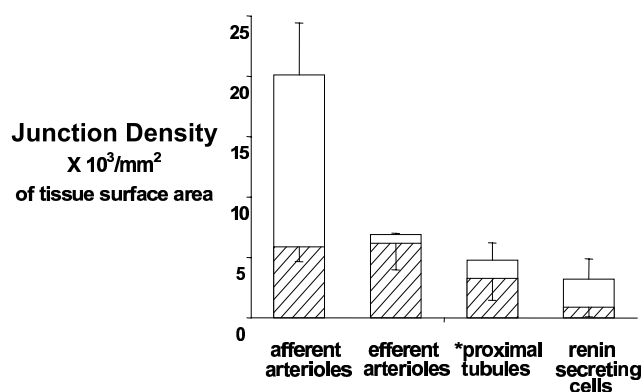


Figure 2. Stacked bar graph of the density of neuroeffector junctions of TYPE I (open bar) and TYPE II (hatched bar) axons on the afferent arterioles, efferent arterioles, proximal tubules (*only those adjacent to the afferent arterioles were innervated) and renin secreting cells. The combined bar equals the total junction density on each effector tissue.

I axons lack neuropeptide Y²⁹. Our findings are in good accord with the study of Reinecke *et al.*³⁰ who reported that the density of neuropeptide Y positive terminals was very similar on the afferent and efferent arterioles; that is, similar to the distribution of TYPE II axons. This provides further evidence that TYPE I and II axons originate from separate populations of neurons. The search for a neuropeptide specific to TYPE I axons is on going.

Hypothesis

On the basis of our morphological and immuno-histochemical evidence, we hypothesised that different patterns of sympathetic outflow to the kidney may evoke selective changes in pre- and post-glomerular vascular resistance to regulate GFR.

We hypothesise, based on the distribution of the TYPE I and TYPE II nerves on the afferent and efferent arterioles that (see Fig. 1 & 3), (i) Selective TYPE I axon activation would result in pre-glomerular vasoconstriction, reduced RBF, a reduction in glomerular capillary pressure and a fall in GFR. (ii) Selective TYPE II axon activation would result in pre- and post-glomerular vasoconstriction and decreased RBF. However, the effect on resistance would be greater on the efferent arteriole, since it is a smaller vessel (Poiseuille's law), leading to little effect on glomerular capillary pressure resulting in the maintenance of GFR¹⁷. (iii) Activation of both TYPE I and II axons would cause a predominant decrease in pre-glomerular vascular resistance due to the greater innervation density of the afferent arteriole. We have pursued this possibility in physiological studies outlined below.

Differential sympathetic outflow

The sympathetic nervous system is capable of producing selective changes in efferent outflow to different organs (see ³¹⁻³³). Increasing knowledge of central autonomic nervous system organisation, indicates that the output to different sympathetic pre-ganglionic neurons depends on the relative contributions of a wide range of brain nuclei and on the particular pattern of inputs to those nuclei (baroreceptor, chemoreceptor, somatic receptors and inputs from all areas of the brain)³¹. We are proposing within the kidney, as has been demonstrated in other organs (eg there are at least 3 distinct types of sympathetic neurons in the gut²⁸), that there is further differentiation of the signal such that specific effector tissues may be selectively activated, depending on the nature and severity of the stimulus. In the literature there is limited and conflicting evidence as to whether subpopulations of renal post-ganglionic nerves can selectively regulate different renal functions^{34,35}.

Physiological studies

Current views on the neural regulation of renal function rely mainly on data from electrical stimulation studies, or even the effects of simple acute denervation. It has been widely accepted that individual renal nerves innervate multiple tissues (vascular smooth muscle, renin secreting cells and proximal tubules)¹⁹ and that renal function is affected entirely by the frequency of their firing, with low to moderate frequencies stimulating increased renin release and sodium reabsorption and only high frequencies stimulating a decrease in renal blood flow and GFR (see ²¹). According to this view renal sympathetic nerve activity (RSNA) is generally too low to influence renal vascular resistance and glomerular ultrafiltration

under normal physiologic conditions²¹. This does not accord however with a large body of physiological and clinical evidence that suggests that renal hemodynamics are under the control of RSNA during daily events (see ⁹).

Not surprisingly, since the afferent arteriole is much more densely innervated than the efferent arteriole²⁰, electrical stimulation of the renal nerves results in a predominant increase in pre-glomerular resistance³⁶. This causes glomerular capillary pressure and GFR to decrease, as predicted when both TYPE I and II nerves are fired simultaneously (see Fig 3). These studies therefore shed no light on the possible effects of selective physiological recruitment of different populations of renal nerves on the renal resistance vessels.

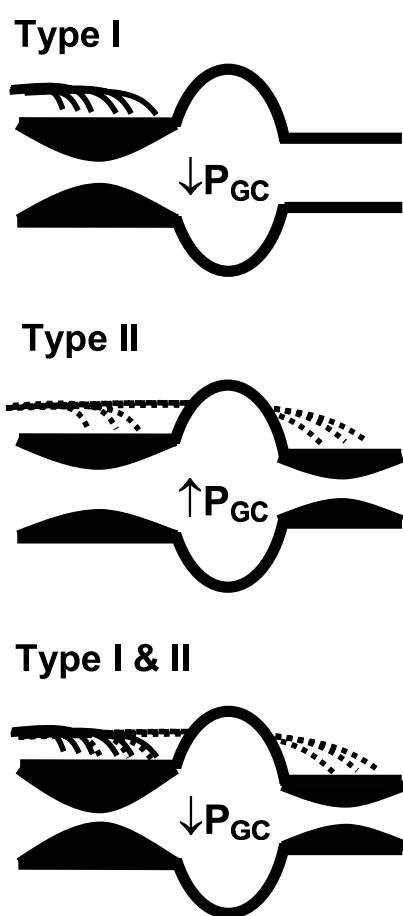


Figure 3. Diagram demonstrating the hypothetical effects of selective activation of TYPE I (upper panel), TYPE II (middle panel) or both TYPE I and II (lower panel) axons innervating the afferent and efferent arteriole, on glomerular capillary pressure (P_{gc}). See text for explanation.

RSNA varies in both the frequency (reflecting the rhythms of the central generating circuits and baroreflex input) and amplitude of its discharge (reflecting the relative number of activated nerves)^{37,38}. Thus, whereas electrical stimulation activates all nerves simultaneously, it is now evident that relatively few individual nerves are active at

rest and that the number of nerves activated during physiological bursts of nerve activity varies widely³⁹. Physiological activation of the renal sympathetic nerves is therefore fundamentally different to electrical stimulation.

The influence of RSNA on GFR

A number of studies have examined the kidney's response to reflex activation of the renal sympathetic nerves. Again not surprisingly, in response to severe increases in RSNA, when many nerves are firing, RBF and GFR decrease (see ²¹), indicative of TYPE I and/or II nerve firing (see Fig. 3). However, in several studies no change in GFR was reported in response to moderate increases in RSNA⁴⁰⁻⁴³. It is quite possible that in these studies subtle changes in pre- and post-glomerular vascular resistances were occurring to maintain glomerular capillary pressure and GFR. However, no study measured glomerular capillary pressure to verify such a conclusion.

Renal micropuncture allows discrimination of pre- & post-glomerular vascular resistance.

At this time, it is not possible to identify individual Type I versus Type II nerves *in vivo*, and thus selectively record or stimulate these neurons. However, we do have tools whereby we can determine whether the pattern of changes in pre- and post-glomerular vascular resistance in response to reflex stimulation of RSNA is presumptive of TYPE I nerve recruitment, TYPE II nerve recruitment or both. *In vivo* micropuncture is a challenging and time consuming procedure, but it is the only means whereby pressure can be directly measured in the glomerular capillaries and is thus essential in studies evaluating the contribution of the pre- and post-glomerular vessels to changes in renal hemodynamics and glomerular function^{13,14}.

Differential recruitment of TYPE I and II nerves

To begin to investigate this hypothesis, we examined the effects of physiologically induced increases in renal sympathetic nerve activity (RSNA) in response to graded hypoxia on pre- and post-glomerular vascular resistances in anaesthetised rabbits¹⁰. We chose hypoxia to reflexly increase RSNA because we had previously shown that it produces graded increases in the amplitude of renal nerve firing (i.e. graded recruitment of individual nerves)⁴⁴. Hypoxia has the further advantage that it does not significantly alter arterial pressure in the rabbit, thereby avoiding confounding autoregulatory effects on renal haemodynamics⁴⁴. In the first study of its kind we measured simultaneously glomerular capillary pressure, renal nerve activity and whole kidney function, while subjecting the rabbits to different degrees of hypoxia¹⁰. The results were clear-cut, and compatible with the hypothesis that TYPE I and II axons can be differentially activated (see Fig. 3).

We found that moderate (14% O_2) and severe (10% O_2) hypoxia increased total RSNA by 60 % and 170 %

respectively, chiefly by increasing the amplitude of the sympathetic bursts rather than their frequency. Moderate hypoxia decreased RBF (26%), increased glomerular capillary pressure and maintained GFR (Fig. 4). Both pre- and post-glomerular vascular resistances were increased; but there was a predominant effect on the post-glomerular vasculature. This greater effect on the efferent arteriole, when the TYPE II innervation density is similar on both afferent and efferent arterioles, can be explained on the basis of Poiseuille's Law and the smaller resting diameter of the efferent arteriole¹⁰. In short, the recruitment of nerves in response to moderate hypoxia appeared to be predominantly TYPE II nerves (Fig. 3). In contrast, severe hypoxia decreased RBF (56%), with a significant fall in glomerular capillary pressure and GFR (Fig. 4). This pattern reflects a substantially greater pre-glomerular than post-glomerular vasoconstriction that is compatible with the further recruitment of nerves by severe hypoxia being predominantly TYPE I nerves (Fig. 3). These results provide evidence that different levels of reflexly induced increases in RSNA may differentially control pre- and post-glomerular vascular resistance, compatible with selective activation of TYPE I and II renal sympathetic nerves.

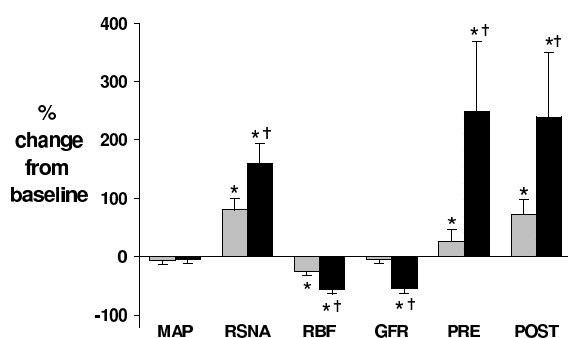


Figure 4. Responses to moderate (14% O₂; grey) and severe (10% O₂; black) hypoxia in anaesthetised rabbits. Values (means \pm s.e.m. $n = 7$) are the percentage change from baseline (room air, 21% O₂) for mean arterial pressure (MAP), renal sympathetic nerve activity (RSNA), renal blood flow (RBF), glomerular filtration rate (GFR) and pre (PRE) and post (POST) glomerular vascular resistance. * $P < 0.05$ change from baseline, † $P < 0.05$ 14% O₂ vs 10% O₂.

We are confident that the effects of hypoxia were mediated via the renal nerves as we have previously demonstrated the absence of any renal action of hypoxia following renal denervation^{42,45}. However, neurally mediated renin release may have contributed to the response to increased RSNA, as renin cells are innervated by both TYPE I and II axons²⁰. In particular, the renal response during moderate hypoxia might be explained on the basis of an increase in renin release being responsible for the rise in post-glomerular resistance. Though plasma

renin activity was not increased in response to moderate hypoxia, intrarenal effects cannot be discounted¹⁰.

Contribution of ANGII

The question of the involvement of the renin-angiotensin system in the response to moderate (14% O₂) hypoxia was investigated. The renin-angiotensin system was rendered unresponsive by the simultaneous infusion of an angiotensin converting enzyme inhibitor and ANGII to restore normal blood pressure ('ANGII clamp'). Measurements were made in rabbits receiving either the 'ANGII clamp' or vehicle infusion before (room air, i.e. 21% O₂) and during moderate hypoxia (14% O₂)⁴⁶. As seen in our previous study¹⁰, in the vehicle group RSNA increased in response to 14% O₂, and this decreased RBF, without effecting GFR or arterial pressure. Though the response was attenuated in the 'ANGII clamp' group, glomerular capillary pressure increased in both the vehicle and 'ANGII clamp' groups during 14% O₂ (Fig. 5). These results are consistent with the notion that direct actions of TYPE II nerves on the efferent arterioles are responsible in part for the increase in post-glomerular resistance in response to 14% O₂⁴⁶. These results further support our hypothesis that different populations of renal nerves selectively control pre- and post-glomerular resistance and hence glomerular pressure and ultrafiltration. Future studies will extend these findings by examining the renal microvascular response to stimulation of central nuclei involved in cardiovascular control³¹.

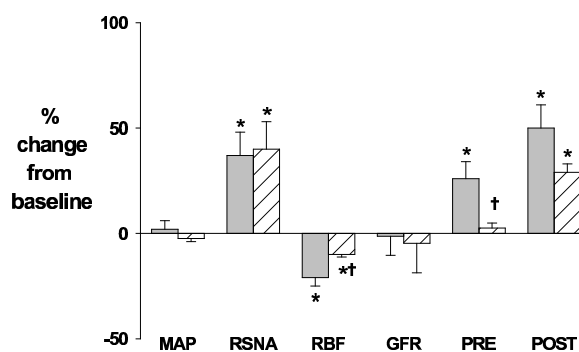


Figure 5. Responses to moderate (14% O₂) hypoxia in anaesthetised rabbits treated throughout the study with vehicle (grey) or 'ANGII clamp' (infusion of an angiotensin converting enzyme inhibitor plus ANG II to restore blood pressure to normal; hatched). Values (means \pm s.e.m. $n = 6$) are the percentage change from baseline (room air, 21% O₂) for mean arterial pressure (MAP), renal sympathetic nerve activity (RSNA), renal blood flow (RBF), glomerular filtration rate (GFR) and pre (PRE) and post (POST) glomerular vascular resistance. * $P < 0.05$ change from baseline, † $P < 0.05$ vehicle vs ANGII clamp.

Perspective

Alterations in renal sympathetic nerve activity produce important effects on renal function, which contribute to the kidney's main task of regulating body fluid balance. Our data suggest that there are functionally specific post-ganglionic renal nerves that can be selectively activated. Based on our evidence, we propose that TYPE II nerves predominate in the physiological control of arteriole resistance to maintain GFR constant during daily activity, whereas Type I nerves play a role when the animal is under stress (hemorrhage, dehydration or exercise), when blood flow is required for other organs at the expense of renal function. Overactivity of the renal nerves has been implicated in the pathophysiology of hypertension⁷, congestive heart failure⁶ and chronic renal failure⁸. Studies examining whether one or other of the populations of renal nerves are involved in these diseases offer possibilities of new therapeutic targets.

Acknowledgements

This work was supported by grants from the National Health and Medical Research Council of Australia (97/0426, 236821). Dr Kate M Denton is the recipient of a Research Fellowship awarded by the Foundation for High Blood Pressure Research, Australia. The technical assistance of Rebecca Flower is gratefully acknowledged.

References

- Bernard C. *Lecon sur les proprietes physiologiques et les alterations pathologiques des liquides de l'organisme*, Vol. 2. Bailliere et Fils, Paris. 1859; 170-171.
- Smith HW. *The kidney: Structure and function*. Oxford University Press, New York, USA. 1951.
- Anonymous. The wisdom of the kidney. *N. Engl. J. Med.* 1969; **280**:106-107.
- Barajas L, Muller J. The innervation of the juxtaglomerular apparatus and surrounding tubules: A quantitative analysis by serial section electron microscopy. *J. Ultrastruct. Res.* 1973; **43**:107-132.
- DiBona GF. Renal innervation and denervation: Lessons from renal transplantation reconsidered. *Artif. Organs.* 1987; **11**:457-462.
- DiBona G, Sawin L. Role of renal nerves in sodium retention of cirrhosis and congestive heart failure. *Am. J. Physiol.* 1991; **260**:R298-R305.
- Esler M. Sympathetic nervous system: Contribution to human hypertension and related cardiovascular diseases. *J. Cardiovasc. Pharmacol.* 1995; **26**(suppl 2):S24-28.
- Orth SR, Amann K, Strojek K, Ritz E. Sympathetic overactivity and arterial hypertension in renal failure. *Nephrol. Dial. Transplant.* 2001; **16**:67-69.
- Malpas S, Leonard BL. Neural regulation of renal blood flow; a re-examination. *Clin. Exp. Pharmacol. Physiol.* 2000; **27**:956-964.
- Denton KM, Shweta A, Anderson WP. Preglomerular and postglomerular resistance responses to different levels of sympathetic activation by hypoxia. *J. Am. Soc. Nephrol.* 2002; **13**:27-34.
- Maddox DA, Brenner BM. Glomerular ultrafiltration. In: Brenner BM (ed). *Brenner & Rector's The Kidney*, 6th edn, Vol 1. WB Saunders, Philadelphia. 2000; 286-333.
- Kriz W, Gretz N, Lemley KV. Progression of glomerular diseases: Is the podocyte the culprit? *Kid. Int.* 1998; **54**:687-697.
- Arendshorst WJ, Gottschalk CW. Glomerular ultrafiltration dynamics: Historical perspective. *Am. J. Physiol.* 1985; **248**:F163-174.
- Denton KM, Anderson WP. Glomerular ultrafiltration in rabbits with superficial glomeruli. *Pflügers. Arch.* 1991; **419**:235-242.
- Trueta J, Barclay AE, Daniel PM, Franklin KJ, Pritchard MML. *Studies of the renal circulation*. Blackwell Scientific Publications. Oxford. 1947.
- Kaissling B, Kriz W. Structural analysis of the rabbit kidney. *Adv. Anat. Embryol. Cell. Biol.* 1979; **56**:7-12.
- Denton KM, Anderson WP, Sinniah R. Effects of angiotensin II on regional afferent and efferent arteriole dimensions and the glomerular pole. *Am. J. Physiol.* 2000; **279**:R629-638.
- Denton KM, Fennessy PA, Alcorn D, Anderson WP. Morphometric analysis of the actions of angiotensin ii on renal arterioles and glomeruli. *Am. J. Physiol.* 1992; **262**:F367-372.
- Barajas L, Liu L, Powers K. Anatomy of the renal innervation: Intrarenal aspects and ganglia of origin. *Can. J. Physiol. Pharmacol.* 1992; **70**:735-749.
- Luff SE, Hengstberger SG, McLachlan EM, Anderson WP. Distribution of sympathetic neuroeffector junctions in the juxtaglomerular region of the rabbit kidney. *J. Auton. Nerv. Syst.* 1992; **40**:239-254.
- DiBona GF, Kopp UC. Neural control of renal function. *Physiol. Rev.* 1997; **77**:75-197.
- Luff SE. Ultrastructure of sympathetic axons and their structural relationship with vascular smooth muscle. *Anat. Embryol.* 1996; **193**:515-531.
- Luff SE, Hengstberger SG, McLachlan EM, Anderson WP. Two types of sympathetic axon innervating the juxtaglomerular arterioles of the rabbit and rat kidney differ structurally from those supplying other arteries. *J. Neurocytol.* 1991; **20**:781-795.
- DiBona GF, Sawin LL, Jones SY. Differentiated sympathetic neural control of the kidney. *Am. J. Physiol.* 1996; **271**:R84-90.
- Kopp UC, Dibona GF. Effects of the renal nerves and neurotransmitters on renal function. In: Brenner BM (ed). *Brenner & Rector's The Kidney*, 5th edn, Vol 1. WB Saunders, Philadelphia. 1996; 789-816.
- Kopp UC, Dibona GF. The neural control of renal function. In: Seldin DW, Giebisch G, (eds). *The Kidney, Physiology and Pathophysiology*. 3rd edn. Vol. 1. Raven Press, New York. 2000; 1157-1204.
- Grkovic I, Anderson CR. Calbindin D28k-

- immunoreactivity identifies distinct subpopulations of sympathetic pre- and postganglionic neurons in the rat. *J. Comp. Neurol.* 1997; **386**:245-259.
28. Furness JB, Morris JL, Gibbins IL, Costa M. Chemical coding of neurons and plurichemical transmission. *Annu. Rev. Pharmacol. Toxicol.* 1989; **29**:289-306.
29. Luff SE, Anderson WP, Denton KM, Young SB. Neuropeptide Y is specifically localised in type ii sympathetic axons innervating the afferent and efferent arterioles in the rabbit kidney. *International Union of Physiological Sciences.* 2001; ID1037 (Abstract).
30. Reinecke M, Forssmann WG. Neuropeptide (neuropeptide Y, neurotensin, vasoactive intestinal polypeptide, substance p, calcitonin gene-related peptide, somatostatin) immunohistochemistry and ultrastructure of renal nerves. *Histochem.* 1988; **89**:1-9.
31. Dampney RA. Functional organization of central pathways regulating the cardiovascular system. *Physiol. Rev.* 1994; **74**:323-364.
32. McAllen RM, Malpas SC. Sympathetic burst activity: Characteristics and significance. *Clin. Exp. Pharmacol. Physiol.* 1997; **24**:791-799.
33. Kenney MJ, Weiss ML, Patel KP, Wang Y, Fels RJ. Paraventricular nucleus bicuculline alters frequency components of sympathetic nerve discharge bursts. *Am. J. Physiol.* 2001; **281**:H1233-1241.
34. Dorward PK, Burke SL, Janig W, Cassell J. Reflex responses to baroreceptor, chemoreceptor, nociceptor inputs in single renal sympathetic neurones in the rabbit and the effects of anaesthesia on them. *J. Auton. Nerv. System.* 1987; **18**:39-54.
35. Stein RD, Weaver LC. Multi- and single-fiber mesenteric and renal sympathetic responses to chemical stimulation of the intestinal receptors in cats. *J. Physiol.* 1988; **396**:155-172.
36. Kon V. Neural control of renal circulation. *Miner. Electrol. Metabol.* 1989; **15**:33-43.
37. Malpas SC, Ninomiya I. A new approach to analysis of synchronized sympathetic nerve activity. *Am. J. Physiol.* 1992; **263**:H1311-1317.
38. Ninomiya I, Malpas SC, Matsukawa K, Shindo T, Akiyama T. The amplitude of synchronized cardiac sympathetic nerve activity reflects the number of activated pre- and postganglionic fibers in anesthetized cats. *J. Auton. Nerv. System.* 1993; **45**:139-147.
39. Malpas SC, Evans RG. Do different levels and patterns of sympathetic activation all provoke renal vasoconstriction? *J. Auton. Nerv. System.* 1998; **69**:72-82.
40. Handa RK, Johns EJ. A study of the renal responses in the rat to electrical stimulation of the afferent nerves of the brachial plexus. *Quart. J. Exp. Physiol.* 1988; **73**:915-929.
41. Osborn JW, Livingstone RH, Schramm LP. Elevated renal nerve activity after spinal transection: Effects on renal function. *Am. J. Physiol.* 1987; **253**:R619-R625.
42. Malpas SC, Shweta A, Anderson WP, Head GA. Functional response to graded increases in renal nerve activity during hypoxia in conscious rabbits. *Am. J. Physiol.* 1996; **271**:R1489-1499.
43. Malpas SC, Head GA, Anderson WP. Renal responses to increases in renal sympathetic nerve activity induced by brainstem stimulation in rabbits. *J. Auton. Nerv. System.* 1996; **61**:70-78.
44. Malpas SC, Bendle RD, Head GA, Ricketts JH. Frequency and amplitude of sympathetic discharges by baroreflexes during hypoxia in conscious rabbits. *Am. J. Physiol.* 1996; **271**:H2563-2574.
45. Leonard BL, Malpas SC, Denton KM, Madden AC, Evans RG. Differential control of intrarenal blood flow during reflex increases in sympathetic nerve activity. *Am. J. Physiol.* 2001; **280**:R62-68.
46. Denton KM, Flower RL, Anderson WP. Increased glomerular capillary pressure following moderate reflex activation of renal nerves is not due to angII; studies in rabbits with superficial glomeruli. *Hypertension* 2002; **40**:408 (Abstract).

Received 30 October 2003; in revised form January 14 2004. Accepted 29 January 2004.

©K.M. Denton 2004

Author for correspondence:

Dr Kate Denton
Department of Physiology,
Monash University,
Victoria 3800, Australia

Tel: +61 3 9905 2503

Email: kate.denton@med.monash.edu.au

Neural control of renal medullary perfusion

Gabriela A. Eppel¹, Simon C. Malpas², Kate M. Denton¹ & Roger G. Evans¹

¹Department of Physiology, Monash University, Melbourne, Vic 3800, Australia and

²Circulatory Control Laboratory, Department of Physiology, University of Auckland, New Zealand.

Summary

1. There is strong evidence that the renal medullary circulation plays a key role in long-term blood pressure control. This, and evidence implicating sympathetic overactivity in development of hypertension, provides the need for understanding how sympathetic nerves affect medullary blood flow (MBF).

2. The precise vascular elements that regulate MBF under physiological conditions are unknown, but likely include the outer medullary portions of descending vasa recta, and afferent and efferent arterioles of juxtamedullary glomeruli, all of which receive dense sympathetic innervation.

3. Many early studies of the impact of sympathetic drive on MBF were flawed, both because of the methods used for measuring MBF, and because single and often intense neural stimuli were tested.

4. Recent studies have established that MBF is less sensitive than cortical blood flow (CBF) to electrical renal nerve stimulation, particularly at low stimulus intensities. Indeed, MBF appears to be refractory to increases in endogenous renal sympathetic nerve activity within the physiological range in all but the most extreme cases.

5. Multiple mechanisms appear to operate in concert to blunt the impact of sympathetic drive on MBF, including counter-regulatory roles of nitric oxide, and perhaps even paradoxical angiotensin II-induced vasodilatation. Regional differences in the geometry of glomerular arterioles are also likely to predispose MBF to be less sensitive than CBF to any given vasoconstrictor stimulus.

6. Failure of these mechanisms would promote reductions in MBF in response to physiological activation of the renal nerves, which could in turn lead to salt and water retention and hypertension.

Introduction

'Neural control of the capillary circulation in specific regions of the kidney has not been adequately studied'. This statement from Pomeranz *et al.* in 1968¹ could reasonably have been made almost 30 years later, with little progress being made in this field in the intervening period. However, renewed activity in this area since 1995² has increased our understanding of the influence of renal sympathetic drive on regional kidney blood flow. As we will describe in this review, there is now strong evidence that medullary blood flow (MBF) is less sensitive than cortical blood flow (CBF) to increases in renal sympathetic drive within the physiological range. This has important implications for the control of renal function, and in particular, the long-term regulation of arterial pressure. Nitric oxide appears to play

a critical role in protecting the renal medulla from ischaemia due to renal nerve activation, but is not the only factor involved. For example, unique structural aspects of the medullary circulation probably contribute, and angiotensin II may have a surprising role as a counter-regulatory vasodilator within the medullary microcirculation. There is also the potential for neurochemical differences between nerves innervating vascular elements controlling MBF and CBF to contribute.

The aim of this review is to examine the mechanisms, and implications, of the neural regulation of MBF. However, we must first discuss three important issues: the unique vascular architecture of the kidney that underlies the differential control of MBF and CBF, the physiological imperatives of precise regulation of MBF, and the nature of the renal sympathetic innervation and its role in blood pressure control. We will then consider the evidence of differential neural control of CBF and MBF, and the potential mechanisms that underlie it.

The renal medullary circulation: structure and function

The blood supply to the renal medulla arises from the efferent arterioles of juxtamedullary glomeruli, which comprise ~10% of all glomeruli in the kidney (Figure 1). Thus, while all blood flow to the kidney enters the renal cortex, only ~10% of this enters the renal medulla. In rats and dogs, reliable estimates of regional kidney blood flow have ranged from 2.6-7.4 ml/min/g in the cortex, 1.3-3.2 ml/min/g in the outer medulla, and 0.2-5.9 ml/min/g in the inner medulla³. Although these estimates show considerable variability between various studies (and species), it is widely regarded that blood flow per unit tissue weight in the outer and inner medulla is approximately 40% and 10%, respectively, that in the cortex. The maintenance of a relatively low MBF appears to be critical for maintaining the cortico-medullary solute gradient, and so urinary concentrating mechanisms³. On the other hand, because the renal medulla is a hypoxic environment even under normal conditions, there must be some trade off in the control of MBF, between maintenance of the cortico-medullary solute gradient (and so normal tubular function), and the supply of oxygen within the renal medulla (Figure 2). As will be described in detail below (see *MBF and blood pressure control*), there is also strong evidence that the level of MBF is a key factor in long-term control of blood pressure.

The precise vascular elements that regulate MBF under physiological conditions remain unknown. However, from a theoretical perspective changes in vascular resistance in juxtamedullary arterioles, or in downstream vascular elements within the medulla itself (eg, outer medullary descending vasa recta), could lead to large

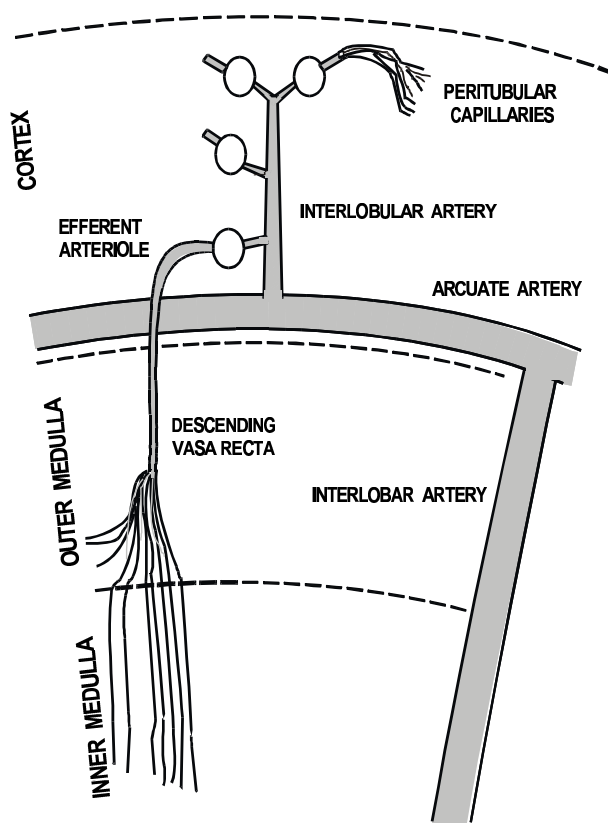


Figure 1. Schematic diagram of the architecture of the renal vasculature, and the extent of renal innervation to various vascular elements (shaded). Based on original figures by others^{3,71}. Innervation data adapted from Barajas & Powers²⁴.

changes in MBF without significant alterations in total CBF. On the other hand, because juxtamedullary afferent arterioles arise near the origin of interlobular arteries (Figure 1), changes in interlobular artery calibre would be expected to impact less on MBF (and juxtamedullary cortical blood flow) than on the bulk of CBF.

Heterogeneity of the geometry of glomerular arterioles may also contribute to the differential regulation of CBF and MBF. Afferent and (particularly) efferent arterioles of juxtamedullary glomeruli have considerably greater calibre than their counterparts in the mid- and outer-cortex⁴ (Figure 1). Because vascular resistance is inversely proportional to vessel radius to the power of 4, comparable changes in vessel radius result in lesser absolute change in vascular resistance in the larger juxtamedullary arterioles, than in their counterparts in other regions of the cortex⁴.

MBF and blood pressure control

Although the precise aetiology of essential hypertension remains unknown, there is persuasive evidence that the initial trigger resides within the kidney⁵. One line of evidence in support of this notion arose from the seminal work of Guyton and colleagues⁶, showing that

the pressure diuresis/natriuresis mechanism provides a 'non-adapting' feedback system by which arterial pressure can be controlled in the long-term. The relationship, between renal perfusion pressure and salt and water excretion (pressure diuresis/natriuresis), is set at higher pressures in all forms of hypertension that have been studied, and hypertension can be ameliorated by treatments that restore this relationship towards normal. Another important line of evidence comes from studies of renal transplantation between hypertensive and normotensive subjects. Both in rats and humans, there is good evidence that 'the blood pressure follows the kidney'⁷. That is, when a kidney from a normotensive subject is transplanted into a hypertensive subject, arterial pressure falls. Conversely, when the kidney from a hypertensive subject, or a normotensive subject genetically pre-disposed to hypertension, is transplanted into a normotensive subject, hypertension develops.

In a series of elegant studies reviewed in detail previously⁸⁻¹¹, Cowley, Roman, Mattson and colleagues have provided persuasive evidence that MBF is a critical factor in the long-term control of arterial pressure. They have utilised a conscious rat model in which CBF and MBF are measured chronically using implanted optical fibres, while vasoactive agents are administered directly into the renal medulla. Chronic medullary interstitial infusion of vasoconstrictors, at doses that reduce MBF, produce hypertension, whereas similar infusions of vasodilators that increase MBF can ameliorate hypertension. This effect seems to be mediated through alterations in the pressure diuresis/natriuresis relationship, which is shifted to higher pressures by both chronic and acute medullary interstitial infusions of vasoconstrictors, and shifted to lower pressures by medullary interstitial infusions of vasodilators. We have confirmed some of these observations in a different species, showing that acute medullary interstitial (but not intravenous) infusion of noradrenaline shifts the pressure diuresis/natriuresis relationship to higher pressures in anaesthetized rabbits^{12,13}.

The precise mechanisms by which reductions in MBF shift the pressure diuresis/natriuresis relationship to higher pressure remain a matter of controversy. Cowley and colleagues have developed the hypothesis, for which there is considerable experimental support,⁸⁻¹¹ that increases in MBF in response to increased renal perfusion pressure actually mediate pressure diuresis/natriuresis. Increased vasa recta capillary hydrostatic pressure (secondary to increased vasa recta blood flow) will result in increased medullary interstitial hydrostatic pressure, which will be transmitted throughout the kidney because of the low compliance of the kidney due to the presence of the renal capsule. Increased renal interstitial hydrostatic pressure reduces sodium reabsorption in a number of segments of the nephron, probably in part through enhanced back-leak along paracellular pathways. However, the integrity of this hypothesis depends on the idea that MBF, unlike total renal blood flow (RBF) and CBF, is relatively poorly autoregulated. The degree to which MBF is autoregulated remains a matter of controversy,^{14,15} probably in part

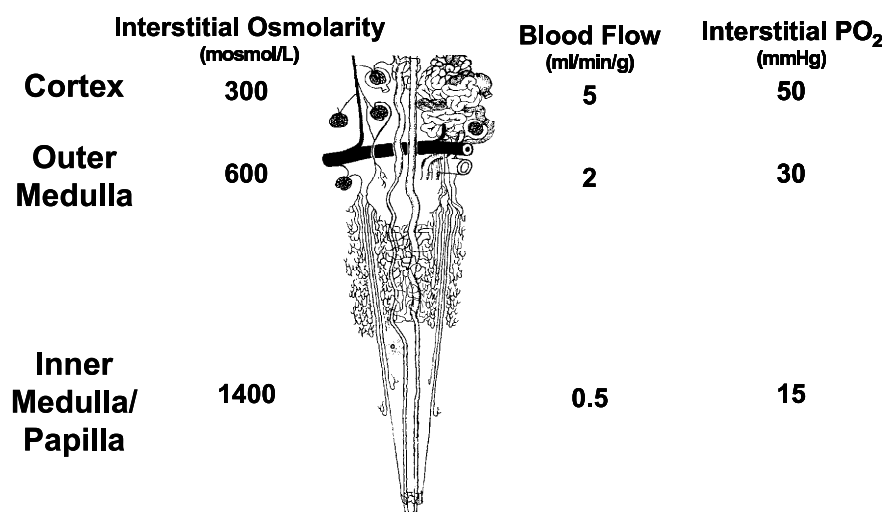


Figure 2. The trade-off between maintenance of the cortico-medullary solute gradient and medullary hypoxic damage. Diagram of the renal vasculature adapted from Beeuwkes & Bonventre⁷³. Data relating to interstitial osmolarity, blood flow and interstitial PO₂ compiled from Vander⁷⁴, Pallone et al.³, and Lübbers & Baumgärtl⁷⁵ respectively.

because of limitations in available methods for estimating MBF.

Renal nerves and blood pressure control

There is clear evidence that renal sympathetic drive is increased during the development of hypertension both in the spontaneously hypertensive rat (SHR) and in human essential hypertension. Thus, basal post-ganglionic sympathetic nerve activity¹⁶, and emotional stress-induced increases in post-ganglionic sympathetic nerve activity and reductions in sodium excretion¹⁷, are enhanced in SHR compared with normotensive Wistar Kyoto control rats (WKY). Furthermore, renal sympathetic drive, as measured by noradrenaline spillover, is also increased in human essential hypertension¹⁸. Increased renal sympathetic drive appears to contribute to the pathogenesis of hypertension, since in SHR chronic bilateral renal denervation, achieved by repeated denervation between weeks 4 and 16 after birth, blocks 30-40% of the expected progressive elevation of arterial pressure¹⁹. A similar regimen of bilateral renal denervation in WKY has no effect on arterial pressure¹⁹.

The precise mechanisms by which increased renal sympathetic drive contributes to the pathogenesis of hypertension remain unknown. The fact that reductions in MBF can shift the pressure diuresis/natriuresis relationship to higher pressures (right-ward shift), which if maintained chronically produces hypertension, provides the impetus for our interest in the neural control of MBF.

Innervation of vascular elements controlling MBF

The origin of the efferent sympathetic innervation of the kidney differs among species, but in general arises from multiple ganglia of the celiac plexus, the lumbar splanchnic nerve and the intermesenteric plexus²⁰. Post-ganglionic

nerves enter the kidney in association with the renal vasculature, and follow the course of the renal arterial tree as it branches to form interlobar, arcuate, and interlobular arteries. These neurones in turn innervate the afferent and efferent arterioles, and the outer medullary portions of descending vasa recta, but not vascular elements within the inner medulla and papilla²¹ (Figure 1). Consistent with these anatomical observations, juxtamedullary afferent and efferent arterioles of the rat hydronephrotic kidney constrict in response to renal nerve stimulation²².

Previous studies of regional differences in innervation density within the kidney indicate that juxtamedullary afferent and efferent arterioles, and their associated outer medullary descending vasa recta, are densely innervated. For example, McKenna & Angelakos found the juxtamedullary cortex and outer medulla to have the greatest concentration of noradrenaline within the dog kidney, levels being ~40-60% less in the mid- and subcapsular-cortex, and low in the inner medulla²³. Barajas and Powers provided more direct evidence of dense juxtamedullary vascular innervation, using autoradiography to detect uptake of exogenous [³H]-noradrenaline (presumptively by sympathetic nerves) in rat kidney²⁴. They found greater density of autoradiographic grains on afferent, compared with efferent arterioles throughout the cortex, but autoradiographic grain density was similar in each of these vascular elements in the outer- mid- and juxtamedullary cortex. Quantitative analysis of the innervation density of outer medullary descending vasa recta was not included in their study, although the amount of autoradiographic grains overlapping the vasculature was greater in the outer stripe of the outer medulla than in any other kidney region. It must be born in mind, however, that the techniques that have been applied to this problem have considerable limitations. Most evidence suggests that

sympathetic neurotransmission in blood vessels occurs chiefly via specialised neuromuscular junctions, at which varicosities form a close contact (< 100 nm) with arteriolar smooth muscle cells²⁵. In the rabbit kidney, ~80% of sympathetic varicosities within the arteriolar region form these specialised neuromuscular junctions²⁶. On the other hand, it has also been argued that sympathetic neurotransmitters can also act at some distance from their site of release within the kidney, particularly in the control of tubular function²⁰. Nevertheless, the relative distribution of specialised neuromuscular junctions in vascular elements controlling CBF and MBF would better reflect the density of 'functional' sympathetic innervation in the renal vasculature, than measures of tissue noradrenaline content *per se*²³, or the density of sites of noradrenaline uptake²⁴. There is a need, therefore, for further detailed studies of the innervation of vascular elements controlling MBF and CBF.

Neurochemistry of renal sympathetic nerves

Most evidence suggests that the predominant neurotransmitter in renal sympathetic nerves is noradrenaline. Thus, while dopamine also appears to be present in these nerves as a precursor of noradrenaline synthesis, there is little compelling evidence of specific dopaminergic nerves within the kidney²⁰. Moreover, while acetylcholine is found within the kidney, it appears not to be associated with renal nerves²⁰. Nevertheless, there is now strong evidence that co-transmitters, including neuropeptide Y and ATP participate in renal sympathetic neurotransmission²⁰ and partially mediate renal nerve stimulation induced-reductions in global RBF²⁷⁻³⁰. Other neurotransmitters, including vasoactive intestinal polypeptide and neurotensin, have been identified within the renal vasculature³¹, and galanin has been identified in a proportion of the neurons innervating the kidney³². Their roles in renal sympathetic neurotransmission and in regulating renal function remain to be determined. Neuropeptide Y³¹ and its binding sites³³, and also neurotensin and vasoactive intestinal polypeptide³¹ have been localised to vascular elements of the medullary circulation (including juxtamedullary afferent and efferent arterioles), raising the possibility that these sympathetic co-transmitters could contribute to the neural control of MBF.

Neural control of MBF: early studies

All available methods for estimating regional kidney blood flow have limitations that must be considered in the interpretation of experimental data^{3,34}. Methods used in early studies of the control of MBF, based on para-aminohippuric acid clearance, washout of diffusible tracers such as ⁸⁵Kr, H₂, and heat (thermodilution), renal extraction of diffusible indicators such as ⁴²K and ⁸⁶Rb, indicator transit time, albumin accumulation and microspheres have been shown to be (more or less) invalid from either practical or theoretical standpoints^{3,33}. For the most part, these methods are also limited by the fact that they do not provide 'real time' measurements of blood flow in individual animals. A further limitation of many early

studies of the neural control of intrarenal blood flow is that they often employed single, intense stimuli, well beyond what one might consider to be physiologically relevant. However, it is worthwhile for us to briefly consider the results of studies using these techniques, because they allow us to appreciate both the heroic efforts of earlier investigators, and the evolution of our understanding, of the neural control of intrarenal blood flow.

Trueta *et al.* were the first to study this issue (in 1947), using the intrarenal distribution of injected radiocontrast material and Indian ink as markers of blood flow in anaesthetized rabbits³⁵. Their observations were entirely qualitative, but prophetic, in that they suggested that renal nerve stimulation induced redistribution of blood flow from the outer cortex to the inner cortex and medulla. In contrast, Houck (in 1951), who also used the Indian ink distribution method in anaesthetized dogs, to study the effects of intense electrical stimulation of the renal nerves, concluding that CBF and MBF were similarly dramatically decreased by intense renal nerve stimulation³⁶. Similar conclusions were drawn by Aukland in 1968, using a method for determining local H₂ gas clearance within the outer medulla in anaesthetized dogs. They found that total RBF and outer cortical H₂ gas clearance both fell by ~40% during intense renal nerve stimulation, but also conceded that 'due to the counter current exchange of gas between ascending and descending vasa recta, the clearance is not necessarily linearly related to blood flow'³⁷. Similar observations, using a similar technique in anesthetized rats, were reported by Chapman *et al.* in 1982³⁸. Thus, with the exception of the initial study by Trueta *et al.*, the unanimous conclusion from the studies described above was that CBF and MBF are similarly sensitive to the effects of activation of the renal sympathetic nerves.

Some studies were performed in which graded neural stimuli were applied, but the picture arising from them was far from clear. Pomeranz *et al.* (1968) used the ⁸⁵Kr autoradiography technique in both anaesthetized and conscious dogs, and concluded that although intense renal nerve activity reduced both CBF and MBF, mild stimulation of the renal nerves actually increased MBF¹. In almost direct contrast, Hermansson *et al.* reported their study using ⁸⁶Rb uptake in anaesthetized rats in 1984, concluding that MBF was more sensitive than CBF to the ischaemic effects of low frequency renal nerve stimulation³⁹. These observations are clearly at odds with the results of more recent studies using laser Doppler flowmetry.

Studies using laser Doppler flowmetry

At present, the most widely used method for estimation of blood flow in specific regions of the kidney is laser Doppler flowmetry. This technique has the advantage that measurements can be made in real-time, and in anatomically specific regions of the kidney. There is good evidence of a direct relationship between laser Doppler flux and erythrocyte velocity both in model systems *in vitro*^{15,40-42}, and in the kidney *in vivo*^{15,40,43,44}. However, it must also be recognised that in highly perfused tissues such

as the kidney, laser Doppler flux is relatively insensitive to changes in the volume fraction of red blood cells in the tissue^{15,40,41}. Therefore, changes in MBF due to changes in the number of perfused capillaries (capillary recruitment) are unlikely to be detected by laser Doppler flowmetry. Nevertheless, this method does represent a considerable technical breakthrough in the study of regional kidney blood flow. Over the last decade, studies from a number of separate research groups using this technique have led to the unequivocal conclusion that MBF is relatively insensitive to renal sympathetic drive, especially at stimulus intensities within the physiological range.

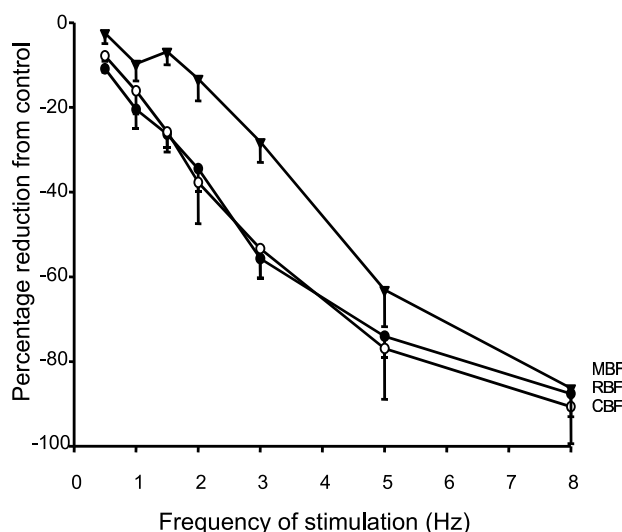


Figure 3. Mean responses of total renal blood flow (RBF, ●), and laser Doppler flowmetry measurements of cortical blood flow (CBF, ○) and medullary blood flow (MBF, ▼), to graded frequencies of renal nerve stimulation (supramaximal voltage, 2 ms duration) in anaesthetized rabbits. Symbols represent mean \pm s.e. mean of observations in 8 rabbits. Note that analysis of variance showed that, across all frequencies of electrical stimulation, responses of MBF differed from those of RBF and CBF ($P < 0.001$). In contrast, responses of RBF and CBF were indistinguishable ($P > 0.05$). Redrawn from Leonard et al.⁴⁵

Rudenstam *et al.* showed that graded renal nerve stimulation (2-5 Hz at 5 V and 1 ms duration) in anaesthetized rats produced progressive reductions in RBF and CBF, but only small changes in blood flow in the renal papilla (the very inner part of the medulla)². We subsequently performed similar studies in anaesthetized rabbits, showing that in this species inner MBF was reduced in a progressive fashion by graded (frequency or amplitude) renal nerve stimulation, but that MBF was reduced less than RBF or CBF, particularly at stimulation frequencies of 3 Hz or less⁴⁵ (Figure 3). Collectively, these studies suggested that the medullary circulation is relatively insensitive to the ischaemic effects of renal sympathetic drive, but also raised the possibility that some regional differences in sensitivity

might exist within the medulla. To investigate this latter possibility, we tested the effects of graded renal nerve stimulation on laser Doppler blood flow measurements at 2 mm intervals from the surface of the cortex to close to the tip of the papilla⁴². We found that responses to renal nerve stimulation in the renal cortex (≤ 3 mm below the kidney surface) were always greater than those within the medulla (≥ 5 mm below the kidney surface), but that responses within the inner and outer medulla were indistinguishable. Thus, while these data confirm that renal nerve activation can differentially affect CBF and MBF, they do not support the notion that it can differentially affect perfusion at different levels of the medulla.

Impact of endogenous renal sympathetic nerve activity on MBF

Electrical stimulation of the renal sympathetic nerves is a useful technique for producing graded increases in renal sympathetic drive, but it does not mimic naturally occurring renal sympathetic nerve activity (RSNA)⁴⁶. Endogenous RSNA has a bursting pattern, with the amplitude of each burst probably largely reflecting the recruitment of individual axons⁴⁷. In most cases, reflex changes in RSNA mainly reflect changes in the amplitude of bursts, rather than changes in their frequency^{48,49}. Relating the frequency of electrical stimulation to changes in endogenous RSNA is therefore problematic⁴⁶. Given this caveat, we can at least say that similar reductions in CBF of $\sim 20\%$ are achieved in anaesthetized rabbits with 1 Hz electrical stimulation⁴⁵, and a hypoxic stimulus that increases RSNA by $\sim 80\%$ ⁵⁰. Therefore, our observation that the relative insensitivity of MBF to renal nerve stimulation is most clearly seen at low frequencies of stimulation raises the possibility that MBF might be refractory to the basal level of RSNA, and to reflex increases in RSNA associated with physiological manoeuvres that reduce RBF. This does indeed seem to be the case. For example, CBF but not MBF is reduced by arterial chemoreceptor stimulation in conscious rats⁵¹ and hypoxia in anaesthetized rabbits⁵⁰ (Figure 4). Furthermore, while hypotensive haemorrhage consistently reduces CBF, MBF has been observed to either remain unchanged or to increase^{52,53}, or to be reduced less than CBF⁵⁴⁻⁵⁶. Conversely, renal denervation in anaesthetized rats increases CBF but not MBF⁵⁷.

On the other hand, MBF does not appear to be entirely insensitive to reflex increases in RSNA. Evoking the nasopharyngeal reflex in conscious rabbits, by exposure to cigarette smoke, transiently increased RSNA by $\sim 135\%$ ⁴⁸. This reflex is accompanied by little change in arterial pressure, but falls in cardiac output, RBF, CBF and MBF are observed⁵⁸ (Figure 5). Indeed, MBF and CBF were reduced similarly by the nasopharyngeal reflex in conscious rabbits, which seems at odds with the notion that MBF is less sensitive than CBF to reflex increases in RSNA. An explanation for this paradox might lie in differences between the dynamic responses of CBF and MBF to neural activation. In particular, MBF seems able to respond faster to renal sympathetic activation⁵⁹, and to be

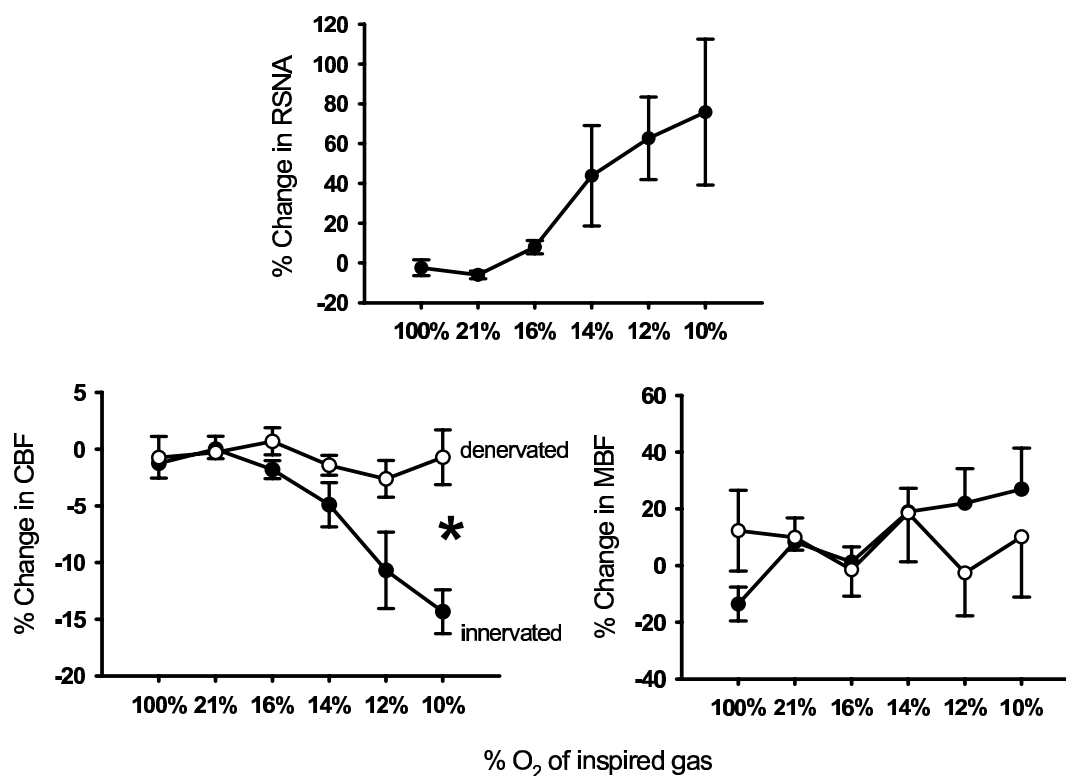


Figure 4. Responses of renal sympathetic nerve activity, and laser Doppler measurements of cortical blood flow (CBF) and medullary blood flow (MBF) to progressive hypoxia. Experiments were performed in anaesthetized, artificially ventilated rabbits, and hypoxaemia was induced by exposure to progressively hypoxic gas mixtures. Responses of CBF and MBF were determined in rabbits with intact renal nerves (●; $n = 7$) and in rabbits in which the renal nerves were destroyed (○; $n = 6$). Symbols and error bars represent mean \pm s.e.mean. * $P < 0.05$ for interaction term between 'state' (intact or denervated) and the response to progressive hypoxia, from analysis of variance. Data redrawn from Leonard et al.⁵⁰

more sensitive than CBF or total RBF to oscillations in RSNA at frequencies normally present in endogenous RSNA⁴⁵. This might increase the relative responsiveness of MBF to transient increases in RSNA associated with manoeuvres such as the nasopharyngeal reflex. The mechanistic and anatomical bases of the differing frequency response characteristics of CBF and MBF remain unknown.

Mechanisms underlying the relative insensitivity of MBF to sympathetic drive

Because MBF is refractory to mild to moderate increases in RSNA, it seems likely that the renal nerves play little role in its physiological regulation. However, in pathological conditions such as heart failure, where RSNA can increase by over 200%⁶⁰, MBF might be chronically reduced, which would exacerbate salt and water retention. Furthermore, MBF might also be chronically reduced if its sensitivity to RSNA were somehow increased, perhaps through failure of mechanisms protecting the medulla from the ischaemic effects of sympathetic activation. Potentially, this could lead to the development of hypertension. Much of our recent research, therefore, has focussed on elucidating the mechanisms underlying the relative insensitivity of MBF to renal sympathetic drive. From a

theoretical perspective, a number of potential mechanisms could contribute, which are discussed separately below.

Regional heterogeneity of glomerular arteriole geometry

As discussed earlier, (see *The renal medullary circulation: structure and function*), the fact that juxtamedullary afferent and (particularly) efferent arterioles have greater calibre than their counterparts in other regions of the kidney, should theoretically predispose MBF to be less sensitive than the bulk of CBF to virtually all vasoconstrictor stimuli. In support of this notion, we have found that while some vasoconstrictors preferentially reduce MBF more than CBF (eg vasopressin peptides), most reduce CBF more than MBF (eg RSNA, angiotensin II, endothelin peptides)^{58,61-67}. Furthermore, renal arterial infusions of angiotensin II⁴ and endothelin-1⁶⁶ constrict juxtamedullary afferent and efferent arterioles similarly to their counterparts in other regions of the kidney (determined by vascular casting methods), yet MBF is little affected by these agents in the face of large changes in total RBF and CBF^{65,66}. It seems likely, therefore, that the vascular architecture of the kidney is arranged in a way that protects the medulla from the ischaemic effects of a range of vasoconstrictor stimuli, including sympathetic nerve

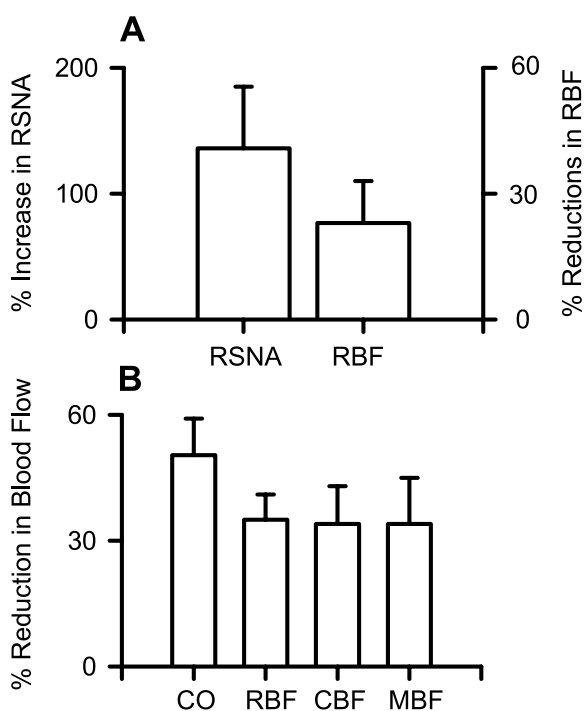


Figure 5. Responses in conscious rabbits of renal sympathetic nerve activity (RSNA), renal blood flow (RBF), cardiac output (CO), cortical blood flow (CBF) and medullary blood flow (MBF) to exposure to cigarette smoke (the nasopharyngeal reflex). Panel A represents the results of a study in rabbits equipped for simultaneous measurement of RSNA and RBF in the left kidney⁴⁸. Note that changes in RSNA and RBF are shown on different scales. Panel B shows the results of an experiment in rabbits equipped for simultaneous measurement of CO, and RBF, CBF and MBF in the left kidney⁵⁸. The reflex comprises transient reductions in heart rate, CO and RBF that usually reach a maximum within the first 5 s after exposure to smoke. Data represent the mean \pm s.e.mean ($n = 8-12$) of maximum changes from control. Note that responses of RBF in the two experiments are comparable, and that both CBF and MBF are reduced by this reflex which more than doubles RSNA.

activation.

Regional differences in the density of nerve bundles and/or varicosities innervating vascular elements controlling CBF and MBF

As previously mentioned (see *Innervation of vascular elements controlling MBF*), available evidence suggests that juxtamedullary glomerular arterioles and outer medullary descending vasa recta are richly innervated, so this seems unlikely to account for the relative insensitivity of MBF to sympathetic activation. However, more detailed information at the ultrastructural level, regarding the density of neuromuscular junctions on the various vascular

elements within the kidney, is required before this potential mechanism can be completely excluded.

Regional differences in sympathetic co-transmitter function in vascular elements controlling CBF and MBF

We recently tested the effects of blockade of α_1 -adrenoceptors on regional kidney blood flow responses to renal nerve stimulation⁶⁸. As expected, the α_1 -adrenoceptor antagonist prazosin greatly blunted responses of RBF and CBF to renal nerve stimulation, but to our surprise, had no detectable effect on responses of MBF. We can exclude roles for α_2 -adrenoceptors in mediating the post-junctional response to renal nerve stimulation, because the α_2 -adrenoceptor antagonist rauwolscine did not inhibit responses of MBF to renal nerve stimulation. These observations raise the interesting possibility that sympathetic co-transmitters make an important contribution to mediating the effects of sympathetic nerve activity on MBF.

Interactions between hormonal and neural mediators of renal vascular tone: paracrine hormones

The role of the vascular endothelium in modulating responses to vasoactive factors is well established¹⁰. More recently, it has become clear that such factors are also released from the tubular epithelium, and that so-called 'tubulovascular cross-talk' plays a key role in the regulation of renal vascular tone¹⁰. Previous studies of the contribution of these mechanisms to the neural control of regional kidney blood flow have, for the most part, relied on intravascular administration of noradrenaline as a surrogate for neural noradrenaline release. Such experiments must be interpreted with care, since noradrenaline infusion does not adequately mimic sympathetic nerve activation, which likely involves neurotransmitter (including co-transmitter) release at specialised neuromuscular junctions²⁵. Nevertheless, these experiments have provided important mechanistic information that has formed the basis of our research in this area.

The relative insensitivity of MBF to noradrenaline infusions (intravenous or renal arterial) appears to be largely due to nitric oxide release^{61,69}. Our recent results suggest that a similar mechanism might operate to protect the medulla from the ischaemic effects of sympathetic nerve activation, since blockade of nitric oxide synthesis⁶² enhances MBF responses to renal nerve stimulation in rabbits. However, even after nitric oxide synthase blockade, renal nerve stimulation still reduces MBF less than CBF⁶², indicating that other mechanisms also contribute to the relative insensitivity of the medullary circulation to sympathetic activation. Prostanoids appear to have little net role in modulating renal vascular responses to activation of the sympathetic nerves, as the cyclooxygenase inhibitor ibuprofen did not significantly affect responses of RBF, CBF or MBF to renal nerve stimulation in anaesthetized rabbits⁷⁰. However, we also recently found that under conditions of prior cyclooxygenase blockade, nitric oxide synthase blockade did not enhance the response of MBF to

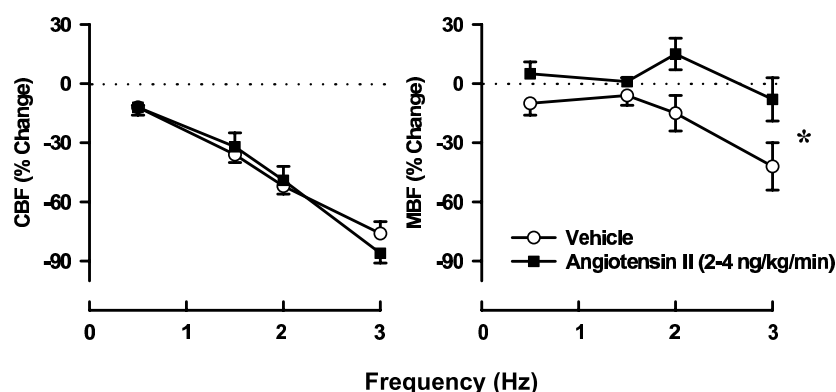


Figure 6. Responses of cortical blood flow (CBF) and medullary blood flow (MBF) to renal nerve stimulation in anaesthetized rabbits receiving a renal arterial infusion of isotonic saline (\circ), or angiotensin II (2-4 ng/kg/min, \blacksquare) ($n = 9$). Saline infusion did not significantly affect baseline CBF or MBF, whereas angiotensin II infusion significantly reduced baseline CBF (by $14 \pm 5\%$) but not MBF. * $P < 0.05$ for significant difference, across all frequencies, in the responses to renal nerve stimulation during angiotensin II infusion, compared with the responses during saline infusion. Data redrawn from Guild et al.⁶³

renal nerve stimulation⁷⁰. These observations contrast directly with those of our previous study under conditions of intact cyclooxygenase activity⁶², and raise the intriguing possibility, that the impact of nitric oxide synthase blockade on responses of MBF to renal nerve stimulation, are at least partly mediated through vasoconstrictor products of cyclooxygenase.

Interactions between hormonal and neural mediators of renal vascular tone: endocrine hormones

We recently obtained evidence that circulating hormones such as angiotensin II and arginine vasopressin could play a key role in determining the nature of the regional renal haemodynamic response to increased renal sympathetic drive⁶³. For example, angiotensin II is known to act at a number of levels to enhance sympathetic neurotransmission⁷¹, but this endocrine/paracrine/autocrine hormone also has a unique action within the medullary circulation, in that it can induce vasodilation through activation of AT_1 -receptors, and subsequent release of nitric oxide and vasodilator prostaglandins^{10,61,64,65}. To test whether angiotensin II might differentially affect responses to sympathetic activation in the medullary and cortical circulations, we tested the effects, on responses to renal nerve stimulation, of renal arterial infusion of angiotensin II in anaesthetized rabbits, at a dose that slightly reduced basal RBF and CBF but did not significantly affect basal MBF⁶³. We found that the angiotensin II infusion virtually abolished reductions in MBF induced by renal nerve stimulation, without affecting responses of RBF and CBF (Figure 6). Thus, elevated intrarenal levels of angiotensin II

appear to selectively inhibit renal nerve stimulation-induced ischaemia in the medullary circulation. The physiological significance of this phenomenon, and the mechanisms mediating it, remain to be determined.

Conclusions and future directions

There is now strong evidence that activation of the renal sympathetic nerves has less impact on MBF than CBF, particularly at moderate stimulus intensities. Indeed, the medullary circulation appears to be refractory to basal levels of endogenous sympathetic nerve activity, and to all but the most profound reflex increases in sympathetic drive. The precise nature of the mechanisms that limit the sensitivity of MBF to sympathetic drive remain unknown, although recent experiments suggest roles for nitric oxide and possibly angiotensin II. It also seems likely that regional differences in the geometry of glomerular arterioles pre-disposes MBF to respond less than CBF to any given vasoconstrictor stimulus (Figure 7). Other mechanisms, including the potential for roles of sympathetic co-transmitters, require investigation.

Dysfunction of the mechanisms that protect the medullary circulation from ischaemia due to activation of the renal nerves would increase the sensitivity of MBF to renal sympathetic drive. This could potentially lead to chronic reductions in MBF, salt and water retention, and the subsequent development of hypertension (Figure 7). Future studies should aim to directly test this hypothesis, and determine whether neurally-mediated reductions in MBF contribute to the development of essential hypertension, and also to salt and water retention in pathological conditions

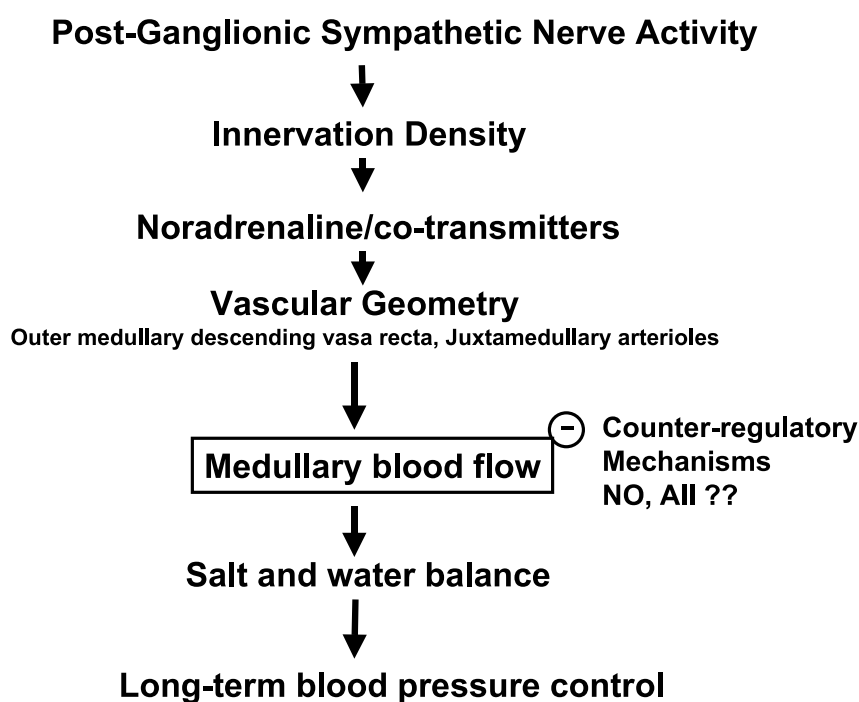


Figure 7. Working hypothesis of the factors underlying the relative insensitivity of renal medullary blood flow (MBF) to renal sympathetic drive. Responses of MBF to sympathetic activation will depend on the level of post-ganglionic sympathetic nerve activity, the functional density of the sympathetic innervation of vascular elements controlling MBF, on the nature of neurotransmission in these neurones, and on the basal calibre of vascular elements controlling MBF relative to those in the bulk of the renal cortex. Nitric oxide (NO), and perhaps also circulating angiotensin II (AII), seem to play key roles in blunting responses of MBF to renal nerve stimulation. Failure of these mechanisms could lead to salt and water retention under conditions of sympatho-adrenal activation, and so the development of hypertension.

associated with increased sympathetic drive, such as heart failure.

Acknowledgements

Original studies by the authors described in this article were supported by grants from the National Health and Medical Research Council of Australia (143603, 143785), the National Heart Foundation of Australia (G 98M 0125), the Ramaciotti Foundations (A 6370, RA 159/98), the Marsden Fund of New Zealand, and the Auckland Medical Research Foundation.

References

1. Pomeranz BH, Birtch AG, Barger AC. Neural control of intrarenal blood flow. *Am. J. Physiol.* 1968; **215**: 1067-1081.
2. Rudenstam J, Bergström G, Taghipour K, Göthberg G, Karlström G. Efferent renal sympathetic nerve stimulation *in vivo*. Effects on regional renal haemodynamics in the Wistar rat, studied by laser-Doppler technique. *Acta Physiol. Scand.* 1995; **154**: 387-394.
3. Pallone TL, Robertson CR, Jamison RL. Renal medullary microcirculation. *Physiol. Rev.* 1990; **70**: 885-920.
4. Denton KM, Anderson WP, Sinniah R. Effects of angiotensin II on regional afferent and efferent arteriole dimensions and the glomerular pole. *Am. J. Physiol.* 2000; **279**: R629-R638.
5. Luke RG. Essential hypertension: a renal disease? A review and update of the evidence. *Hypertension* 1993; **21**: 380-390.
6. Guyton AC. Long-term arterial pressure control: an analysis from animal experiments and computer and graphic models. *Am. J. Physiol.* 1990; **259**: R865-R877.
7. Rettig R, Schmitt B, Peilzl B, Speck T. The kidney and primary hypertension. Contributions from renal transplantation studies in animals and humans. *J. Hypertension* 1993; **11**: 883-891.
8. Roman RJ, Zou A-P. Influence of the renal medullary circulation on the control of sodium excretion. *Am. J. Physiol.* 1993; **265**: R963-R973.
9. Cowley AWJr. Role of the renal medulla in volume and arterial pressure regulation. *Am. J. Physiol.* 1997; **273**: R1-R15.
10. Cowley AWJr, Mori T, Mattson D, Zou A-P. Role of renal NO production in the regulation of medullary blood flow. *Am. J. Physiol.* 2003; **284**:

- R1355-R1369.
11. Mattson D. Importance of the renal medullary circulation in the control of sodium excretion and blood pressure. *Am. J. Physiol.* 2003; **284**: R13-R27.
 12. Correia AG, Bergström G, Lawrence AJ, Evans RG. Renal medullary interstitial infusion of norepinephrine in anesthetized rabbits: methodological considerations. *Am. J. Physiol.* 1999; **277**: R112-R122.
 13. Correia AG, Madden AC, Bergström G, Evans RG. Effects of renal medullary and intravenous norepinephrine on renal antihypertensive function. *Hypertension* 2000; **35**: 965-970.
 14. Majid DS, Said K, Omoro SA, Navar LG. Nitric oxide dependency of arterial pressure-induced changes in renal interstitial hydrostatic pressure in dogs. *Circ. Res.* 2001; **88**: 347-351.
 15. Eppel GA, Bergström G, Anderson WP, Evans RG. Autoregulation of renal medullary blood flow in rabbits. *Am. J. Physiol.* 2003; **284**: R233-R244.
 16. Lundin S, Ricksten S-E, Thoren P. Renal sympathetic activity in spontaneously hypertensive rats and normotensive controls, as studied by three different methods. *Acta Physiol. Scand.* 1984; **120**: 265-272.
 17. Lundin S, Thoren P. Renal function and sympathetic activity during mental stress in normotensive and spontaneously hypertensive rats. *Acta Physiol. Scand.* 1982; **115**: 115-124.
 18. Esler MG, Lambert G, Jennings G. Increased regional sympathetic nervous activity in human hypertension: causes and consequences. *J. Hypertens.* 1990; **8(Suppl 7)**: S53-S57.
 19. Norman RA, Dzielak DJ. Role of renal nerves in onset and maintenance of spontaneous hypertension. *Am. J. Physiol.* 1982; **243**: H284-H288.
 20. DiBona GF, Kopp UC. Neural control of renal function. *Physiol. Rev.* 1997; **77**: 75-197.
 21. Barajas L, Liu L, Powers K. Anatomy of the renal innervation: intrarenal aspects and ganglia of origin. *Can. J. Physiol. Pharmacol.* 1992; **70**: 735-749.
 22. Chen J, Fleming JT. Juxtamedullary afferent and efferent arterioles constrict to renal nerve stimulation. *Kid. Int.* 1993; **44**: 684-691.
 23. McKenna OC, Angelakos ET. Adrenergic innervation of the canine kidney. *Circ. Res.* 1968; **22**: 345-354.
 24. Barajas L, Powers K. Monoaminergic innervation of the rat kidney: a quantitative study. *Am. J. Physiol.* 1990; **259**: F503-F511.
 25. Brock JA, Cunnane T. Electrophysiology of neuroeffector transmission in smooth muscle. In: Burnstock G, Hoyle CHV (eds). *Autonomic Neuroeffector Mechanisms*. Harwood Academic Publishers: Chur. 1992; pp 121-211.
 26. Luff SE, Hengstberger SG, McLachlan EM, Anderson WP. Distribution of sympathetic neuroeffector junctions in the juxtglomerular region of the rabbit kidney. *J. Auton. Nerv. Syst.* 1992; **40**: 239-254.
 27. DiBona GF, Sawin LL. Role of neuropeptide Y in renal sympathetic vasoconstriction: studies in normal and congestive heart failure rats. *J. Lab. Clin. Med.* 2001; **138**: 119-129.
 28. Malmström RE, Balmér KC, Lundberg JM. The neuropeptide Y (NPY) Y₁ receptor antagonist BIBP 3226: equal effects on vascular responses to exogenous and endogenous NPY in the pig *in vivo*. *Br. J. Pharmacol.* 1997; **121**: 595-603.
 29. Pernow J, Lundberg JM. Release and vasoconstrictor effects of neuropeptide Y in relation to non-adrenergic sympathetic control of renal blood flow in the pig. *Acta Physiol. Scand.* 1989; **136**: 507-517.
 30. Schwartz DD, Malik KU. Renal periarterial nerve stimulation-induced vasoconstriction at low frequencies is primarily due to release of a purinergic transmitter in the rat. *J. Pharmacol. Exp. Ther.* 1989; **250**: 764-771.
 31. Reinecke M, Forssmann WG. Neuropeptide (neuropeptide Y, neurotensin, vasoactive intestinal polypeptide, substance P, calcitonin gene-related peptide, somatostatin) immunohistochemistry and ultrastructure of renal nerves. *Histochem.* 1988; **89**: 1-9.
 32. Longley CD, Weaver LC. Proportions of renal and splenic postganglionic sympathetic populations containing galanin and dopamine beta hydroxylase. *Neuroscience* 1993; **55**: 253-261.
 33. Leys K, Schachter M, Sever P. Autoradiographic localisation of NPY receptors in rabbit kidney: comparison with rat, guinea-pig and human. *Eur. J. Pharmacol.* 1987; **134**: 233-237.
 34. Hansell P. Evaluation of methods for estimating renal medullary blood flow. *Renal Physiol. Biochem.* 1992; **15**: 217-230.
 35. Trueta J, Barclay AE, Daniel PM, Franklin KJ, Prichard MML. *Studies of the Renal Circulation*. 1947, Oxford, Blackwell Scientific Publications.
 36. Houck CR. Alterations in renal hemodynamics and function in separate kidneys during stimulation of renal artery nerves in dogs. *Am. J. Physiol.* 1951; **167**: 523-530.
 37. Aukland K. Effect of adrenaline, noradrenaline, angiotensin and renal nerve stimulation on intrarenal distribution of blood flow in dogs. *Acta Physiol. Scand.* 1968; **72**: 498-509.
 38. Chapman BJ, Horn NM, Robertson MJ. Renal blood-flow changes during renal nerve stimulation in rats treated with α -adrenergic and dopaminergic blockers. *J. Physiol.* 1982; **325**: 67-77.
 39. Hermansson K, Öjteg G, Wolgast M. The cortical and medullary blood flow at different levels of renal nerve activity. *Acta Physiol. Scand.* 1984; **120**: 161-169.
 40. Roman RJ, Smits C. Laser-Doppler determination of papillary blood flow in young and adult rats. *Am. J. Physiol.* 1986; **251**: F115-F124.
 41. Almond NE, Wheatley AM. Measurement of hepatic perfusion in rats by laser Doppler flowmetry. *Am. J. Physiol.* 1992; **262**: G203-G209.
 42. Guild S-J, Eppel GA, Malpas SC, Rajapakse NW,

- Stewart A, Evans RG. Regional responsiveness of renal perfusion to activation of the renal nerves. *Am. J. Physiol.* 2002; **283**: R1177-R1186.
43. Stern MD, Bowen PD, Parma R, Osgood RW, Bowman RL, Stein JH. Measurement of renal cortical and medullary blood flow by laser-Doppler spectroscopy in the rat. *Am. J. Physiol.* 1979; **236**: F80-F87.
 44. Fenoy FJ, Roman RJ. Effect of volume expansion on papillary blood flow and sodium excretion. *Am. J. Physiol.* 1991; **260**: F813-F822.
 45. Leonard BL, Evans RG, Navakatikyan MA, Malpas SC. Differential neural control of intrarenal blood flow. *Am. J. Physiol.* 2000; **279**: R907-R916.
 46. Malpas SC, Guild S-J, Evans RG. Responsiveness of the renal vasculature: relating electrical stimulation to endogenous nerve activity is problematic. *Am. J. Physiol.* 2003; **284**: F594-F596.
 47. Malpas SC. The rhythmicity of sympathetic nerve activity. *Prog. Neurobiol.* 1998; **56**: 65-96.
 48. Malpas SC, Evans RG. Do different levels and patterns of sympathetic activation all provoke renal vasoconstriction? *J. Auton. Nerv. Syst.* 1998; **69**: 72-82.
 49. Malpas SC, Evans RG, Head GA, Lukoshkova EV. Contribution of renal nerves to renal blood flow variability during hemorrhage. *Am. J. Physiol.* 1998; **274**: R1283-R1294.
 50. Leonard BL, Malpas SC, Denton KM, Madden AC, Evans RG. Differential control of intrarenal blood flow during reflex increases in sympathetic nerve activity. *Am. J. Physiol.* 2001; **280**: R62-R68.
 51. Ledderhos C, Gross V, Cowley AWJr. Pharmacological stimulation of arterial chemoreceptors in conscious rats produces differential responses in renal cortical and medullary blood flow. *Clin. Exp. Pharmacol. Physiol.* 1998; **25**: 536-540.
 52. Brezis M, Heyman SN, Epstein FH. Determinants of intrarenal oxygenation II: Hemodynamic effects. *Am. J. Physiol.* 1994; **267**: F1063-F1068.
 53. Ganguli M, Tobian L. Hypertension from carotid occlusion decreases renal papillary blood flow, hypotension from hemorrhage increases it, an autoregulatory paradox. *Hypertens. Res.* 1996; **19**: 17-22.
 54. Fischer R, Ikeda S, Sarma JSM, Bing RJ. The effects of indomethacin, 6-hydroxydopamine, saralasin and hemorrhage on renal hemodynamics. *J. Clin. Pharmacol.* 1977; **17**: 5-12.
 55. Neiberger RE, Passmore J. Effects of dopamine on canine intrarenal blood flow distribution during hemorrhage. *Kid. Int.* 1979; **15**: 219-226.
 56. Jaschke W, Sievers RS, Lipton MJ, Cogan MG. Cine-computed tomographic assessment of regional renal blood flow. *Acta Radiol.* 1990; **31**: 77-81.
 57. Kompanowska-Jeziarska E, Walkowska A, Johns EJ, Sadowski J. Early effects of renal denervation in the anaesthetised rat: natriuresis and increased cortical blood flow. *J. Physiol.* 2001; **531**: 527-534.
 58. Evans RG, Madden AC, Denton KM. Diversity of responses of renal cortical and medullary blood flow to vasoconstrictors in conscious rabbits. *Acta Physiol. Scand.* 2000; **169**: 297-308.
 59. Navakatikyan MA, Leonard BL, Evans RG, Malpas SC. Modelling the neural control of intrarenal blood flow. *Clin. Exp. Pharmacol. Physiol.* 2000; **27**: 650-652.
 60. Zucker IH, Wang W, Brandle M, Schultz HD, Patel KP. Neural regulation of sympathetic nerve activity in heart failure. *Prog. Cardiovasc. Dis.* 1995; **37**: 397-414.
 61. Rajapakse NW, Oliver JJ, Evans RG. Nitric oxide in responses of regional kidney blood flow to vasoactive agents in anesthetized rabbits. *J. Cardiovasc. Pharmacol.* 2002; **40**: 210-219.
 62. Eppel GA, Denton KM, Malpas SC, Evans RG. Nitric oxide in responses of regional kidney perfusion renal nerve stimulation and renal ischaemia. *Pflügers Arch.* 2003; **447**: 205-213.
 63. Guild S-J, Barrett CJ, Evans RG, Malpas SC. Interactions between neural and hormonal mediators of renal vascular tone in anaesthetized rabbits. *Exp. Physiol.* 2003; **88**: 229-241.
 64. Oliver JJ, Rajapakse NW, Evans RG. Effects of indomethacin on responses of regional kidney perfusion to vasoactive agents in rabbits. *Clin. Exp. Pharmacol. Physiol.* 2002; **29**: 873-879.
 65. Duke LM, Eppel GA, Widdop RE, Evans RG. Disparate roles of AT₂-receptors in the renal cortical and medullary circulations of anesthetized rabbits. *Hypertension* 2003; **42**: 200-205.
 66. Denton KM, Finkelstein L, Flower RL, Shweta A, Evans RG, Anderson WP. Constriction of juxtamedullary arterioles in response to endothelin does not decrease medullary blood flow. *FASEB J.* 2003; **17 (5 part II)**: 587.5 (Abstract).
 67. Correia AG, Denton KM, Evans RG. Effects of activation of vasopressin V₁-receptors on regional kidney blood flow and glomerular arteriole diameters. *J. Hypertens.* 2001; **19**: 649-657.
 68. Lee LL, Evans RG, Eppel GA. Roles of α -adrenoceptor subtypes in regional renal vascular responses to renal nerve stimulation in rabbits. *Clin. Exp. Pharmacol. Physiol.* 2003; **30**: A66 (Abstract).
 69. Zou A-P, Cowley AWJr. α_2 -Adrenergic receptor-mediated increase in NO production buffers renal medullary vasoconstriction. *Am. J. Physiol.* 2000; **279**: R769-R777.
 70. Rajapakse NW, Eppel GA, Denton KM, Malpas SC, Evans RG. Do nitric oxide and prostaglandins protect the renal medullary circulation from ischemia during renal nerve stimulation? *FASEB J.* 2003. **17 (5 part II)**: 587.22 (Abstract).
 71. Zimmerman BG. Actions of angiotensin on adrenergic nerve endings. *Fed. Proc.* 1978; **37**: 199-202.
 72. Bankir L, Bouby N, Trinh-Trang-Tan M-M. Heterogeneity of nephron anatomy. *Kid. Int.* 1987; **31(suppl. 20)**: S-25-S-39.

73. Beeuwkes R, Bonventre JV. Tubular organization and vascular-tubular relations in the dog kidney. *Am. J. Physiol.* 1975; **229**: 695-713.
74. Vander A. *Renal Physiology*. 1995, New York: McGraw Hill.
75. Lübbers DW, Baumgärtl H. Heterogeneities and profiles of oxygen pressure in brain and kidney as examples of the pO₂ distribution in the living tissue. *Kid. Int.* 1997; **51**: 372-380.

Received 30 October 2003; in revised form January 28 2004. Accepted 29 January 2004.

©G.A. Eppel 2004

Author for correspondence:

Dr Roger G. Evans
Department of Physiology,
Monash University,
Vic 3800, Australia

Tel: +61 3 9905 1466

Email: Roger.Evans@med.monash.edu.au

Functional Imaging Introduction: Gaining new insight from biophotonic imaging

Mark B. Cannell

*Department of Physiology, School of Medical Sciences,
The University of Auckland, Auckland, New Zealand*

Over the past 2 decades, there has been an explosive growth in the range of measurement modalities available to the physiologist. Today, a very large part of the electromagnetic spectrum is used to probe and record physiological function from the level of the whole body to tissue, cell and even organelle. This use of photonic methods includes radio waves in the form of nuclear magnetic resonance imaging, through light in, for example, microscopy and video imaging, and on to real time fluoroscopy with Xrays. Even gamma rays from radioisotopes find some imaging applications with gamma ray cameras. Perhaps the most common use of photonics in physiological research is in the area of microscopy and cell biology. Here we see methods that employ almost most of the fundamental features of light itself to generate physiological images; for example polarization and interference are routinely used to help generate contrast within unlabelled cells.

The effort to clarify cell function has been aided by the development of a wide variety of probes that reveal elements of cell function that cannot be directly observed through other contrast enhancement methods. With these probes we can now image intracellular ion levels, vesicle trafficking and even protein synthesis and degradation within living cells. Although today we talk about "cell biology", "neuroscience" and "developmental biology" as cutting edge disciplines, in reality they are simply physiological research repackaged to detach the term "physiology". It is possible that a part of this has arisen from the view that the more classical forms of physiology involved rather more quantification, mathematics and physics than is palatable for many students. This is a pity, for careful measurement can often be more revealing than cursory examination. For example, digital imaging microscopy is routinely used in all of the above disciplines but detailed analysis of the already digitized data is rarely performed. Unfortunately, the massive amount of real data contained in microscopic images is frequently ignored and image processing applied to only "beautify" images rather than provide feature extraction and quantification. I cannot help but wonder what Bernstein and Starling would have made of this "science".

Measurement within new imaging methods has given powerful insight in to cell function. As an example, our discovery and quantification of microscopic calcium sparks¹⁻³ has shown that signal transduction occurs in microscopic domains where behaviour cannot be deduced from whole cell measurements. Such experiments have firmly established the need for confocal microscopy in live cell imaging. Today, I am still amazed that we have been now been able to directly measure microscopic gradients of

calcium within sarcomeres with a fast confocal line scanning method⁴. Two decades ago, such gradients could only be deduced from computer models of my rather poor quality calcium signals obtained using aequorin^{5,6}. That such exquisitely sensitive methods can now be routinely applied to follow cellular processes promises great insight into cell physiology. This has been aided by the co-development of better probes for cell function (as well as instrumentation).

In the area of calcium metabolism, calcium imaging inside cells is not new; for example in 1928 Pollack⁷ injected an amoeba with alarazin which precipitated as a calcium salt at the site of pseudopod formation. With increasing awareness of the multiple roles of calcium new methods were developed to image Ca and obtain sub-cellular resolution. Autoradiographic imaging of ⁴⁵Ca with electron microscopy was applied to muscle in the 1960's^{8,9}. The development of calcium measurement techniques occurred quite rapidly around 1980 (see 10 for review). To improve temporal response and the ability to directly measure function in living cells required the development and application of more sensitive compounds (e.g. aequorin and metallochromic indicators) and ultimately fluorescent probes such as fura-2^{11,12}. The high signal strength of the fluorescent probes made real time video fluorescence imaging possible^{13,14}. The spatial resolution of the fluorescent microscope was been improved by the development and application of laser scanning confocal microscopy¹⁵⁻¹⁸. Such laser scanning methods promise resolution to the level of single molecules within cells – although it is always questionable whether the study of the interactions of single molecules really falls under the umbrella of "physiology". More uncommon microscopic imaging modalities are still developed in areas such as non-linear excitation in multiphoton microscopy, fluorescence energy transfer, quantitative birefringence and quantitative phase microscopy. These methods are bringing a new generation of physicists and engineers into the life sciences and helping to further accelerate our development and application of new methods.

That visible light has proved so useful for studying cell function is easy to explain. In order to measure something it must be probed by energy in some form and to maximize the signal to noise ratio, you need to employ the highest possible energy levels. Since the energy of the visible wavelength photon (~2 eV) is somewhat lower than that of a typical chemical bond, molecules can be repeatedly probed by visible wavelength photons without destroying them. Of course, the energy difference is not so large that damage can be ignored, but with careful experimental design we can record cell function and cell

responses to many stimuli and bracket responses with controls. In live cell imaging, noisy signals are to be expected and not to be confused with poor experimentation. Therein lies the true artistry of vital imaging: to achieve the clearest possible imaging results while treading carefully along the boundary of cell damage. In connection with this point, we should also not forget that introducing any probe carries the risk of changing cell function and that molecular biological manipulation to make the cell report its own functions is also not without the risk of changing cell function/behaviour.

In summary, I suggest that the greatest advances in understanding physiological function have come about from the development and application of new measurement methods and the physiologist has always been quick and creative in applying new methods to problems in his/her area of research. Application of these new methods is always harder than using well established methods but the rewards are also greater. Thus while imaging is not new in physiological research, new imaging modalities are giving fresh insight into cell behaviour. The application of new imaging technologies within the life sciences is likely to continue to reveal unexpected complexity in physiology and life. In the following four papers presented in this symposium, we can see examples of the latest quantitative imaging techniques. As we continue this work, we can also take a moment to enjoy the beauty of the images that can be made.

References

- Cheng H, Lederer WJ, Cannell MB. Calcium sparks: elementary events underlying excitation-contraction coupling in heart muscle. *Science* 1993;**262**(5134):740-4.
- Cannell MB, Cheng H, Lederer WJ. Spatial non-uniformities in $[Ca^{2+}]_i$ during excitation-contraction coupling in cardiac myocytes. *Biophys. J.* 1994;**67**(5):1942-56.
- Cannell MB, Cheng H, Lederer WJ. The control of calcium release in heart muscle. *Science* 1995;**268**(5213):1045-9.
- Hollingworth S, Soeller C, Baylor SM, Cannell MB. Sarcomeric Ca^{2+} gradients during activation of frog skeletal muscle fibres imaged with confocal and two-photon microscopy. *J. Physiol.* 2000;**526 Pt 3**:551-60.
- Cannell MB, Allen DG. Model of calcium movements during activation in the sarcomere of frog skeletal muscle. *Biophys. J.* 1984;**45**(5):913-25.
- Cannell MB. Effect of tetanus duration on the free calcium during the relaxation of frog skeletal muscle fibres. *J. Physiol.* 1986;**376**:203-18.
- Pollack H. Micrurgical studies in cell physiology. IV. Calcium ions in living protoplasm. *J. Gen. Physiol.* 1928;**11**: p. 539-545.
- Winegrad, S., Autoradiographic studies of intracellular calcium in frog skeletal muscle. *J. Gen. Physiol.* 1965;**48**:455-79.
- Winegrad, S., Intracellular calcium movements of frog skeletal muscle during recovery from tetanus. *J. Gen. Physiol.* 1968;**51**(1):65-83.
- Blinks JR, Wier WG, Hess P, Prendergast FG. Measurement of Ca^{2+} concentrations in living cells. *Prog. Biophys. Mol. Biol.* 1982;**40**(1-2):1-114.
- Grynkiewicz G, Poenie M, Tsien RY. A new generation of Ca^{2+} indicators with greatly improved fluorescence properties. *J. Biol. Chem.* 1985;**260**(6):3440-50.
- Poenie M, Tsien R. Fura-2: a powerful new tool for measuring and imaging $[Ca^{2+}]_i$ in single cells. *Prog. Clin. Biol. Res.* 1986;**210**:53-6.
- Wier WG, Cannell MB, Berlin JR, Marban E, Lederer WJ. Cellular and subcellular heterogeneity of $[Ca^{2+}]_i$ in single heart cells revealed by fura-2. *Science* 1987;**235**(4786):325-8.
- Cannell MB, Berlin JR, Lederer WJ. Intracellular calcium in cardiac myocytes: calcium transients measured using fluorescence imaging. *Soc. Gen. Physiol. Ser.* 1987;**42**:201-14.
- Brakenhoff GJ, van der Voort HT, van Spronsen EA, Linnemans WA, Nanninga N. Three-dimensional chromatin distribution in neuroblastoma nuclei shown by confocal scanning laser microscopy. *Nature* 1985;**317**(6039):748-9.
- White JG, Amos WB, Fordham M. An evaluation of confocal versus conventional imaging of biological structures by fluorescence light microscopy. *J. Cell Biol.* 1987;**105**(1):41-8.
- Brakenhoff GJ, van der Voort HT, van Spronsen EA, Nanninga N. Three-dimensional imaging by confocal scanning fluorescence microscopy. *Ann. N.Y. Acad. Sci.* 1986;**483**:405-15.
- Carlsson K. Three-dimensional microscopy using a confocal laser scanning microscope. *Optics Letters* 1985;**10**:53-55.

Received 6 August 2004. Accepted 16 August 2004.

©M.B. Cannell 2004.

Author for correspondence:
M.B. Cannell
Department of Physiology,
School of Medical Sciences,
The University of Auckland,
Auckland, New Zealand

Tel: +64 9373 7599 x86201
Fax: +64 9373 7499
E-mail: m.cannell@auckland.ac.nz

Development of low affinity, membrane targeted Ca²⁺ sensors suitable for measuring presynaptic Ca²⁺

M. Monif, M.L. Smart, C.A. Reid & D.A. Williams

*Department of Physiology,
The University of Melbourne,
Grattan St, Parkville,
Melbourne, 3010, Australia*

Summary

1. Our aim is to measure near-membrane Ca²⁺ flux within presynaptic terminals of central neurons by modifying new genetically encoded Ca²⁺ sensors to develop tools capable of measuring localised Ca²⁺ signals.

2. We used standard recombinant DNA technologies to generate the DNA coding for a fusion construct of a modified fluorescent "pericam" Ca²⁺ biosensor with a presynaptic P2X7 receptor (P2X7R). The Ca²⁺ sensitivity of the biosensor was modified by rational site-directed mutagenesis of the calmodulin portion of the pericam.

3. Biosensor-receptor fusions were transfected into expression systems for evaluation. Expression studies in Human Embryonic Kidney-293 (HEK-293) cells showed that biosensor-receptor fusion construct delivered protein was localised exclusively to the plasma membrane, confirming that fusion did not affect the ability of the receptor to undergo normal protein synthesis and trafficking.

4. The Ca²⁺-dependent fluorescence of the pericam portion of the fusion protein was also retained. Site-direct mutagenesis within the calmodulin moiety of the pericam significantly reduced the Ca²⁺ affinity of the complex. The dynamic range of the sensor following this modification is better matched to the higher Ca²⁺ levels expected within presynaptic Ca²⁺ micro-domains.

Introduction

Ca²⁺ is a ubiquitous cellular messenger controlling a diverse array of physiological processes from fertilisation through to gene transcription, muscle contraction, cell proliferation and migration, cell differentiation and ultimately, cell death. Tight control of the spatial, temporal and concentration profile of Ca²⁺ influx is therefore required to define specific functional roles in cells. This is important in the neuronal setting, especially within the presynaptic terminal where the release of transmitter is critically dependent upon small changes in Ca²⁺ concentrations¹. The invasion of an action potential into the presynaptic terminal opens voltage-dependent Ca²⁺ channels allowing the rapid influx of Ca²⁺ ions, giving rise to a small local volume (microdomain) of elevated Ca²⁺²⁻⁴. Ca²⁺ microdomains coincide with active zones that are areas of presynaptic membrane densely packed with Ca²⁺ channels and docked with neurotransmitter vesicles³. At these microdomains the Ca²⁺ concentration reaches

approximately 100µM⁵ within 800 microseconds⁶, over distances of less than 1 µm from the point of entry⁷. Ca²⁺ microdomains are determinants of neurotransmitter release² and play an important role in the modulation of synaptic strength⁸. Historically, it has been a challenging exercise to measure Ca²⁺ microdomains due to their small spatio-temporal profiles, with the most reliable data derived from modelling and simulation studies⁹. The difficulty in measuring Ca²⁺ microdomains means that a wide range of Ca²⁺-specific signalling processes may go undetected by the current 'volume-averaged' methods routinely used. There is clearly a need for a biosensor that is capable of sensing Ca²⁺ microdomains. Genetically encoded Ca²⁺ sensors based on green fluorescent protein (GFP) provide an exciting opportunity to develop tools to measure these localised signals.

GFP derived from *Aequorea Victoria* jelly fish is a 238 amino acid protein with an apparent molecular weight of 27-30kDa¹⁰. Several GFP mutants with distinct spectral qualities have been established as sensors of cellular dynamics, for example, in monitoring local pH or Ca²⁺ concentration inside cells¹¹. A powerful example of this technology has been the recent development of pericams¹² that consist of a single GFP variant sensitive to physiologically relevant substrates such as Ca²⁺ ions. To construct the pericams, circularly permuted enhanced yellow fluorescent proteins (cpEYFP) were used in which the amino and carboxyl portions had been interchanged and reconnected by a short spacer between the original termini. Calmodulin was fused to the C terminus of cpEYFP and its target peptide, M13, to the N terminus. The pericam was shown to be fluorescent with its spectral properties changing reversibly with the amount of Ca²⁺. Of the three major pericams developed, ratiometric-pericam (RP) appeared to be most promising, in that due to its capacity for dual excitation nature, it has potential for quantitative imaging.

Insertions of genetically encoded sensor into host receptors that already have localisation signals offers a new strategy for measuring localised Ca²⁺. Our goal is to measure Ca²⁺ microdomains within presynaptic terminals. The requirement therefore is a receptor that localises to the presynaptic membrane, but does not play a critical role in evoked release. The P2X7Rs are ligand-gated ion channels that are gated by ATP and other nucleotides¹³⁻¹⁵. Studies of expression patterns of P2X7R have confirmed localisation in presynaptic nerve terminals in both central and peripheral neurons¹⁶. Further, immunoreactivity studies in the

hippocampus indicate that P2X7Rs colocalise with the vesicular glutamate transporter, (VGLUT1), placing them within excitatory terminals¹⁷. This makes P2X7R an ideal tool for targeting Ca²⁺ sensors to excitatory presynaptic nerve terminals in the hippocampus. Smart and colleagues have revealed that fusion of the purinergic P2X7R to GFP directed the complex to the plasma membrane in the simple HEK expression system¹⁸. Here we use this simple expression system to characterise a RP-P2X7R construct, determining its trafficking and Ca²⁺ sensing ability.

As Ca²⁺ concentrations within the presynaptic microdomains are thought to be in the 50-100µM range, the dissociation constant (Kd) of RP, reported to be 1.7µM, is therefore lower than required. As part of fine-tuning the Ca²⁺ affinities of a previous Ca²⁺ sensor, cameleons¹⁹, a number of mutations were performed in the calmodulin moiety of this construct to optimise the Kd for this reporting range. In particular a substitution mutation in the first Ca²⁺ binding loop of calmodulin, where the 31st amino acid was changed from glutamic acid (E) to glutamine (Q), shifted the titration curve of cameleon-1 to the right reflecting an increase in the Kd of its low affinity component from 11µM to 700µM¹⁹. Here we use a similar strategy to lower the affinity of the RP, making it more suitable for measuring the high Ca²⁺ concentrations expected in presynaptic microdomains.

Methods

Gene construction

To incorporate the E31Q mutation into RP a total of three PCR reactions were performed. First the cDNA of the 5' portion of RP(E31Q) was amplified with a sense primer containing a HindIII restriction site and a reverse primer 5' C GGT GCC AAG TT G CTT TGT GGT GAT GG (with the base change introducing the mutation of interest being underlined). For both RP and RP(E31Q) a glycine-rich spacer sequence, GGA GGT GCA GGT AGT GGA GGT corresponding to Gly-Gly-Ala-Gly-Ser-Gly-Gly, was included upstream of the start codon in the forward primer. In the second PCR reaction, the cDNA of the 3' portion of RP(E31Q) was amplified with a forward primer: 5'CC ATC ACC ACA AAG C AA CTT GGC ACC G, and a reverse primer containing a XhoI restriction site. Finally the entire cDNA of RP(E31Q) was amplified with the HindIII and XhoI sites containing primers by using a mixture of the first and second PCR fragments as the template. The restricted product was cloned in-frame into the HindIII/XhoI sites of pcDNA3.1 (Invitrogen) vector. To generate the chimeric sensors, P2X7R-RP and P2X7R-RP(E31Q), a subcloning strategy was employed. The cDNA encoding P2X7R was amplified by using primers containing 5'NheI and 3'HindIII restriction sites. The restricted PCR fragments were ligated to the 5' end of RP or RP(E31Q) gene in pcDNA3.1 to yield the tagged Ca²⁺ sensor constructs of P2X7R-RP and P2X7R-RP(E31Q).

In vitro spectroscopy

To assess the spectral characteristics of the RP and RP(E31Q) proteins, HEK-293 cells were transfected with each DNA construct using LipofectamineTM2000 (Life Technologies). Transfected HEK-293 cells were lysed 3 days post transfection and liberated cytosolic proteins (RP and RP(E31Q)) were collected. To determine the Kds of RP and RP(E31Q), a Ca²⁺ Calibration Buffer Kit (Molecular Probes, C-3009) was used. The spectral properties of the proteins were measured using a Hitachi F-4010 Fluorescence Spectrophotometer. In separate experiments RP and RP(E31Q) were excited at 480nm, with an emission wavelength scan performed from 480 to 650nm. The solutions were maintained at pH 7.20 and 24°C. The Kd of both indicators (RP and RP(E31Q)) was calculated from a linearised (Hill) plot of fluorescence intensity as a function of Ca²⁺ concentration. Data were generated by scanning the emission spectrum of the indicator in the presence of different Ca²⁺ concentrations. All data for RP or RP(E31Q) were corrected for the fluorescence or a reference solution containing non-transfected HEK-293 cells (autofluorescence).

Imaging

Fluorescence-based approaches were used to characterise the Ca²⁺ sensors. Two or three days after cDNA transfection with LipofectamineTM2000, HEK-293 adherent on poly-L-lysine-coated coverslips were analysed microscopically. Cells bathed in HEPES buffer (mM: NaCl 147, KCl 2, HEPES 10, Glucose 10, CaCl₂ 1 pH: 7.4) were imaged at 24°C on a laser scanning confocal (Biorad MRC-1024ES) employing an argon-ion laser, coupled to a Nikon Diaphot 300 microscope. Both the tagged and untagged RPs were illuminated at 488 nm, which excited the YFP portion of the constructs. YFP fluorescence emission of the RP was collected through a 510 long pass dichroic mirror and OG515 emission filter (>515nm). Fluorescence distribution patterns of tagged and untagged biosensors were achieved by collecting 512×512 pixel confocal images (slow scan rate – 1 s/image), a bright field or transmitted image, and a simultaneous image showing the colocalisation of the confocal signal with the transmitted image which revealed fluorescent cellular structures. Some images were taken as an average of 4 consecutive scans (Kalman algorithm) to smooth random noise fluctuations. For assessment of the Ca²⁺ sensing ability of the Ca²⁺ sensors the acquisition package 'Timecourse' was used. In any given field of cells several regions of interest (ROI) were defined. Examination of the Ca²⁺ sensing properties of the RP, RP(E31Q) or chimeric constructs was performed in transfected HEK-293 cells being exposed to 2.5µM ionomycin (Sigma).

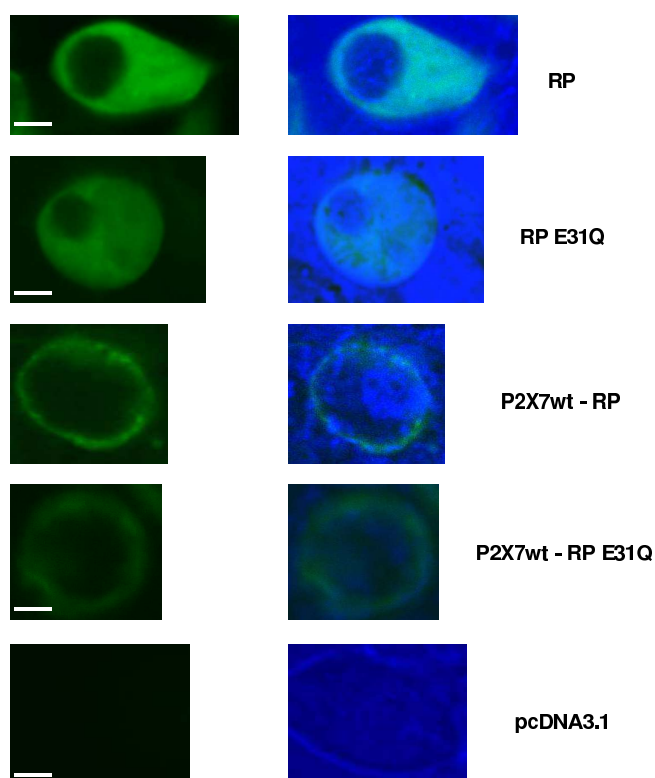


Figure 1. Sub-cellular localisation of tagged and untagged Ca^{2+} sensor constructs expressed in HEK-293 cells.

Images were captured using a laser scanning confocal microscope (488 excitation, >510 emission). Left panel represents the fluorescence images, displayed at identical gain and black level settings. Right panel is the co-registration of the fluorescence image with transmission light image of the same field. Transmission light images reveal the cell outline and presence of organelles. Scale bar = $5\mu m$.

A Ratiometric Pericam (RP)

B Ratiometric Pericam E31Q (RP(E31Q))

C P2X7R-RP

D P2X7R-RP(E31Q)

E pcDNA3.1 vector (control) which shows no fluorescence

Results and Discussion

Development of a near-membrane Ca^{2+} sensor

A fusion between a ratiometric pericam and a membrane targeted protein, the P2X7R was carried out using standard molecular biology techniques. This was revealed by imaging HEK-293 cells transfected with either the tagged (localised) or untagged (unlocalised) pericams and comparing fluorescence distribution patterns. As expected, untagged ratiometric pericams (RP) displayed a bright fluorescence intensity, which was confined to the cytosol but excluded from the nucleus (Figure 1A). Our targeting strategy of fusing the RP to P2X7R was tested

next. P2X7R-GFP is known to localise to the plasma membrane in the HEK expression system¹⁸. P2X7R-RP exhibits an identical expression pattern (Figure 1C) to that of P2X7R-GFP, suggesting that the normal P2X7R trafficking is not disrupted by the addition of RP. The signal sequence on the P2X7R therefore directed the ratiometric pericams exclusively to the plasma membrane. Confirming the locality of the sensors provides us with the potential for exclusively reporting near-membrane Ca^{2+} signals.

Fine-tuning the K_d of ratiometric pericams to measure high Ca^{2+} concentrations

The high affinity of RP makes it unsuitable to accurately measure the large Ca^{2+} flux expected at presynaptic microdomains. Site-directed mutagenesis within the calmodulin portion of the Ca^{2+} sensor, cameleon-1, shifts the fluorescence- Ca^{2+} relationship¹⁹. A single glutamic acid to glutamine mutation (RP(E31Q)) weakens the interaction between Ca^{2+} and its binding loop, decreasing the affinity of the sensor and increasing its dynamic range¹⁹. The mutation was introduced using a standard PCR protocol and it was confirmed by direct sequencing. RP and RP(E31Q) displayed virtually identical emission spectra, with an emission maximum at approximately 515nm, coinciding with the emission peak of the YFP portion of each pericam (Figure 2A). This observation confirms that the E31Q mutation did not alter the spectral characteristics of the protein. The E31Q mutation in RP altered the K_d from $2.1\mu M$ to $19.1\mu M$ effectively improving the dynamic range of $0.25\mu M$ - $19\mu M$ to approximately $2\mu M$ - $170\mu M$ (Figure 2B). RP(E31Q) expressed in HEK cells is uniformly distributed through the cytoplasm, but is excluded from the nucleus (Figure 1B). The P2X7R-RP(E31Q) construct was also generated and displayed an identical expression pattern to P2X7R-RP, limited to the plasma membrane (Figure 1D). The lower fluorescent signal seen with RP(E31Q) is consistent with its lower Ca^{2+} affinity (Figure 1C,D).

Will the sensors be sensitive enough to measure Ca^{2+} microdomains?

In turtle hair cells the Ca^{2+} concentration in Ca^{2+} microdomains was found to be at least $85\mu M$ ⁷. Others have reported microdomain Ca^{2+} concentrations of 100 - $200\mu M$, necessary to produce rapid neurotransmitter secretion⁵. With a dynamic range of $0.25\mu M$ - $19\mu M$ the original RP indicator would be expected to saturate at these high concentrations. However, the RP(E31Q), with a dynamic range of $2\mu M$ - $171\mu M$, is ideally suited to the expected levels of Ca^{2+} concentrations within presynaptic microdomains.

Sensing Ca^{2+} in a mammalian expression system using genetically encoded sensors

HEK-293 cells transfected with each pericam were exposed to the ionophore ionomycin ($2.5\mu M$). Both the

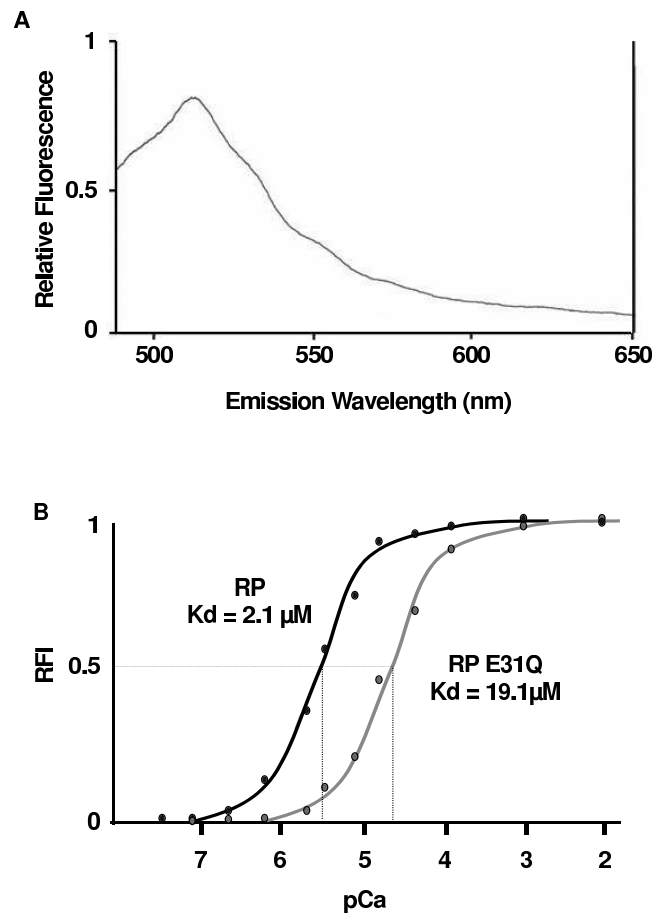


Figure 2. In-vitro properties of ratiometric pericams.

A Fluorescence emission spectrum of ratiometric pericam E31Q (RP(E31Q)). HEK-293 cells transfected with RP(E31Q) were lysed and the liberated cytosolic proteins containing RP(E31Q) were diluted in phosphor-buffered saline (PBS). Emission wavelength scans (490nm-650nm) were obtained using a spectrophotometer. The spectrum was measured at 24°C and pH 7.20, and the results corrected for with a reference solution identical in composition to the sample except for the absence of RP(E31Q). The results were similar to YFP spectra, showing an emission peak at approximately 515nm. A very similar emission spectrum was obtained for RP (results not shown) with a maximum peak at 510nm, indicating the maintenance of YFP spectral properties.

B Dose response curves of ratiometric pericams, showing relative fluorescence intensity (RFI) as a function of pCa ($-\log_{10}[\text{Ca}^{2+}]_{\text{free}}$). The curves were generated by scanning the emission of the indicator (RP or RP(E31Q)) at 515nm. The concentration of free Ca^{2+} ions in solution was varied by cross dilution of Ca^{2+} (“high Ca^{2+} solution”) and EGTA (“low Ca^{2+} solution”) to produce a series of eleven solutions with increasing $[\text{Ca}^{2+}]$ while keeping the concentration of the indicator (RP or RP(E31Q)) constant. The pH was kept at 7.2 during experimentation. The E31Q mutation shifted the dose response curve to the right, reflecting a change in Kd from 2.1 μM for RP to 19.1 μM for RP(E31Q).

P2X7R-RP and P2X7-RP(E31Q) sensors demonstrated an increase in fluorescence intensity in response to application of ionomycin (Figure 3). As expected, P2X7R-RP showed a significantly larger change in fluorescence intensity than the lower affinity sensor, P2X7-RP(E31Q). These experiments demonstrate that the Ca^{2+} sensing abilities of the RP and RP(E31Q) are not altered when fused to the P2X7R and expressed in a mammalian cell line. Further studies are required to demonstrate this in primary neuronal cultures and other neuronal preparations.

Will the sensor only measure Ca^{2+} from presynaptic Ca^{2+} microdomains?

Using simulation studies, Fogelson and colleagues⁹ predicted with a three dimensional model that Ca^{2+} enters the presynaptic terminal through discrete membrane channels and acts to release transmitter within 50nm of the entry point. In turtle hair cells the initial diameter of Ca^{2+} microdomains was found to be less than 1 μm , as estimated by confocal microscopy⁷. Hence, Ca^{2+} microdomains can have very restricted spatial profiles and restricting even a sensor to the membrane may not guarantee localisation within Ca^{2+} microdomains (e.g. in neurons). However, one could still expect much better signal-to-noise ratios with a

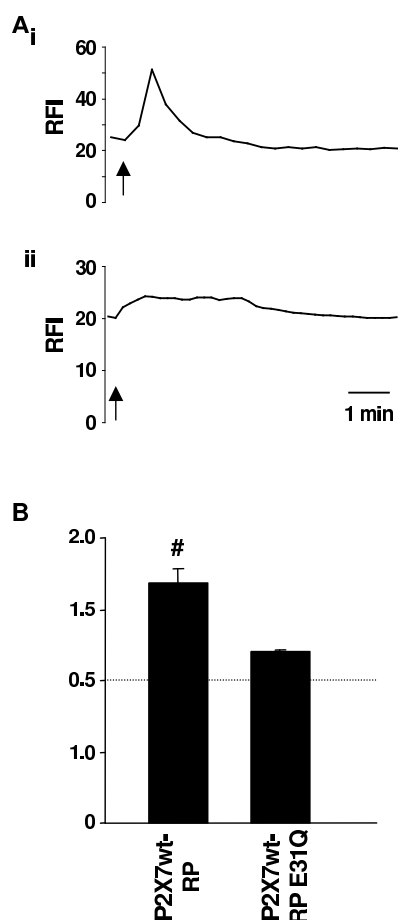


Figure 3. Responses of chimeric Ca^{2+} sensor constructs when expressed in HEK-293 cells to $2.5 \mu\text{M}$ ionomycin.

A Typical responses of HEK-293 cells expressing: (i) P2X7R-RP, (ii) P2X7R-RP(E31Q) upon application of ionomycin ($2.5 \mu\text{M}$) as indicated by the upward arrows below each trace. RFI indicates relative fluorescence intensity. Application of ionomycin caused a transient increase in relative fluorescence intensity in each case, but the response of P2X7R-RP(E31Q) was smaller as compared to the response of P2X7R-RP. All experiments were performed in HEPES solution containing 1mM CaCl_2 . For each trace the horizontal bar indicates 1 minute.

B Collated responses of HEK-293 cells expressing each of the chimeric Ca^{2+} sensor constructs, P2X7R-RP ($n=13$ cells), P2X7R-RP(E31Q) ($n=9$ cells) to $2.5 \mu\text{M}$ ionomycin. F/F_0 indicates peak fluorescence intensity over basal fluorescence intensity. Responses are expressed as mean $F/F_0 \pm \text{s.e.m.}$ # $P < 0.05$ (one-way Anova) significantly different to P2X7R-RP(E31Q).

membrane-delimited sensor as opposed to a generalised cytosolic sensor. Therefore, a localised biosensor responding selectively to Ca^{2+} signals near the presynaptic membrane will provide a valuable tool to more accurately measure these signals. Further experiments will determine how close we can get.

Conclusion and Future Directions

The Ca^{2+} microdomains within presynaptic nerve terminals are highly localised and the concentrations of Ca^{2+} within these regions are thought to be significantly larger than the global cytosolic concentration. By measuring 'volume-averaged' global signals in response to stimuli, important information about these compartmentalised functions remains undetected. In this study biosensors have been designed with characteristics suited to investigating Ca^{2+} microdomains within presynaptic terminals. We generated a fusion protein of a ratiometric pericam (with modified Ca^{2+} -sensing ability) and a P2X7 receptor, a protein known to localise to the presynaptic membrane of excitatory neurons. Fusion proteins successfully trafficked to the plasma membrane distribution of HEK cells and were capable of responding to changes in intracellular Ca^{2+} . Our next goal is to characterise these sensors in a neuronal setting, confirming localisation and Ca^{2+} sensing ability and refining these properties where necessary. Ultimately, we hope to study Ca^{2+} dynamics in brain slices derived from various mouse and rat models of relevant human diseases. The generation of genetically encoded fluorescent biosensors described is expected to continue to expand and provide exciting new insights into normal physiological and pathological processes in neurons.

Acknowledgments

Supported by funding from NHMRC and ARC (Australia). We are grateful for the careful proofreading of Samantha Ferguson.

References:

1. Reid CA, Bekkers JM, Clements JD. N- and P/Q-type Ca^{2+} channels mediate transmitter release with a similar cooperativity at rat hippocampal autapses. *J. Neurosci.* Apr 15 1998;18(8):2849-2855.
2. Augustine GJ. How does calcium trigger neurotransmitter release? *Curr Opin Neurobiol.* Jun 2001;11(3):320-326.
3. Llinas R, Sugimori M, Silver RB. Microdomains of high calcium concentration in a presynaptic terminal. *Science.* May 1 1992;256(5057):677-679.
4. Jarvis SE, Zamponi GW. Interactions between presynaptic Ca^{2+} channels, cytoplasmic messengers and proteins of the synaptic vesicle release complex. *Trends Pharmacol Sci.* Oct 2001;22(10):519-525.
5. Heidelberger R, Heinemann C, Neher E, Matthews G. Calcium dependence of the rate of exocytosis in a synaptic terminal. *Nature.* Oct 6 1994;371(6497):513-515.
6. Sugimori M, Lang EJ, Silver RB, Llinas R. High-resolution measurement of the time course of calcium-concentration microdomains at squid presynaptic terminals. *Biol. Bull.* Dec 1994;187(3):300-303.
7. Tucker T, Fettiplace R. Confocal imaging of calcium

- microdomains and calcium extrusion in turtle hair cells. *Neuron*. Dec 1995;15(6):1323-1335.
8. Zucker RS. Calcium- and activity-dependent synaptic plasticity. *Curr Opin Neurobiol*. Jun 1999;9(3):305-313.
 9. Fogelson AL, Zucker RS. Presynaptic calcium diffusion from various arrays of single channels. Implications for transmitter release and synaptic facilitation. *Biophys. J*. Dec 1985;48(6):1003-1017.
 10. Tsien RY. The green fluorescent protein. *Annu. Rev. Biochem.* 1998;67:509-544.
 11. Gerdes HH, Kaether C. Green fluorescent protein: applications in cell biology. *FEBS Lett*. Jun 24 1996;389(1):44-47.
 12. Nagai T, Sawano A, Park ES, Miyawaki A. Circularly permuted green fluorescent proteins engineered to sense Ca²⁺. *Proc. Natl. Acad. Sci. USA*. Mar 13 2001;98(6):3197-3202.
 13. North RA, Surprenant A. Pharmacology of cloned P2X receptors. *Annu. Rev. Pharmacol. Toxicol.* 2000;40:563-580.
 14. Paukert M, Hidayat S, Grunder S. The P2X(7) receptor from *Xenopus laevis*: formation of a large pore in *Xenopus* oocytes. *FEBS Lett*. Feb 27 2002;513(2-3):253-258.
 15. Rassendren F, Buell GN, Virginio C, Collo G, North RA, Surprenant A. The permeabilizing ATP receptor, P2X7. Cloning and expression of a human cDNA. *J. Biol. Chem.* Feb 28 1997;272(9):5482-5486.
 16. Deuchars SA, Atkinson L, Brooke RE, et al. Neuronal P2X7 receptors are targeted to presynaptic terminals in the central and peripheral nervous systems. *J Neurosci*. Sep 15 2001;21(18):7143-7152.
 17. Atkinson L, Batten TF, Moores TS, Varoqui H, Erickson JD, Deuchars J. Differential co-localisation of the P2X7 receptor subunit with vesicular glutamate transporters VGLUT1 and VGLUT2 in rat CNS. *Neuroscience*. 2004;123(3):761-768.
 18. Smart ML. Molecular Basis of P2X7R Pore Formation (Thesis). The laboratory of Biophysics and Molecular Biology. Department of Physiology, The University of Melbourne. 2002.
 19. Miyawaki A, Llopis J, Heim R, et al. Fluorescent indicators for Ca²⁺ based on green fluorescent proteins and calmodulin. *Nature*. Aug 28 1997;388(6645):882-887.

Author for correspondence:

Prof. David A. Williams
Department of Physiology
The University of Melbourne
Grattan St,
Melbourne, Vic 3010
Australia

Tel: +61 3 8344 5845

Fax: +61 3 8344 5818

Email: davidaw@unimelb.edu.au

Received 8 June 2004, in revised form 30 June 2004.

Accepted 3 July 2004.

©D.A. Williams 2004.

Functional imaging: new views on lens structure and function

Paul J. Donaldson, Angus C. Grey, B. Rachele Merriman-Smith, A.M.G. Sisley,
Christian Soeller, Mark B. Cannell & Marc D. Jacobs

*Department of Physiology, School of Medical Sciences,
The University of Auckland, Auckland, New Zealand*

Summary

1. We have developed an experimental imaging approach that allows the distribution of lens membrane proteins to be mapped with subcellular resolution over large distances, as a function of fibre cell differentiation.

2. Using this approach in the rat lens, we have precisely localised histological sites of Cx46 cleavage, quantitatively mapped changes in gap junction distribution and fibre cell morphology, and correlated these changes to differences in intercellular dye transfer.

3. Profiling of glucose transporter isoform expression showed that lens epithelial cells express GLUT1 while deeper, cortical fibre cells express the higher-affinity GLUT3 isoform. Near the lens periphery, GLUT3 was located in the cytoplasm of fibre cells, but it underwent a differentiation-dependent membrane insertion.

4. Similarly, the putative adhesion protein MP20 is inserted into the fibre cell membranes, at the stage when the cells lose their nuclei. This redistribution is strikingly rapid in terms of fibre cell differentiation and correlates with a barrier to extracellular diffusion.

5. Our imaging-oriented approach has facilitated new insights into the relationships between fibre cell differentiation and lens function. Taken together, our results indicate that a number of strategies are utilised by the lens during the course of normal differentiation, to change the subcellular distribution, gross spatial location and functional properties of key membrane transport proteins.

Introduction

The transparency of the lens is closely linked to the unique structure and function of its fibre cells. These highly differentiated cells are derived from equatorial epithelial cells, which exit the cell cycle and embark upon a differentiation process that produces extensive cellular elongation, the loss of cellular organelles and nuclei and the expression of fibre-specific proteins^{1,2}. Since this process continues throughout life, a gradient of fibre cells at different stages of differentiation is established around an internalised core of mature, anucleate fibre cells. To maintain its structural organization, and hence, its transparency, the lens is believed to have an internal microcirculation system that delivers nutrients, removes waste products, and imposes the negative membrane potential required to maintain the steady-state volume of the

fibre cells³. This system is thought to be generated by spatial differences in ion transport processes that generate a circulating flux of ions which enters the lens via the extracellular clefts between fibre cells, crosses fibre cell membranes, then flows from cell to cell towards the surface of the lens, via an intracellular pathway mediated by gap junction channels. This circulating current creates a net flux of solute that generates fluid flow. The extracellular flow of water conveys nutrients toward the deeper-lying fibre cells, while the intracellular flow removes wastes and creates a well-stirred intracellular compartment.

The experimental evidence in support of this model of lens circulation has primarily been provided by macroscopic measurements of whole-lens electrical properties³. More recently, our laboratory has provided additional evidence in favour of the model by identifying, and localising at the cellular level, key components of the circulation system⁴. This work has involved a number of functional imaging approaches which correlate membrane protein distribution to function in spatially distinct regions of the lens⁵⁻⁸. Here we compare and contrast the results obtained for three diverse types of membrane proteins: cell-to-cell channel proteins (connexins); glucose transporter proteins (GLUTs); and an adhesion protein (MP20). While our initial goal was to provide a molecular inventory of key components of the lens circulation system, our results have revealed that the lens uses a number of different strategies to establish and maintain spatial differences in membrane transport proteins during the course of fibre cell differentiation.

Mapping spatial differences in transport proteins: a question of scale

To investigate these questions we have developed an experimental approach that allows the distribution of lens membrane proteins to be mapped with subcellular resolution over large distances. Since fibre cells continually differentiate from epithelial cells at the lens periphery and are progressively internalised with age, the spatial layout of fibre cells from the lens periphery to the centre also represents a temporal profile of fibre cell differentiation. The technical procedures we have developed⁹ to map membrane protein distributions across this differentiation gradient, utilize high-quality cryosections that are systematically imaged to produce a continuous, high-resolution data set (Figure 1). Such an image data set contains information not only on how the gross spatial distribution of a labeled membrane protein changes as a

function of fibre cell differentiation, but also on the changing subcellular distribution of the protein (Figure 2). This is important because differentiating fibre cells are essentially elongated epithelial cells, which retain distinct apical, basal and lateral membrane domains¹⁰. In these cells the lateral membranes are further divided into broad and narrow sides, which contribute to the distinctive hexagonal profile of the fibre cells. Thus in addition to radial differences in membrane protein distribution which can occur as a consequence of fibre cell differentiation, other changes may be evident in an axial direction (pole-equator-pole) along the length of a fibre cell or between the lateral membrane domains (broad versus narrow side).

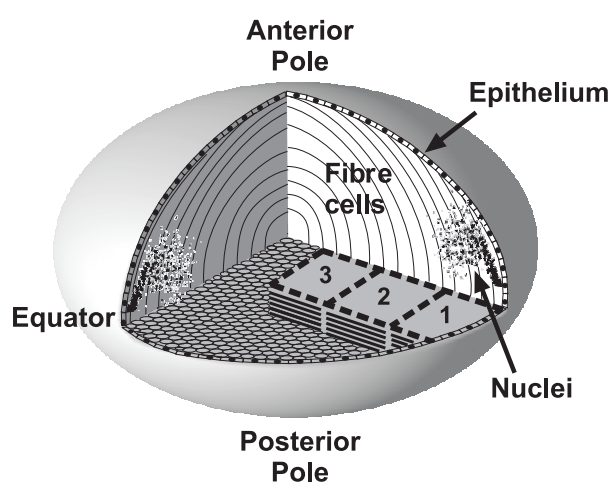


Figure 1. High-resolution long-range imaging in the lens. This diagram illustrates our application of quantitative two-photon, and confocal imaging in the equatorial region of the lens. Overlapping, large image stacks (1-3) can be collected from high-quality cryosections at diffraction-limited resolution, and precisely aligned by correlation analysis⁹ to form a continuous 3D data set spanning a large proportion of the lens radius (see Figure 2). Expression patterns of immunofluorescence-labeled proteins can be examined qualitatively by extracting high-magnification views from exact locations within the data set, or analyzed quantitatively as a function of fibre cell age using custom-written image processing software. Fibre cell nuclei disperse axially (i.e. toward the poles) and degrade as the cells age, providing a convenient differentiation marker when stained with a DNA-binding fluorochrome such as propidium iodide. Nuclear degradation, and protein expression in fibre cell lateral membrane domains, can be precisely localised in equatorial sections showing transverse views of fibre cells. Nuclear dispersal, degradation and longitudinal protein expression patterns, can be localised in axial sections showing the fibre cell lengths.

Fibre cell gap junctions: structure, dispersal and age-dependent processing

Because of their central importance to lens function, the fibre cell gap junctions have been extensively studied¹¹. Gap junctions are formed by the connexin family of proteins¹² and lens fibre cells express two connexin isoforms, Cx46¹³ and Cx50¹⁴. Functional studies indicate that the density of gap junctions is highest near the equator of the lens so as to direct the outward component of the circulating current to the equatorial epithelial cells, which contain the highest density of Na/K pumps¹⁵. Qualitative assessments showed that in the young, equatorial fibre cells, gap junctions are particularly concentrated on the broad sides while in older, inner fibre cells, the gap junctions are more evenly distributed throughout the cell membrane.¹⁶⁻¹⁸ Furthermore, biochemical studies have shown that the cytoplasmic tails of Cx46¹⁹ and Cx50^{20,21} are cleaved in the lens, the latter by the protease calpain²¹, in order to maintain cell coupling at low pH deep in the lens²².

In a more recent study which utilised our high-resolution imaging techniques, we have precisely localised the histological sites of Cx46 cleavage, by quantitative analysis of signal density profiles obtained from antibodies directed against the cytoplasmic loop and tail of Cx46⁸. Our analysis revealed that Cx46 cleavage occurs at two distinct stages during fibre cell differentiation (Figure 3A). The major stage occurs at a normalized radial distance (r/a) ~ 0.9 in 3-week-old lenses, and coincides with an axial dispersal of fibre cell nuclei; the second stage occurs at $r/a \sim 0.7$ and is associated with the complete loss of fibre cell nuclei.

In addition to Cx46 cleavage, we have quantitatively mapped the changing gap junction distributions (Figure 2A-C) as a function of fibre cell differentiation. Radial changes in cell shape and gap junction plaque size and distribution were measured automatically by quantitative morphometric analysis of our image data⁸. A fibre cell 'ellipticity index' was found to increase smoothly from the lens periphery inward, reflecting a gradual change from the hexagonal peripheral cell cross-section to a more circular cross-section. We also quantified a rapid peripheral decrease in the size of broad side plaques which is followed by an apparent fragmentation and dispersal of the plaques around the cell perimeter. These precise radial measurements of fibre cell changes show that the sudden gap junction cleavage and shrinkage events do not correspond to sudden changes in cellular morphology. However, the loss of the hexagonal cell profile is closely associated with gap junction plaque dispersal, and both follow the major stage of Cx46 cleavage, suggesting a possible role for cleavage in gap junction and cell remodeling⁸.

To investigate the functional consequences of these changes, we performed two-photon flash photolysis (TPFP) on lenses loaded with CMNB-caged fluorescein and assessed regional gap junction coupling patterns⁸. By applying TFPF inside a single fibre cell, a microscopic source of uncaged fluorescein was created and its diffusion to neighbouring cells was monitored by simultaneous

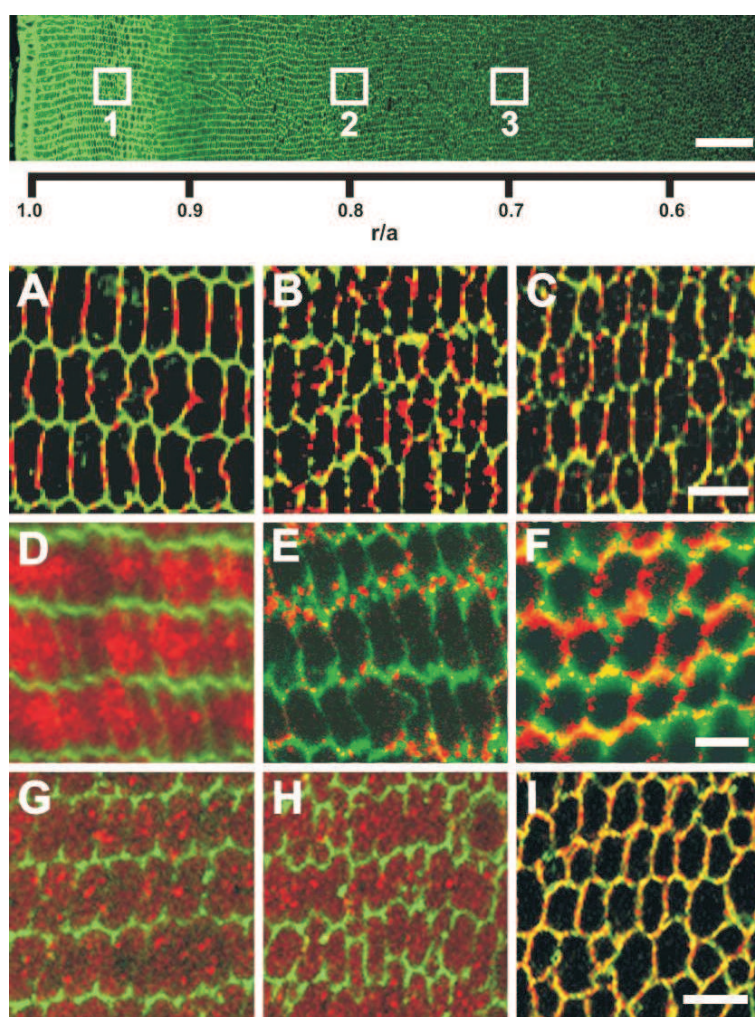


Figure 2. Differentiation-dependent changes in the subcellular distribution of 3 diverse lens proteins.

Top: Four 1024 x 1024 image stacks were assembled as described (Figure 1) to form a continuous, high-resolution immunofluorescence data set extending over half the rat lens radius. The image shows cell membranes labeled with wheat germ agglutinin conjugated to AlexaFluor 350. High-magnification images of the proteins (A-I) were extracted from the approximate locations designated with white boxes to view changes in their distribution as a function of fibre cell age.

A-C: The gap junction protein Cx46 forms large plaques on the broad sides of fibre cells near the lens periphery, with small punctate plaques on the narrow sides (A). As fibre cells age they become rounder, the large plaques become smaller (B), and they fragment and disperse around the cell membrane by the time they reach $r/a \sim 0.7$ (C).

D-F: The GLUT3 glucose transporter protein labels the cytoplasm of peripheral fibre cells (D) but this signal re-locates predominantly to the narrow sides of the cells by $r/a \sim 0.8$ (E); later, at $r/a \sim 0.7$, GLUT3 signal is widely distributed around the rounded fibre cell membranes.

G-I: The membrane protein MP20 is distributed in a granular pattern resembling cytoplasmic vesicles, from the lens periphery to $r/a \sim 0.7$ (G, H), where it is rapidly targeted to the plasma membrane (I). Scale bars: Top, 50 μm ; A-C, D-F and G-I, 5 μm .

confocal microscopy. These experiments revealed different patterns of cell-cell coupling at different radial locations. In peripheral fibre cells, where large broad side plaques predominate, dye diffusion occurred primarily in a radial direction (Figure 3B). In contrast, at locations beyond the zone of nuclear loss, where plaques were distributed more evenly around the fibre cell membrane, the pattern of fluorescein diffusion was approximately isotropic (Figure 3C). Thus the local pattern of intercellular coupling changed from a radial direction in the lens periphery to a

more uniform pattern in the deeper fibre cells, consistent with the differentiation-dependent remodeling of gap junction plaques. It appears, then, that the structure of gap junctions is modified by precise connexin processing and plaque remodeling, which create functional specializations in sub-regions of the organ and allow the maintenance of lens circulation, homeostasis and transparency.

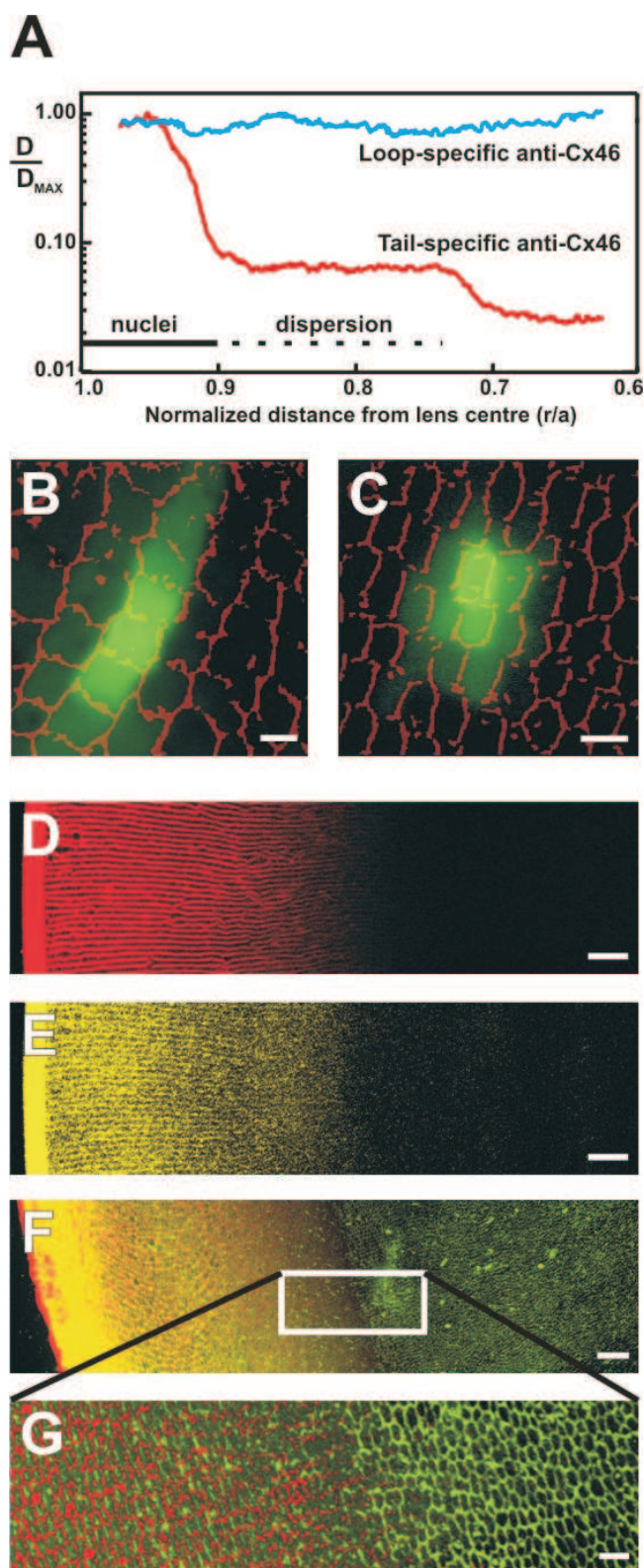


Figure 3. Novel insights gained from an image-based approach to lens function.

A: Precise in situ localization of two cleavage zones of Cx46, in relation to fibre cell differentiation markers. Two antibodies, specific to the cytoplasmic loop or the carboxy terminus ‘tail’ of Cx46, were used to label rat lens sections by immunofluorescence. Fluorescence signal density was imaged and quantified using a two-photon microscope and custom-written software. The density of membrane signal from the Cx46 tail antibody declined rapidly in two discrete zones located at $r/a \sim 0.9$ and ~ 0.7 , while the Cx46 loop antibody signal remained relatively constant, indicating cleavage of the carboxy tail in the two zones, with retention of the rest of the protein in the membrane. The solid and dotted horizontal lines designate the locations of axially clustered or dispersed fibre cell nuclei, respectively, preceding complete nuclear degradation.

B, C: Position-dependent patterns of local cell-cell coupling in the rat lens revealed by dye transfer. Two-photon flash photolysis was used to optically release caged fluorescein within individual fibre cells. Simultaneous confocal imaging of the time course of dye diffusion revealed that cell coupling was predominantly in a radial direction at the lens periphery (B) but was more isotropic deep in the lens ($r/a < 0.7$; C). These patterns correlate with the subcellular distributions of gap junction channels in the respective areas.

D, E: Restricted dye diffusion into the lens. Cultured rat lenses were incubated for 4 hours in Texas Red-dextran (D) or Lucifer yellow (E), then fixed, sectioned and imaged. Both dyes penetrated the lens via the extracellular space to a depth of only $\sim 400 \mu\text{m}$, corresponding to the zone of nuclear degradation.

F, G: Antibodies to MP20 were applied to lens sections following dye treatment as in (D) for 18 hours. Immunofluorescent imaging of the sections showed that localization of MP20 to the cell membranes occurs at a depth corresponding to the limit of extracellular dye diffusion (F: red, Texas Red-dextran; green, MP20; G: high-magnification view), suggesting a possible role for MP20 in this ‘diffusion barrier’. Scale bars: B, C, $5 \mu\text{m}$; D-F, $50 \mu\text{m}$; G, $10 \mu\text{m}$.

Glucose transporters: differential expression and membrane insertion

Glucose is the principal fuel used by the lens to support growth and homeostasis²³. In the lens, epithelial

and differentiating fibre cells are capable of oxidative phosphorylation, while the mature fibre cells, having lost their mitochondria, must rely solely on glycolysis for energy production². The lens is bathed by the aqueous humor, which contains glucose levels that mirror those in

the plasma. Hence, lens cells near the periphery have access to an abundant supply of glucose, while the supply of glucose to the deeper-lying fibre cells is likely to be limited by a decreasing glucose gradient. However, the circulating current is thought to create a net flux of solutes that generates an extracellular fluid flow^{4,17}, which in turn conveys nutrients toward the deeper-lying fibre cells by advection. Thus, from the model one might predict that both the peripheral and deeper-lying cells would be exposed to external glucose, though at different concentrations, and might express glucose transporters. To address this issue we performed a molecular profiling of GLUT isoform expression in the rat lens²⁴. We found that epithelial cells express GLUT1 while cortical fibre cells express the higher-affinity GLUT3 isoform. This differential expression pattern is consistent with the probable glucose environments these cells are exposed to. In epithelial cells, the expression of GLUT1 appears to determine that the K_m of the glucose transporter is appropriate for the glucose concentration in the aqueous humor. In cortical fibre cells, the lower K_m of GLUT3 is likely to be more appropriate for extracting glucose from the extracellular fluid, which at this distance into the lens should have a relatively low glucose concentration.

Subsequent analysis of GLUT3 expression using our high-resolution image mapping approach revealed an intriguing pattern. Near the lens periphery, GLUT3 was located in the cytoplasm of fibre cells (Figure 2D); but with increasing depth into the lens, GLUT3 labeling became associated with the membrane, suggesting that GLUT3 undergoes a differentiation-dependent membrane insertion⁵. Interestingly, this membrane insertion of GLUT3 was initially targeted to the narrow sides of fibre cell membranes (Figure 2E). Then at a later stage of fibre cell differentiation, GLUT3 became more uniformly dispersed around the entire cell membrane (Figure 2F). The dispersal of GLUT3 from the narrow sides to the rest of the membrane appears to coincide with dispersal of the gap junction plaques which are initially located on the broad sides of fibre cells (Figure 2A-C). This observation reinforces our impression that the distinct sub-domains of fibre cell lateral membranes are lost during the course of differentiation. Our findings also suggest that GLUT3 is initially produced in the younger, peripheral fibre cells (which are capable of protein synthesis) and can be stored in the cytoplasm until a differentiation-dependent signal triggers its insertion into the membrane.

Fibre cell adhesion: MP20 membrane insertion and extracellular diffusion

Membrane insertion would appear to be a common phenomenon in the lens. High-resolution mapping of the distribution of the second most abundant lens membrane protein, MP20, revealed that like GLUT3 it undergoes a differentiation-dependent membrane insertion. Despite its relative abundance, the function of MP20 in the lens is still not definitively known. MP20 has been implicated as a component of membrane junctions between lens fibre

cells^{19,25}, and more recently it was shown that MP20 acts as a ligand for galectin-3²⁶, a known modulator of cell-cell adhesion in other tissues²⁷. These results are consistent with a role for MP20 in cell-cell adhesion, however, the precise role of MP20 in lens structure, and its impact on lens function, have yet to be determined.

Using image-based immunofluorescent mapping, we assessed the relative distributions of MP20 and another abundant membrane protein, the water channel AQP0, as a function of fibre cell differentiation. We found that MP20, but not AQP0, is inserted into the fibre cell membranes at the stage when the cells lose their nuclei⁶. We showed that while MP20 labeling is intracellular in the younger fibre cells of the cortex, it redistributes to the plasma membranes as the cells mature (Figure 2G-I). Furthermore, the redistribution from the cytoplasm to the plasma membrane is relatively rapid and occurs over a small number of cell layers. If MP20 is indeed an adhesion molecule then the insertion of MP20 into the membranes of mature fibre cells might be expected to increase adhesion between the cells. This suggested to us the possibility that upon insertion of MP20, the extracellular space might become effectively smaller or more tortuous, restricting extracellular diffusion of molecules deeper into the lens. To test this hypothesis, we organ-cultured lenses in the presence of two fluorescent extracellular space markers, Texas Red-dextran (MW 10 kDa) and Lucifer yellow (MW 456 Da), for varying times. Regardless of the incubation period (2 to 18 hours), Texas Red-dextran diffusion into the lens only occurred up to a distance of some 400 μm in from the capsule (Figure 3D). This consistency in the depth of tracer penetration observed at all time points indicated that the Texas Red-dextran movement via the extracellular space was not diffusion-limited, but restricted by a physical barrier. In support of this, the extracellular diffusion of the smaller molecular weight dye, Lucifer yellow, also became restricted at around the same depth (Figure 3E). This indicates that the barrier to extracellular diffusion has a molecular weight cut-off of at most ~ 450 Da. Subsequent immunolabelling with MP20 antibodies of sections derived from a lens incubated in Texas Red-dextran for 18 hours indicated that the barrier to extracellular diffusion coincides with the zone where MP20 is inserted into the membrane (Figure 3F, G). Thus the insertion of MP20 correlates with the formation of a diffusion barrier that restricts the further extracellular movement of tracer dye molecules into the lens core. These results are consistent with the view that membrane insertion of MP20 contributes to the establishment of interactions between adjacent fibre cells, which act in the lens to limit the movement of molecules via the extracellular space.

Conclusions and future challenges

Our adoption of a functional imaging approach to investigate key components of the lens microcirculation system has reaped unforeseen insights into lens biology. It appears that the lens adopts a number of strategies to compensate for the inability of its older anucleate fibre cells to synthesise new membrane proteins. These strategies

involve the processing, redistribution and differential targeting of proteins as fibre cells age. The gap junction proteins Cx46 and Cx50 undergo specific, differentiation-dependent post-translational modifications that remove their cytoplasmic tails: events which cause a loss of junctional pH sensitivity and which bracket (temporally and spatially) a dramatic redistribution of gap junction plaques. This redistribution correlates with a major redirection of the local cell-cell coupling which underpins the lens microcirculation system. In a similar vein, the differentiation-dependent expression of glucose transporters, which targets the GLUT1 isoform to epithelial cells and the GLUT3 isoform to cortical cells, appears to match transporter affinity with local glucose availability. In order to achieve this, GLUT3 undergoes insertion into fibre cell narrow side membranes, apparently from a pre-designated cytoplasmic pool. Like GLUT3, MP20 also undergoes a membrane insertion event, but at a later stage of fibre cell differentiation, suggesting that the signals responsible for the insertion of these two membrane proteins are different. Insertion of MP20 correlates with the formation of an extracellular diffusion barrier. Taken together, our results show that as fibre cells mature and their ability to synthesise new membrane proteins is lost, the lens deploys a panoply of post-translational processing and targeting mechanisms to enable fibre cells to meet the physiological challenges associated with being buried ever deeper in the lens mass.

Since the lens is continually adding new fibre cells at its equator, it is interesting to speculate that establishing and maintaining spatial differences in membrane transport proteins is an integral part of the fibre cell differentiation programme. Having developed image-based methods to precisely map, with high resolution, spatial changes in membrane protein distribution, the next challenge is to identify the differentiation signals that trigger the very precise changes we have observed. If this is achieved, the lens will not only be an excellent model system in which to study generic aspects of cell differentiation but could also become a unique system in which to study how differentiation processes modulate overall tissue function.

Acknowledgements

Research work in the authors' laboratories was supported by: the Health Research Council of New Zealand, the Marsden Fund (NZ), the Wellcome Trust (UK), the Lotteries Grant Board (NZ), the University of Auckland Research Committee and the Auckland Medical Research Foundation.

References

- Menko AS. Lens epithelial cell differentiation. *Exp. Eye Res.* 2002; 75: 485-490.
- Bassnett S. Lens organelle degradation. *Exp. Eye Res.* 2002; 74: 1-6.
- Mathias RT, Rae JL, Baldo GJ. Physiological properties of the normal lens. *Phys. Rev.* 1997; 77: 21-50.
- Donaldson P, Kistler J, Mathias RT. Molecular solutions to mammalian lens transparency. *News Phys. Sci.* 2001; 16: 118-123.
- Merriman-Smith BR, Krushinsky A, Kistler J, Donaldson PJ. Expression patterns for glucose transporters GLUT1 and GLUT3 in the normal rat lens and in models of diabetic cataract. *Invest. Ophthalmol. Vis. Sci.* 2003; 44: 3458-3466.
- Grey AC, Jacobs MD, Gonen T, Kistler J, Donaldson PJ. Insertion of MP20 into lens fibre cell plasma membranes correlates with the formation of an extracellular diffusion barrier. *Exp. Eye Res.* 2003; 77: 567-574.
- Young MA, Tunstall MJ, Kistler J, Donaldson PJ. Blocking chloride channels in the rat lens: Localized changes in tissue hydration support the existence of a circulating chloride flux. *Invest. Ophthalmol. Vis. Sci.* 2000; 41: 3049-3055.
- Jacobs MD, Soeller C, Sisley AMG, Cannell MB, Donaldson P. Gap junction processing and redistribution revealed by quantitative optical measurements of connexin46 epitopes in the lens. *Invest. Ophthalmol. Vis. Sci.* 2004; 45: 191-199.
- Jacobs MD, Donaldson PJ, Cannell MB, Soeller C. Resolving morphology and antibody labeling over large distances in tissue sections. *Microsc. Res. Tech.* 2003; 62: 83-91.
- Bassnett S, Missey H, Vucemilo I. Molecular architecture of the lens fiber cell basal membrane complex. *J. Cell Sci.* 1999; 112: 2155-2165.
- Goodenough DA. The crystalline lens. A system networked by gap junctional intercellular communication. *Semin. Cell Biol.* 1992; 3: 49-58.
- Willecke K, Eiberger J, Degen J et al. Structural and functional diversity of connexin genes in the mouse and human genome. *J. Biol. Chem.* 2002; 277: 725-737.
- Paul DL, Ebihara L, Takemoto LJ, Swenson KI, Goodenough DA. Connexin46, a novel lens gap junction protein, induces voltage-gated currents in nonjunctional plasma membrane of *Xenopus* oocytes. *J. Cell Biol.* 1991; 115: 1077-1089.
- White TW, Bruzzone R, Goodenough DA, Paul DL. Mouse Cx50, a functional member of the connexin family of gap junction proteins, is the lens fiber protein, MP70. *Mol. Biol. Cell* 1992; 3: 711-720.
- Gao J, Sun X, Yatsula V, Wymore RS, Mathias RT. Isoform specific function and distribution of Na/K pumps in the frog lens epithelium. *J. Membr. Biol.* 2000; 178: 89-101.
- Gruijters WTM, Kistler J, Bullivant S. Formation, distribution and dissociation of intercellular junctions in the lens. *J. Cell. Sci.* 1987; 88: 351-359.
- Baldo GJ, Mathias RT. Spatial variations in membrane properties in the intact rat lens. *Biophys. J.* 1992; 63: 518-29.
- Gong XH, Baldo GJ, Kumar NM, Gilula NB, Mathias RT. Gap junctional coupling in lenses lacking alpha(3) connexin. *Proc. Nat. Acad. Sci.* 1998; 95: 15303-15308.

19. Tenbroek E, Arneson M, Jarvis L, Louis C. The distribution of the fiber cell intrinsic membrane proteins MP20 and connexin46 in the bovine lens. *J. Cell Sci.* 1992; 103: 245-57.
20. Kistler J, Bullivant S. Protein processing in lens intercellular junctions: cleavage of MP70 to MP38. *Invest. Ophthalmol. Vis. Sci.* 1987; 28: 1687-1692.
21. Lin JS, Fitzgerald S, Dong YM, Knight C, Donaldson P, Kistler J. Processing of the gap junction protein connexin50 in the ocular lens is accomplished by calpain. *Eur. J. Cell Biol.* 1997; 73: 141-149.
22. Lin JS, Eckert R, Kistler J, Donaldson P. Spatial differences in gap junction gating in the lens are a consequence of connexin cleavage. *Eur. J. Cell Biol.* 1998; 76: 246-250.
23. Berman ER. *Biochemistry of the Eye*. New York: Plenum Press, 1991.
24. Merriman-Smith R, Donaldson P, Kistler J. Differential expression of facilitative glucose transporters GLUT1 and GLUT3 in the lens. *Invest. Ophthalmol. Vis. Sci.* 1999; 40: 3224-3230.
25. Arneson ML, Louis CF. Structural Arrangement Of Lens Fiber Cell Plasma Membrane Protein Mp20. *Exp. Eye Res.* 1998; 66: 495-509.
26. Gonen T, Grey AC, Jacobs MD, Donaldson PJ, Kistler J. MP20, the second most abundant lens membrane protein and member of the tetraspanin superfamily, joins the list of ligands of galectin-3. *BMC Cell Biol.* 2001;17.
27. Perillo NL, Marcus ME, Baum LG. Galectins: versatile modulators of cell adhesion, cell proliferation, and cell death. *J. Mol. Med.* 1998; 76: 402-412.

Received 22 June 2004, in revised form 23 July 2004.

Accepted 24 July 2004.

©P.J. Donaldson 2004.

Author for correspondence:

Paul Donaldson

Department of Physiology

School of Medical Sciences

University of Auckland

Private Bag 92019

Auckland, New Zealand

Phone: +64 9 3737599

Fax: +64 9 3737499

E-mail: p.donaldson@auckland.ac.nz

Quantitative phase microscopy – a new tool for investigating the structure and function of unstained live cells

Claire L. Curl, Catherine J. Bellair*, Peter J. Harris, Brendan E. Allman†,
Ann Roberts*, Keith A. Nugent* & Lea M.D. Delbridge

*Department of Physiology and *School of Physics, University of Melbourne, Victoria 3010, Australia
and*

†Imaging Division, IATIA Ltd., 2/935 Station St, Box Hill Nth, Victoria 3129, Australia

Summary

1. The optical transparency of unstained live cell specimens limits the extent to which information can be recovered from bright field microscopic images as these specimens generally lack visible, amplitude modulating components. However, visualization of the phase modulation which occurs when light traverses these specimens can provide additional information.

2. Optical phase microscopy, and derivatives of this technique such as Differential Interference Contrast (DIC) and Hoffman Modulation Contrast (HMC) have been widely used in the study of cellular materials. With these techniques enhanced contrast is achieved, which is useful in viewing specimens, but does not allow quantitative information to be extracted from the phase content available in the images.

3. An innovative computational approach to phase microscopy, which provides mathematically derived information about specimen phase modulating characteristics, has recently been described. Known as Quantitative Phase Microscopy (QPM), this method derives quantitative phase measurements from images captured using a bright-field microscope without phase or interference contrast optics.

4. The phase map generated from the bright field images by the QPM method can be used to emulate other contrast image modes (including DIC and HMC) for qualitative viewing. QPM achieves improved discrimination of cellular detail, which permits more rigorous image analysis procedures to be undertaken when compared with conventional optical methods.

5. The phase map contains information about cell thickness and refractive index and can allow quantitation of cellular morphology under experimental conditions. As an example, the proliferative properties of smooth muscle cells have been evaluated using QPM to track growth and confluency of cell cultures. QPM has also been used to investigate erythrocyte cell volume and morphology in different osmotic environments.

6. QPM is a valuable new non-destructive, non-interventional experimental tool for structural and functional cellular investigations.

Introduction

One of the major difficulties in visualizing and imaging cellular material is the lack of contrast inherent in

these translucent specimens. With fixed specimens contrast may be created using staining techniques, but for work with live cells this is usually not possible. To facilitate the visualization of viable cellular specimens, a number of different forms of phase microscopy have been devised where contrast is enhanced by manipulation of the optical path. In this review the principles underlying these methods of optical phase microscopy and the limitations associated with their implementation are discussed. A recently developed new form of phase microscopy, Quantitative Phase Microscopy (QPM), is described. The utility of QPM, which incorporates qualitative aspects of established phase techniques and also offers the capacity to undertake quantitative structural analysis, is evaluated. Finally some applications of the QPM methodology are briefly presented.

Light Propagation and Phase Properties of Cellular Material

When light waves traverse a stained sample some light is absorbed by the localised pigment. Thus the amplitude of the light waves emergent from specific regions of the specimen are altered relative to the background or medium.¹ This modulation allows visualisation by the human eye, and sensitivity to differences in amplitude are perceived as variation in brightness and colour. When light traverses an unstained sample there is little change in the amplitude of the light since the unpigmented sample does not have substantial absorption properties in the visible wavelengths usually employed for microscopy. A lack of amplitude modulating structure renders the sample translucent and morphology difficult to discern. However, light propagated through a translucent sample is altered so that the phase is displaced with respect to the light which has passed through the surrounding medium only. Such a displacement is termed phase retardation or phase shift.²

The 'phase shift effect' produced by a sample simply reflects the extent to which light wave propagation is slowed down by passage through the sample. Waves passing through a thick sample will be slowed to a greater degree than those passing through a thin sample. This effect is illustrated in Figure 1. Incident light waves are initially 'in phase', and as sample regions of different thickness and different composition (relative to the medium) influence the passage of the light, a variable degree of phase retardation is induced. The extent to which the emergent light waves are 'out of phase' with each other is termed the relative

phase shift and is measured in radians.^{2,3} Unlike amplitude variations, differences in phase cannot be perceived by the eye or by photographic film.

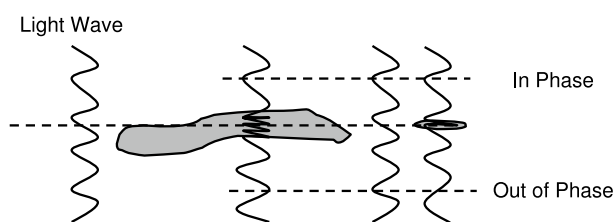


Figure 1. Schematic representation of the phase retardation of light as it passes through a sample.

Light waves are 'in phase' before passing through the specimen, but are 'out of phase' emerging from cell regions of non-uniform thickness due to the effects of phase retardation.

Optical Phase Microscopy

The optical phase microscope was developed to allow visualisation of the phase properties of unstained cellular material and works by converting phase properties to amplitude differences that can be detected by eye. Different forms of optical phase microscopy utilise various optical devices that change the way light is refracted and reflected and these have served for many years as useful tools for qualitative examination of unstained live cells. An overview of the major types of phase microscopy is provided below, and the advantages and disadvantages of each are briefly considered.

Zernike Phase Microscopy

The 'standard' (Zernike) phase microscope, invented in the 1930's by the Dutch physicist Fritz Zernike,⁴ uses a phase plate to alter the passage of light passing directly through a sample by a specified wavelength fraction. This method results in destructive interference of light and allows details of the normally transparent cellular specimen to appear relatively dark against a light background. That is, the phase differences are converted into amplitude differences and observed as intensity contrast. The extent of phase shift induced is determined by a combination of the refractive index and thickness of a specimen at any point.⁵ By this means, structures of unstained living cells, not evident using bright field microscopy, can be visualised using optical phase microscopy. A major disadvantage of Zernike phase microscopy is the appearance of light halos at the edges of specimen components where the phase shift gradient is most steep, resulting in poor boundary localisation. These boundary halo effects are particularly problematic if quantification of cell size and/or structure is required.^{1,6-8}

Differential Interference Contrast (DIC)

Differential interference contrast microscopy was invented in the 1950's by the French optics theoretician, George Nomarski.⁹ DIC is based on modification of the Wollaston prism which is used for detecting optical gradients in specimens and converting them into intensity differences.² The equipment needed for DIC microscopy includes a polarizer, a beam-splitting modified Wollaston prism below the condenser, another prism above the objective, and an analyzer above the upper prism.¹⁰ The prisms allow for splitting of the incident light in the optical path before reaching the specimen and re-combination of the split beams beyond the specimen. As a result the paths of the parallel beams are of unequal length and when re-combined allow differences in intensity to be discerned.¹¹ Under DIC conditions one side of the specimen appears bright while the other side appears dark, conferring a three-dimensional 'shadow relief' appearance.⁸ An aesthetic colour effect may also be achieved with DIC when there is a further phase shift produced by a wave plate inserted in the light path. A major advantage of DIC is that it makes full use of the numerical aperture of the system and permits focus in a thin plane section of a thick specimen, with reduced contributions from specimen regions above or below the plane of focus. Thus DIC provides superior resolution to Zernike phase contrast microscopy¹⁰ and when coupled with other equipment allows optical sectioning.¹² DIC has the additional advantage that the 'halo' edge effects produced by standard phase microscopy are largely absent.¹⁰ Unfortunately DIC is expensive to set up due to the cost of the accessory optical components, requires significant increases in incident light levels and is not conducive to imaging with plastic culture dishes (which mix the phase retardation effects with birefringence). Implementation of DIC can also be physically restrictive, as the condenser position over the stage of an inverted microscope can obstruct access for placement of experimental tools (ie recording electrodes, solution spritzers).

Hoffman Modulation Contrast (HMC)

Hoffman Modulation Contrast, invented by Robert Hoffman in 1975,^{13,14} is similar to DIC, but works by the conversion of optical gradients into variations in light intensity.^{15,8} The components of the HMC system comprise an amplitude spatial filter (the 'modulator') placed at the back focal plane of an objective, and an off-centre slit partially covered by a polarizer located at the front plane of the condenser. Hoffman images have a three-dimensional appearance arising from the directional effect of the optical gradients. Like DIC, a major advantage of HMC is that fuller use of the numerical aperture results in excellent resolution of detail together with good specimen contrast and visibility. HMC can be used for imaging through plastic culture ware, and it is for this application that the technique is most widely utilised. Although the Hoffman 'view' takes on a three-dimensional appearance, localisation of image detail at a particular depth within the sample is relatively

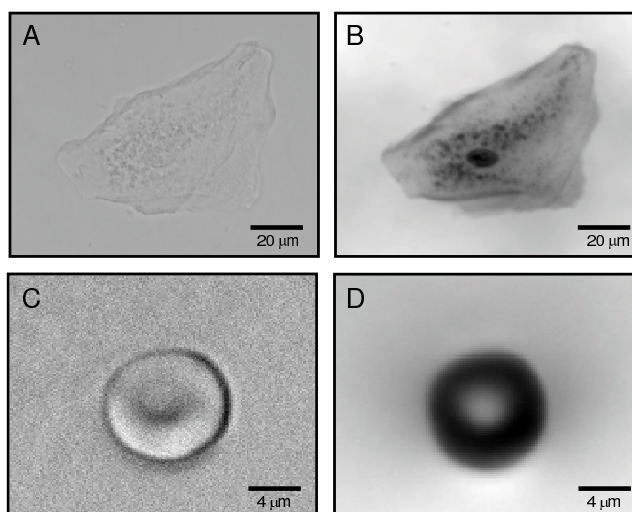


Figure 2. Example of the ability of QPM to highlight cellular morphology by creating of phase maps.

All bright field images presented in Figures were acquired using a black and white 1300 × 1030 pixel Coolsnap FX CCD camera (Roper Scientific) mounted on a Zeiss Axiovert 100M inverted microscope. The defocus images were obtained using a piezoelectric positioning device (PiFoc, Physik Instrumente, Karlsruhe, Germany) for objective translation. Bright field images were processed to generate phase maps using QPm software (v2.0 IATIA Ltd, Australia).

A: Bright field image of human buccal epithelial cell (Achromplan, ×40, NA 0.60).

B: Phase map of cell shown in A, showing prominent phase-dense (darker) nucleus.

C: Bright field image of mouse erythrocyte (Achromplan, ×63, NA 0.80).

D: Phase map of erythrocyte shown in C, with biconcavity depicted as a darkened annulus of increased phase.

imprecise¹ and this can make spatial navigation through a specimen visually difficult. As with DIC, HMC also involves a number of ancillary optical components and is relatively expensive to implement.

Quantitative Phase Microscopy

It is important to emphasise that the optical microscopy techniques discussed above, whilst very useful in many different observational and imaging situations, generally only provide qualitative information about cellular morphology.⁷ An innovative computational approach to phase microscopy, which provides mathematically derived information about specimen phase modulating characteristics, has recently been described.^{16,17} Known as Quantitative Phase Microscopy (QPM), this method combines the useful qualitative attributes of previous phase imaging approaches with the additional advantage of quantitative representation of specimen phase parameters. With QPM, a phase-based analysis of cell structure, morphology and composition is possible using a relatively simple wide field microscope. In optical phase microscopy the amplitude and phase image components are inextricably embedded in the image generated, whereas with QPM it is possible to separate these specimen qualities in the images produced.

The implementation of QPM involves the calculation of a 'phase map' from a triplicate set of images captured under standard bright field microscopy.⁵ A computational algorithm is applied to the analysis of an in-focus image and a pair of equidistant positive and negative de-focus

images. The mathematical processes involved have been described in detail elsewhere, but essentially the procedure entails calculation of the rate of change of light intensity between the three images in order to determine the phase shift induced by the specimen.⁵ The de-focus images may be obtained either by positioning a mirror at specified points in the optical path or by translating the objective to positions above and below the designated plane of focus. Both the image acquisition and the computational processes for QPM can be directed by commercially available hardware and software (QPm software, IATIA Ltd, Box Hill Nth, Australia).

Using QPM for Qualitative Evaluation of Cell Morphology

QPM is particularly valuable for examining cellular morphology, especially when visualising phase dense components of cellular structures such as the nucleus, organelles or intracellular inclusions. Figure 2A shows an example of a typical bright field image of a buccal epithelial cell, from which little evidence of detailed intracellular structure can be gleaned. When a phase map is generated from bright field images using QPM methods (Figure 2B), the phase information within the cell becomes apparent with visualisation of the intracellular organelles, including the very obvious phase dense (dark) nucleus. As a further example, Figure 2C shows a bright field image of an erythrocyte exhibiting a characteristic biconcave disk-like shape. The calculation of the phase map using QPM (Figure 2D) allows more detailed representation of the cell

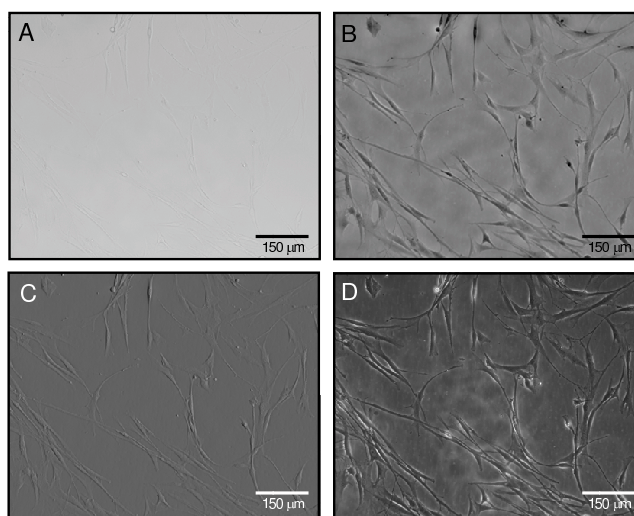


Figure 3. Illustration of the different simulated imaging modalities generated using QPM applied to smooth muscle cells in culture (Achromplan $\times 10$, NA 0.30).

A: Bright field image of human airway smooth muscle cells.

B: Phase map produced using bright field image in Panel A.

C: Differential Interference Contrast (DIC) image calculated from phase map.

D: Hoffman Modulation Contrast (HMC) image calculated from phase map.

geometry, with the biconcavity appearing as a well defined annulus of increased cell 'phase' thickness.

The phase information which is extracted from wide field cell imaging by QPM analysis may also be utilized to simulate optical phase and to reproduce different imaging modalities. For example in Figure 3A, a bright field image of a smooth muscle cell culture is shown, notable for the lack of contrast and definition. In Figure 3B the phase map calculated from the triplicate set of bright field images of the same cell field exhibits considerably enhanced contrast and cellular delineation. Based on the information within the phase map, mathematical procedures can be applied to allow calculation and creation of images usually associated with optical imaging modalities such as DIC (Figure 3C), Hoffman Modulation Contrast (Figure 3D), Zernike Phase Contrast and Dark Field. This is a useful and efficient extension of the QPM analysis approach, as these different image modes are all derived from the same initial bright field image set without any specialized optical equipment. Compared with other techniques, QPM is optically and practically simple, requiring only a bright field microscope and a CCD camera to generate a range of imaging modalities. An additional convenience is that with QPM, the bright field imaging conditions do not require that a condenser be positioned close above the inverted microscope stage, and this allows for improved access of other equipment such as electrodes and pipettes.

Using QPM for Quantitative Assessment of Cellular Morphology

The use of QPM for quantitative assessment of cell attributes has considerable potential, and a number of such

applications have already been developed.^{18,19} These include the tracking of culture confluency and growth²⁰ to investigate cell proliferative properties, and the development of cell volume measurement techniques²¹ to evaluate variations in erythrocyte morphology.

Tracking Cell Culture Confluency and Growth

The relatively high degree of contrast which is achieved in phase maps generated by QPM analysis make these images especially amenable to segmentation and thresholding manipulations. This feature of QPM has been exploited to develop new tools for the quantitative evaluation of cell growth in culture, using repeated imaging of cultures to assess the progression towards confluency over designated periods of time.²⁰ It is important to appreciate that methodologies previously established for the measurement of cell growth in culture are either destructive or extremely laborious. These include cell size measurement with fluorescence activated cell sorting (FACS, which requires removal of cells from their substrate by trypsinization), cell protein synthesis estimation (using tritiated leucine uptake) or manual cell counting by haemocytometry.²²⁻²⁵ The ability of QPM to provide quantitative information regarding the growth of cells *in situ* in culture provides a significant advance on these techniques.

The first step in the processing of QPM-derived phase maps to quantify the amount of cellular material involves the generation of a pixel intensity histogram to differentiate the phase values associated with cellular and non-cellular regions of the culture dish. From this histogram a threshold grey level is obtained at which segmentation of cellular from non-cellular material can be achieved to produce a

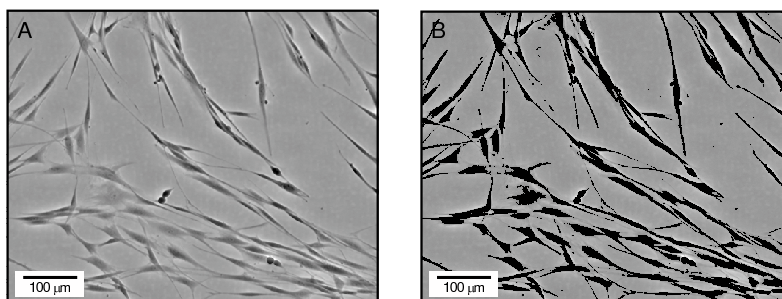


Figure 4. Demonstration of the segmentation process used for assessing confluency of human airway smooth muscle cell cultures (Achromplan $\times 10$, NA 0.3).

A: Phase map of human airway smooth muscle cell culture.

B: Segmented image of phase map in A, generated using the threshold value determined by axis intercept. (Image-Pro Plus software v3.0 Media Cybernetics, USA) See text for method details.

binary image (for a more detailed explanation of curve fitting and extrapolation procedures see Curl *et al* 2004²⁰). This image manipulation process is illustrated in Figure 4 which shows a smooth muscle cell culture phase map (Figure 4A) calculated from a bright field image, and the segmented cell-delineated image produced by this thresholding process (Figure 4B). The area summation of the segmented cellular material on the culture plate provides a measure of the confluency of the cell culture, expressed as a percentage of the total field area examined (in this example calculated to be 17.05% of total field). The precision of this measurement relies on the threshold grey level extrapolated by curve-fitting methods applied to the image pixel intensity histogram²⁰ and is entirely reproducible for a given image. The extent to which histogram distributions vary from image to image will determine the measurement variability, and this should be evaluated empirically for different imaging conditions. As this methodology does not require the cells to be manipulated in any fashion (ie by staining or trypsinization), repeated measurements of the same cell field may be made over a specified time period to derive a growth curve. The high contrast phase visualization produced by the QPM technique makes these measurements feasible – the contrast available in bright field and even in conventional optical phase images is generally not adequate to permit reproducible image thresholding and reliable cell delineation.

Cellular Volume Measurement

Cell volume regulation is a fundamental cellular homeostatic mechanism.²⁶ Accurate measurements of cell volume can provide important information about many physiological regulatory and growth processes, but such measurements are particularly difficult to undertake *in situ*.^{12,27}

As the extent of phase shift induced when light passes through a translucent cellular specimen is determined by a combination of the refractive index and thickness of the cell, it follows that, where refractive index

may be established (or is known already) it is also possible to use QPM to measure the thickness of a cell. Thus, the volume of an individual cell or of a field of cells may be measured by the integration of thickness values extracted from designated areas of the phase map. Erythrocytes, which adopt predictable and well characterized geometric shapes in different osmotic environments,²⁸⁻³¹ are a particularly convenient cell type for the demonstration of this application of QPM.²¹

When exposed to a sufficiently hypotonic solution, erythrocytes expand their isotonic biconcavity and take on spherical shape. In this condition, the red blood cell thickness (depth) may be equated with the width (measured in the x-y plane). From a specific cell a certain phase value can be correlated with the measured thickness/width. By averaging over many cells, a 'generic' erythrocyte refractive index can be determined.²¹ This refractive index can then be applied to any similar cell, or fields of cells under equivalent circumstances to convert the phase values contained in the phase map (such as that shown in Figure 2D) to an estimate of cellular volume. Erythrocyte volume calculations performed using this methodology compare favourably with those previously reported using more laborious and destructive methods.^{32,33} For other cell types with less convenient geometry, essentially the same process can be used to undertake volume measurement, although somewhat more complex procedures (ie confocal microscopy combined with QPM³⁴) may be required to initially establish a value for refractive index when this is not independently available. As phase shift is simply the product of specimen thickness and refractive index, any error in the determination of the refractive index will be linearly reflected in the calculated volume. A refractive index of 1.59-1.63 is commonly reported for erythrocytes,³⁵ and taking values at either extreme of this range would produce about a 2.5% variation in computed volume. In most applications, where the refractive index is not expected to alter under experimental circumstances for a given cell type, phase changes can be taken to be directly proportional to changes in cell thickness (and therefore volume) for relative measurements.

As a newly devised microscopy technique, QPM has demonstrated application in the evaluation of cellular structure and morphology. The full value of QPM as a non-destructive, non-interventional experimental tool for functional imaging of 'real time' cellular process will become evident as this technique is more widely implemented.

Acknowledgements

The authors thank Mr David Stewart of Zeiss Australia for assistance with optical and software components and Assoc Prof. Alastair Stewart and Ms Trudi Harris (Department of Pharmacology, University of Melbourne) for generous assistance with cell culture preparation. The support of the Australian Research Council and IATIA Ltd is acknowledged. The quantitative phase microscopy system described is marketed by IATIA Ltd ('QPm', www.iatia.com.au) and we declare that KAN has a financial interest in that company.

References

1. DiBona DR, Kirk KL, Johnson RD. Microscopic investigation of structure and function in living epithelial tissues. *FASEB Fed. Proc.* 1985; **44**:2693-2703.
2. Ross KFA. Phase contrast and interference microscopy for cell biologists. Edward Arnold (Publishers) Ltd, London 1967.
3. McMahon PJ, Barone-Nugent ED, Allman BE, Nugent KA. Quantitative phase-amplitude microscopy II: differential interference contrast imaging for biological TEM. *J. Microsc.* 2002; **206**:204-208.
4. Zernike F. Phase contrast, a new method for the microscopic observation of transparent objects. *Physica* 1942; **9**:686-693.
5. Barty A, Nugent KA, Roberts A, Paganin D. Quantitative phase microscopy. *Opt. Lett.* 1998; **23**:817-819.
6. Delbridge LMD, Kabbara AA, Bellair CJ, Allman BE, Nassis L, Roberts A, Nugent KA. Quantitative phase imaging – a new way to 'see' cells. *Today's Life Science.* 2002; **14**:28-32.
7. Barer R. Refractometry and interferometry of living cells. *J. Opt. Soc. Am.* 1957; **47**:545-556.
8. Simon I, Pound CR, Partin AW, Clemens JQ, Christens-Barry WA. Automated image analysis system for detecting boundaries of live prostate cancer cells. *Cytometry.* 1998; **31**:287-294.
9. Nomarski G & Weill AR. Application a la metallographie des methods interferentielles a deux ondes polarises. *Rev. Metall.* 1955; **2**:121-128.
10. Salmon ED, Tran P. High-resolution video-enhanced differential interference contrast (VE-DIC) light microscopy. *Meth. Cell Biol.* 1998; **56**:153-184.
11. Allen RD, David GB, Nomarski G. The Zeiss-Nomarski differential interference equipment for transmitted-light microscopy. *Z. Wiss Mikrosk. Tech.* 1969; **69**:193-221.
12. Kimelberg HK, O'Connor ER, Sankar P, Keese C. Methods for determination of cell volume in tissue culture. *Can. J. Physiol. Pharmacol.* 1991; **70**:S323-S333.
13. Hoffman R & Gross L. The modulation contrast microscope. *Nature.* 1975; **254**:586-588.
14. Hoffman R, Gross L. Modulation contrast microscopy. *Appl. Optics.* 1975; **14**:1169-1171.
15. www.micro.magnet.fsu.edu/primer/techniques/hoffman/hoffmanintro.html
16. Paganin D & Nugent KA. Non-interferometric phase imaging with partially coherent light. *Phys. Rev. Lett.* 1998; **80**:2586-2589.
17. Barone-Nugent ED, Barty A, Nugent KA. Quantitative phase-amplitude microscopy I: optical microscopy. *J. Microsc.* 2002; **206**:194-203.
18. Allman BE, Nassis L, von Bibra ML, Bellair CJ, Kabbara AA, Barone-Nugent E, Gaeth AP, Delbridge LMD, Nugent KA. Optical phase microscopy: quantitative imaging and conventional phase analogs. *Microsc. Analy.* 2002; **52**:13-15.
19. Bellair CJ, Curl CL, Allman BE, Harris PJ, Roberts A, Delbridge LMD, Nugent KA. Quantitative phase-amplitude microscopy IV: imaging thick specimens. *J. Microsc.* 2004; **214**:62-70.
20. Curl, CL, Harris T, Harris PJ, Allman BE, Stewart AG, Delbridge LMD. Quantitative phase microscopy: a new tool for measurement of cell culture growth and confluency in situ. *Pflugers Archiv.* 2004; **448**:462-468.
21. Curl CL, Bellair CJ, Allman BE, Roberts A, Nugent KA, Harris PJ, Delbridge LMD. Measurement of erythrocyte volume changes in response to osmotic stimuli using quantitative phase microscopy. *Proc. Exp. Biol.* 2003: LB65.
22. Fernandes DJ, Guida E, Kalafatis V, Harris T, Wilson J, Stewart AG. Glucocorticoids inhibit proliferation, cyclin D1 expression and retinoblastoma protein phosphorylation, but not mitogen-activated protein kinase activity in human cultured airway smooth muscle. *Am. J. Resp. Cell. Mol. Biol.* 1999; **21**:77-88.
23. Lepore DA, Hurley JV, Stewart AG, Morrison WA, Anderson RL. Prior heat stress improves the survival of ischemic-reperfused skeletal muscle in vivo: role of HSP 70. *Muscle Nerve.* 2000; **23**:1847-55.
24. Ravenhall CR, Guida E, Harris T, Koutsoubos V, Vadiceolo P, Stewart AG. The importance of ERK activity in the regulation of cyclin D1 levels in DNA synthesis in human cultured airway smooth muscle. *Br. J. Pharmacol.* 2000; **131**:17-28.
25. Stewart AG. Airway wall remodelling and hyper-responsiveness: modelling remodelling in vitro and in vivo. *Pulm. Pharmacol. Ther.* 2001; **14**:255-265.
26. Korchev YE, Gorelik J, Lab MJ, Sviderskaya EV, Johnston CL, Coombes CR, Vodanoy I, Edwards CRW. Cell volume measurement using scanning ion conductance microscopy. *Biophys. J.* 2000; **78**:451-457.

27. Reuss L. Changes in cell volume measured with an electrophysiologic technique. *Proc. Natl. Acad. Sci.* 1985; **82**:6014-6018.
28. Orlov SN, Pokudin NI, Kotelevtsev YV, Gulak PV. Volume-dependent regulation of ion transport and membrane phosphorylation in human and rat erythrocytes. *J. Membr. Biol.* 1989; **107**:105-117.
29. MacKnight ADC, Gordon LGM, Purves RD. Problems in the understanding of cell volume regulation. *J. Exp. Zool.* 1994; **268**:80-89.
30. Schneider AS, Harmatz D. An experimental method correcting for absorption flattening and scattering in suspensions of absorbing particles: circular dichroism and absorption spectra of hemoglobin in situ in red blood cells. *Biochemistry.* 1976; **15**:4158-4162.
31. Gitter-Amir A, Rosenheck K, Schneider AS. Angular scattering analysis of the circular dichroism of biological cells. 1. The red blood cell membrane. *Biochemistry.* 1976; **15**:3131-3137.
32. Ponder E: Hemolysis and related phenomena, Grune & Statton, New York, 1948.
33. Altman PL, Dittmer DS: *Biology Data Book*, Federation of American Societies of Experimental Biology, Washington DC, 1964.
34. www.iatia.com.au/applications/apps_confocal.asp
35. Mazarevica G, Freivalds T, Jurka A. Properties of erythrocyte light refraction in diabetic patients. *J. Biomed. Optics* 2002; **7**:244-247.

Received 7 July 2004, in revised form 27 July 2004.

Accepted 12 August 2004.

©L.M.D. Delbridge 2004.

Author for correspondence:

Lea Delbridge

Department of Physiology

University of Melbourne

Victoria, 3010

Australia

Tel: +61 3 8344 5853

Fax: +61 3 8344 5897

E-mail: lmd@unimelb.edu.au

Microscopic imaging of extended tissue volumes

Ian LeGrice, Greg Sands, Darren Hooks, Dane Gerneke & Bruce Smaill

Bioengineering Institute & Department of Physiology, University of Auckland, New Zealand

Summary

1. Detailed information about 3D structure is key to understanding biological function

2. Confocal laser microscopy has made it possible to reconstruct 3D organization with exquisite resolution at cellular and subcellular levels

3. There have been few attempts to acquire large image volumes using the confocal laser scanning microscope.

4. We have previously used manual techniques to construct extended volumes (several mm in extent, at 1.5 μm voxel size) of myocardial tissue.

5. We are now developing equipment and efficient automated methods for acquiring extended morphometric databases using confocal laser scanning microscopy.

Introduction

The association between form and function is a central principle of the biological sciences and one that has contributed to the growth of the field over many years. The linkage is probably more important today than ever before. It is widely accepted that detailed information about three-dimensional (3D) structure is key to understanding biological function from molecule to organ and with the development of new imaging modalities there has been an explosion in the quality and volume of data that can be acquired at each of these scales. For instance, the confocal laser microscope has made it possible to reconstruct three-dimensional organization with exquisite resolution at cellular and subcellular levels. Moreover, using the array of immuno-histochemical techniques now available, it is also possible to probe the link between structure and function directly, for instance by quantifying the co-location of labelled proteins such as gap junctions or receptors with other anatomic structures.

For the most part, confocal imaging has not been used to reconstruct 3D tissue organization in a systematic fashion and there have been few attempts to acquire large image volumes as has been done with MRI or micro-CT. This reflects the physical constraints on the technology. Acquisition rates are limited by the sensitivity of photodetectors and the need to scan points sequentially throughout the tissue volume, while the dimensions that can be imaged are set by the working field of the microscope objective and critically, with respect to Z direction, by absorption and scattering of light in the tissue investigated. That said, there is a clear need for databases that incorporate structural information across the scales addressed by confocal microscopy for normal and

pathologically changed organ systems at different developmental stages. Extended morphometric databases of this kind are required to characterize more fully the structural changes associated with various dysfunctional states and to support the computer models that are increasingly being used to integrate experimental information at cell, tissue and organ levels.

Manual technique for acquiring extended confocal microscope images of biological samples

In the remainder of this section, we summarize ongoing research at the University of Auckland which is directed toward the development of efficient methods for acquiring extended morphometric databases using confocal laser microscopy. The work flows from initial studies in which high-resolution volume images were assembled of myocyte arrangement and connective tissue organization across the heart wall¹. Transmural segments (800 μm \times 800 μm \times 4.5 mm) were cut from the left ventricle free wall of rat hearts, previously perfused with Bouin's solution for fixation and then with the dye picosirius red which binds non-sterically to collagen². The specimen was dehydrated with a graded series of alcohols, embedded in epoxy resin and the upper surface of the block was then planed flat using an ultramicrotome. A motorized stage was used to control the horizontal position of the specimen and contiguous z-series image stacks were acquired at different x-y locations. In this way, an extended volume image was generated over the upper surface of the transmural specimen to a depth of around 60 μm . The block was then removed from the microscope and mounted in an ultramicrotome where the upper 50 μm was removed. The specimen was then returned to the microscope and the cycle of imaging and trimming was completed sequentially until the complete volume was imaged. Painstaking alignment of the upper surface of the tissue block in both the microtome and the confocal microscope was required at each stage in this process to ensure that image registration was, as far as possible, preserved (See Figures 1 and 2). Moreover, further *post-hoc* spatial transformation of image sub-volumes was still required to optimize registration when assembling the complete image volume.

Digital reslicing, segmentation and volume rendering methods can be applied to the resulting volumes to provide quantitative structural data about the 3D organization of myocytes, extracellular collagen matrix and the vascular network. These data have not previously been available and provide a powerful basis for further analysis of function. For example, it is a relatively trivial matter to quantify the transmural variation of perimysial collagen once it has been

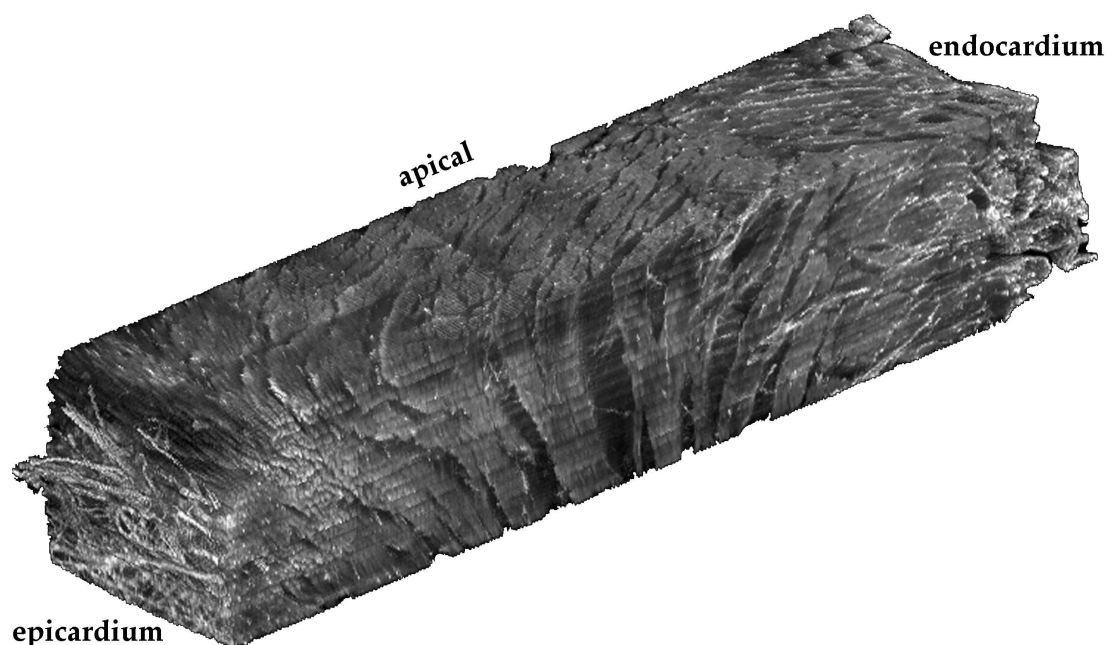


Figure 1. Oblique view of extended volume image from left ventricle of rat heart obtained using confocal microscopy. Note the laminar organization and collagen (white) interconnecting layers of myocytes. The epicardial collagen weave is clearly seen along with cleavage planes between myocardial layers. (From 1, with permission from the Royal Microscopical Society).

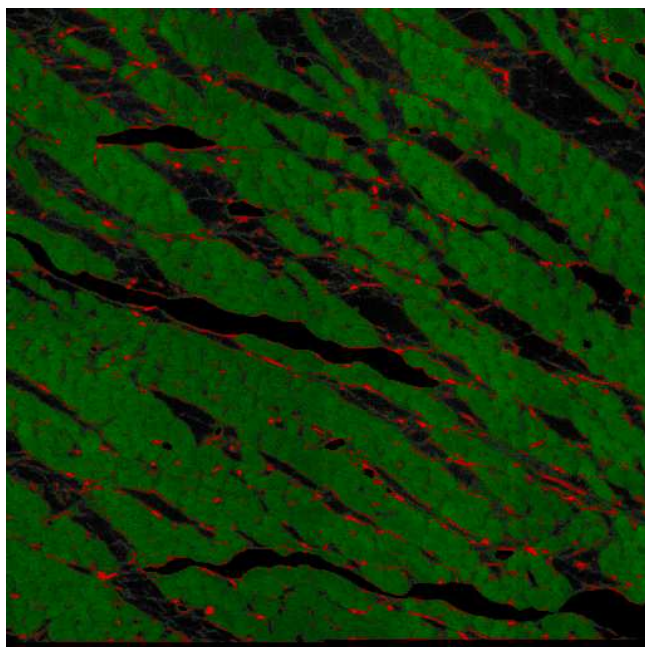


Figure 2. Image slice from left ventricular midwall of rat heart ($800 \times 800 \mu\text{m}$) illustrating laminar organization of myocytes. Plane of optical section is perpendicular to myocyte axis. Red dots are perimysial collagen cords running parallel to myocyte axis.

segmented out of an extended volume image as shown in Figure 3b. The heart wall remodelling associated with many types of cardiac disease involves changes in the extent and

distribution of collagen and detailed information about the time-course of these changes is necessary to better understand the disease processes involved. It follows that extended volume imaging provides a pathway for systematic acquisition of such data. It can also be used for the development of computer models, which make it possible to examine the effects of myocardial structure on the function of the heart. For instance, we have extracted the 3D arrangement of cleavage planes and myocyte orientation from an extended volume image of rat left ventricular myocardium ($3.8\text{mm} \times 0.8\text{mm} \times 0.8\text{mm}$ at $1.5\mu\text{m}$ pixel size, 0.72×10^9 voxels).

This application illustrates well the utility of being able to gather detailed microscopic information over extended volumes. The myocardial layers and cleavage planes are defined by connective tissue and myocytes interconnections that are visible at levels of a few micrometers and it is details of these structures that are needed to define the local electrical and mechanical properties of the laminar myocardium. However, the cleavage planes can extend for two to three millimetres. In order to fully describe the structure and associated material properties, for instance when developing a computer model of myocardium it is necessary to have information across a wide scale range, the system we have developed provides the tools to acquire this information. The extended volume image of rat myocardium has been incorporated into a structurally detailed, finite element model of ventricular myocardium that has been used to study the influence of discontinuous myocyte organization on the propagation of electrical activation in the heart³.

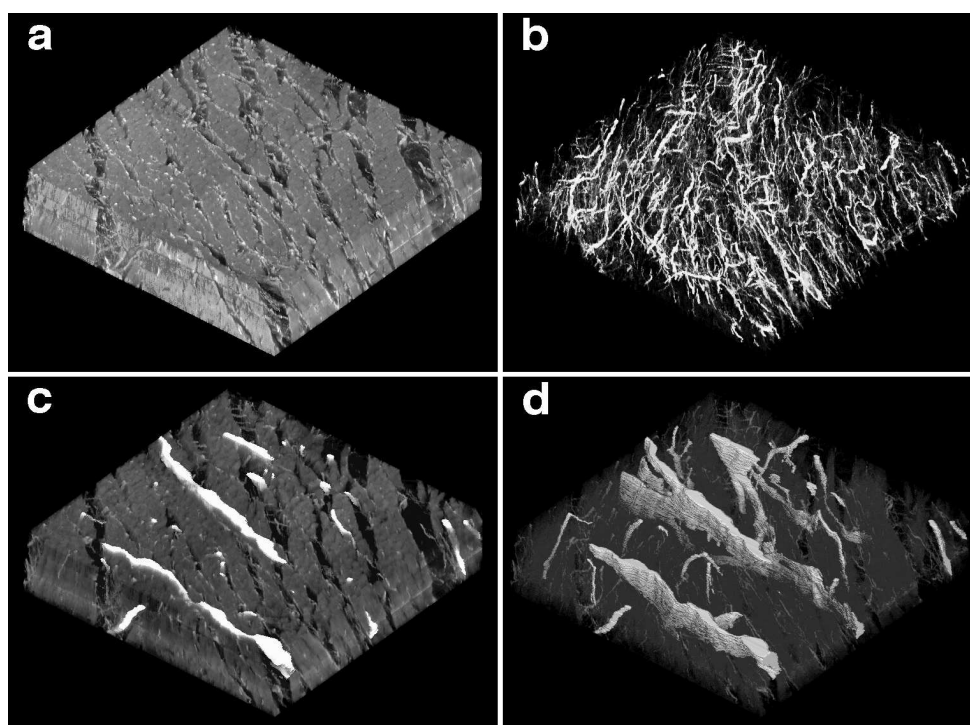


Figure 3. Reconstructed subvolumes ($800 \times 800 \times 100 \mu\text{m}$). In the upper panel collagen is segmented and rendered (a) with and (b) without background due to myocytes. In the lower panel venous sinuses are segmented and rendered, (c) with, and, (d), without background. (From 1, with permission from the Royal Microscopical Society).

Development of automated techniques for acquiring extended volume images

Unfortunately, acquisition of an image volume such as that presented in Figure 1 requires weeks of painstaking work and this precludes the use of the manual approach outlined above for systematic morphometric analysis. For this reason, we are now developing an automated system that provides for computer controlled confocal imaging and milling of embedded tissue samples over extended volumes. The system consists of (i) a confocal microscope (Leica TCS 4D) with a Kr/Ar laser (Omnichrome) (ii) a variable speed Ultramill (Leica) which cuts to $1\mu\text{m}$ over a 75mm path using diamond or tungsten carbide tips, and (iii) a three-axis translation stage (Aerotech) with xyz movement of 1000, 200 and 75mm, respectively at 100nm step size. The stage controls the positioning of specimens for imaging and milling (See Figure 4). Microscope and mill are supported above the translation stage using rigid mounting systems designed to facilitate alignment of imaging and cutting planes. The system is mounted on an anti-vibration table (Newport). Z-stack volume images are acquired for overlapping x-y areas that cover the region of interest. The imaged volume is then milled off and the process is repeated. A major advantage of this method is that alignment of the sample elements is maintained throughout the imaging and milling operations, thereby preserving spatial registration and making reconstruction of the complete volume image easier and faster.

The system is controlled using a dedicated computer

(Dell P4, 1.8GHz, 1GB RAM, Windows 2000) using custom software written using the LabVIEW™ programming language. A single user interface has been developed that enables image acquisition and milling to be controlled interactively or automatically and allows the operator to process, reconstruct and visualize the image volumes. The flexible user interface provides the ability to image chosen sub-volumes at high resolution, but placing them within the context of a large volume imaged at lower resolution.

Preliminary studies carried out with cardiac tissue specimens demonstrate that the system has the capacity to acquire 62.5 million voxels per hour, each averaged over 8 scans. This means that a fully-registered 1mm^3 image volume can be acquired at $1\mu\text{m}$ resolution (10^9 voxels) with 8× averaging, in 16 hours. This is a more than ten fold improvement with respect to our initial manual approach and further more modest improvement is seen to be possible with optimization of scanning and signal acquisition protocols.

The imaging rig is currently being used in a series of different projects including a longitudinal study of cardiac remodelling in spontaneously hypertensive rats throughout the course of their progress to heart failure and an analysis of the 3D organization of renal tubules and blood vessels in nephron segments. Particular emphasis is being given to extending the range of embedding and staining techniques that can be used with this automated volume imaging system.

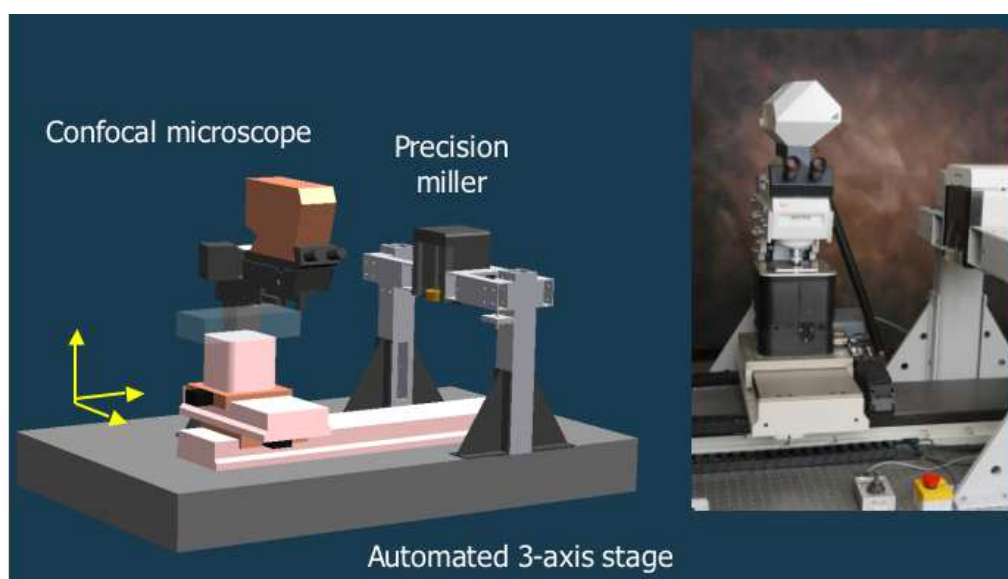


Figure 4. *The automated confocal imaging rig.* The schematic indicates the arrangement of the confocal microscope, the ultramill and the three-axis translation stage. The inset photograph shows all three components and the anti-vibration table on which they are mounted.

Acknowledgments:

Development of this imaging system was made possible by a grant from the Wellcome Trust.

References:

1. Young AA, LeGrice IJ, Young MA, Smaill BH. Extended confocal microscopy of myocardial laminae and collagen network. *J. Microsc.* 1998; **192**: 139-150.
2. Dolber PC, Spach MS. Conventional and confocal fluorescence microscopy of collagen fibres in the heart. *J. Histochem. Cytochem.* 1993; **41(3)**: 465-469.
3. Hooks DA, Tomlinson KA, Marsden SG, LeGrice IJ, Smaill BH, Pullan AJ, Hunter JP. Cardiac microstructure: implications for electrical propagation and defibrillation in the heart. *Circ. Res.* 2002; **91**: 331-338.

Author for correspondence:

Ian LeGrice
Department of Physiology,
University of Auckland,
Auckland, New Zealand

Tel: +64 9 373 7599 ext 86206
Fax: +64 9 373 7599
Email: i.legrice@auckland.ac.nz

Received 27 July 2004, in revised form 17 August 2004.

Accepted 19 August 2004.

©I. LeGrice 2004.

Inherited cardiac arrhythmia syndromes: What have they taught us about arrhythmias and anti-arrhythmic therapy?

Rajesh N. Subbiah, Terence J. Campbell & Jamie I. Vandenberg

*Electrophysiology and Biophysics Program,
Victor Chang Cardiac Research Institute,
Darlinghurst, NSW 2010, Australia
and
Department of Medicine,
St. Vincent's Hospital,
University of NSW, NSW 2052, Australia*

Summary

1. In recent years, the identification of the gene defects in a vast array of monogenic disorders has revolutionised our understanding of the basic mechanisms underlying numerous disease processes.

2. Mutations in cardiac ion channels have been identified as the basis of a wide range of inherited arrhythmia syndromes, including the congenital Long QT syndromes, Brugada syndrome, Lenegre syndrome, Andersen's disease and Familial atrial fibrillation.

3. Identification of mutations in the human-ether-a-go-go related gene (HERG) K⁺ channel as the molecular basis of congenital long QT syndrome type 2 also led to the discovery that HERG is the molecular target for the vast majority of drugs (both cardiac and non-cardiac) that cause drug-induced arrhythmias. This has had profound implications not only for the development of anti-arrhythmic agents but for drug development in general.

4. The sequencing of the human genome in a sense represents the pinnacle of the reductionist era of molecular medicine. The great challenge now is to re-integrate the information gathered during the "reductionist era" to provide a better understanding of the intact organism. Computer modelling is likely to be a key component of that re-integration process.

Introduction

The processes of disease are so complex that it is excessively difficult to search out the laws which control them, and, although we have seen a complete revolution in our ideas, what has been accomplished by the new school of medicine is only an earnest of what the future has in store." (William Osler, 1849 - 1919)

In recent years, the identification of the gene defects in a vast array of monogenic disorders (<http://www.ncbi.nlm.nih.gov/omim/>) has revolutionised our understanding of the basic mechanisms underlying numerous disease processes. In the case of ventricular arrhythmias, the unraveling of the molecular genetics of the Long QT syndrome (LQTS, see below) is one such example. Such studies, and the wider effort of sequencing the human genome have undoubtedly advanced our knowledge of the molecular basis of disease; the great challenge now is to translate this revolution into improving

the delivery and outcome of clinical practice.

Electrical activity of the heart

Cardiac function is dependent upon the synchronised contraction of each of the millions of cardiac myocytes that make up the heart. This synchronisation is achieved by an electrical network that is composed of a specialised conducting system, including the sinoatrial node, atrioventricular node and His-Purkinje fibres, and by the presence of ion channels in the cell membrane surrounding every cardiac myocyte. Electrical signals that originate in the sinoatrial node travel through this network of fibres and trigger action potentials in the cardiac myocytes, which in turn induce the influx of calcium into the myocytes that initiate the contractile cycle.¹ It is perhaps not surprising then that a disruption of this electrical network, or more specifically dysfunction of cardiac ion channels, greatly increases the risk of cardiac arrhythmias.² However, it is a relatively recent concept that the underlying substrate in cardiac arrhythmias is abnormal ion channel function and this is in a large part is due to the dissection of the rare genetic causes of cardiac arrhythmias.³

Cardiac arrhythmias

Cardiac arrhythmias may be classified into two broad groups, according to the underlying rate, i.e. tachyarrhythmias (excessively fast) and bradyarrhythmias (excessively slow). Furthermore, cardiac arrhythmias can be divided into subgroups depending on whether they originate from the atria or ventricles. Cardiac arrhythmias are associated with both significant morbidity and mortality. In particular, they can result in syncope, a transient loss of consciousness due to insufficient blood supply to the brain, or more significantly, lead to death, which is classically described as "sudden cardiac death". Death due to cardiac arrhythmia is most commonly associated with ventricular tachyarrhythmias and is believed to account for over 50% of the 49,741 deaths per annum attributable to cardiovascular disease in Australia (<http://www.heartfoundation.com.au>) and probably >350,000 deaths in the U.S.A.,⁴ making it one of the commonest individual causes of death. Furthermore, this group of arrhythmias has been the focus of the majority of genetic studies in recent years.²

Table 1:
Cardiac Ion Channelopathies

Syndrome	Gene	Channel	Reference
1. Long QT syndrome			
LQTS 1	KCNQ1 ^a	I_{Ks}	13
LQTS 2	KCNH2 ^b	I_{Kr}	10
LQTS 3	SCN5a ^c	I_{Na}	42
LQTS 4	β -ankyrin ^d	β -ankyrin	15
LQTS 5	KCNE1 ^e	I_{Ks}	43
LQTS 6	KCNE2 ^f	I_{Kr}	16
2. Short QT syndrome			
	KCNH2 ^g	I_{Kr}	27
3. Brugada syndrome			
	SCN5a ^h	I_{Na}	29
4. Lenegre syndrome			
	SCN5a ^h	I_{Na}	33
5. Andersen's syndrome			
	KCNJ2 ⁱ	I_{K1}	34
6. Familial Atrial Fibrillation			
	KCNQ1 ^j	I_{Ks}	37

- a.* Loss of function mutations in *KCNQ1* lead to a reduction in the repolarising I_{Ks} current
- b.* Loss of function mutations in *KCNH2* lead to a reduction in the repolarising I_{Kr} current
- c.* Gain of function mutations in *SCN5a* lead to an increase in the depolarising I_{Na} current
- d.* β -ankyrin modulates sodium currents
- e.* Loss of function mutations in *KCNE1*, an auxiliary subunit in I_{Ks} channels, leads to a reduction in the repolarising I_{Ks} current
- f.* Loss of function mutations in *KCNE1*, an auxiliary subunit in I_{Ks} channels, leads to a reduction in the repolarising I_{Ks} current
- g.* Gain-of-function mutations in *KCNH2* (*HERG*) cause a short QT syndrome, i.e. the opposite to the effect of loss of function mutations in *KCNH2* which cause long QT syndrome.
- h.* Both Brugada syndrome and Lenegre's syndrome are caused by loss of function mutations in *SCN5a* leading to a reduction in I_{Na} current and hence slowed conduction.
- i.* Andersen's syndrome is due to loss of function mutations in *KCNJ2* which encodes the inward rectifier current, I_{K1}
- j.* Gain of function mutations in *KCNQ1* can cause familial atrial fibrillation. The mechanism underlying this syndrome has not yet been elucidated.

Cardiac arrhythmias most often occur in the context of structurally abnormal hearts (e.g. post myocardial infarction or in the context of dilated or hypertrophic cardiomyopathy) but for nearly 50 years it has also been recognised that some people will develop lethal cardiac arrhythmias despite having structurally normal hearts. It has also been known for over 40 years that these rare instances of "unexplained sudden death" were often familial and so likely to have a genetic basis.^{5,6} In the past 10 years the genetic basis of many of these rare congenital arrhythmia syndromes has been identified (see below). The most extensively studied is the congenital LQTS, which is now known to be caused by defects in at least 6 different gene loci, all of which encode ion channels or in the case of LQTS type 4 a protein that regulates ion channel function (see Table 1).

Congenital long QT syndrome

Congenital LQTS is associated with prolongation of the QT interval on the surface electrocardiogram (see Fig. 1), ventricular arrhythmias, syncope, and sudden death.

LQTS is now sub-classified according to the gene locus. The first locus was found in 1991⁷ although it was not until 1996 that the specific gene, *KCNQ1*^{*}, was identified.⁸ *KCNQ1* encodes the α -subunit of the slow component of the delayed rectifier K^+ channel,^{8,9} I_{Ks} , which contributes to phase III repolarisation of the cardiac action potential (see Fig. 1). Thus loss of function mutations in *KCNQ1* result in less K^+ efflux through I_{Ks} channels and thence delayed repolarisation of the cardiac action potential. LQTS2 is caused by mutations in the *KCNH2* gene (previously known as *HERG*),¹⁰ which encodes the α -subunit of the rapid component of the delayed rectifier K^+ channel, I_{Kr} .¹¹

* The convention for naming ion channel genes is the first letter denotes the ion species (K for potassium, S for sodium, Ca for calcium). CN stands for channel. A fourth letter when present is an arbitrary sub-family classification. For example, members of the slowly activating delayed rectifier family have been classified as subfamily Q. The final number denotes (usually in chronological order of discovery) individual subfamily members – thus *KCNQ1* was the first member of the Q-subfamily of K^+ channels discovered.

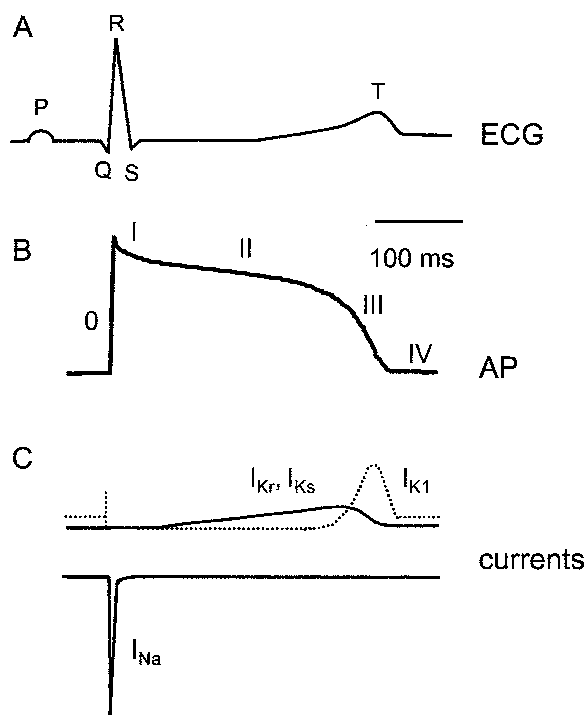


Figure 1: Cardiac Electrical Activity

A. The electrocardiogram (ECG) recorded from the body surface shows three major deflections denoted the P-wave, QRS complex and T-wave. The P-wave corresponds to atrial depolarisation, the QRS complex to ventricular depolarisation and the T-wave to ventricular repolarisation. The QT interval measured from the start of the QRS complex to the end of the T-wave is a measure of the duration of repolarisation. The ECG represents the integrated signal from all the cells that contribute to cardiac electrical activity.

B. A typical action potential recorded from a ventricular myocyte. The electrical activity in a myocyte is divided into 5 phases: 0, rapid depolarisation; I, early repolarisation; II, plateau; III, terminal repolarisation and IV, diastolic or resting potential. The cardiac action potential represents the integrated signal from all the individual ion channels present in the cell.

C. Mutations in at least four ion channel complexes are associated with an increased risk of cardiac arrhythmias (see Table 1). The cardiac Na^+ channel (I_{Na}) contributes to depolarisation (inward currents are shown as downward deflections, by convention). The delayed rectifier K^+ channels (I_{Kr} , I_{Ks}) contribute to the end of the plateau and early phases of terminal repolarisation. The inward rectifier K^+ channel (I_{K1}) contributes to rapid terminal repolarisation as well as maintenance of the diastolic potential.

Like I_{Ks} , I_{Kr} contributes to phase III repolarisation of the

cardiac action potential. Thus loss of function mutations in *KCNH2* result in less K^+ efflux during the repolarisation phase of the action potential and hence delayed repolarisation. Since its identification as the channel responsible for LQTS2, the HERG K^+ channel has been extensively studied and much of this interest is because the HERG K^+ channel is also the molecular target for the vast majority of drugs (over 700 now identified) that cause drug-induced LQTS, see below.¹² LQTS3 is caused by mutations in the *SCN5A* gene, which encodes the α -subunit of the cardiac Na^+ channel.¹³ The Na^+ channel is primarily responsible for the rapid depolarisation of the cardiac action potential. Interestingly, mutations in *SCN5A* that cause LQTS are “gain of function” mutations that result in the channels not switching off during the plateau of the action potential, thereby resulting in an increased influx of positive charge and a prolongation of the plateau phase of the cardiac action potential.¹⁴ More recently, it has been found that loss of function mutations in *SCN5A* can also cause cardiac arrhythmias (Brugada syndrome and Lenegre syndrome, see below), but via a distinct mechanism to that which causes LQTS. LQTS4 is due to loss of function in the ankyrin B gene.¹⁵ Ankyrin B regulates the activity of cardiac Na^+ channels and hence the mechanism of arrhythmia in these patients is thought to be similar to that in LQTS3. LQTS5 is caused by mutations in *KCNE1*¹⁸, the β -subunit of I_{Ks} ^{8,9} and LQTS6 is caused by mutations in *KCNE2*, the β -subunit of I_{Kr} .¹⁶ Thus it is thought that LQTS5 and LQTS6 are likely to be similar to LQTS1 and LQTS2 respectively, although these channel subunits have not been as well studied as the corresponding α -subunits.

Mechanism of arrhythmia in LQTS: The case of HERG K^+ channels

In many instances arrhythmias in LQTS are precipitated by ectopic or premature beats.¹⁷ The mechanism underlying the increased risk of arrhythmias is subtly different in each of the subtypes of LQTS, but in essence they reflect an imbalance between repolarisation currents and reactivation of depolarisation currents. This can be most clearly illustrated in the case of HERG K^+ channel mutations. HERG K^+ channels have unusual kinetics characterised by slow activation and deactivation but rapid and voltage-dependent inactivation.¹⁸ Consequently, HERG K^+ channels pass little current during the plateau of the action potential, but the channels recover from inactivation during the repolarisation phase and therefore contribute to the rapidity of repolarisation (see Fig. 2). However, due to slow deactivation HERG K^+ channels remain open for tens of milliseconds following repolarisation but pass little current during this period, because the electrochemical gradient for K^+ is minimal at the normal resting membrane potential, ~ -85 mV. However, if a premature stimulus arrives during this period HERG K^+ channels will pass a large outward current that will help to suppress propagation of the premature beat (see Fig. 2). Consequently, patients who have loss of function mutations in HERG (i.e. patients with LQTS type 2), lack this

“endogenous anti-arrhythmic mechanism”.

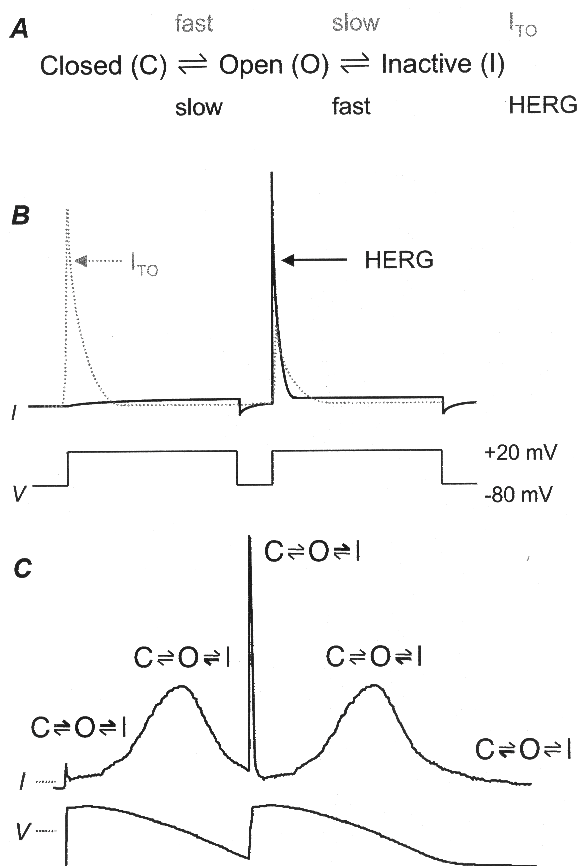


Figure 2: Mechanism of arrhythmia in LQTS2

A. Voltage-gated K^+ channels can exist in one of three main conformations, closed (C), open (O) and inactive (I). In the vast majority of voltage-gated K^+ channels the rates of opening (activation) and closing (deactivation) are very rapid, whilst the rates of transition between the open and inactivate states (inactivation and recovery from inactivation) are slow. Conversely, for HERG K^+ channels the rates of opening and closing are slow but inactivation is very rapid and voltage-dependent.

B. During a double pulse protocol, I_{TO} channels (member of the voltage-gated K^+ channel family present in the heart) opens rapidly giving rise to a large outward current which then decays slowly due to inactivation (dashed line). If a second stimulus is given shortly after the first pulse there is a much smaller outward current as the channels have not had time to recover from inactivation. Conversely, for HERG K^+ channels there is relatively little current during the first pulse as the channels open slowly and as soon as they open they inactivate. In the interval between the two pulses, HERG K^+ channels rapidly recover from inactivation but close slowly and therefore during a second pulse there is a much larger current (as most of the channels are in the open state), which then inactivates very rapidly.

C. The clinical importance of the unusual kinetics of HERG K^+ channels can be seen from the response of HERG

K^+ channels to premature action potential waveforms. In the example shown, two action potentials have been recorded, one following a normally paced stimulus and the second following a premature stimulus delivered at the point of 90% repolarisation of the first action potential. This voltage waveform has then been used to voltage clamp a CHO cell transfected with HERG K^+ channels. At the resting membrane potential HERG channels are in the closed state (C). During the early phases of the action potential the HERG K^+ channels open (O) slowly but inactivate (I) rapidly; therefore passing little current (similar to that shown in B). As the voltage decreases the channels recover from inactivation thereby passing more current; the increase in outward current peaks at about -40 mV. The current then decreases due to a combination of a decrease in the driving force for K^+ and slow deactivation. However as many of the channels are still in the open state, albeit passing little current, if a premature stimulus arrives there is a large increase in outward current (i.e. there is now a much larger electrochemical driving force for K^+). This large outward current however decays quickly due to the rapid inactivation of the channels at depolarised potentials. The profile of current flow during the remainder of the second action potential is very similar to that recorded during the first action potential. The large outward current in response to a premature stimulus would oppose cellular depolarisation and thereby help to suppress the propagation of premature beats, and hence arrhythmias initiated by premature beats.⁴⁴

Possibility of subtype specific therapy for LQTS

By elucidating the molecular mechanisms of LQTS, we have gained considerable insight into the substrate and possible triggering events of malignant cardiac arrhythmias. Previously, our understanding of the role of ion channels in cardiac arrhythmias prompted the widespread use of anti-arrhythmic drugs as either preventative or therapeutic agents. However, given the effects of such drugs on the cardiac action potential and the heterogeneity of the underlying arrhythmia substrate in LQTS, there continues to be a definite pro-arrhythmic risk involved with the use of these agents. With a limited number of effective drugs for LQTS, development of ion channel disease specific drugs has been much anticipated. At present, the mainstream pharmacological therapy for LQTS has involved the use of beta-receptor blocking drugs, which have been shown to significantly reduce mortality.¹⁹ However, there remain a considerable percentage of patients who either fail or cannot tolerate this therapy. For this group of patients, a limited range of options exist, including the surgical option of a left cervical sympathectomy or the implantation of a pacemaker or a cardiac defibrillator in conjunction with beta-receptor blocking therapy. The rationale of channelopathy-specific therapy is to use drugs with pharmacological properties that are able to either counteract or reverse the effects of the particular ion channel disorder. For instance, patients with the SCN5A and HERG

mutations have differential responses to Na⁺ channel blockade (with mexiletine) and increases in heart rate.²⁰ In particular, mexiletine shortened the QT interval in patients with the SCN5A gain in function mutation, but had no effect on the HERG mutation patients. Patients with HERG mutations had an insufficient adaptation of their QT interval to exercise and hence were more likely to benefit from beta-receptor blockade.

Drug induced long QT syndrome

Many prescription medications are known to increase the risk of cardiac arrhythmias. This was first clearly identified in the Cardiac Arrhythmia Suppression Trial (CAST). In the CAST study, patients with asymptomatic or mildly symptomatic ventricular arrhythmias after myocardial infarction, who were treated with the Na⁺ channel blockers encainide or flecainide had a higher rate of death from arrhythmia than the patients assigned to placebo.²¹ More recently, it has been realised that the HERG K⁺ channel is particularly susceptible to blockade by a wide range of drugs. Administration of these drugs can result in a phenotype very similar to the congenital LQTS type 2.²² Inhibition of HERG has now been reported for a large range of both cardiac and non-cardiac drugs. These include antihistamines (e.g. terfenadine), gastrointestinal prokinetic agents (e.g. cisapride), many psychoactive agents (e.g. amitriptyline, chlorpromazine, haloperidol and thioridazine), and some antimicrobials (e.g. macrolide antibiotics, cotrimoxazole, and the antimalarial agent halofantrine).¹² Terfenadine and Cisapride have recently been removed from the market by the Food and Drug Administration in the United States because of the risk of lethal ventricular arrhythmias and the ready availability of alternate drugs with similar therapeutic activity but lower risk of drug-induced arrhythmias.

One of the more intriguing observations in this field has been that while drug-induced LQTS could theoretically result from blockade of any of the outward potassium currents contributing to repolarisation, (or alternately from drug induced failure of inactivation of the inward sodium current), almost all of the drugs known to cause acquired Long QT syndrome appear to do so by blocking HERG.²³ Mutagenesis studies on the HERG K⁺ channel have identified the drug binding pocket in the pore region of the channel.²⁴ This pocket consists of two aromatic side chains which are able to interact with the aromatic groups present in almost all the drugs that inhibit HERG K⁺ channels. Recently Cavalli and colleagues²⁵ have carried out a quantitative structure-activity relationship analysis of drugs that inhibit HERG and identified a generic "pharmacophore" for HERG binding. The pharmacophore consist of three centres of mass (usually aromatic rings) and an amino group (usually charged at physiological pH) which together form a flattened tetrahedron. It is hoped that such pharmacophore models will be useful for "in silico" screening of new drugs for HERG binding activity.

Drug-induced LQTS is an important illustration of how basic science studies, in this case, unravelling of the

molecular genetics of the congenital LQTS, can provide very useful insights into significant clinical problems and lead to changes in clinical practice.

Short QT syndrome

In 2003, Gaita and colleagues identified 2 families with an inherited arrhythmia syndrome characterised by shortening of the QT interval.²⁶ Subsequent genetic studies identified a mutation in the HERG K⁺ channel that resulted in a loss of inactivation and hence an increase in I_{Kr} current.²⁷ Thus a "gain of function" in HERG results in a shortening of the QT interval whereas a loss of function results in a lengthening of the QT interval (see above). The increased risk of cardiac arrhythmias with either loss of function or gain of function mutations in the one ion channel subunit illustrates the delicate balance of control of electrical activity in the heart.

Brugada Syndrome

In 1992, Brugada *et al.*,²⁸ described a clinical entity, now called Brugada syndrome, in which specific electrocardiographic features in patients with a structurally normal heart were associated with an increased incidence of fatal cardiac arrhythmias. In the ensuing years, there was increasing evidence of a familial propensity with this syndrome and Chen *et al.*,²⁹ in 1998 was the first to describe mutations in the SCN5A gene in some patients with Brugada syndrome. Prior to this, in the 1980's the Centers for Disease Control in Atlanta reported an abnormally high incidence of sudden death in young immigrants from Southeast Asia, which was described as the Sudden Unexplained Nocturnal Death Syndrome (SUNDS). In Japan it was called *Pokkuri* (unexpected sudden death at night), in the Philippines, *Bangungut* (scream followed by sudden death) and in northeast Thailand, *Lai Tai* (death during sleep). Interestingly, Brugada syndrome resembles SUNDS, the most common cause of sudden cardiac death in young adults in Asia, and recent clinical and genetic evidence have suggested that both these syndromes are caused by mutations in SCN5A.³⁰ The global loss of Na⁺ channel function in the context of a heterogeneous distribution of repolarising potassium channel activity, in particular the transient outward K⁺ current (I_{TO}), results in an abbreviated upstroke of the cardiac action potential and variation in the shape of the plateau phase of the action potential across the wall of the ventricle. The variation in the shape and duration of the plateau of the action potential (i.e. phase 2 of the action potential, see Figure 1) in different regions of the ventricles can result in those cells with a long plateau triggering re-excitation of cells in which phase 2 was very short.³¹ This has been termed phase two re-entry and can result in the generation of life threatening arrhythmias. At present, no pharmacological agents have been shown to improve survival in patients with Brugada syndrome, although a role has been proposed for quinidine, a drug that has marked I_{TO} blocking properties, leading to a reduction in the transmural gradient and hence the likelihood of phase 2 reentry.³²

Currently, the only effective therapy is the implantation of a cardiac defibrillator.

Lenegre / Progressive cardiac conduction defect (PCCD)

PCCD or Lenegre syndrome as it is sometimes called can also be caused by loss of function mutations in SCN5A.³³ PCCD is characterised by slowed AV conduction. This raises the intriguing question as to why do some loss of function mutations in SCN5A result in Brugada syndrome whilst others result in PCCD. This implies that there must be other unidentified modifying influences. One possibility may be that patients with slightly lower gap junction conductance may be more prone to PCCD (i.e. decreased gap junction conductance would exacerbate the slow intercellular conduction).

Andersens' syndrome

Andersen's syndrome is characterised by periodic paralysis, cardiac arrhythmias, and dysmorphic features. Plaster *et al.*,³⁴ recently identified mutations in the gene KCNJ2 which encodes for the background inwardly rectifying Kir2.1 current in cardiac myocytes, as a cause of Andersen's syndrome. Kir2.1 plays an important role in terminal repolarisation of the cardiac action potential (see Fig. 1). Furthermore, it has been suggested that some patients with mild loss of function mutations in Kir2.1 may not exhibit the dysmorphic features, but still have the cardiac arrhythmia phenotype, associated with a mild prolongation of the QT interval. Therefore, mutations in Kir2.1 should be considered a seventh locus for congenital LQTS.³⁵

Familial Atrial Fibrillation

Atrial Fibrillation (AF) is the most common cardiac arrhythmia, with an incidence of ~6% in patients over the age of 65 and ~20% in patients over the age of 80. AF is associated with very significant morbidity, such as an increased risk of embolic stroke.³⁶ The molecular basis of atrial arrhythmias is not well understood, however, in 2003, Chen and colleagues identified a mutation in the KCNQ1 gene (i.e. the same gene that causes LQTS type 1, see above) in one large family with familial AF.³⁷ The mutation identified resulted in a gain of function, and they suggested that the initiation and maintenance of AF in these patients was likely to be caused by a reduction in action potential duration and effective refractory period in atrial myocytes. Many groups around the world are actively investigating the presence of these mutations in other patients with AF but to date none has been found.

Mutations in non-ion channel genes can also increase risk of arrhythmias

Over the last 10 years it has been discovered that there are a number of other monogenic disorders caused by mutations in non-ion channel genes that are associated with an increased risk of cardiac arrhythmias. The most extensively characterised of these are the inherited

cardiomyopathies and in particular familial hypertrophic cardiomyopathy.³⁸ In the context of cardiomyopathies, the mutations occur in structural proteins that cause gross morphological changes in the heart and presumably interfere with the conduction of signals between cells. Interesting disorders within this group are those that cause Catecholaminergic Polymorphic Ventricular Tachycardia (CPVT). CPVT is characterised by exercise-induced ventricular tachycardia and sudden death in the absence of gross myocardial disease or QT prolongation. The defects are in proteins that regulate calcium homeostasis, including the ryanodine receptor³⁹ and calsequestrin.⁴⁰ The significance of non-ion channel genetic disorders is that they illustrate the importance of the interrelationship between calcium handling and ion channel activity (both directly and indirectly).

What does the future hold?

The most direct result of the identification of the cardiac ion channelopathies is the confirmation that ion channels are crucial for electrical regulation of the heart and any abnormality in ion channel function, whether it be direct or indirect, will greatly increase the risk of cardiac arrhythmias. Consequently there has been considerable interest in understanding how cardiac ion channels function and how they are integrated to produce the synchronised activity of the heart. In the past 10 years the major ion channels have been identified and their specific functions elucidated. Thus it is likely that in the next decade, the breakthroughs will be in understanding how the activities of these channels are regulated both acutely (e.g. by phosphorylation) and chronically (e.g. via gene transcription), and in re-integrating the information gathered during the "reductionist era" to provide a better understanding of the electrical activity of the intact heart. In this respect the role of computer modelling is likely to be a key component of that "re-integration process".⁴¹

References

1. Bers, D.M. *Excitation-contraction coupling and cardiac contractile force*. Kluwer Academic Publishers, Dordrecht, 1991
2. Keating M, Atkinson D, Dunn C, Timothy K, Vincent GM, Leppert M. Linkage of a cardiac arrhythmia, the long QT syndrome, and the Harvey ras-1 gene. *Science* 1991; **252**: 704-6.
3. Marban E. Cardiac channelopathies. *Nature* 2002; **415**: 213-8.
4. Zipes DP, Wellens HJ. Sudden cardiac death. *Circulation* 1998; **98**: 2334-51.
5. Jervell, A., Lange-Neilson, F. Congenital deaf-mutism, functional heart disease with prolongation of QT interval and sudden death. *Am. Heart J.* 1957; **54**: 59-68
6. Ward OC. A new familial cardiac syndrome in children. *J. Iri. Med. Assoc.* 1964; **54**: 103-6
7. Keating MT, Sanguinetti MC. Molecular and cellular mechanisms of cardiac arrhythmias. *Cell* 2001; **104**:

- 569-80.
8. Barhanin J, Lesage F, Guillemare E, Fink M, Lazdunski M, Romey G. K(V)LQT1 and IsK (minK) proteins associate to form the I(Ks) cardiac potassium current. *Nature* 1996; **384**: 78-80.
 9. Sanguinetti MC, Jiang C, Curran ME, Keating MT. A mechanistic link between an inherited and an acquired cardiac arrhythmia: HERG encodes the IKr potassium channel. *Cell* 1995; **81**: 299-307.
 10. Curran ME, Splawski I, Timothy KW, Vincent GM, Green ED, Keating MT. A molecular basis for cardiac arrhythmia: HERG mutations cause long QT syndrome. *Cell* 1995; **80**: 795-803.
 11. Sanguinetti MC, Curran ME, Zou A, *et al.* Coassembly of K(V)LQT1 and minK (IsK) proteins to form cardiac I(Ks) potassium channel. *Nature* 1996; **384**: 80-3.
 12. Vandenberg JI, Walker BD, Campbell TJ. HERG K⁺ channels: friend and foe. *Trends Pharmacol. Sci.* 2001; **22**: 240-6.
 13. Wang Q, Curran ME, Splawski I, *et al.* Positional cloning of a novel potassium channel gene: KVLQT1 mutations cause cardiac arrhythmias. *Nat. Genet.* 1996; **12**: 17-23.
 14. Balser JR. Sodium "channelopathies" and sudden death: must you be so sensitive? *Circ. Res.* 1999; **85**: 872-4.
 15. Mohler PJ, Schott JJ, Gramolini AO, *et al.* Ankyrin-B mutation causes type 4 long-QT cardiac arrhythmia and sudden cardiac death. *Nature* 2003; **421**: 634-9.
 16. Abbott GW, Sesti F, Splawski I, *et al.* MiRP1 forms IKr potassium channels with HERG and is associated with cardiac arrhythmia. *Cell* 1999; **97**: 175-87.
 17. Benhorin J, Medina A. Images in clinical medicine. Congenital long-QT syndrome. *N. Engl. J. Med.* 1997; **336**: 1568.
 18. Vandenberg JI, Torres AM, Campbell TJ, Kuchel PW. The HERG K(+) channel: progress in understanding the molecular basis of its unusual gating kinetics. *Eur. Biophys. J.* 2004; **33**: 89-97
 19. Moss AJ, Zareba W, Hall WJ, *et al.* Effectiveness and limitations of beta-blocker therapy in congenital long-QT syndrome. *Circulation* 2000; **101**: 616-23.
 20. Schwartz PJ, Priori SG, Locati EH, *et al.* Long QT syndrome patients with mutations of the SCN5A and HERG genes have differential responses to Na⁺ channel blockade and to increases in heart rate. Implications for gene-specific therapy. *Circulation* 1995; **92**: 3381-6.
 21. Investigators C. Preliminary report: effect of encainide and flecainide on mortality in a randomized trial of arrhythmia suppression after myocardial infarction. The Cardiac Arrhythmia Suppression Trial (CAST) Investigators. *N. Engl. J. Med.* 1989; **321**: 406-12.
 22. Walker BD, Krahn AD, Klein GJ, *et al.* Congenital and acquired long QT syndromes. *Can. J. Cardiol.* 2003; **19**: 76-87.
 23. Haverkamp W, Breithardt G, Camm AJ, *et al.* The potential for QT prolongation and pro-arrhythmia by non-anti-arrhythmic drugs: clinical and regulatory implications. Report on a Policy Conference of the European Society of Cardiology. *Cardiovasc. Res.* 2000; **47**: 219-33.
 24. Mitcheson JS, Chen J, Lin M, Culbertson C, Sanguinetti MC. A structural basis for drug-induced long QT syndrome. *Proc. Natl. Acad. Sci. USA* 2000; **97**: 12329-33.
 25. Cavalli A, Poluzzi E, De Ponti F, Recanatini M. Toward a pharmacophore for drugs inducing the long QT syndrome: insights from a CoMFA study of HERG K(+) channel blockers. *J. Med. Chem.* 2002; **45**: 3844-53.
 26. Gaita F, Giustetto C, Bianchi F *et al.* Short QT Syndrome: a familial cause of sudden death. *Circulation.* 2003; **108**: 965-70
 27. Brugada R, Hong K, Dumaine R *et al.* Sudden death associated with short-QT syndrome linked to mutations in HERG. *Circulation* 2004; **109**: 30-5
 28. Brugada P, Brugada J. Right bundle branch block, persistent ST segment elevation and sudden cardiac death: a distinct clinical and electrocardiographic syndrome. A multicenter report. *J. Am. Coll. Cardiol.* 1992; **20**: 1391-6.
 29. Chen Q, Kirsch GE, Zhang D, *et al.* Genetic basis and molecular mechanism for idiopathic ventricular fibrillation. *Nature* 1998; **392**: 293-6.
 30. Vatta M, Dumaine R, Varghese G, *et al.* Genetic and biophysical basis of sudden unexplained nocturnal death syndrome (SUNDS), a disease allelic to Brugada syndrome. *Hum. Mol. Genet.* 2002; **11**: 337-45.
 31. Krishnan SC, Antzelevitch C. Sodium channel block produces opposite electrophysiological effects in canine ventricular epicardium and endocardium. *Circ. Res.* 1991; **69**: 277-291
 32. Alings M, Dekker L, Sadee A, Wilde A. Quinidine induced electrocardiographic normalization in two patients with Brugada syndrome. *Pacing Clin. Electrophysiol.* 2001; **24**: 1420-2.
 33. Tan HL, Bink-Boelkens MT, Bezzina CR, *et al.* A sodium-channel mutation causes isolated cardiac conduction disease. *Nature* 2001; **409**: 1043-7.
 34. Plaster NM, Tawil R, Tristani-Firouzi M, *et al.* Mutations in Kir2.1 cause the developmental and episodic electrical phenotypes of Andersen's syndrome. *Cell* 2001; **105**: 511-9.
 35. Tristani-Firouzi M, Jensen JL, Donaldson MR, *et al.* Functional and clinical characterization of KCNJ2 mutations associated with LQT7 (Andersen syndrome). *J. Clin. Invest.* 2002; **110**: 381-8.
 36. Alpert JS, Petersen P, Godtfredsen J. Atrial fibrillation: natural history, complications, and management. *Annu. Rev. Med.* 1988; **39**: 41-52.
 37. Chen YH, Xu SJ, Bendahhou S, *et al.* KCNQ1 gain-of-function mutation in familial atrial fibrillation. *Science* 2003; **299**: 251-4.
 38. Towbin JA, Bowles NE. Arrhythmogenic inherited

- heart muscle diseases in children. *J. Electrocardiol.* 2001; **34** Suppl:151-65.
39. Priori SG, Napolitano C, Memmi M, *et al.* Clinical and molecular characterization of patients with catecholaminergic polymorphic ventricular tachycardia. *Circulation* 2002; **106**: 69-74.
 40. Lahat H, Pras E, Olender T, *et al.* A missense mutation in a highly conserved region of CASQ2 is associated with autosomal recessive catecholamine-induced polymorphic ventricular tachycardia in Bedouin families from Israel. *Am. J. Hum. Genet.* 2001; **69**: 1378-84.
 41. Hunter PJ, Pullan AJ, Smaill BH. Modeling total heart function. *Annu. Rev. Biomed. Eng.* 2003; **5**: 147-77.
 42. Wang Q, Shen J, Splawski I, *et al.* SCN5A mutations associated with an inherited cardiac arrhythmia, long QT syndrome. *Cell.* 1995; **80**: 805-11.
 43. Splawski I, Tristani-Firouzi M, Lehmann MH, Sanguinetti MC, Keating MT. Mutations in the hminK gene cause long QT syndrome and suppress IKs function. *Nat. Genet.* 1997; **17**: 338-40.
 44. Lu Y, Mahaut-Smith MP, Varghese A, Huang CL, Kemp PR, Vandenberg JI. Effects of premature stimulation on HERG K(+) channels. *J. Physiol.* 2001; **537**: 843-51.

Received 19 April 2004, in revised form 10 May 2004.

Accepted 12 May 2004.

©J.I. Vandenberg 2004.

Cardiac structure and electrical activation: Models and measurement

Bruce H. Smaill, Ian J. LeGrice, Darren A. Hooks, Andrew J. Pullan, Bryan J. Caldwell & Peter J. Hunter

*Bioengineering Institute & Department of Physiology, University of Auckland,
Private Bag 92019, Auckland, New Zealand*

Summary

1. Our group has developed finite element models of ventricular anatomy which incorporate detailed structural information. These have been used to study normal electrical activation and re-entrant arrhythmia.

2. A model based on the actual 3D microstructure of a transmural LV segment predicts that cleavage planes between muscle layers may give rise to non-uniform, anisotropic electrical propagation and also provide a substrate for bulk resetting of the myocardium during defibrillation.

3. The model predictions are consistent with the results of preliminary experiments in which a novel fibre optic probe is used to record transmembrane potentials at multiple intramural sites in the intact heart. Extracellular potentials are recorded at adjacent LV sites in these studies.

4. We conclude that structural discontinuities in ventricular myocardium may play a role in the initiation of re-entrant arrhythmia and discuss future studies that address this hypothesis.

Introduction

We have a robust understanding of the factors which influence cardiac electrical activation at the cellular level. This is grounded in systematic experimental study of the time-dependent characteristics of transmembrane ion channels, membrane-bound ion transporters and pumps carried out over many years, in a variety of cardiac cell types. These data have been assembled into biophysically-based computer models that reproduce the observed electrical behaviour of atrial and ventricular myocytes, as well as cells of the specialized conduction system¹⁻⁴.

However, our knowledge of the factors that underlie electrical activation in the intact heart and, more particularly, those that give rise to re-entrant arrhythmia and fibrillation is more qualitative. There are a number of reasons for this. Normal and re-entrant activation are 3D events that involve relatively large tissue volumes and are influenced by regional variation of the electrical properties of cardiac tissue and by the complex architecture of the heart. Spach⁵ recently listed three primary mechanisms that may give rise to re-entry: (1) regional heterogeneity of cellular electrical properties; (2) anisotropic discontinuities in which the discrete nature of cellular organization cause slow propagation in particular directions; and (3) wavefront dynamics, in which abrupt changes of wavefront curvature in regions where structure is discontinuous or exhibits

marked spatial variation may give rise to sustained re-entrant wave motion. While electric potentials can be recorded with high spatial and temporal resolution at the heart surfaces^{6,7}, it is often difficult to relate these data to intramural electrical activity. Moreover, while it is possible to make intramural measurements of extracellular potential^{8,9} and membrane potential¹⁰, these techniques lack the spatial resolution to reconstruct fully the 3D spread of electrical activation. Within this context, mathematical modelling provides a powerful tool with which to interpret and interpolate experimental observations. Thus mathematical models which incorporate representations of actual microscopic structure offer insight into microscopic electrical effects and will become increasingly important for understanding the generation and maintenance of re-entrant arrhythmias as well as their ultimate prevention⁵.

It is relatively straightforward to specify the features of the computer models necessary to drive advances in this field. They include: descriptions of cellular architecture and cardiac boundary geometry at a scale appropriate to the problems addressed; an adequate representation of the main time-dependent processes that determine cellular electrical activity; and a realistic description of the spatial variation of cellular electrical properties. However, such models also need to be computationally efficient so that repeated cycles of re-entrant electrical activity can be simulated within a reasonable time-frame. Finally, model validation is a critical element in this process. Innovative techniques must be developed for mapping both transmembrane and extracellular potentials not just on the heart surfaces, but also intramurally. While it is not yet possible to realize all of these requirements simultaneously, they are for the first time within our grasp. In this article, we outline the efforts of researchers working in this field at the Auckland Bioengineering Institute.

Three dimensional structure of right and left ventricles

We have made detailed measurements of three-dimensional ventricular surface geometry in passive dog¹¹ and pig hearts¹² fixed in an unloaded state. These data have been incorporated into a high order finite element model that provides a compact representation of ventricular geometry, including a realistic description of atrio-ventricular valve ring topology and the structure of the ventricular apices¹².

The muscular architecture of the heart is a crucial determinant of its electrical function. Streeter and co-workers¹³ described ventricular myocardium as a continuum in which myofibre orientation varied smoothly

across the ventricular wall. They measured the transmural variation of myocyte orientation at limited numbers of representative ventricular sites in different species and demonstrated that fibre angle varies by up to 180° transmurally. Our research group has made exhaustive measurements of myofibre orientation throughout walls of right and left ventricles in dog¹¹ and pig¹², and have shown that there is significant local variation of fibre orientation, particularly at the junctions of the free walls of right ventricle (RV) and left ventricle (LV), and in the interventricular septum. This information has been incorporated into our finite element model of cardiac anatomy (see Figure 1) and is not captured fully in the more restricted datasets published earlier.

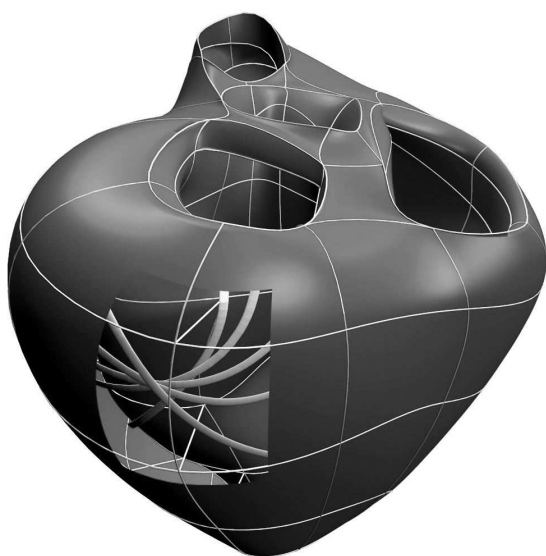


Figure 1. Finite element representation of ventricular anatomy in the pig heart, incorporating accurate topology for inlet and outlet valve orifices. Epicardial and endocardial surfaces are rendered and surface element boundaries are shown. The inset region in the LV free wall indicates the transmural variation of myofibre orientation from around -60° with respect to the circumferential axis close to the epicardial surface to near longitudinal in the subendocardium.

In most continuum models of the heart, it has been assumed that the material properties of ventricular myocardium are transversely isotropic with respect to the myofibre axis, reflecting the view that neighbouring myocytes are uniformly coupled. However, it is now clear that ventricular myocardium is structurally orthotropic, with myocytes arranged in layers that are typically four cells thick^{14,15}. Adjacent layers are separated by cleavage planes which have a characteristic radial orientation in base-apex ventricular sections and are significant in extent, particularly in the LV midwall¹⁵. Therefore, at any point within the ventricles, it is possible to define three

structurally based material axes: (i) in the fibre direction, (ii) perpendicular to the fibre direction within a muscle layer, and (iii) normal to the muscle layer. A continuous representation of these local structural axes has been incorporated into finite element models of ventricular anatomy in dog¹⁶ and pig¹² based on systematic measurements of transmural muscle layer organization and matched myofibre orientation data obtained separately for these species

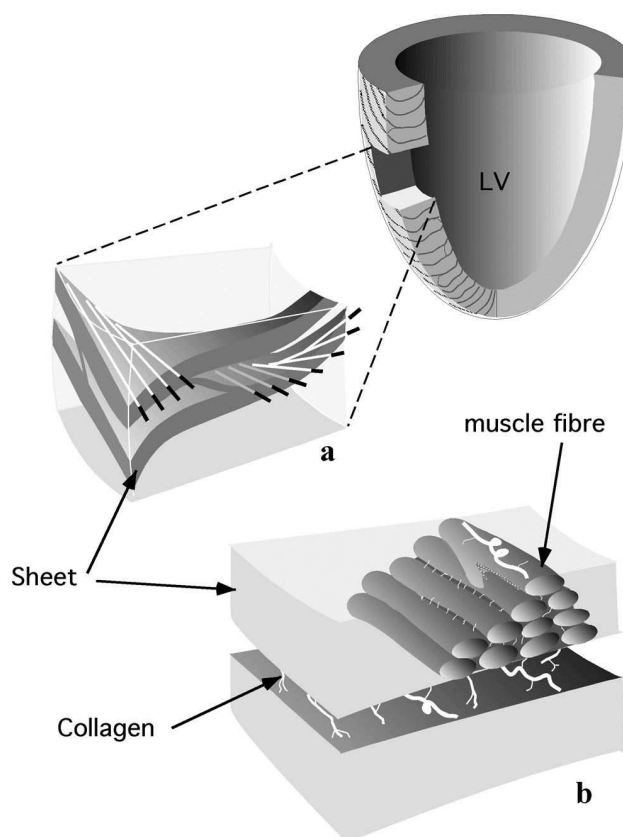


Figure 2. Schematic of cardiac microstructure.

(a) A transmurally cut block from the ventricular wall shows the macroscopic arrangement of muscle layers. Note the transmural variation of myofibre orientation.

(b) The muscle fibres are shown forming a layer three to four cells thick. Endomysial collagen connects adjacent cells within a sheet while perimysial collagen links adjacent sheets. (Modified from LeGrice et al.¹⁵)

We have also established techniques that enable us to image and visualize 3D microscopic structures in extended volumes of cardiac tissue. Initially, a confocal microscope was used to acquire "stacks" of optical sections to depths of around 60µm at contiguous sites across the upper surface of resin-embedded myocardial specimens. The top layer was then trimmed off using a glass microtome and the sequence of imaging and sectioning was repeated to assemble large, high-resolution volume images of ventricular tissue¹⁷. Unfortunately, this process requires repeated manual steps

to preserve image registration and, as a result, is very time-consuming. We have recently completed development of an automated system that enables extended volume images to be acquired much more efficiently. A high precision three-axis translation stage is coupled with a confocal microscope and histological ultramill under the control of a central computer. It is now feasible routinely to capture extended 3D images of ventricular myocardium such as that shown in Figure 3. Digital reslicing, segmentation and volume rendering methods can be applied to the resulting volumes to provide quantitative information about the 3D organization of myocytes, extracellular collagen matrix and blood vessel network of the heart not previously available. More detailed information about these techniques is outlined in a companion article in this volume¹⁸.

Modelling electrical activation in ventricular myocardium

The Auckland heart model has been used by ourselves and others to study normal cardiac electrical activation¹⁹ and the mechanisms that underlie re-entrant ventricular arrhythmia^{20,21}.

We have also used detailed microstructure-based tissue models to address three specific hypotheses²². These are (1) that early propagation from a focal activation can be accurately described only by a discontinuous model of myocardium (2) that the laminar organization of myocytes determines unique propagation velocities in three microstructurally defined directions at any point in the myocardium, and (3) that interlaminar clefts, or cleavage planes, provide a means by which an externally applied shock can influence a sufficient volume of heart tissue to terminate cardiac fibrillation. The studies were carried out using an extended volume image acquired from a transmural segment of rat LV free wall (0.8×0.8×3.7 mm) and consists of 6.07×10^8 cubic voxels at 1.56 μm resolution* (see Figure 3A). The spatial arrangement of muscle layers was quantified as follows: Cleavage planes were manually segmented and represented as bilinear finite element surface patches, while the transmural variation of myocyte orientation was characterized throughout the volume and represented as a linear function. A bidomain formulation was used to model the spread of electrical activation in this tissue volume. Ventricular myocytes and extracellular space were represented as overlapping domains, while cleavage planes were modelled as boundaries to current flow in the intracellular domain. Unlike the monodomain formulation, in which the extracellular space is assumed to be infinitely conducting, the extracellular field is explicitly represented in the bidomain approach. In practice, external electrical interventions such as intramural stimulation or defibrillating shocks are delivered extracellularly and the bidomain model enables phenomena such as these to be studied directly.

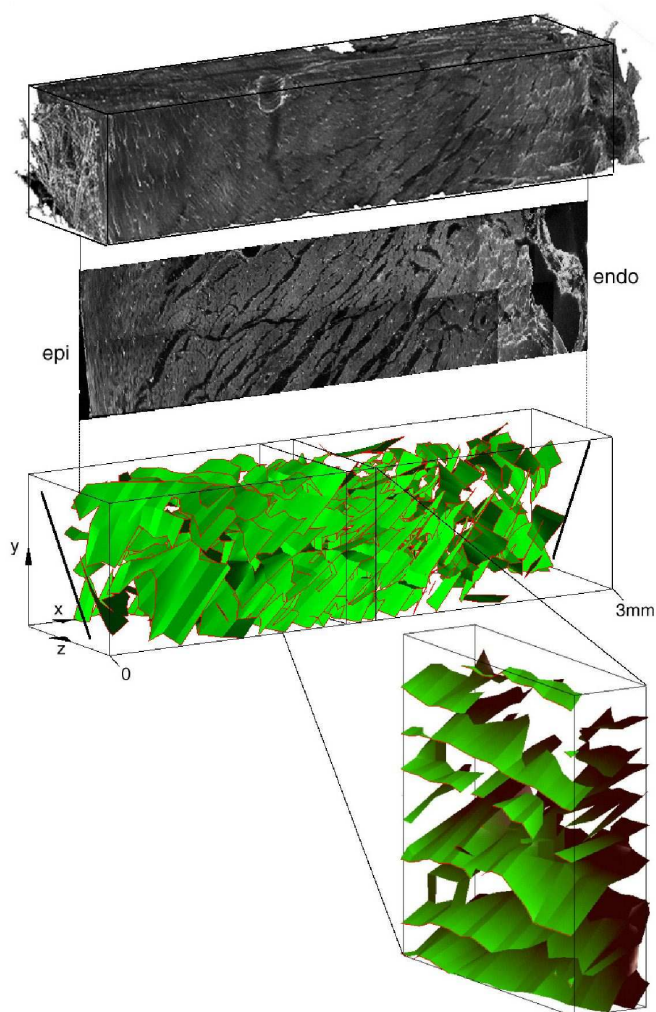


Figure 3.

Top: reconstructed volume of rat LV free-wall.

Middle: transmural slice from the reconstructed volume showing a complex network of cleavage planes which course between myocyte laminae.

Bottom: bilinear finite element description of cleavage planes through the entire tissue block, and a smaller midwall subsection. Myofibre orientation is shown on the epi- (epi), and endo- (endo) cardiac surfaces. (From Hooks et al.²²)

The isopotential regions in Figure 4 indicate the spread of electrical activation from a point stimulus at the centre of the tissue segment. Activation was simulated using a simple cubic ionic current model²³. Two cases were considered. In Figure 4A, we present results for the spread of activation where the discontinuities due to cleavage planes were explicitly represented. It was assumed that electrical conductivity in intracellular and extracellular domains are transversely isotropic with respect to local myocyte orientation. Comparable data, presented in Figure 4B, were obtained using a continuous model in which it was assumed that conductivity is orthotropic with respect to

* The reader is referred to Young *et al.*¹⁷ for more detailed information about this data-set.

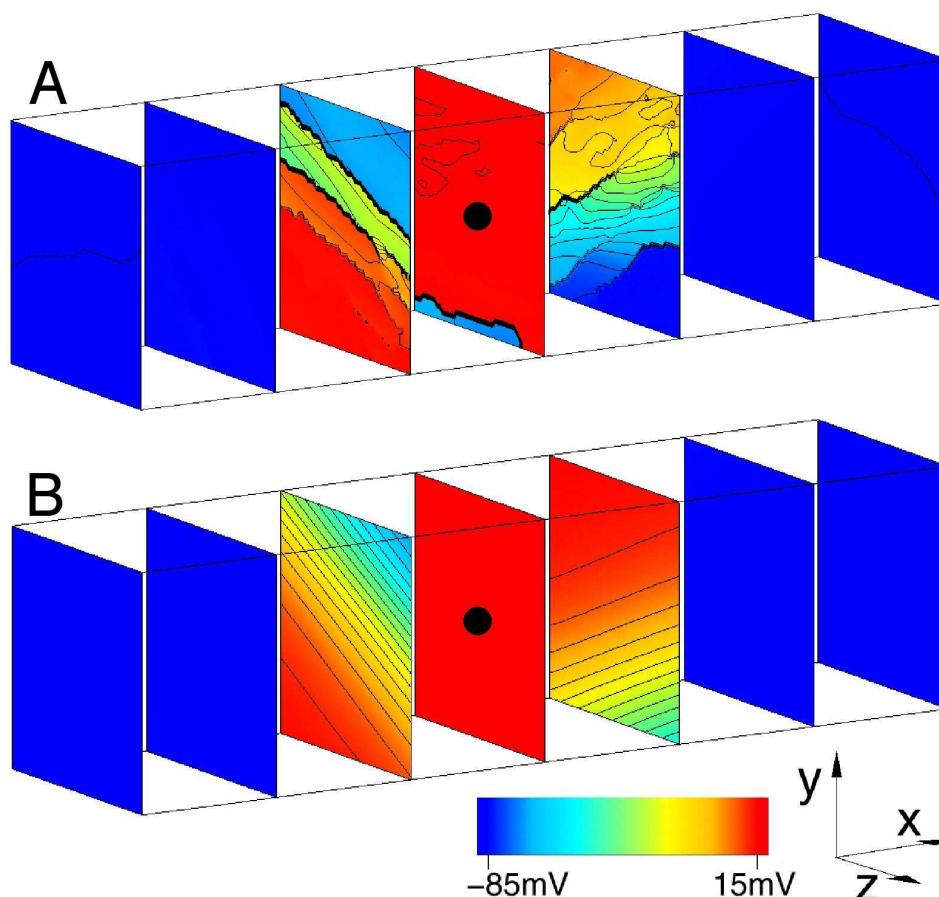


Figure 4. Ectopic activation of (A) discontinuous model and (B) continuous model. Transmembrane potentials are mapped on 7 equi-spaced surfaces through the reconstructed tissue volume, at 8ms following midwall stimulation. Isopotential lines at 5mV intervals are shown in black. Site of stimulation is shown with black dot at centre of volume. The cleavage plane obstacles in (A) lead to a highly discontinuous form of propagation, which is, however, well approximated by the continuous model. (Modified from Hooks et al.²²)

three microstructurally defined material axes. These three conductivity parameters were adjusted to best fit the propagation patterns predicted by the discontinuous model. This analysis suggests that the spread of electrical activation from an intramural point stimulus in the LV is highly anisotropic due to discontinuities associated with cleavage planes between muscle layers. Propagation is most rapid along the myocyte axis, somewhat slower transverse to the cell axis in muscle layers, but much slower again in the direction perpendicular to the muscle layers.

Despite this global correspondence between discontinuous and continuous orthotropic model, the latter cannot reproduce the complex local patterns of activation that occur along the activation wave front. Nearly all signals from the discontinuous model show some degree of fractionation, which is greatest in extent adjacent to the stimulus site. Moreover, the down stroke duration of signals recorded close to the stimulus site was considerably longer in the discontinuous model, than in the continuous model. It has previously been argued that nonuniform wave

front propagation due to tissue heterogeneity and discontinuities may give rise to such complex polyphasic (fractionated) extracellular potential recordings^{24,25}.

The effects of applying a large potential difference between epi- and endocardial surfaces of the transmural tissue segment are shown in Figure 5, where results for discontinuous (Figure 5A) and orthotropic continuous (Figure 5B) structural models are contrasted. Constant current (10ms duration; uniform density 0.14mA/mm²) was applied to the extracellular domain at the epicardial (cathodal) and endocardial (anodal) surfaces inducing an extracellular potential gradient of approximately 1V/mm across the ventricle wall. The shock response was modelled using a Beeler-Reuter ionic current model¹ modified to account for large externally applied potentials^{26,27}.

The progression of activation through the tissue volume during the 10 ms for which the shock was applied is very different for the continuous and discontinuous solutions. In the former case, the transmural shock initially produced steep potential gradients in sub-endocardial and

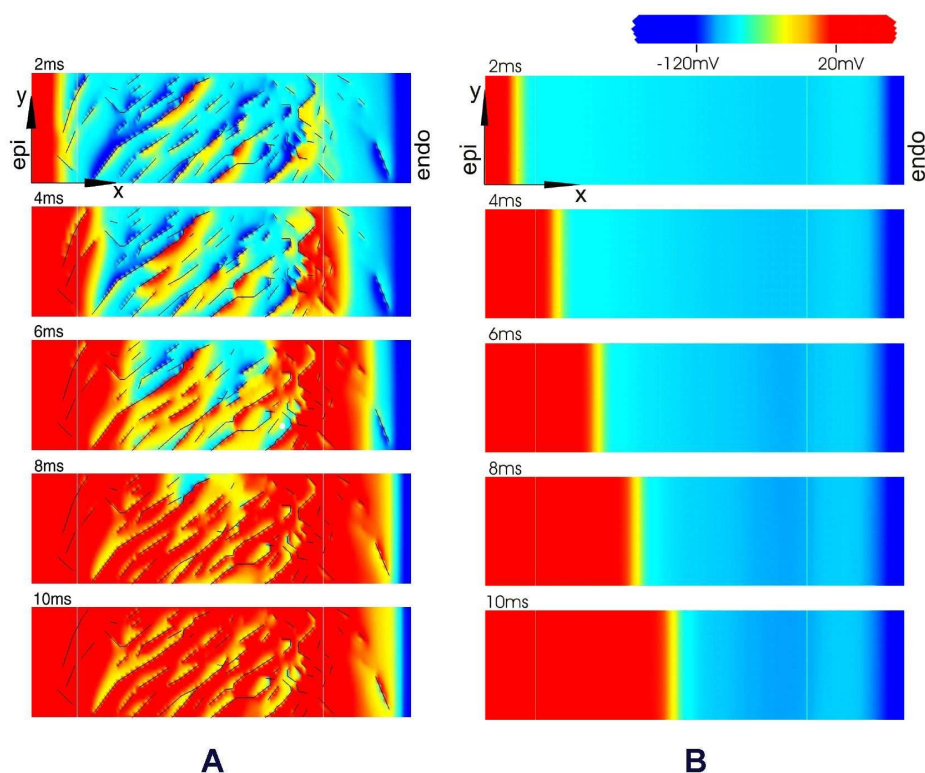


Figure 5. Effects of cleavage planes on activation after application of a large transmural shock. (Constant current: 10ms duration; $0.14\text{mA}/\text{mm}^2$.) Transmembrane potentials are mapped on a single plane at the centre of the reconstructed transmural segment at 2ms time increments following onset of shock.

(A) Discontinuous model, with cleavage planes indicated by broken black lines.

(B) Continuous model.

(Modified from Hooks et al.²²)

sub-epicardial regions generating activation that at 10 ms had spread only about 1 mm from the epicardial surface. On the other hand, application of the transmural shock to the discontinuous tissue volume produced a series of sharp intramural voltage steps centred on the cleavage planes that separate muscle layers. These local potential gradients were generated by current in the extracellular space adjacent to cleavage planes and acted as secondary sources to "seed" near-complete activation at 10 ms. Very similar findings were obtained with cultured myocytes laid down in separated strands²⁸. More recently, Sharifov *et al.*²⁹ reported on experimental studies that approximate the simulations outlined here. Optical techniques were used to map membrane potential across the surface of a perfused, transmural segment removed from the LV free wall of the pig heart and transmural shocks of similar magnitude to those employed in this work led to the formation of widely distributed virtual sources.

Intramural measurement of cardiac electrical activity

Direct validation of the model predictions reported in the previous section is technically difficult. To date, attempts to reconstruct the 3D spread of electrical activation through the ventricular wall using extracellular plunge electrodes have provided relatively coarse global information at best⁸. Moreover, it has not been previously possible to measure transmembrane potentials at sites across the intact heart wall. Recently, however, we have developed techniques that enable both transmembrane and extracellular potentials to be measured at multiple intramural sites in the LV.

Transmembrane potentials are recorded using a novel optical probe or optrode¹⁰ that consists of seven, hexagonally packed optical fibres inserted into a tapered glass micropipette (400 μm OD). Fibres terminate at 1.4 mm spacings and address a tissue volume radial to the optrode, each staggered by 60° . The principal elements of the optical system are illustrated in Figure 6, below. Excitation light (488 nm) from a water-cooled argon ion

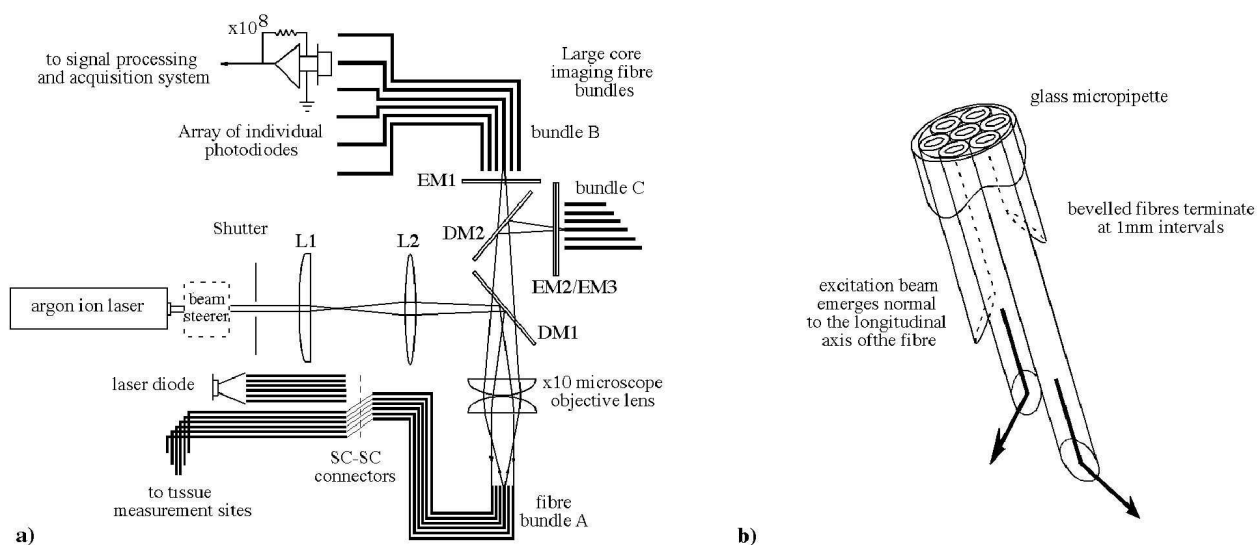


Figure 6. Schematic diagrams of a) optical mapping system and b) optrode. Nomenclature in (a) is as follows: S, shutter; L1&2, converging lenses, DM1&2, dichroic mirrors; EM1&2, 600nm and 520nm long pass filters; EM3, 600nm short pass filter. Optical fibres in bundles B and C have greater core:outer diameter ratio than those in C to maximize coupling efficiency and facilitate alignment. (Modified from Hooks et al.¹⁰)

laser is delivered to the optrode and excites the membrane potential sensitive dye di-4-ANEPPS (Molecular Probes Inc.) adjacent to the fibre ends. Fluorescent light returns via the same path, and is split into long and short wavelength bands that are routed to separate photo-detectors. Either dual wavelength ratiometry or a modified subtraction technique³⁰ are used to minimize light source noise and remove artifact due to motion and fluorescence bleaching[†]. Intramural extracellular potentials are recorded using epoxy coated plunge needles each containing 12 unipolar silver wire (70 μm) electrodes at 1 mm separation⁹.

We have completed preliminary studies in which transmembrane and extracellular potentials have been measured at multiple intramural sites in the intact pig. These experiments were carried out using an isolated Langendorff-perfused pig heart preparation, similar to that used by Chattipakorn and colleagues³¹, which enabled us to suppress "motion artifact" with the electromechanical uncoupler 2,3-butanedione monoxime (BDM). However, to provide an *in vivo* control, intramural extracellular potentials were first recorded in anaesthetized pigs employing identical experimental protocols. Young pigs (20 - 30 kg) were anaesthetized initially with tiletamine-zolazepam (Zoletil, 10 mg/kg im) and maintained with halothane (2-5%) in oxygen. The heart was exposed via a thoracotomy and three needle probes were introduced into the anterior free wall of the LV. An intramural bipolar

pacing probe was placed adjacent to the extracellular recording probes. Extracellular potentials were monitored at all 36 intramural sites until ST segment elevation returned to baseline and then in sinus rhythm and during ventricular pacing (1 - 3 Hz) using a constant current stimulator (duration 2 ms; current 1.5x capture threshold). The heart was then excised with needle probes in place and mounted in a modified Langendorff perfusion apparatus. The heart was perfused with oxygenated Tyrode's solution (37°C, 95% O₂ and 5% CO₂), BDM (7.5 - 12.5 mmol/L) was added to the perfusate and the potential-sensitive dye di-4-ANEPPS (Molecular Probes Inc.; 15 ml, 75 $\mu\text{mol/L}$) was infused into the left anterior descending coronary artery. An optrode was positioned at the centre of the dyed region adjacent to the pacing probe and the pacing protocols carried out *in vivo* were repeated in the isolated heart. Extracellular potentials and optical signals were acquired at 1 kHz and stored. Data were averaged over 8 to 12 successive heart beats.

The results of the preliminary studies were as follows. For *in vivo* hearts in sinus rhythm, extracellular potentials exhibited a smooth negative deflection of short duration and there was a rapid transmural spread of activation from subendocardium to subepicardium. Polyphasic (fractionated) electrograms were rarely observed. For subendocardial and mid-wall pacing, however, the duration of the negative deflection was increased with respect to sinus rhythm, particularly at intramural sites close to the stimulus and electrograms were commonly fractionated in this region also. The transmural progression of activation from the stimulus site toward the subendocardium was slower than for sinus rhythm. The

[†] This is possible because di-4 ANEPPS is a ratiometric dye. While modulation due to membrane potential change is opposite in sense in short and long wavelength bands, photobleaching and motion artifact etc produce comparable changes in both.

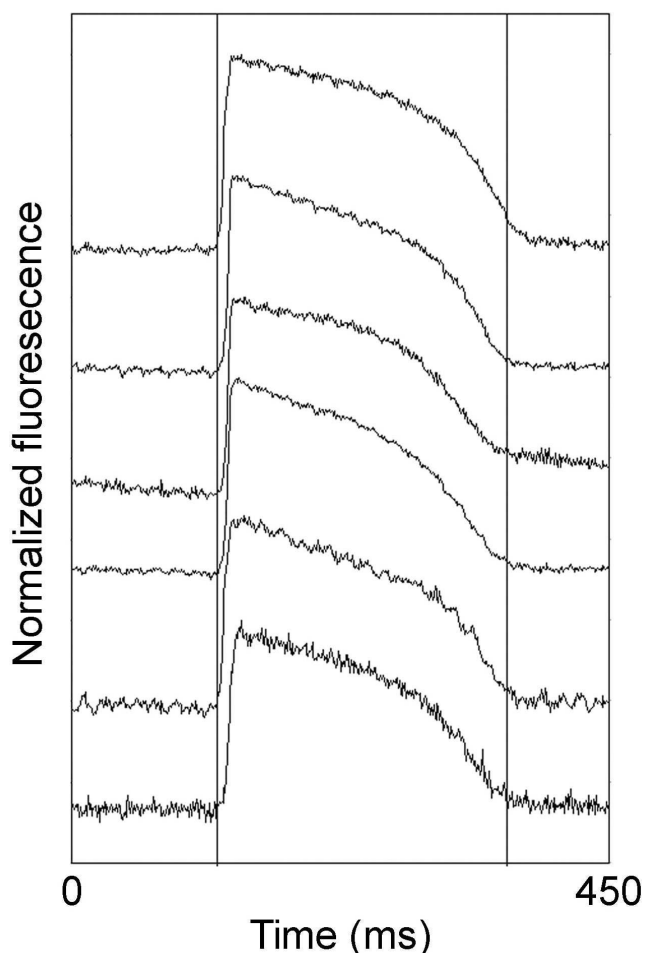


Figure 7. Intramural transmembrane potentials recorded at six sites in the pig LV free wall in sinus rhythm. Action potentials are ordered by depth below the epicardial surface with the most superficial record uppermost. The optical records were averaged over 16 cycles and obtained at transmural depths of 1.9, 3.3, 4.7, 6.1, 7.5 and 8.9 mm.

extracellular potentials observed in the isolated heart preparation were very similar to those seen for comparable experimental protocols *in vivo*. In general, though, propagation was slower in the isolated heart and the extent of fractionation significantly greater. Intramural transmembrane potential was also measured adjacent to the stimulus probe and to the plunge electrode closest to it. Membrane potential exhibited the expected behaviour with a rapid upstroke on depolarization prolonged plateau and a slow recovery to baseline during repolarization. There was close correlation between the transmural patterns of activation seen with optrode and adjacent extracellular needle probes, although activation times estimated from the optical potentials were more variable than those obtained from the extracellular potentials. Despite the fractionation of the extracellular electrograms, polyphasic activity was

never detected in the upstroke of the membrane potentials during ventricular pacing.

These preliminary results are consistent with model predictions and reinforce the hypothesis that structural discontinuity may give rise to non-uniform, anisotropic propagation of electrical activation. The fact that polyphasic activation is not seen in membrane potentials suggests that the nonuniform electrical activity that gives rise to fractionation is occurring in volumes larger than those addressed by the optrode.

Conclusions and future developments

At the start of this article, we argued that computer models provide a particularly important means of investigating cardiac electrical activation, but that modelling and controlled experimental measurement must be seen as complementary parts of an iterative process in which understanding is developed through a sequence of hypothesis formation, prediction and validation. We are using this approach to investigate the effect of discontinuities associated with muscle layers on the spread of electrical activation in ventricular myocardium. A structurally detailed tissue model has been set up and novel experimental techniques for characterizing intramural electrical activity in the intact heart have also been developed. On this basis, we have argued that the standard view of ventricular myocardium as a uniformly coupled electrical continuum, transversely isotropic with respect to fibre direction, is likely to be incorrect and we have demonstrated that interlaminar clefts could play a significant role in the termination of fibrillation by an externally applied shock²².

The role of interlaminar clefts in the development and maintenance of re-entrant electrical activity has not yet been resolved. The results outlined here indicate that the spread of electrical activation from an ectopic stimulus is slow in the direction perpendicular to cleavage planes and this could contribute to the formation of macroscopic re-entrant electrical circuits, particularly in the ischaemic heart. However, it is more difficult to establish whether or not discontinuities associated with muscle layers provide a potential substrate for micro re-entry.

It is appropriate at this stage to restate the three mechanisms listed by Spach⁵ as likely causes of re-entry: (1) regional heterogeneity of cellular electrical properties; (2) anisotropic discontinuities in which the discrete nature of cellular organization cause slow propagation in particular directions; and (3) wavefront dynamics, in which abrupt changes of wavefront curvature in regions where structure is discontinuous or exhibits marked spatial variation may give rise to sustained re-entrant wave motion. Within this context, it seems logical to include what we have learnt about the effects of myocardial cellular architecture in full atrial or ventricular models with realistic boundary geometry which also incorporate accurate information about the spatial variation of cellular electrical properties. We are extending our capacity to model key aspects of cardiac anatomy and are acquiring comprehensive data on

ventricular tissue architecture in a range of different animal models of cardiac disease. We are also setting up a computer model of atrial anatomy that will include detailed morphometric information on atrial surface geometry, myocyte arrangement and organization of specialized conduction tracts. More systematic information on the regional expression of membrane ion channels, transporters and gap junctions in normal and pathologic hearts is now becoming available^{32,33} and it is anticipated that the volume of such data will increase markedly over the next two to three years. To utilize such information fully, it will be necessary to develop computationally efficient models that capture the main electrical mechanisms responsible for re-entrant arrhythmia, but also to have access to serious computing power. Both goals are entirely realizable in the immediate future. As a result, we and other groups working in this field have the opportunity to apply a more integrative approach to cardiac electrophysiology, in which realistic, structure-based computer models will be used routinely in parallel with experimental measurement to investigate the formation, maintenance and prevention of re-entrant arrhythmias.

Acknowledgments

This work has been funded by a number of different agencies. We gratefully acknowledge the support of the Health Research Council of New Zealand, the New Zealand Marsden Fund, the Auckland Medical Research Foundation, the Wellcome Trust (UK) and the Maurice and Phyllis Paykel Trust.

References

1. Beeler GW, Reuter H. Reconstruction of the action potential of ventricular myocardial fibres. *J. Physiol.* 1977; **268**: 177-210.
2. Francesco D, Noble D. A model of cardiac electrical activity incorporating ionic pumps and concentration changes *Phil. Trans. R. Soc. Lond.* 1985; **B307**: 353-398.
3. Courtemanche M, Ramirez RJ, Nattel S. Ionic mechanisms underlying human atrial action potentials: insights from a mathematical model. *Am. J. Physiol.* 1998; **275**: H310-H321.
4. Luo C-H, Rudy Y. A dynamic model of the cardiac ventricular action potential. I. Simulations of ionic currents and concentration changes. *Circ. Res.* 1994; **74**: 1071-1096.
5. Spach MS. Mechanisms of the dynamics of reentry in a fibrillating myocardium. *Circ. Res.* 2001; **88**: 753-755.
6. Gray RA, Ayers G, Jalifé J. Video imaging of atrial defibrillation in the sheep heart. *Circulation* 1997; **95**: 1038-1047.
7. Knisley SB. Optical mapping of cardiac electrical stimulation. *J. Electrocardiol.* 1998; **30** supplement: 11-18.
8. Frazier DW, Krassowska W, Chen P-S, Wolf PD, Daniele ND, Smith WM, Ideker RE. Transmural activations and stimulus potentials in three-dimensional anisotropic canine myocardium. *Circ. Res.* 1988; **63**: 135-146.
9. Rogers JM, Melnick SB, Huang J. Fiberglass needle electrodes for transmural cardiac mapping. *IEEE Trans. Biomed. Eng.* 2002; **49**:1639-1641.
10. Hooks DA, LeGrice IJ, Harvey JD, Smaill BH. Intramural optical mapping of transmembrane potential in the heart. *Biophys. J.* 2001; **81**: 2671-2680.
11. Nielsen PMF, LeGrice IJ, Smaill BH, Hunter PJ. Mathematical model of geometry and fibrous structure of the heart. *Am. J. Physiol.* 1991; **260**: H1365-H1378.
12. Stevens C, Remme E, LeGrice IJ, Hunter PJ. Ventricular mechanics in diastole: material parameter sensitivity. *J. Biomech.* 2003; **36**: 737-748.
13. Streeter DDJ, Bassett DL. 1966 An engineering analysis of myocardial fiber orientation in pig's left ventricle in systole. *Anat. Rec.* 1966; **155**: 503-511.
14. Caulfield JB, Borg TK. The collagen network of the heart. *Lab. Invest.* 1979; **40**: 364-72.
15. LeGrice, IJ, Smaill BH, Chai LZ, Edgar SG, Gavin JB, Hunter PJ. Laminar structure of the heart: ventricular myocyte arrangement and connective tissue architecture in the dog. *Am. J. Physiol.* 1995; **269**: H571-H582.
16. LeGrice IJ, Hunter PJ, Smaill BH. Laminar structure of the heart: a mathematical model. *Am. J. Physiol.* 1997; **272**: H2466-H2476.
17. Young AA, LeGrice IJ, Young MA, Smaill BH. Extended confocal microscopy of myocardial laminae and collagen network. *J. Microsc.* 1998; **192**: 139-150.
18. LeGrice I, Sands G, Hooks D, Gernecke D, Smaill B. Microscopic Imaging of Extended Tissue Volumes. *Proc. Aust. Physiol. Pharmacol. Soc.* 2004; **34**: 129-132.
19. Hunter PJ, Nash MP, Sands GB. Computational electro-mechanics of the heart. In: *Computational Biology of the Heart* (eds A.V Panfilov & AV Holden), John Wiley & Sons, 1997; 347-409.
20. Panfilov AV. Modelling of re-entrant patterns in an anatomical model of the heart. In: *Computational Biology of the Heart* (eds A.V Panfilov & AV Holden), John Wiley and Sons, 1997; 259-276.
21. Berenfeld O, Jalife J. Purkinje-muscle reentry as a mechanism of polymorphic ventricular arrhythmias in a 3-dimensional model of the ventricles. *Circ. Res.* 1998; **82**: 1063-1077.
22. Hooks DA, Tomlinson KA, Marsden SG, LeGrice IJ, Smaill BH, Pullan AJ, Hunter PJ. Cardiac microstructure: implications for electrical propagation and fibrillation. *Circ. Res.* 2002; **91**: 331-338.
23. Hunter PJ, McNaughton PA, Noble D. Analytical models of propagation in excitable cells. *Prog. Biophys. Mol. Biol.* 1975; **30**: 99-144.

24. Spach MS, Dolber PC. Relating extracellular potentials and their derivatives to anisotropic propagation at the microscopic level in human cardiac muscle: evidence for electrical uncoupling of side-to-side fiber connections with increasing age. *Circ. Res.* 1986; **58**: 356-371.
25. Ellis WS, Auslander DM, Lesh MD. Fractionated electrograms from a computer model of heterogeneously uncoupled anisotropic ventricular myocardium. *Circulation* 1995; **92**: 1619-1626.
26. Drouhard JP, Roberge FA. A simulation study of the ventricular myocardial action potential. *IEEE Trans. Biomed. Eng.* 1982; **29**:494-502.
27. Skouibine KB, Trayanova NA, Moore PK. Anode/cathode make and break phenomena in a model of defibrillation. *IEEE Trans. Biomed. Eng.* 1999; **46**: 769-777.
28. Fast VG, Rohr S, Ideker RE. Nonlinear changes of transmembrane potential caused by defibrillation shocks in strands of cultured myocytes. *Am. J. Physiol.* 2000; **278**: H688-H697.
29. Sharifov OF, Fast VG. Optical mapping of transmural activation induced by electric shocks in isolated left ventricular wall wedge preparations. *J. Cardiovasc. Electrophysiol.* 2003; **14**:1215-1222.
30. Tai DC-S, Caldwell BJ, LeGrice IJ, Hooks DA, Pullan AJ, Smaill BH. Correction of motion artifact in transmembrane voltage-sensitive fluorescent dye emission in hearts. *Am. J. Physiol.* 2004; **287**: H985-H993.
31. Chattipakorn NI, Banville I, Gray RA, Ideker RE. Mechanisms of ventricular defibrillation for near-defibrillation threshold shocks - a whole-heart optical mapping study in swine. *Circulation* 2001; **104**: 1313-1319.
32. Li D, Zhang L, Kneller J, Nattel S. Potential ionic mechanism for repolarization differences between canine right and left atrium. *Circ. Res.* 2001; **88**: 1168-1175.
33. Tan JH, Liu W, Saint D. Differential expression of the mechanosensitive potassium channel TREK-1 in epicardial and endocardial myocytes in rat ventricle. *Exp. Physiol.* 2004; **89**: 237-242.

Received 25 August 2004, in revised form 22 September 2004. Accepted 24 September 2004.

©B.H. Smaill 2004.

Author for correspondence:

Bruce H. Smaill
Bioengineering Institute & Department of Physiology,
University of Auckland,
Private Bag 92019,
Auckland, New Zealand

Tel: +64 9 373 7599 x86208

Fax: +64 9 373 7499

E-mail: b.smaill@auckland.ac.nz

John Atherton Young AO, FAA FRACP (1936-2004)

D.I. Cook

Department of Physiology, University of Sydney, NSW 2006, Australia

For almost 40 years John Young was one of the leading figures in physiology in Australia. The importance of his contributions to scientific knowledge were recognized by election to Fellowship of the Australian Academy of Sciences, where he rose to be Vice-President and Secretary (Biological) and by the award of the prestigious Research Professorship of the Alexander von Humboldt Stiftung.

As long-term members of the Society will be aware, however, John Young was not only a leading researcher, he also played a major role in promoting physiology within Australia and internationally. He, together with a handful of others including Ian McCance, Chris Bell, Trefor Morgan, Dave Davey and Alan Boura, was one of the key personalities who kept the Australian Physiological and Pharmacological Society running efficiently and effectively from the 1970s through to the 1990s, serving as Councillor (1969-1973), Editor of the Proceedings (1973-1975), National Secretary (1983-1988) and President (1995-2000). He also served on the National Committee for Physiology of the Australian Academy of Sciences (1984-1990). Internationally, he was instrumental in the establishment of the Federation of Asian and Oceanian Physiological Societies (FAOPS) and was an inaugural member of its Council (1990-1994) before being elected Vice-President (1994-1998) and President (1998-2002). He also served as a member of the Council of the International Union of Physiological Sciences (1993-2001) where his presence ensured that the interests of Australian physiologists were adequately catered for in the Congresses organised by the Union. His impact in promoting linkages between Australian physiologists and between physiologists in Australia and those overseas was substantial. His impact on individuals was equally great. Many will have fond memories of impromptu sightseeing tours or visits to the opera organised by John to fill in lulls in the scientific program and have been amused and educated by his knowledgeable and witty conversation over meals in interesting restaurants in cities all over the world.

Doctoral Training (1962-1964)

John Young undertook his doctoral studies at the Kanematsu Memorial Institute at Sydney Hospital under the supervision of Dr K.D.G. Edwards. His project was to investigate the renal handling of the anti-hypertensive methyldopa and in particular to establish whether therapy with methyldopa, an α -amino acid, interfered with renal handling of other amino acids. To carry out this project, he successfully adapted the technique of stop-flow analysis¹ which had been just recently developed in the dog kidney² for studies in rats. To validate the technique, he first demonstrated that phenolsulphonphthalein secretion is localised to the proximal tubule³ and then determined the

tubular segments responsible for transporting a wide variety of amino acids and other substances⁴. This work confirmed that previous findings in dogs (see for example⁵) were also applicable to rats. He then conducted an extensive pharmacological investigation of the absorption, metabolism and excretion of methyldopa and related catecholamines in order to characterise the extent of renal elimination of α -methyldopa and its metabolites⁶ and used the stop-flow technique to demonstrate that as predicted, the L-stereo-isomer of α -methyl-dopa interferes with proximal tubular absorption of neutral amino acids such as histidine and serine^{6,7}. Finally, he followed up the observation that the D-stereo-isomer of α -methyldopa is not orally absorbed⁶ by showing that in the rat jejunum, as in the proximal tubule, α -methyldopa is absorbed by the same system that absorbs neutral amino acids⁸. These studies led to the award of the degree of MD from the University of Queensland in 1965. They also provided the basis of his first presentation to the Australian Physiological Society (as it then was) at its Sixth Meeting held at Monash from 20 to 22 May 1964.

Post-doctoral Training (1965-1966)

John began working on the physiology of salivary glands in 1965 in the laboratory of Professor K.J. Ullrich at the Physiologisches Institut of the Free University in Berlin. At this time, Karl Ullrich was already well known for his studies on renal concentrating mechanisms, and John was expecting to continue working on renal physiology. Ullrich's group, however, was pioneering the application of micropuncture techniques to epithelial organs other than the kidney. In particular, J.R. Martinez had begun micropuncture studies on unstimulated rat mandibular glands⁹ in order to test the applicability of the Thaysen 2-stage hypothesis to them. Ricardo had, however, returned to El Salvador, and the task of extending his work to rat mandibular glands during parasympathetic stimulation fell to John. John succeeded in confirming that, as predicted, the fluid in the intercalated ducts had a plasma-like composition which did not vary with secretion rate. The findings were of such importance, that the then doyen of salivary physiology, Sir Arnold Burgen FRS, when he heard John present his findings at a meeting of the Physiological Society at London Zoo, sought permission to include the data in a lecture he was giving at a conference in Birmingham, Alabama, as well as securing John an invitation to give a Plenary Lecture at the same conference.

While in Berlin, he collaborated with Eberhard Frömter who many Members will have met during his trips to Australia to visit John. Together they developed *in vivo* perfusion methods that permitted them to establish that the main excretory duct actively transported both Na⁺ and K⁺

and that the apical membrane of this epithelium behaved like a Na⁺-selective electrode¹⁰. This work formed the basis of John's second presentation to the Australian Physiological Society, given at the tenth Meeting of the Society in Adelaide (24-26 May 1967) following his return to Australia.

The Department of Physiology in Sydney (1966-2004)

In late 1966, John returned to Australia to a Senior Lectureship in Physiology at the University of Sydney. The choice between this position and one in Zoology at Macquarie University having been made on his behalf by the Heads of the two Departments in a chance meeting in a supermarket aisle. In order to more rigorously test the general applicability of the Thaysen 2-stage hypothesis, he extended his micropuncture studies to a wide variety of species and gland types, including the rat sublingual, the cat sublingual, the cat mandibular, the sheep parotid, and the rabbit mandibular glands as well as the parotid, mandibular and sublingual glands of a monotreme (the echidna, *Tachyglossus aculeatus*) (reviewed in^{11,12}).

He also continued to study the mechanisms of ductal ion transport. His studies on ductal HCO₃⁻ transport, in particular, led to the demonstration that ductal transport could be influenced by parasympathomimetic agonists¹³, an idea that he had first canvassed on the basis of his studies on the intact rat mandibular gland¹⁴. This finding, which was confirmed and extended to sympathomimetic agonists in subsequent studies^{15,16}, disproved the then dogma that the rate of ductal electrolyte transport would be determined solely by the composition of the luminal fluid. The exploitation of its implications became the major focus of his work in the 1970s. Initially these studies were based on the mandibular duct perfused *in vivo*¹⁵, but during a sabbatical leave spent in the Max Planck Institut für Biophysik in Frankfurt am Main in 1971, he started to perfuse these ducts *in vitro*, using a technique that had just been developed by H. Knauf in Frankfurt. He exploited this technique to investigate the effects on ductal transport of a wide variety of hormones and neurotransmitters (see, for example^{17,18}).

His interests were not, however, limited to salivary epithelia. He continued to carry out work on renal amino acid transport in collaboration with Akos Györy and Jennifer Lingard. In collaboration with Peter Harris he found that the concentration-response relation for angiotensin II on proximal tubular Na⁺ transport is biphasic; low concentrations of angiotensin II being stimulatory and high concentrations being inhibitory¹⁹.

During this period, John became one of the stalwarts of the Society. He acted as the Local Secretary for the 13th meeting of the Society held in Sydney in August 1969. Importantly, the Society's meetings also provided the venue at which the succession of highly talented medical students who worked with John presented their micropuncture and duct perfusion data. In 1973, John presented the Society's Invited Lecture using the title "Electrolyte Transport by Salivary Epithelia". In it he made a point of making

particular mention of his students whose work had made the talk possible.

During the late 1970s and early 1980s, John started to investigate the mechanisms by which salivary endpiece cells secrete saliva. Research in this area had been impeded by the lack of a suitable *in vitro* preparation for studying salivary secretion. He had had some success in developing an *in vitro* perfused salivary gland preparation in the mid 1970s, but it was only when Maynard Case spent a sabbatical leave in his laboratory in 1977, that Arthur Conigrave and Ivana Novak succeeded in establishing a convincing *in vitro* preparation of the rabbit mandibular gland²⁰. Subsequently, in collaboration with Ricardo Martinez in Columbia, Missouri, an isolated perfused preparation of the rat mandibular and sublingual glands was also developed²¹, which Masataka Murakami was later to make extensive use of in John's laboratories. These preparations permitted analysis of the mechanisms of salivary secretion at a level of detail that had never previously been possible. In rapid succession major studies were published on the role of HCO₃⁻²², H⁺²³ and Cl⁻²⁴ in maintaining salivary secretion. This work culminated in the pharmacological identification of the transport proteins that underlie fluid and electrolyte secretion by the rat and the rabbit mandibular glands^{25,26}.

Finally, during the 1980s and 1990s, John and I collaborated in studies that ranged from the mechanisms by which sheep salivary glands secrete, through to the mechanisms by which epithelial Na⁺ channels are regulated by intracellular ions²⁷.

John has also made substantial contributions to the study of the exocrine pancreas. These contributions include characterising the protein, fluid and electrolyte secretory responses of the rat pancreas^{28,29} and the rabbit pancreas³⁰ to stimulation with secretin and cholecystokinin. They also include the development with Jennifer Lingard of an isolated and perfused rat pancreas preparation³¹. The driving force for the development of this preparation was the need for information on pancreatic secretory mechanisms that could be compared with the data emerging from studies on isolated and perfused salivary glands³². From these studies it became clear that rat pancreatic acinar cells secreted by a markedly different mechanism to that seen in salivary endpiece cells^{33,34}.

John also exerted great influence on salivary and exocrine physiology through the reviews he wrote. These covered salivary morphology³⁵, the composition of saliva³⁶, salivary myoepithelial cells³⁷ and salivary electrolyte transport mechanisms^{11,12,38-40} as well as more general overviews of the physiology of salivary glands⁴¹⁻⁴⁴ and salt glands⁴⁵. Of particular note were those written together with Ernst Van Lennep (e.g.^{12,35,45}).

Administration (1976-2004)

John's success in research led to his rapid promotion. He was promoted to Associate Professor in 1972, and then appointed to one of the two chairs of Physiology in 1976. Once he became Professor, university

administration took up an ever greater proportion of his life. This was not simply due to the need to alternate with Liam Burke as Head of Department. It was also because John took on an amazingly wide range of tasks within the University. The first sign of this was his election, in 1976, to the Council of the Sydney Association of University Teachers, the academic staff union, of which he was President in 1977. He also served as Deputy Chair of the Academic Board (1978-1980), a position which required chairing of many key University Committees, including the Library Committee, the Admissions Committee, the Matriculation Committee, and the PhD Committee and he served on the University Senate (1978-81, 1984-85, 1988-89, 1990-93). Within the Faculty of Medicine, he became Sub-Dean of Academic Affairs in 1978 and remained in that post until his elevation to Dean of the Faculty in 1989. His activities while Dean of Medicine and later Pro-Vice-Chancellor in charge of the Faculties of Medicine, Dentistry, Health Sciences and Nursing (1994-2003) have been dealt extensively elsewhere; here it is sufficient to remind Members of John Young's role in the establishment of the Graduate Medical Curriculum at the University of Sydney and in the establishment of the Canberra Clinical School, which has subsequently developed to become the School of Medicine at the Australian National University.

John Young and the Australian Physiological Society

As I have already mentioned, John played a leading role in the Society. While his students made major contributions to the scientific program of the meeting, he perhaps had his greatest impact during Annual General Meetings, where his tireless use of the Socratic method to get to the core of issues coupled with his enthusiastic support for the aims of the Society and a solid knowledge of Joske's *The Law and Procedure at Meetings in Australia and New Zealand* (5th edition) ensured a lively and engaging debate. On one memorable occasion, he successfully moved that the meeting would "no longer hear" a Member who had pressed his case in an unduly acrimonious and long-winded manner.

John also had a major impact on the Society's approach to conducting meetings. He believed that meetings should be enjoyable. He thus pushed Local Secretaries to ensure that the all social functions should be of a high quality. For example, the Conference Dinner of one meeting was held on a ferry on Sydney Harbour and facilitated interactions between participants with a keg of sherry. He was strongly of the view that the Society should emulate that famous dining society, the Physiological Society, and recommended to neophyte Local Secretaries that they arrange a meal in a top quality restaurant for the Council following its meeting on the day preceding the opening of the Meeting, and that they budget on one bottle of good wine per person in order to ensure that the "Society's serious interest in wine" was adequately catered for. His wish to emulate the best aspects of Physiological Society practice also included his oversight as Editor of a

system of printing draft books of abstracts before the meeting, which were corrected by meetings through comments and a vote at the completion of each presentation. John seemed pretty keen on the system, which although it needed a dedicated editor, involved audiences in a way we do not see today.

John's belief that the Society's meetings were as much a social event as a scientific event also led to his practice of driving or catching the train to meetings. This habit ensured that meetings became part of a very much larger experience, in which the students (often heavily subsidised by John) and colleagues who accompanied him were exposed to a wide range of culinary and tourist experiences in a wonderfully hospitable atmosphere. The previously mentioned Adelaide meeting, for example, included not only a tour of the Barossa and Clare Valley wine districts in which John acted as the expert guide. It also included one of John's more exuberant 'extra-curricular' contributions to the Society. This was a late-night induction for friends and colleagues to the game of 'slosh' on the precious billiard tables of one of Adelaide University's Residential Colleges. As many of the participants had become thoroughly sloshed during the course of the game it was not altogether surprising that, in the interests of preserving good order in respectable Adelaide, the entire group was unceremoniously asked to vacate the billiard room and not return. Members who were introduced to slosh by John will not be surprised to learn that a game some years later in the august Australian Club in Sydney resulted in one of his former students, Chris Martin, breaking a cue. John, who had recently been elected to the club, was left with a rather delicate and taxing exercise in diplomacy which led to his "donation" of the cue which bears his name in the club's billiard room.

John also contributed to the development of physiology, both in Australia and overseas through the many conferences that he organised. These included several major international symposia at Leura, and at a luxury hotel close to his beloved property at Bowral, as well the Satellite Symposium of the 1983 IUPS meeting held in the spartan conditions of the University of Sydney's Veterinary School at Camden.

Finally, he exerted an influence which, despite being difficult to document, had a major positive impact on Physiology in Australia. Through his service in the Society and on innumerable appointment committees and review boards, he came in contact with every professional physiologist in the country as well as many students. Many of the letters which I, and others, have received since his death have mentioned the profound impact that contact with John had in assisting these people to become more productive and happier scientists. He succeeded in fostering a collegial striving for excellence among Australian physiologists which contributed greatly to the success of the discipline.

Acknowledgements

I would like to thank John's many colleagues and former

students who have shared their memories with me.

References

- Young JA, Edwards KDG. Stop-flow analysis of renal tubular function adapted to the rat. *Proc. Aust. Soc. Med. Res.* 1963; **1**: 83.
- Malvin RL, Wilde WS, Sullivan LP. Localization of nephron transport by stop-flow analysis. *Am. J. Physiol.* 1958; **194**: 135.
- Young JA, Edwards KDG. Stop-flow analysis of phenolsulphonphthalein excretion and visual localization of the site of maximal urine acidification in the rat nephron. *Aust. J. Exp. Biol. Med. Sci.* 1964; **42**: 539-542.
- Young JA, Edwards KDG. Stop-flow analysis of renal tubular function in the rat undergoing osmotic diuresis due to creatinine loading. *Aust. J. Exp. Biol. Med. Sci.* 1964; **42**: 667-688.
- Pitts RF, Gurd RS, Kessler RH, Hierholzer K. Localization of acidification of urine; potassium and ammonia secretion and phosphate reabsorption in the nephron of the dog. *Am. J. Physiol.* 1958; **194**: 125.
- Young JA, Edwards KDG. Studies on the absorption, metabolism and excretion of methyl dopa and other catechols and their influence on amino acid transport in rats. *J. Pharmacol. Exp. Ther.* 1964; **145**: 102-112.
- Young JA, Edwards KDG. Clearance and stop-flow studies on histidine and methyl dopa transport by rat kidney. *Am. J. Physiol.* 1966; **210**: 667-675.
- Young JA, Edwards KDG. Competition for transport between methyl dopa and other amino acids in rat gut loops. *Am. J. Physiol.* 1966; **210**: 1130-1136.
- Martinez JR, Holzgreve H, Frick A. Micropuncture study of submaxillary glands of adult rats. *Pflügers Arch.* 1966; **290**: 124.
- Young JA, Frömter E, Schögel E, Hamann KF. A microperfusion investigation of sodium resorption and potassium secretion by the main excretory duct of the rat submaxillary gland. *Pflügers Arch.* 1967; **295**: 157-172.
- Young JA. Salivary secretion of inorganic electrolytes. In: RK Crane (ed) *International Review of Physiology, Gastrointestinal Physiology III, Volume 19*. University Park Press: Baltimore, 1979; 1-58.
- Young JA, Van Lennep EW. Transport in salivary and salt glands. Part I: Salivary glands. In: G Giebisch, DC Tosteson, HH Ussing (eds) *Membrane Transport in Biology, Volume 4B Transport Organs*. Springer Verlag: Berlin, 1979; 563-674.
- Young JA, Martin CJ, Asz M, Weber FD. A microperfusion investigation of bicarbonate secretion by the rat submaxillary gland. The action of a parasympathomimetic drug on electrolyte transport. *Pflügers Arch.* 1970; **319**: 185-199.
- Young JA, Schögel E. Micropuncture investigation of sodium and potassium excretion in rat submaxillary saliva. *Pflügers Arch.* 1966; **291**: 85-98.
- Martin CJ, Young JA. A microperfusion investigation of the effects of a sympathomimetic and a parasympathomimetic drug on water and electrolyte fluxes in the main duct of the rat submaxillary gland. *Pflügers Arch.* 1971; **327**: 303-323.
- Martin CJ, Young JA. Electrolyte concentrations in primary and final saliva of the rat sublingual gland studied by micropuncture and catheterization techniques. *Pflügers Arch.* 1971; **324**: 344-360.
- Martin CJ, Frömter E, Gebler B, Knauf H, Young JA. The effects of carbachol on water and electrolyte fluxes and transepithelial electrical potential differences of the rabbit submaxillary main duct perfused *in vitro*. *Pflügers Arch.* 1973; **341**: 131-142.
- Denniss AR, Young JA. The action of neurotransmitter hormones and analogues and cyclic nucleotides and theophylline on electrolyte transport by the excretory duct of the rabbit mandibular gland. *Pflügers Arch.* 1975; **357**: 77-89.
- Harris PJ, Young JA. Dose-dependent stimulation and inhibition of proximal tubular sodium reabsorption by angiotensin II in the rat kidney. *Pflügers Arch.* 1977; **367**: 295-297.
- Case RM, Conigrave AD, Novak I, Young JA. Electrolytes and protein secretion by the perfused rabbit mandibular gland stimulated with acetylcholine or catecholamines. *J. Physiol. (Lond.)* 1980; **300**: 467-487.
- Compton J, Martinez JR, Martinez AM, Young JA. Fluid and electrolyte secretion from the isolated, perfused submandibular and sublingual glands of the rat. *Arch. Oral Biol.* 1981; **26**: 555-561.
- Case RM, Conigrave AD, Favalaro EJ, Novak I, Thompson CH, Young JA. The role of buffer anions and protons in secretion by the rabbit mandibular salivary gland. *J. Physiol. (Lond.)* 1982; **322**: 273-286.
- Novak I, Conigrave AD, Case RM, Young JA. Secretory processes in the rabbit mandibular gland. II. The role of H⁺ ions. In: I Schulz, G Sachs, JG Forte, KJ Ullrich (eds) *Hydrogen Ion Transport in Epithelia*. Elsevier: Amsterdam, 1980; 251-258.
- Case RM, Hunter M, Novak I, Young JA. The anionic basis of fluid secretion by the rabbit mandibular gland. *J. Physiol. (Lond.)* 1984; **349**: 619-630.
- Novak I, Young JA. Two independent anion transport systems in rabbit mandibular salivary glands. *Pflügers Arch.* 1986; **407**: 649-656.
- Pirani D, Evans LAR, Cook DI, Young JA. Intracellular pH in the rat mandibular salivary gland: the role of Na-H and Cl-HCO₃ antiports in secretion. *Pflügers Arch.* 1987; **408**: 178-184.
- Dinudom A, Fotia AB, Lefkowitz RJ, Young JA, Kumar S, Cook DI. The kinase Grk2 regulates Nedd4/Nedd4-2-dependent control of epithelial Na⁺ channels. *Proc. Natl. Acad. Sci. U.S.A.* 2004; **101**: 11886-11890.
- Sewell WA, Young JA. Secretion of electrolytes by the

- pancreas of the anaesthetized rat. *J. Physiol. (Lond.)* 1975; **252**: 379-396.
29. Sewell WA, Young JA. The effect of cycloheximide on cholecystokinin-evoked pancreatic juice of the anaesthetized rat. *Aust. J. Exp. Biol. Med. Sci.* 1978; **56**: 385-394.
30. Seow KTFP, Case RM, Young JA. Pancreatic secretion by the anaesthetized rabbit in response to secretin, cholecystokinin and carbachol. *Pancreas* 1990; **6**: 385-391.
31. Lingard JM, Young JA. β -Adrenergic control of exocrine secretion by perfused rat pancreas *in vitro*. *Am. J. Physiol.* 1983; **245**: G690-G696.
32. Case RM, Hunter M, Novak I, Young JA. A comparison of the mechanisms of electrolyte secretion in pancreas and salivary glands. *Scand. J. Gastroenterol.* 1983; **18(Supplement 87)**: 57-67.
33. Seow FKT, Lingard JM, Young JA. The anionic basis of fluid secretion by rat pancreatic acini *in vitro*. *Am. J. Physiol.* 1986; **250**: G140-G148.
34. Evans LAR, Pirani D, Cook DI, Young JA. Intraepithelial current flow in rat pancreatic secretory epithelia. *Pflügers Arch.* 1986; **407(Supplement 2)**: S107-S111.
35. Young JA, Van Lennep EW. *The Morphology of Salivary Glands*. Academic Press: London, 1978.
36. Young JA, Schneyer CA. Composition of saliva in mammalia. *Aust. J. Exp. Biol. Med. Sci.* 1981; **59**: 1-53.
37. Young JA, Van Lennep EW. Morphology and physiology of salivary myoepithelial cells. In: RK Crane (ed) *International Review of Physiology, Gastrointestinal Physiology II, Volume 12*. University Park Press: Baltimore, 1977; 105-125.
38. Schneyer LH, Young JA, Schneyer CA. Salivary secretion of electrolytes. *Physiol. Rev.* 1972; **52**: 720-777.
39. Young JA. Electrolyte transport by salivary epithelia. *Proc. Aust. Physiol. Pharmacol. Soc.* 1973; **4**: 101-121.
40. Cook DI, Young JA. Fluid and electrolyte secretion by salivary glands. In: JG Forte (ed) *Handbook of Physiology. The Gastrointestinal System. Salivary, Pancreatic, Gastric and Hepatobiliary Secretion. (Section 6, Volume III)*. American Physiological Society: Bethesda, 1989; 1-23.
41. Van Lennep EW, Cook DI, Young JA. Morphology and secretory mechanisms of salivary glands. In: P Desnuelle, H Sjöström, O Noren (eds) *Molecular and Cellular Biology of Digestion, Chapter 24*. Elsevier: Amsterdam, 1986; 435-456.
42. Young JA, Cook DI, Van Lennep EW, Roberts ML. Secretion by the major salivary glands. In: L Johnson, J Christensen, M Jackson, E Jacobson, J Walsh (eds) *Physiology of the Gastrointestinal Tract, Volume 2, 2nd Edition*. Raven Press: New York, 1987; 773-815.
43. Cook DI, Van Lennep EW, Roberts ML, Young JA. Secretion by the major salivary glands. In: L Johnson, J Christensen, M Jackson, E Jacobson, J Walsh (eds) *Physiology of the Gastrointestinal Tract, Volume 2, 3rd Edition*. Raven Press: New York, 1994; 1061-1117.
44. Young JA, Cook DI. The major salivary glands. In: R Greger, U Windhorst (eds) *Comprehensive Human Physiology, Volume 2*. Springer-Verlag: Berlin, 1996; 1309-1326.
45. Van Lennep EW, Young JA. Transport in salivary and salt glands. Part II: Salt glands. In: G Giebisch, DC Tosteson, HH Ussing (eds) *Membrane Transport in Biology Volume 4B: Transport Organs*. Springer Verlag: Berlin, 1979; 675-692.

Received 13 August 2004, in revised form 20 August 2004.

Accepted 21 August 2004.

©D.I. Cook 2004.

Author for correspondence:

Prof. D.I. Cook

Department of Physiology F13,

University of Sydney,

NSW 2006, Australia

Tel: +61 2 9351 3477

Fax: +61 2 9351 2058

Email: davidc@physiol.usyd.edu.au

Author Index

Allen, D.G.	1-11,31-37	Hunter, P.J.	141-149
Allman, B.E.	121-127	Iida, M.	65-70
Anderson, W.P.	85-91	Jacobs, M.D.	113-120
Bassett, D.	13-17	Kansui, Y.	65-70
Bellair, C.J.	121-127	Lee, E.M.	75-83
Brockett, C.L.	25-30	LeGrice, I.J.	129-132,141-149
Caldwell, B.J.	141-149	Lok, H.C.	71-74
Campbell, T.J.	133-140	Luff, S.E.	85-91
Cannell, M.B.	105-106,113-120	Lynch, G.S.	39-43
Coleman, H.A.	55-64	Malpas, S.C.	93-104
Conigrave, A.D.	71-74	Merriman-Smith, B.R.	113-120
Cook, D.I.	151-155	Monif, M.	107-112
Curl, C.L.	121-127	Morgan, D.L.	19-23,25-30
Currie, P.D.	13-17	Nugent, K.A.	121-127
Delbridge, L.M.D.	121-127	Parkington, H.C.	55-64
Denton, K.M.	85-91,93-104	Percival, P.	25-30
Donaldson, P.J.	113-120	Pollock, C.A.	75-83
Eppel, G.A.	93-104	Poronnik, P.	75-83
Evans, R.G.	93-104	Proske, U.	19-23,25-30
Fujii, K.	65-70	Pullan, A.J.	141-149
Gerneke, D.	129-132	Reid, C.A.	107-112
Goto, K.	65-70	Roberts, A.	121-127
Grey, A.C.	113-120	Sandow, S.L.	45-54
Harris, P.J.	121-127	Sands, G.	129-132
Hooks, D.A.	129-132,141-149	Shweta, A.	85-91
Hryciw, D.H.	75-83	Sisley, A.M.G.	113-120

Author Index

Smaill, B.H.	129-132,141-149
Smart, M.L.	107-112
Soeller, C.	113-120
Subbiah, R.N.	133-140
Tare, M.	55-64
Vandenberg, J.I.	133-140
Williams, D.A.	107-112
Yeung, E.W.	31-37